Journal of Radioanalytical and Nuclear Chemistry (2024) 333:717–804
https://doi.org/10.1007/s10967-023-09283-8

Extension of recommended cross section database for production of therapeutic isotopes

F. Tárkányi[1] · A. Hermanne[2] · A. V. Ignatyuk[3] · F. Ditrói[1] · S. Takács[1] · R. Capote Noy[4]

Received: 15 September 2023 / Accepted: 15 November 2023 / Published online: 9 January 2024

Abstract

Radionuclide-based diagnostics and therapy require proper selection of production nuclear reaction based on knowledge of the production excitation functions and the achievable yields completed with data on the formation of possible impurities. In the present work the existing IAEA recommended cross section data database for production of therapeutic isotopes is extended to production of the ^{47}Sc,^{47}Ca(^{47}Sc), ^{58m}Co, ^{71}As(^{71}Ge), ^{71}Ge, ^{77}Br, ^{77}Kr(^{77}Br), ^{80m}Br, ^{103}Pd, ^{103}Pd(^{103m}Rh), ^{103}Ru(^{103m}Rh), ^{105}Rh, ^{117m}Sn, ^{119}Sb, ^{119m}Te(^{119}Sb), ^{134}Ce, ^{135}La, ^{149g}Tb, ^{161}Tb, ^{165}Er, ^{165}Tm(^{165}Er), ^{167}Tm, ^{197m}Hg, ^{197g}Hg, ^{198g}Au, and ^{230}Pa(^{230}U) radioisotopes. Nearly 60 nuclear reactions are presented and discussed. The new recommended cross-section data and their uncertainties for the production of these 21 radionuclides will be available on the Web page of the IAEA Nuclear Data Section at https://nds.iaea.org/radionuclides and also at the IAEA medical portal https://nds.iaea.org/medportal.

Keywords Therapeutic radioisotopes · Cross sections · Recommended database

Introduction

Optimization of production for radionuclides of interest in medical applications (clinical and research) is of considerable interest to the IAEA. Several actions to set up a database for recommended cross-sections for various charged-particle reactions used for medically interesting radionuclides production and the underlying nuclear decay data have been launched by the IAEA over the last 25 years. The results and evaluations of the different studies were published on webpages of the IAEA-NDS https://nds.iaea.org/medportal and are documented in [1–9].

Selection of an optimal reaction depends on many factors such as available beam particles and their achievable energy range, target elements and possible recovery problems with enriched target materials, production yield, radionuclidic impurities and necessary chemical separation processes. Reliable cross section data and deduced yields for the extended list of the possible production reactions make this selection easier.

We report here on evaluated reactions for the production of radionuclides with emerging interest for therapeutic use in nuclear medicine, identified mostly by following the report of the IAEA-NDS consultants meeting of December 2018 in Vienna [10]. Results are presented for 62 charged particle induced nuclear reactions interesting for production of the ^{47}Sc, ^{47}Ca(^{47}Sc), ^{58m}Co, ^{71}As(^{71}Ge), ^{71}Ge, ^{77}Br, ^{80m}Br, ^{103}Pd(^{103m}Rh), ^{103}Ru(^{103m}Rh), ^{105}Rh, ^{117m}Sn, ^{119}Sb, ^{134}Ce, ^{135}La, ^{161}Tb, ^{165}Er, ^{165}Tm(^{165}Er), ^{167}Tm, ^{197m}Hg, ^{197g}Hg and ^{230}Pa(^{230}U) radioisotopes. The discussed results include recommended cross section values over well-chosen energy domains with their uncertainties and calculated physical yields based on these recommended data.

Summary of the method of evaluation

Detailed information on the method of collection and selection of experimental data, followed by Padé fitting methodology and obtaining uncertainties of the fit, can be found in the relevant IAEA publications: [1, 3–6, 9]. The main points:

✉ F. Ditrói
ditroi@atomki.hu

1 Institute for Nuclear Research, Debrecen, Hungary

2 Vrije Universiteit, Brussels, Belgium

3 Institute for Physics and Power Engineering, Obninsk, Russia

4 IAEA, Vienna, Austria

- The published datasets were corrected for up-to-date monitor cross sections or nuclear decay characteristics. Unrealistic low uncertainties in publications were enlarged based on other experimental data and the practice of the compilators.
- The experimental data were adopted from original works in EXFOR LIB, Google Scholar databases
- The experimental data sets show in many cases very large disagreements. This is usually due to incorrect determination of the basic experimental parameters like beam current, beam energy, detector efficiency, nuclear data, etc.… It was hence impossible to use the standard evaluation method based on pure statistical methods.
- In practice, the evaluation contains several steps. Collection, if needed correction, and selection of published experimental data sets by an experimentalist. Fitting of the selected data by an expert on model calculation and data evaluation. During this step further deselection occurred of a few separate data, very outlying when compared to the other selected sets, the theoretical predictions and reaction thresholds.
- Problematic cases occur when only a few (two or three) experimental data sets are available with contradicting results. In this case, to fill the energy range where only one data set was available, selection, correction, and normalization were done based on many facts: on the earlier results of the authors, the used experimental techniques, etc.
- For α-particle induced reactions in several cases the data from some publications are lower by a factor of two. We observed this fact earlier while evaluating monitor reactions. Our experimental data show that the sets with too low cross sections result from an improper estimation of the number of incident α-particles (measured by the incoming charge) due to neglecting the double elementary charge of the α-particle.
- For a selection of the best production route by practical users, the most important information is the figures of the excitation function and the yield curves.
- For reactions where only a single experimental data set exists no Padé fit was performed. The selection and fitting may be undertaken only if at least two independent data sets are available.
- Differential yield data are used only if the yields are given from the threshold on and if the mentioned energy steps are small (depending on the behavior of the excitation function).
- For the selection of data sets earlier evaluations and the results of model calculations were taken into account. Critical factors for the selection between contradicting results are data quality and the experience of the experimental group.
- Fit of the selected experimental data was done using the Padé approach (approximant by rational function) [11–13].
- Statistical uncertainties in the fitted results were estimated via a least-squares method and, as discussed in the earlier evaluations [1, 3–6, 9]. As explicitly discussed in [1] and [3] after analyzing the complete set of then available data we concluded that realistic total uncertainties cannot be defined as less than 4% for each of the reactions. Therefore, an additional systematic uncertainty of 4% over the whole energy region has been included as part of each systematic uncertainty derived from statistical analyses.
- Calculation of so-called physical integral production yields [14] is based on the obtained recommended cross section data.
- We decided to include the 2017, 2019 and 2021 versions of the TENDL library to show the change and the improvement of the theoretical predictions by the evolution of the TALYS code.

Some other points on problems encountered during the evaluation process are:

- In a few problematic reactions different Padé fits were done, with the question of which to select: the one based strictly on experimental data or include theory and systematics.
- For practical production the shape of the excitation function and the tabulated yields are important. Hence no covariance calculations were done.
- According to our experience, the pure statistical evaluation methods only work well in cases where a large number of data sets with realistic uncertainties, detailed knowledge of the experiments, and the used nuclear data, are available.
- The reason for disagreement of different data sets lies essentially in:
- Estimation of number of incident particles (Faraday cup, beam stop, monitor in single energy point, monitor in all energy range, etc.).
- Quality of targets in case of different target preparation techniques.
- Technique of spectra measurement, distance, dead time, coincidence losses, corrections.
- Determination of incident energy and control of the energy degradation.
- Properties of the single foil, stacked foil, and rotating wheel irradiation technique.
- Direct measurement vs. after chemical separation.

List of evaluated nuclear reactions and the main decay data

An overview of the reactions evaluated in the present report is presented in Table 1. It contains the list of reactions, the number of available experimental data sets, the maximal energy of the available experimental data (selection and fit only in an energy range useful for practical production), the parameters of the final Padé fit and the number of available experimentally determined yield publications. The main decay data used in the evaluation of the reported radionuclides and the parameters showing their applicability in nuclear medicine are displayed in Table 2 and are available, with decay schemes, in [15].

Discussion of the evaluated nuclear reactions

Following a short comment on the therapeutic application and the decay scheme, subSects. "Production of 47Sc" to "198gAu production" include the figures of all experimental data compared to theoretical TENDL predictions, the selected data with Padé fits and statistical uncertainties. The yields for the evaluated reactions, calculated from recommended data derived from the Padé fit, are presented at the end of each subsection in one or two figures. The full reference list for all compiled reactions related to the production of the discussed therapeutic isotopes is at the end of the publication.

Production of ^{47}Sc

^{47}Sc is a promising β⁻-emitter for targeted radionuclide therapy that forms a theranostic pair with the positron emitters ^{44}Sc or ^{43}Sc. Moreover, it is a theranostic radionuclide as such, as its single dominant 159keV gamma line is suitable for imaging via single photon emission computed tomography (SPECT). It may be produced directly or through the decay of its parent, ^{47}Ca ($T_{1/2}$ = 4.54 d, 100% by β⁻). The decay scheme is available in [15] and decay data are displayed in Table 2.

Evaluated nuclear reactions for ^{47}Ca and ^{47}Sc formation

The ^{nat}V(p,x)^{47}Ca, ^{nat}V(p,x)^{47}Sc, ^{nat}V(d,x)^{47}Sc, ^{nat}V(d,x)^{47}Ca, ^{nat}Ti(p,x)^{47}Sc, ^{nat}Ti(p,x)^{47}Ca, ^{nat}Ti(d,x)^{47}Sc, ^{48}Ca(p,2n)^{47}Sc and ^{48}Ti(p,2p)^{47}Sc reactions were evaluated.

Information on the reactions for formation of ^{47}Ca is important for either limitation of impurity or considering a cumulative production, especially at higher particle energy.

^{nat}V(p,x)^{47}Ca Three data sets were found: Heinninger [16], Hontzeas [17] and Michel [18]. Corrections for outdated decay and monitor data were done. The Hontzeas 1963 [17] data, unrealistic too high, were deselected for fit.

All data, in comparison with TENDL theoretical predictions, are shown in Fig. 1. Selected data and Padé fit are in Fig. 2. The calculated yields, based on the recommended values from the Padé fit, are shown in Fig. 19. No experimental yield data were found in the literature.

^{nat}V(p,x)^{47}Sc Seven experimental data sets were found, published by Heininger [13], Hontzeas [14], Michel [19], Michel [18], Levkovskij [20], Pupillo [21] and Barbaro [22]. The cross sections are cumulative, measured after the complete decay of parent ^{47}Ca.

In Hontzeas [17], Michel [18] and Levkovskij [20] cross sections are reported for the ^{51}V(p,x)^{47}Sc reaction (^{51}V has 99.75% abundance in ^{nat}V). The Pupillo [21] and Barbaro [22] data were found to be identical (two separate reports on the same experiment). Only Barbaro [22] was considered further and was multiplied by a factor of 1.2. The outlying Heiniger [16] and Hontzeas [17] sets were deselected.

All data (with comparison to TENDL theoretical predictions) and Padé fitted selected data are shown in Figs. 3 and 4. The calculated yields, based on the recommended cross sections obtained from the fit, are shown in Fig. 20. Experimental yields were reported by Acerbi [23] and Dmitriev [24].

^{nat}V(d,x)^{47}Ca Qaim [25] and Tárkányi [26] reported cross section data for the ^{nat}V(d,x)^{47}Ca reaction. In Qaim [25] results are reported as ^{51}V(d,x)^{47}Ca. Both data sets were selected and are shown, in comparison with TENDL theoretical predictions, in Fig. 5 while the Padé fit is in Fig. 6. The calculated yields are shown in Fig. 19. No experimental yield data were found.

^{nat}V(d,x)^{47}Sc Three data sets were published: Sonzogni [27], Qaim [25], and Tárkányi [26]. In Qaim [25] and Sonzogni [27] cross sections for the ^{51}V(d,x) ^{47}Sc reaction (99.75% ^{51}V abundance in ^{nat}V) are reported. The data are cumulative as they were measured after the complete decay of the ^{47}Ca parent. All sets were selected for fitting. All data, in comparison with TENDL theoretical predictions, are presented in Fig. 7, while the Padé fit is in Fig. 8. The calculated yields are shown in Fig. 20. No experimental yield data were found.

^{nat}Ti(p,x)^{47}Ca Three data sets were found in the literature: Michel [18], Michel [28] and Neumann [29]. All sets were selected and fitted and are shown in Figs. 9 and 10. The calculated yields are shown in Fig. 19. No experimental yield values were found.

Table 1 List of reactions for the production of therapeutic radioisotopes

Isotope	Reaction	# Sets	E_{max} recom. (MeV)	Pade parameters	Experi-mental yield
^{47}Sc	^{nat}V(p,x)^{47}Ca	3	200	Pade 4, N = 22, χ^2 = 0.52	
	^{nat}V(p,x)^{47}Sc	8	200	Pade 16, N = 104, χ^2 = 1.22	2
	^{nat}V(d,x)^{47}Ca	2	90	Pade 8, N = 27, χ^2 = 0.66	
	^{nat}V(d,x)^{47}Sc	3	90	Pade 11, N = 62, χ^2 = 0.64	
	^{nat}Ti(p,x)^{47}Ca	3	200	Pade 10, N = 60, χ^2 = 0.66	
	^{nat}Ti(p,x)^{47}Sc	16	70	Pade 10, N = 60, χ^2 = 0.66	2
	^{nat}Ti(d,x)^{47}Sc	8	50	Pade 9, N = 220, χ^2 = 1.20	1
	^{48}Ca(p,2n)^{47}Sc	2	30	Pade 8, N = 228, χ^2 = 0.63	*2*
	^{48}Ti(p,2p)^{47}Sc	2	85	Pade 6, N = 26, χ^2 = 1.71	
^{58m}Co	^{58}Fe(p,n)^{58m}Co	2	17	Pade 8, N = 29, χ^2 = 0.70	
	^{55}Mn(α,n)^{58m}Co	3	30	Pade 5, N = 34, χ^2 = 2.14	
^{71}As	^{68}Zn(α,n)^{71}Ge	2	26	Pade 10, N = 33, χ^2 = 0.87	
	^{nat}Ga(α,xn)^{71}As	5	40	Pade 8, N = 64, χ^2 = 0.74	1
	^{nat}Ge(p,xn)^{71}As	5	100	Pade 17, N = 109, χ^2 = 2.70	1
	^{nat}Ge(d,xn)^{71}As	2	50	Pade 17, N = 36, χ^2 = 0.98	
	^{70}Ge(d,n)^{71}As	2	15	Pade 12, N = 14, χ^2 = 1.05	1
	^{72}Ge(p,2n)^{71}As	2	30	Pade 5, N = 25,χ^2 = 1.06	1
^{77}Br	^{77}Se(p,n)^{77}Br	5	30	Pade 9, N = 227, χ^2 = 1.11	3
	^{78}Se(p,2n)^{77}Br	2	65	Pade 9, N = 39, χ^2 = 1.25	2
	^{79}Br(p,3n)^{77}Kr	10	85	Pade 11, N = 83, χ^2 = 1.79	
	^{75}As(α,2n)^{77}Br	5	130	Pade 10, N = 113, χ^2 = 1.44	1
	^{nat}Kr(p,x)^{77}Br	2	100	Pade 18, N = 47, χ^2 = 1.23	
^{80m}Br	^{80}Se(p,n)^{80m}Br	5	30	Pade 9, N = 67, χ^2 = 1.74	1
	^{nat}Se(d,xn)^{80m}Br	2	50	Pade 11c, N = 25, χ^2 = 0.84	
	^{nat}Se(p,xn)^{80m}Br	5	50	Pade 14, N = 63, χ^2 = 2.05	
	^{80}Se(d,2n)^{80m}Br	2	25	Pade 8c, N = 11, χ^2 = 0.65	1
	^{nat}Se(α,x)^{80m}Br	2	50	Pade 6, N = 42, χ^2 = 0.94	
^{103}Pd	^{nat}Ag(p,x)^{103}Pd	2	100	Pade 13, N = 29, χ^2 = 1.43	
^{103}Ru	^{nat}Ru(p,x)^{103}Ru	2	35	Pade 7, N = 30, χ^2 = 1.54	
	^{nat}Ru(d,x)^{103}Ru	2	50	Pade 11, N = 32, χ^2 = 0.72	
	^{100}Mo(α,n)^{103}Ru	4	40	Pade 11, N = 45, χ^2 = 1.10	
^{105}Rh	^{104}Ru(d,n)^{105}Rh	2	50	Pade 7, N = 33, χ^2 = 0.85	
^{117m}Sn	^{114}Cd(α,n)^{117m}Sn	3	40	Pade 7, N = 23, χ^2 = 1.94	
	^{116}Cd(α,3n)^{117m}Sn	10	60	Pade 9, N = 81, χ^2 = 1.54	
	^{115}In(α,x)^{117m}Sn	5	140	Pade 12, N = 58, χ^2 = 1.85	1
	^{nat}Cd(α,xn)^{117m}Sn	7	50	Pade 17, N = 110, χ^2 = 3.36	2
	^{nat}Sb(p,x)^{117m}Sn	4	130	Pade 15, N = 31, χ^2 = 0.83	
^{119}Sb	^{119}Sn(p,n)^{119}Sb	4	18	Pade 15, N = 50, χ^2 = 0.61	
	^{nat}Sb(p,xn)^{119}Te	3	70	Pade 13, N = 54, χ^2 = 1.03	1
^{134}Ce	^{139}La(p,6n)^{134}Ce	3	90	Pade 6, N = 18, χ^2 = 1.67	
^{135}La	^{nat}Ba(p,xn)^{135}La	3	70	Pade 20c, N = 30, χ^2 = 1.48	1
^{149}Tb	^{nat}Gd(p,xn)^{149}Tb	3	140	Pade 10, N = 16, χ^2 = 1.48	
^{161}Tb	^{160}Gd(d,n)^{161}Tb	2	50	Pade 5, N = 32, χ^2 = 1.32	
^{165}Er	^{165}Ho(p,n)^{165}Er	2	40	Pade 11, N = 70, χ^2 = 0.92	1
	^{166}Er(p,2n)^{165}Tm	3	20	Pade 6, N = 10, χ^2 = 1.75	1
	^{165}Ho(d,2n)^{165}Er	3	45	Pade 9, N = 39, χ^2 = 1.62	
	^{nat}Er(p,xn)^{165}Tm	2	45	Pade 11, N = 30, χ^2 = 0.50	2
	^{nat}Er(d,xn)^{165}Tm	3	50	Pade 18, N = 60, χ^2 = 1.66	2
	^{166}Er(d,3n)^{165}Tm	2	20	Pade 5, N = 24, χ^2 = 1.22	2

Table 1 (continued)

Isotope	Reaction	# Sets	E_{max} recom. (MeV)	Pade parameters	Experimental yield
^{167}Tm	^{169}Tm(p,x)^{167}Tm	4	50	Pade 10c, N = 18, χ^2 = 1.05	
	^{169}Tm(d,x)^{167}Tm	3	50	Pade 10, N = 22, χ^2 = 0.86	
	^{nat}Er(d,xn)^{167}Tm	2	50	Pade 14, N = 47, χ^2 = 0.67	2
	^{nat}Er(p,xn)^{167}Tm	4	90	Pade 15, N = 55, χ^2 = 1.45	2
	^{167}Er(p,n)^{167}Tm	3	17	Pade 8, N = 17, χ^2 = 1.53	
	^{165}Ho(α,2n)^{167}Tm	11	60	Pade 9, N = 113, χ^2 = 2.26	1
^{197m}Hg	^{197}Au(p,n)^{197m}Hg	8	80	Pade 6, N = 195, χ^2 = 1.86	2
	^{197}Au(d,2n)^{197m}Hg	10	50	Pade 14, N = 95, χ^2 = 2.11	
^{197g}Hg	^{197}Au(p,n)^{197g}Hg	8	30	Pade 9, N = 58, χ^2 = 1.88	2
	^{197}Au(d,2n)^{197g}Hg	8	50	Pade 11, N = 45, χ^2 = 1.59	
^{198g}Au	^{198}Pt(p,n)^{198g}Au	5	40	Pade 8, N = 39, χ^2 = 0.91	
	^{198}Pt(d,2n)^{198g}Au	2	50	Pade 8, N = 70, χ^2 = 3.12	
^{230}Pa	^{232}Th(p,3n)^{230}Pa	13	200	Pade 13, N = 83, χ^2 = 1.86	1
	^{232}Th(d,4n)^{230}Pa	2	80	Pade 7, N = 23, χ^2 = 0.70	

^{nat}Ti(p,x)^{47}Sc A total of 15 data sets were found in literature: Michel [30], Michel [31], Michel [18], Fink [32], Brodzinski [33], Kopecky [34], Michel [28], Neumann [29], Zarie [35], Khandaker [36], Garrido [37], Parashari [38], Cervenak [39], Azzam [40], Voyles [41] and Liu [42].

Three low-energy data points of Khandaker [36] and 4 low-energy points of Azzam [40] were deselected as they are below the threshold of the ^{48}Ti(p,2p)^{47}Sc reaction. The Liu [42] set was deselected as values contradict other low energy data. Moreover, it is in disagreement with the shape of the excitation function of the ^{48}Ti(p,2p)^{47}Sc reaction (see Sect. 4.1.8). The Fink [32] and Brodzinski [33] data above 100 MeV were not used. All available sets, in comparison with theoretical TENDL predictions, are shown in Fig. 11, and the selected data with Padé fit are in Fig. 12.

The calculated yields are shown in Fig. 20. Thick target yields were reported by Dmitriev [43] and Sabbioni [44].

^{nat}Ti(d,x)^{47}Sc Eight experimental data sets were found in literature: Takács [45], Hermanne [46], Takács [47], Gagnon [48], Khandaker [49], Khandaker [50], Lebeda [51] and Duchemin [52] (Fig. 13). All data were selected and fitted (Fig. 14). The calculated yields are shown in Fig. 20. Experimental yield was reported by Dmitriev [43].

^{48}Ti(p,x)^{47}Sc Two experimental data sets, measured by Gadioli [53] and Levkovskij [54], are available in the literature and were selected. All experimental data, in comparison with the TENDL predictions, are shown in Fig. 15, and the Padé fit in Fig. 16. The calculated yield is in Fig. 20. No experimental yield data were found.

^{48}Ca(p,2n)^{47}Sc In the investigated energy range 3 data sets are available, published by Levenberg [55] (above 100 MeV), Carzaniga [56] and Sitarz [57] (Fig. 17). Sitarz [57] data were converted from differential yield measurements and were multiplied by a factor of 1.4 as was done when using other reactions of this publication in our evaluations. Still no reason was found for the systematic disagreement.

Selected data and Padé fit are shown in Fig. 18. The calculated integral yields are shown in Fig. 20. Thick target yields were measured by Dmitriev [43] and Misiak [58]. The Misiak [58] differential yield data cannot be converted to cross section because two reactions on ^{46}Ca and ^{48}Ca contribute to the production of ^{47}Sc.

Integral yields for ^{47}Ca and ^{47}Sc formation Integral yields of reactions related to the production of ^{47}Sc and parent ^{47}Ca are deduced from the recommended values obtained from Padé fittings and are shown in Figs. 19 and 20.

Production of ^{58m}Co

Being an Auger emitter ^{58m}Co ($T_{1/2}$ = 9.10 h, IT = 100%) forms a theranostic pair with ^{55}Co ($T_{1/2}$ = 17.53 h, β^+ = 77%) used in PET imaging. The decay schemes are available in NUDAT 3.0 [15] and decay data are displayed in Table 2.

Evaluated nuclear reactions for ^{58m}Co formation

The ^{58}Fe(p,n)^{58m}Co and ^{55}Mn(α,n)^{58m}Co reactions were evaluated.

Table 2 Decay data of investigated reaction products: ^{47}Sc, ^{47}Ca(^{47}Sc), ^{58m}Co, ^{71}As(^{71}Ge), ^{71}Ge, ^{77}Br, ^{77}Kr(^{77}Br), ^{80m}Br, ^{103}Pd, ^{103}Pd(^{103m}Rh), ^{103}Ru(^{103m}Rh), ^{105}Rh, ^{117m}Sn, ^{119}Sb, ^{119m}Te(^{119}Sb), ^{134}Ce, ^{135}La, ^{149g}Tb, ^{161}Tb, ^{165}Er, ^{165}Tm(^{165}Er), ^{167}Tm, ^{197m}Hg, ^{197g}Hg, ^{198g}Au, ^{230}Pa

Product (Elevel) (keV)	Half-life and decay (%)	Main gamma-lines E_γ (keV), I_γ (%)	$E_{\alpha,max}$ (keV)	$E_{\beta-,mean}$ $E_{\beta+,mean}$ (keV)	Main electrons E_e (keV), I_e (%) Auger, Conversion(CE)
^{47}Sc	3.3492 d β^-: 100%	159.381 (68.3)		162.0	
^{47}Ca	4.536 d β^-: 100%	489.23 (5.9) 807.86 (5.9) 1297.09 (67)		4.0E+2	
^{58m}Co (24.889)	9.10 h IT: 100%	24.889 (0.0397) XR kα1 6.93 (16.1)			Auger L 0.75 (126.1) Auger K6.07 (44.7)
^{71}As	65.30 h ε: 100% β^+: 28.3%	174.954 (82.4)			
^{71}Ge	11.43 d ε: 100%				Auger L 1.1 (122) Auger K 8.04 (42.3)
^{77}Br	57.04 h ε: 100% β^+ 0.73%	238.98 (23.1) 249.77 (2.98) 297.23 (4.16) 520.69 (22.4)			Auger L 1.32 (114.8) Auger K 9.67 (35.3)
^{80m}Br	4.4205 h IT: 100%				Auger L 1.32 (173.1) Auger K 9.67 (46.9)
^{103}Pd	16.991d, ε: 100% to ^{103m}Rh	39.748 (0.0683) 357.45 (0.0221)			
^{103}Ru	4.439 h β^-: 100%	262.828 (6.93) 316.496 (11.04) 469.347 (18.31) 676.355 (15.82) 724.211 (47.8)		406	
^{103m}Rh (39.75)	56.114 min IT: 100%	39.75			CE L 36.343 (70), CE M 39.128 (14.3) Auger L 2.39 (75.5) Auger K 17.0 (1.77)
^{105}Rh	35.341 h β^-: 100%	306.311 (4.66) 319.231 (16.9)		154.9	
^{117m}Sn (314.58)	14.00 d IT: 100%	156.02 (2.113) 158.56 (86.4)			Auger L 2.95 (92.8) Auger K21.0 (10.8) CE K 126.82 (65.7) CE K 129.360 (11.65) CE L 151.56 (26.5)
^{119}Sb	38.19 h ε: 100%				Auger L2.95 (147.1) Auger K 21.0 (11.9) CE L 19.405 (67.5) CE M 22.986 (13.3)
^{119}Te	16.05 h ε: 100%	644.01 (84.1) 699.85 (10.1)			Auger L 3.8 (77.0) Auger K 27.4 (7.9)
^{134}Ce	3.16 d ε: 100%	130.414 (0.209) 162.306 (0.230)			
^{134}La	6.45 m ε: 100% β^+: 63.6%			1217	
^{135}La	19.5 h ε: 100% β^+: 0.007%	XR kα2 31.817 (21.7) XR kα1 32.194 (39.6)			Auger L 3.67 (77.6) Auger K 26.4 (8.5)
^{149}Tb	4.118 h ε: 83.3% α: 16.70%	164.98 (26.7) 352.24 (29.8) 388.87 (18.6) 652.12 (16.5) 853.43 (15.7)	3967	720	Auger L 4.84 (64) Auger K 34.9 (5.2)

Table 2 (continued)

Product (Elevel) (keV)	Half-life and decay (%)	Main gamma-lines E_γ (keV), I_γ (%)	$E_{\alpha,max}$ (keV)	$E_{\beta-,mean}$ $E_{\beta+,mean}$ (keV)	Main electrons E_e (keV), I_e (%) Auger, Conversion(CE)
^{161}Tb	6.89 d β^-: 100%	74.56669 6 (10.2)		154	
^{165}Er	10.36 h ε: 100%	XR l 6.72 (17.0) XR kα2 46.7 (21.5) XR kα1 47.547 (37.9)			Auger L5.33 (65.6) Auger K 38.4 (4.8)
^{165}Tm	30.06 h ε: 100% β^+: 0.0055%	242.917 (35.5) 297.369 (12.7)			
^{167}Tm	9.25 d ε: 100%	207.801 (42)			Auger L 5.5 (114) Auger K 39.7 (5.8)
^{197m}Hg (298.93)	23.8 h IT: 91.4% EC:8.6%	133.98 (33.5)			Auger L 7.6 (71.4) Auger K 53.8 (1.30) CE K 50.88 (14.095) CE K 81.87 (20.16) CE L 119.14 (32.643) CE M 130.42 (8.47) CE L 150.13 (50.242) CE M 161.41 (15.473)
^{197g}Hg	64.81 h EC:100%	77.351 (18.7) 191.437 (0.632)			Auger L 7.4 (119) CE 64. (70)
^{198g}Au	2.6941 d β^- 100%	411.80205 (95.62)		312.5	Auger L 7.6 (2.17) Auger K 53.8 (0.11)
^{230}Pa	17.4 d α: 0.0032% ε: 92.2%	443.74 (5.8) 508.15 (4.10) 51.88 (29.6)	^{230}U5888.4		

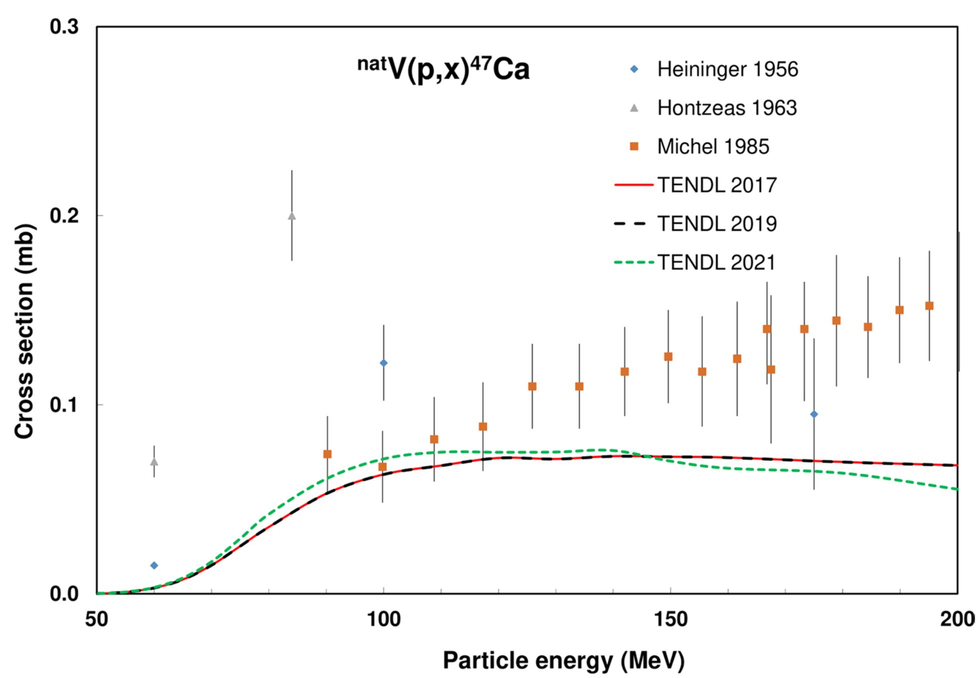

Fig. 1 $^{nat}V(p,x)^{47}Ca$ reaction: all experimental data and the TENDL theoretical excitation functions

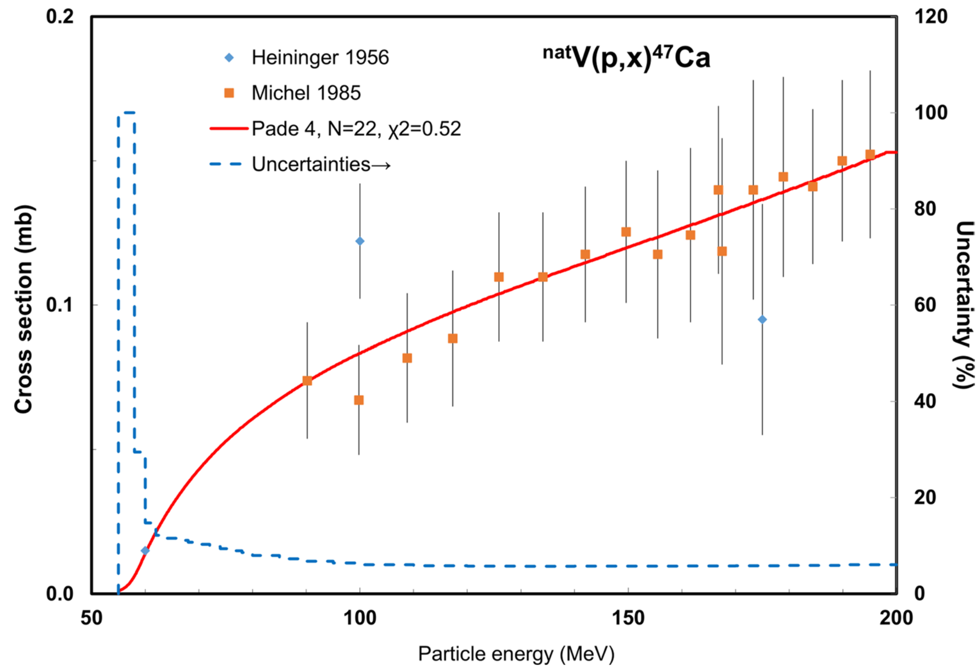

Fig. 2 $^{nat}V(p,x)^{47}Ca$ reaction: selected experimental works and Padé fit (solid line) with total derived uncertainties, including 4% systematic uncertainty (dashed line, right-hand scale)

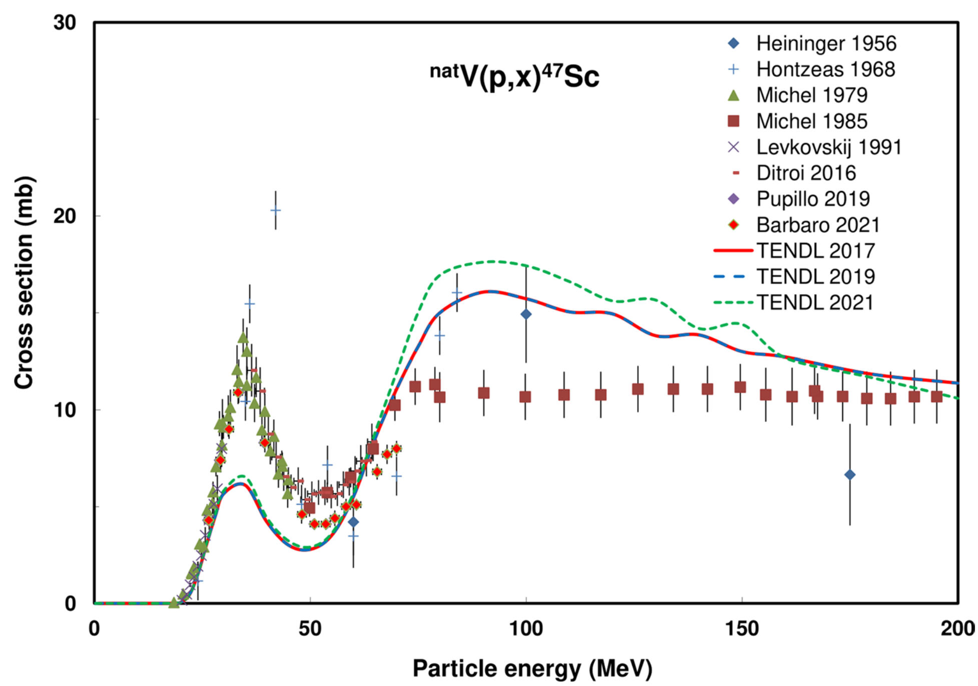

Fig. 3 $^{nat}V(p,x)^{47}Sc$ reaction: all experimental data and the TENDL theoretical excitation functions

$^{58}Fe(p,n)^{58m}Co$ Two experimental data sets exist, reported by Zarubin [59] and Sudar [60] and were selected. The experimental data, in comparison with the theoretical predictions, are shown in Fig. 21, the selected data with Padé fit in Fig. 22 and the calculated physical yield in Fig. 25. No experimental yield data were found.

$^{55}Mn(\alpha,n)^{58m}Co$ Matsuo [61], Long Xianguan [62] and Sudar [60] presented experimental cross section data (Fig. 23). All data were selected and fitted (Fig. 24). The calculated physical yields are shown in Fig. 25. No experimental yield data were found.

Integral yields for ^{58m}Co formation Integral yields of reactions related to the production of.^{58m}Co are deduced from the recommended values obtained from Padé fittings and are shown in Fig. 25

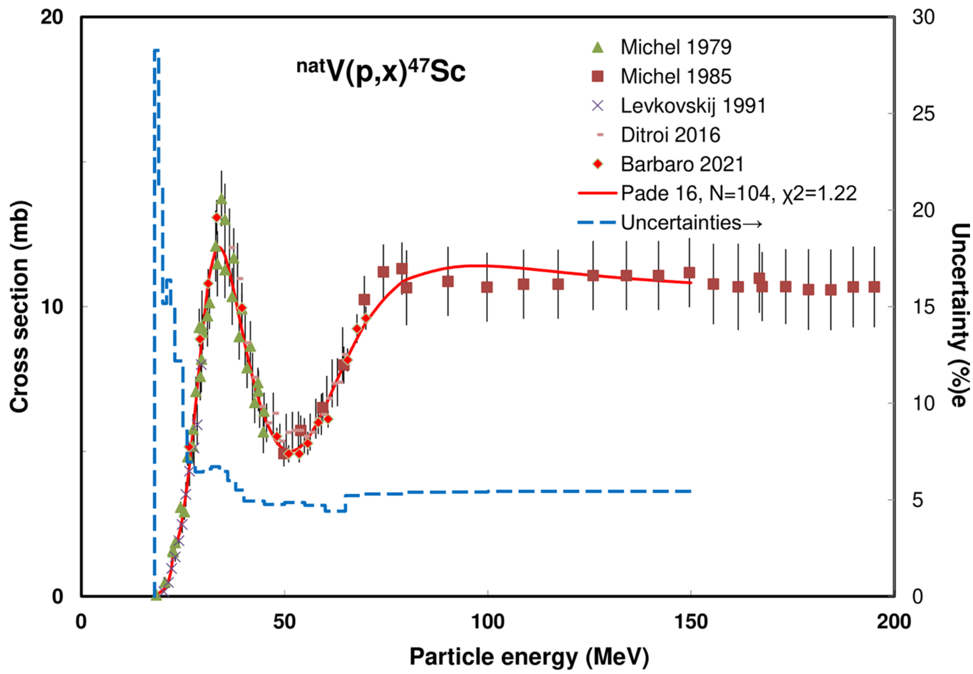

Fig. 4 $^{nat}V(p,x)^{47}Sc$ reaction: selected experimental works and Padé fit (solid line) with total derived uncertainties, including 4% systematic uncertainty (dashed line, right-hand scale)

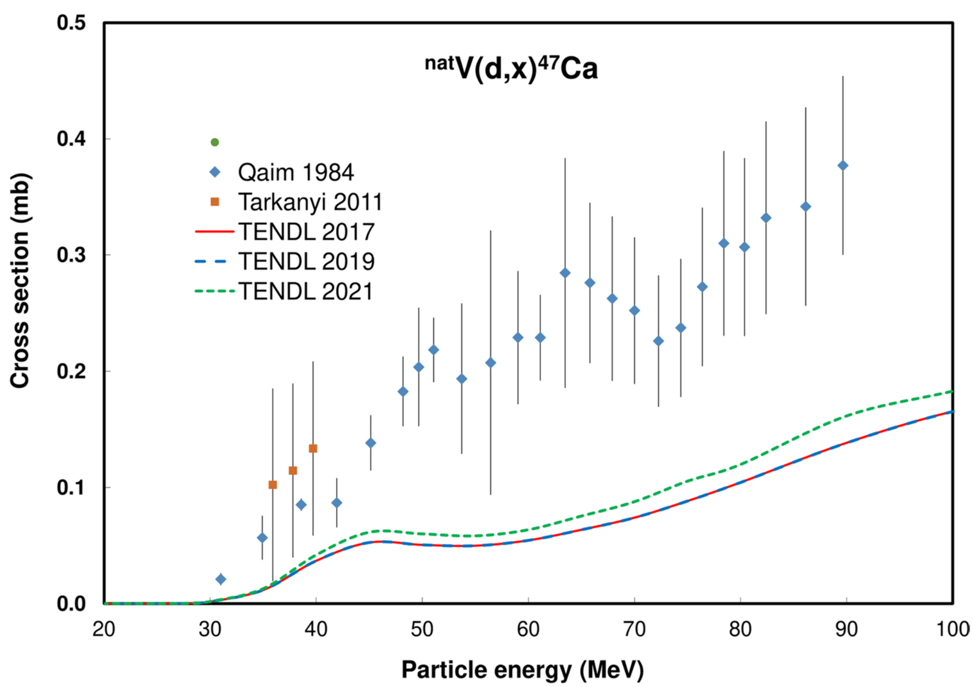

Fig. 5 $^{nat}V(d,x)^{47}Ca$ reaction: all experimental data and the TENDL theoretical excitation functions

^{71}Ge production

The ^{71}Ge ($T_{1/2} = 11.43$ d) decays by pure electron capture (EC) with subsequent Auger electron emission, making it a potential therapeutic isotope. It forms a theranostic pair with the attractive PET isotope ^{69}Ge ($T_{1/2} = 39$ h, 21% β^+, $E_{max} = 1205$ keV). ^{71}Ge can be produced directly and through the decay of the shorter-lived ^{71}As parent isotope ($T_{1/2} = 65.28$ h). The decay schemes are available in [15] and decay data are displayed in Table 2.

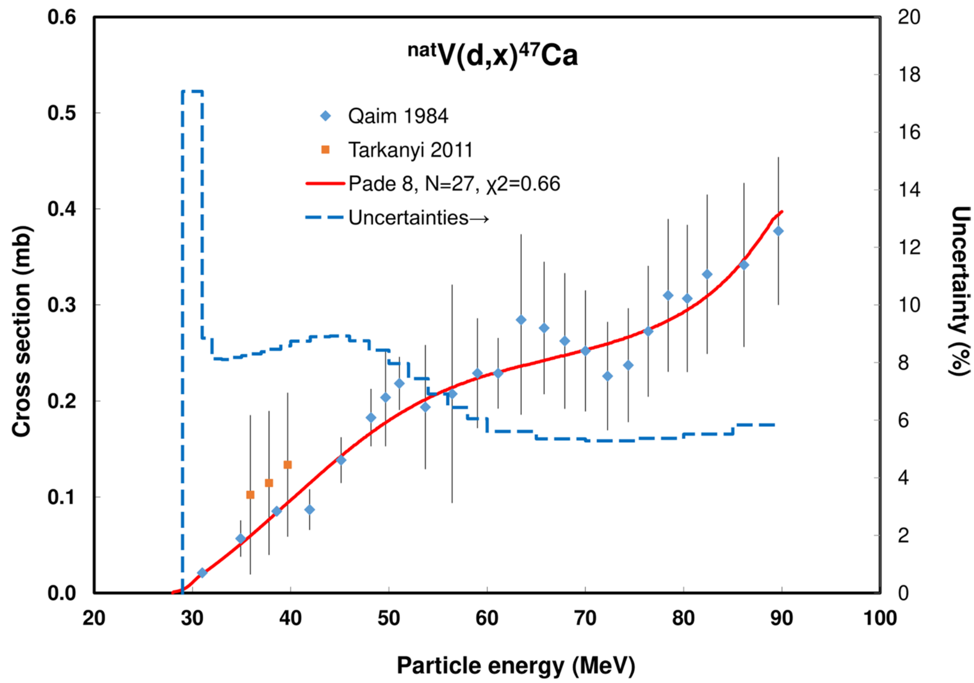

Fig. 6 $^{nat}V(d,x)^{47}Ca$ reaction: selected experimental works and Padé fit (solid line) with total derived uncertainties, including 4% systematic uncertainty (dashed line, right-hand scale)

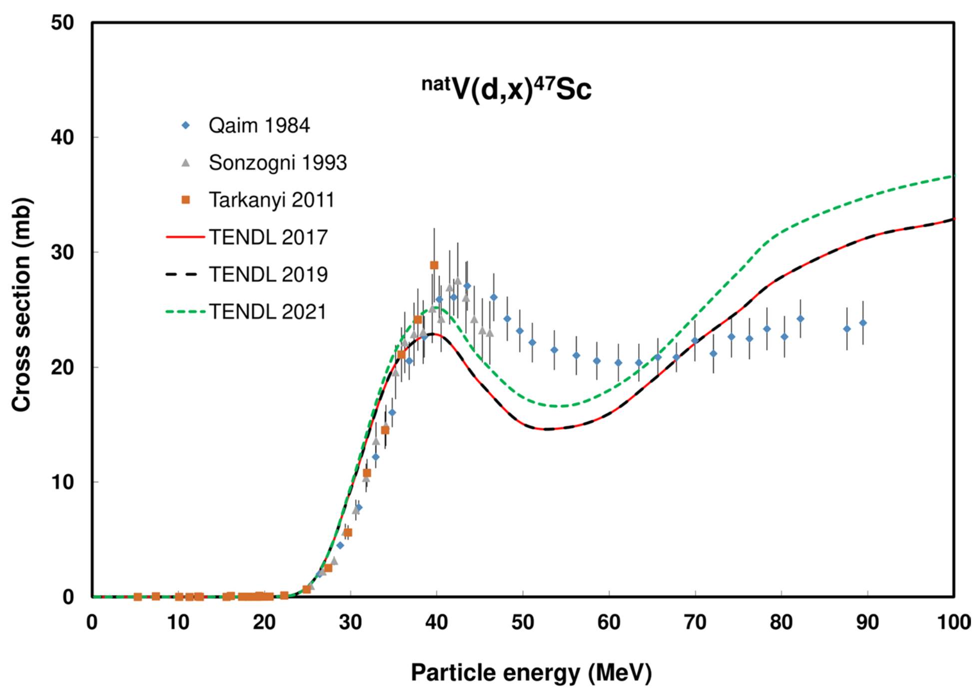

Fig. 7 $^{nat}V(d,x)^{47}Sc$ reaction: all experimental data and the TENDL theoretical excitation functions

Evaluated nuclear reactions for ^{71}As and ^{71}Ge formation

The $^{68}Zn(\alpha,n)^{71}Ge$, $^{nat}Ga(\alpha,x)^{71}As$, $^{nat}Ge(p,xn)^{71}As$, $^{nat}Ge(d,x)^{71}As$, $^{70}Ge(d,n)^{71}As$ and $^{72}Ge(p,2n)^{71}As$ reactions were evaluated.

$^{68}Zn(\alpha,n)$ ^{71}Ge Two data sets were found, published by Stelson [63] and Antropov [64]. Antropov [64] data were energy shifted to correspond better with the TENDL predictions and the highest energy point at 24.2 MeV was deleted. The experimental data, with comparison to the TENDL predictions, are shown in Fig. 26 and the Padé fit on the selected data is displayed in Fig. 27. The calculated integral yield is shown in Fig. 39. No experimental yield was found.

$^{nat}Ga(\alpha,x)^{71}As$ A total of 5 data sets were found in literature: Rizvi 1989 (results on ^{nat}Ga and ^{69}Ga targets) [65], Ismail [66], Levkovskij [54] and Didik [67]. The Rizvi [65] data

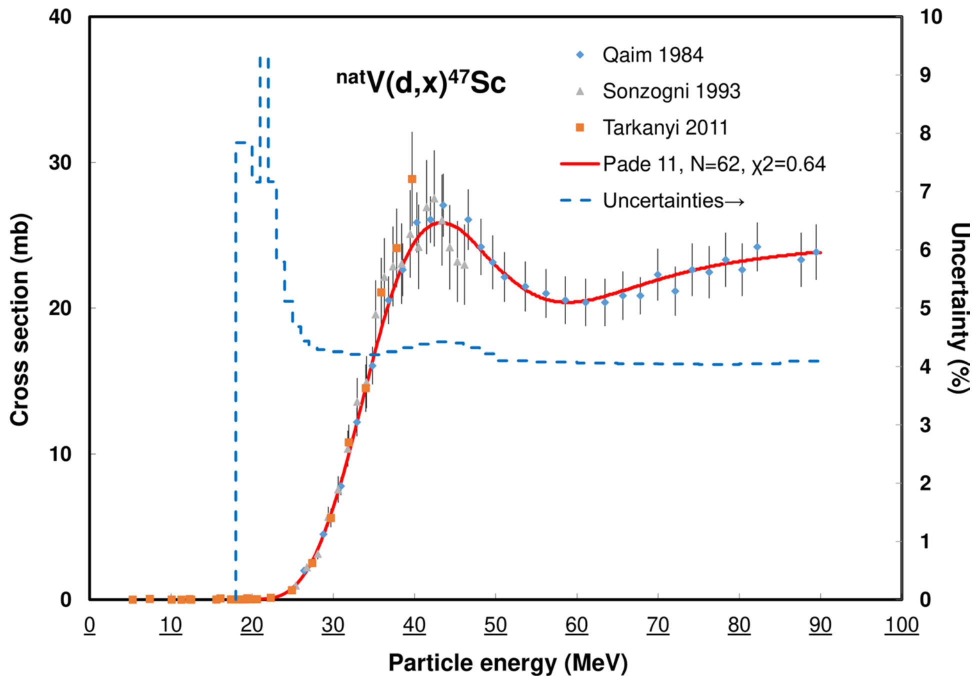

Fig. 8 $^{nat}V(d,x)^{47}Sc$ reaction: selected experimental works and Padé fit (solid line) with total derived uncertainties, including 4% systematic uncertainty (dashed line, right-hand scale)

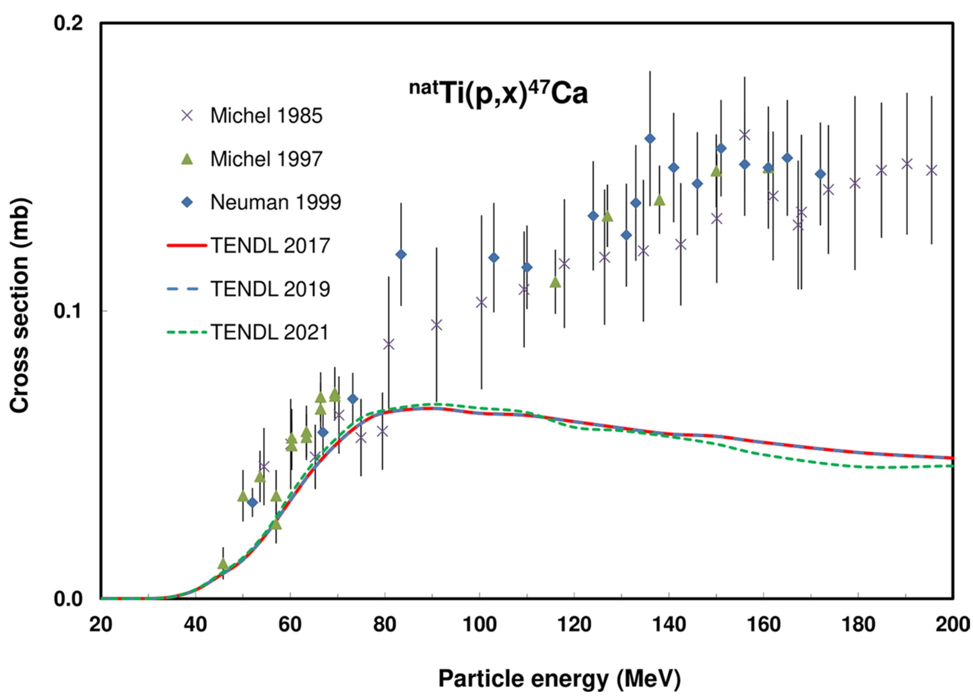

Fig. 9 $^{nat}Ti(p,x)^{47}Ca$ reaction: all experimental data and the TENDL theoretical excitation functions

on natural targets were deleted for the following reasons. According to the publication, ^{nat}Ga targets were used but results for $^{69}Ga(\alpha,2n)$ $^{71}As + ^{71}Ga(\alpha,4n)$ ^{71}As cross sections were presented, which is not identical to $^{nat}Ga(\alpha,xn)$. No information is given how the (α,4n) data were obtained. In addition, the first two points of normalized values of Rizvi [62] obtained on ^{69}Ga targets were deleted.

All data, in comparison with TENDL predictions, are shown in Fig. 28, Padé fitted selected data in Fig. 29, and calculated integral yields in Fig. 38. Experimental yield data were reported by Dmitriev [43].

$^{nat}Ge(p,xn)^{71}As$ A total of five data sets were found in the literature: Basile [68], Horiguchi [69], Levkovskij [54],

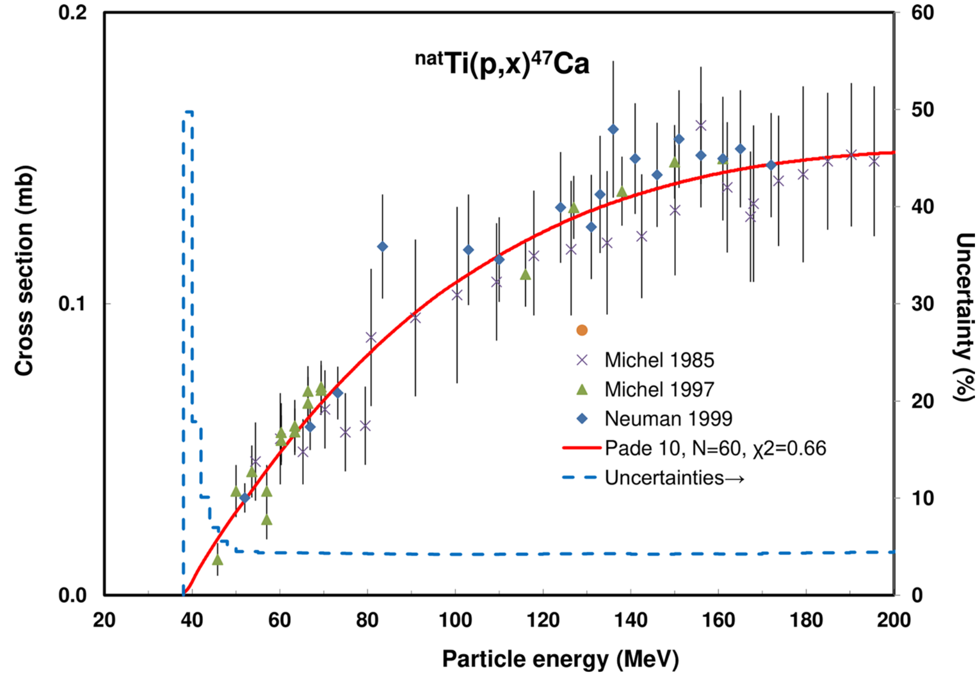

Fig. 10 $^{nat}Ti(p,x)^{47}Ca$ reaction: selected experimental works and Padé fit (solid line) with total derived uncertainties, including 4% systematic uncertainty (dashed line, right-hand scale)

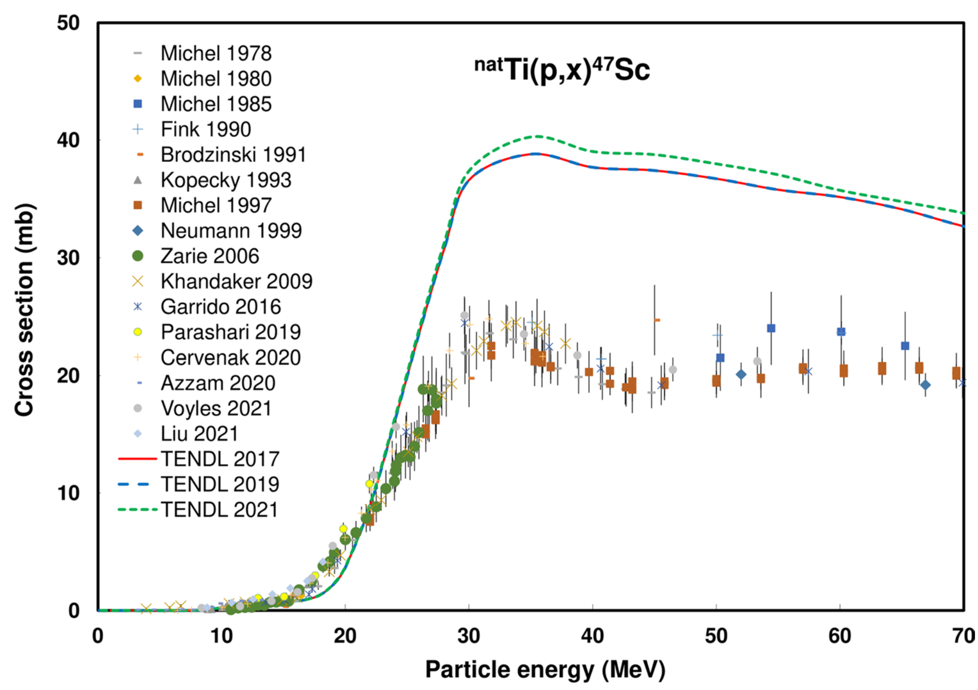

Fig. 11 $^{nat}Ti(p,x)^{47}Sc$ reaction. All experimental data and the TENDL theoretical excitation functions

Spahn [70] and Barabanov [71]. All data were selected. All data, compared to the theoretical predictions, are shown in Fig. 30 while the Padé fit is seen in Fig. 31. The calculated yields are shown in Fig. 38. Dmitriev [43] reported experimental yield data.

$^{nat}Ge(d,x)^{71}As$ For the $^{nat}Ge(d,x)^{71}As$ reaction two experimental data sets exist: Otozai [72] and Takács [73]. Both sets were selected but the uncertainties of the Otozai [72] data at energies above 10 MeV were enlarged.

The experimental data, compared to the TENDL predictions, are shown in Fig. 32, the Padé fit on selected data in Fig. 33, and the calculated integral yield in Fig. 38. An

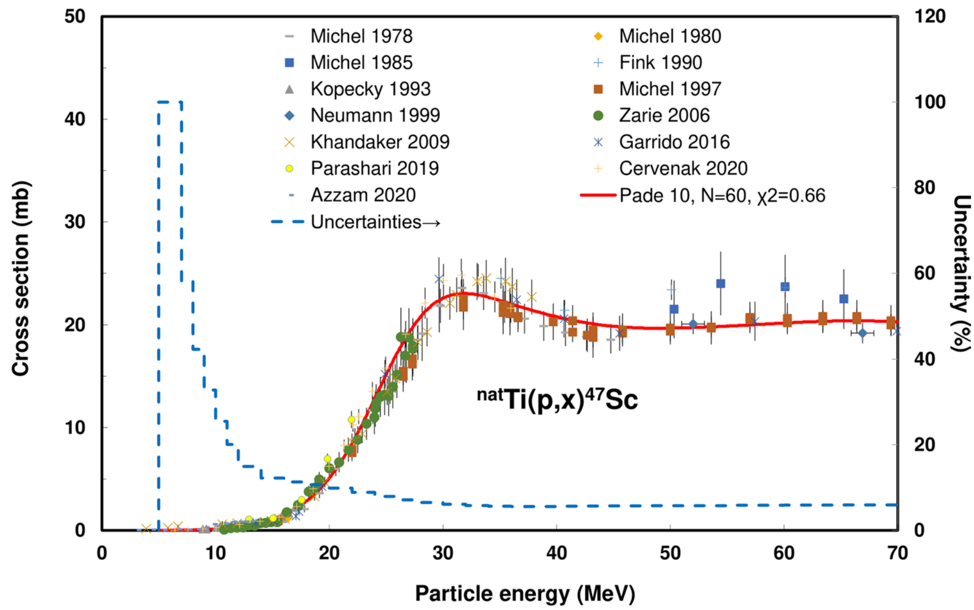

Fig. 12 $^{nat}Ti(p,x)^{47}Sc$ reaction: selected experimental works and Padé fit (solid line) with total derived uncertainties, including 4% systematic uncertainty (dashed line, right-hand scale)

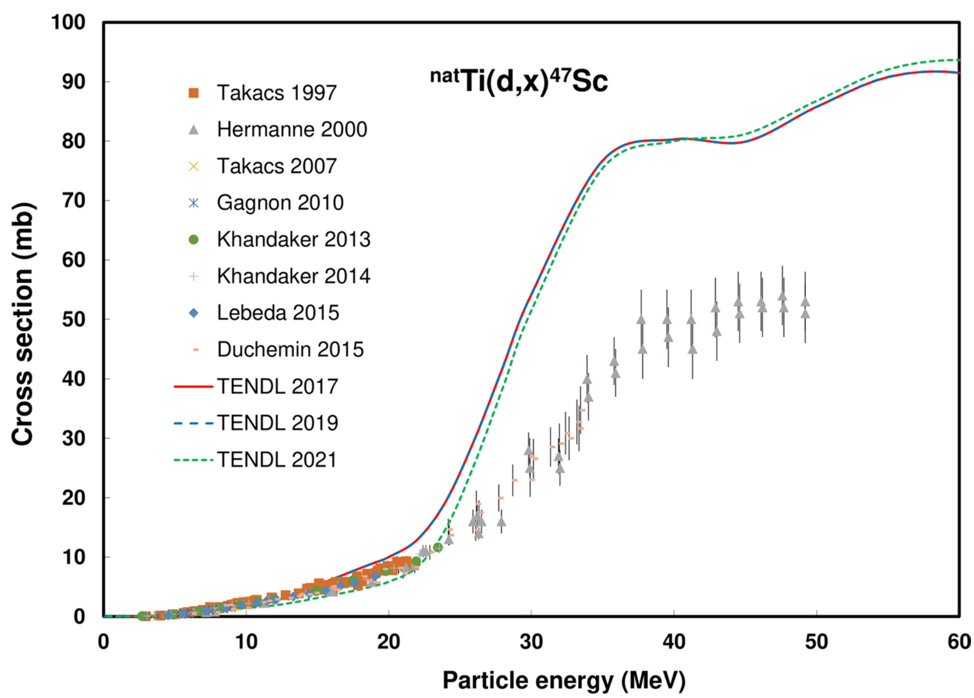

Fig. 13 $^{nat}Ti(d,x)^{47}Sc$ reaction: all experimental data and the TENDL theoretical excitation functions

experimental yield at 22 MeV was reported by Dmitriev [24].

$^{70}Ge(d,n)^{71}As$ Two data sets were published: Otozai [72] and Takács [73] and were selected. The experimental and TENDL theoretical predictions are shown in Fig. 34, and the selected data with the Padé fit in Fig. 35. The calculated physical yields are shown in Fig. 38. No experimental yield data were found.

$^{72}Ge(p,2n)^{71}As$ Three data sets were found in the investigated energy range: Basile [68], Levkovskij [54] and Spahn [74]. All data sets were selected. The uncertainty on Basile's [68] data was enlarged. The experimental data, the theoretical TENDL predictions and the Padé fit are shown in Figs. 36 and 37. The calculated integral yields are presented in Fig. 38.

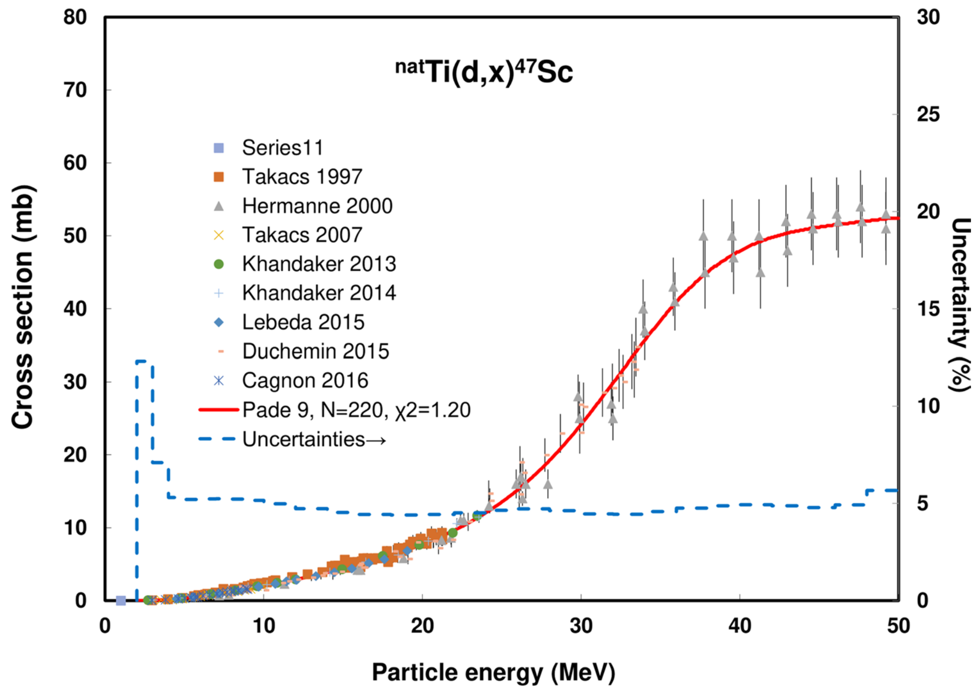

Fig. 14 $^{nat}Ti(d,x)^{47}Sc$ reaction: selected experimental works and Padé fit (solid line) with total derived uncertainties, including 4% systematic uncertainty (dashed line, right-hand scale)

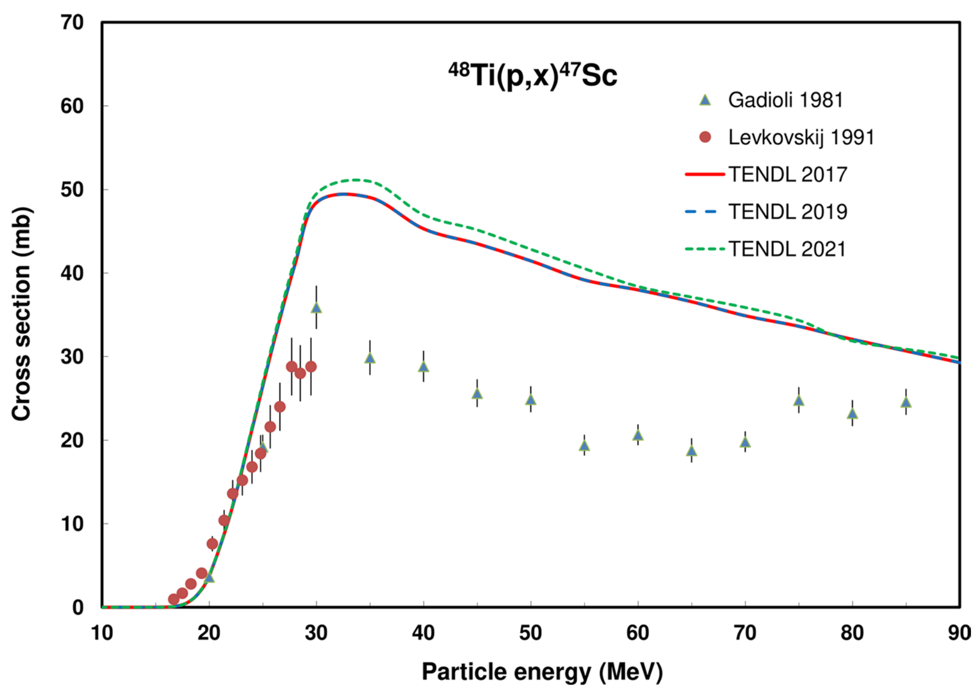

Fig. 15 $^{48}Ti(p,x)^{47}Sc$ reaction: all experimental data and the TENDL theoretical excitation functions

Integral yields for ^{71}As and ^{71}Ge formation Integral yields of reactions related to the production of ^{71}As and parent.^{71}Ge are deduced from the recommended values obtained from Padé fittings and are shown in Figs. 38 and 39

Production of ^{77}Br

The radioisotope ^{77}Br, decaying by electron capture with a half-life of 57 h, can be used in Auger therapy and the emission of a 239 keV γ-line allows imaging by SPECT. It can be produced directly or through the decay of its ^{77}Kr parent isotope. The ^{77}Kr and ^{77}Br decay schemes are available in [15] and decay data are displayed in Table 2.

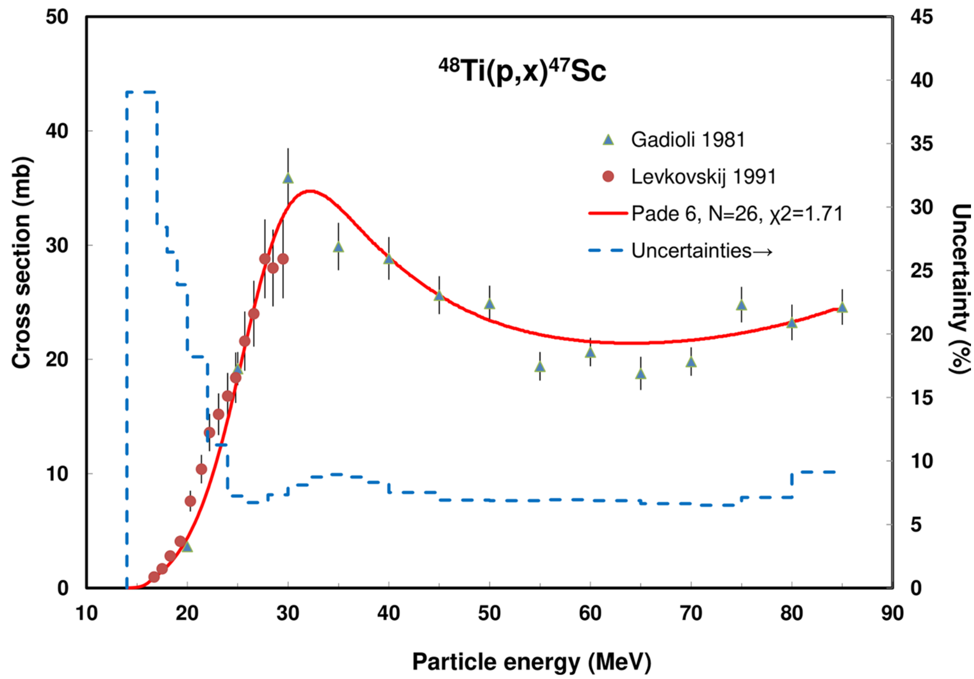

Fig. 16 ^{48}Ti(p,x)^{47}Sc reaction: selected experimental works and Padé fit (solid line) with total derived uncertainties, including 4% systematic uncertainty (dashed line, right-hand scale)

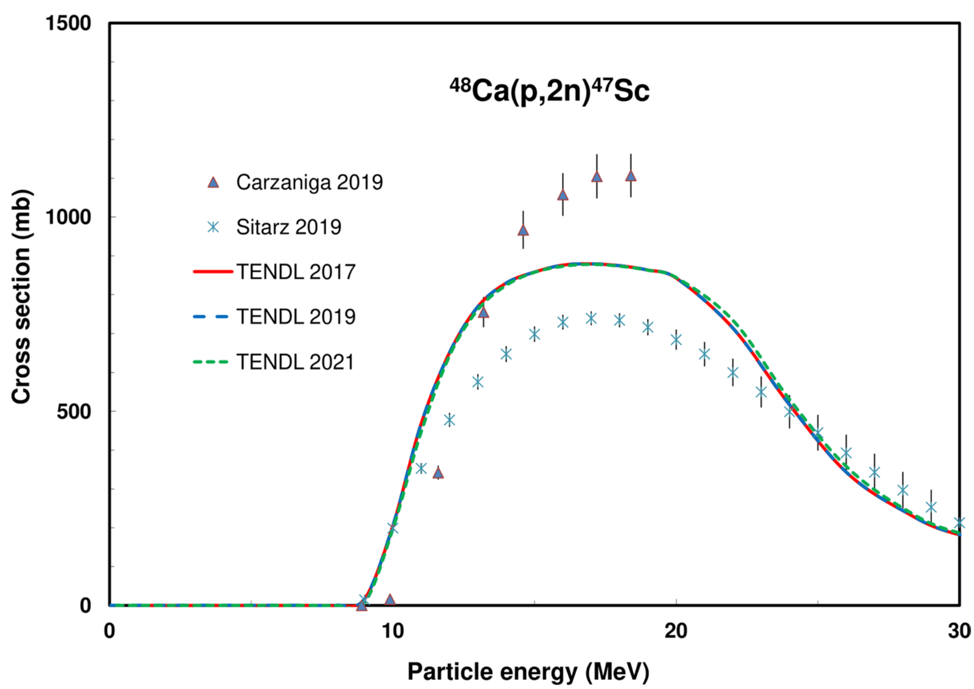

Fig. 17 ^{48}Ca(p,2n)^{47}Sc reaction: all experimental data and the TENDL theoretical excitation functions

Evaluated nuclear reactions for ^{77}Kr and ^{77}Br formation

The ^{77}Se(p,n)^{77}Br, ^{78}Se(p,2n)^{77}Br, ^{79}Br(p,xn)^{77}Kr, ^{75}As(α,2n)^{77}Br and ^{nat}Kr(p,x)^{77}Br reactions were evaluated. For each of the possibly interesting reactions ^{81}Br(p,x)^{77}Kr (E_{max} = 85 MeV), ^{nat}Se(d,x)^{77}Br (E_{max} = 21 MeV), ^{80}Kr(p,x)^{77}Br (E_{max} = 38.8) MeV) and ^{78}Se(α,2n)^{80m}Br (E_{max} = 46 MeV) only a single set of experimental data is available and no evaluation or fit was performed.

^{77}Se(p,n)^{77}Br Ten data sets were found in the literature: Johnson [75], Johnson [76], Johnson [77], Nozaki [78], Levkovskij [54], Gyurky [79], Hassan [80], El Azony [81],

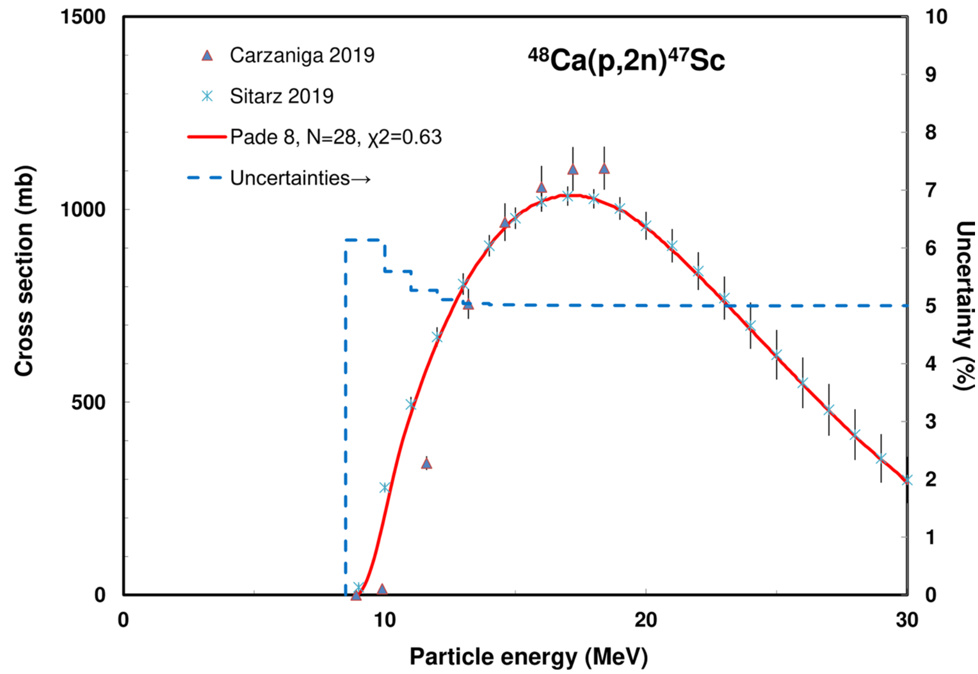

Fig. 18 ^{48}Ca(p,2n)^{47}Sc reaction: selected experimental works and Padé fit (solid line) with total derived uncertainties, including 4% systematic uncertainty (dashed line, right-hand scale)

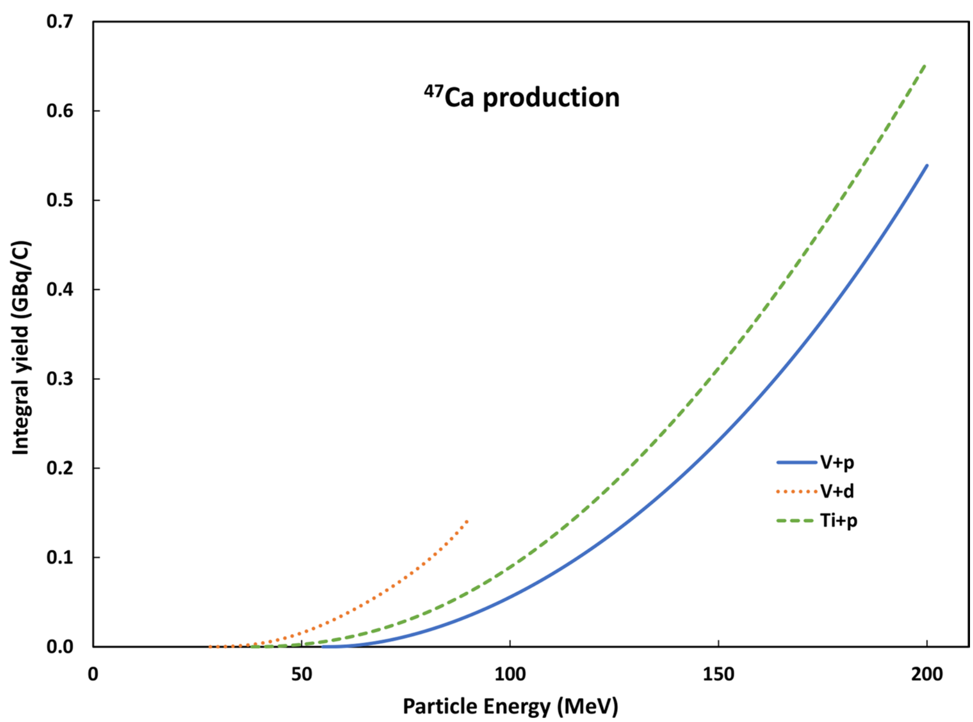

Fig. 19 Yield calculated from the recommended cross sections for ^{47}Ca production

Spahn [82] and Foteinou [83]. The three sets Johnson [75–77] were multiplied by a factor of 0.5 and the uncertainty was considered to be 17%. The 5 data points between 19 and 27 MeV of Hassan [80] were deselected (normalized from data on ^{nat}Se). The too low set by Foteinou [83] was deselected. All data sets and comparison with TENDL prediction are shown in Fig. 40, and the selected data with Padé fit in Fig. 41. The yields for production of ^{77}Br calculated from the fitted results are collected in Fig. 51. Experimental yield data were reported by Janssen [84], Dmitriev 1982 [85] and Nickles [86].

^{78}Se(p,2n)^{77}Br Two data sets were found: Levkovskij [54] and Spahn [82]. The five data points below 30 MeV of Spahn [82] were deselected, due to large disagreement. Data, theory and fit are presented in Figs. 42. and 43.

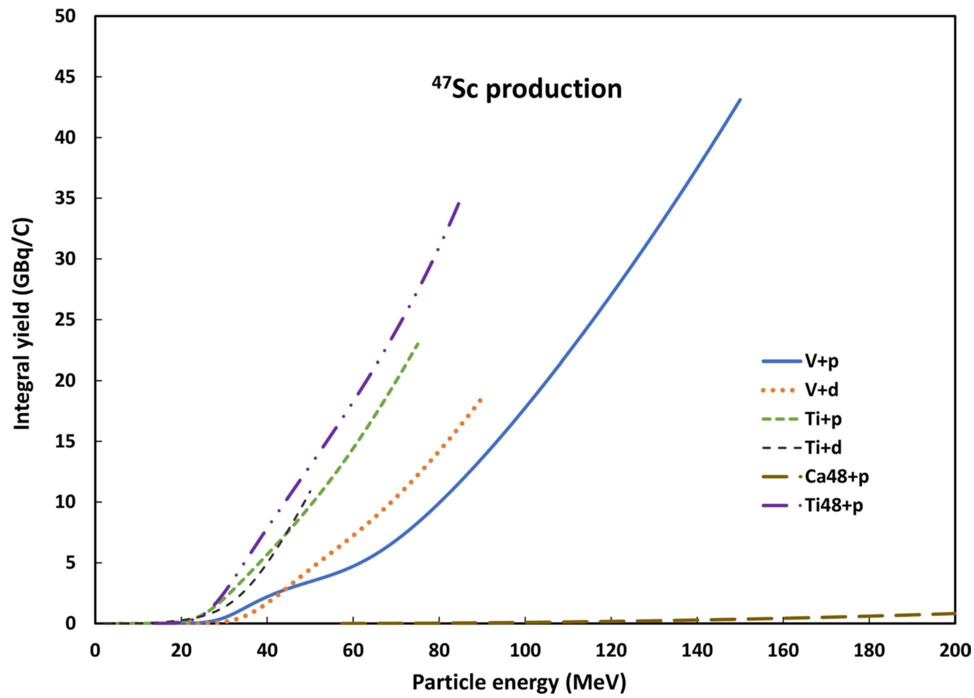

Fig. 20 Yield calculated from the recommended cross sections for ^{47}Sc production

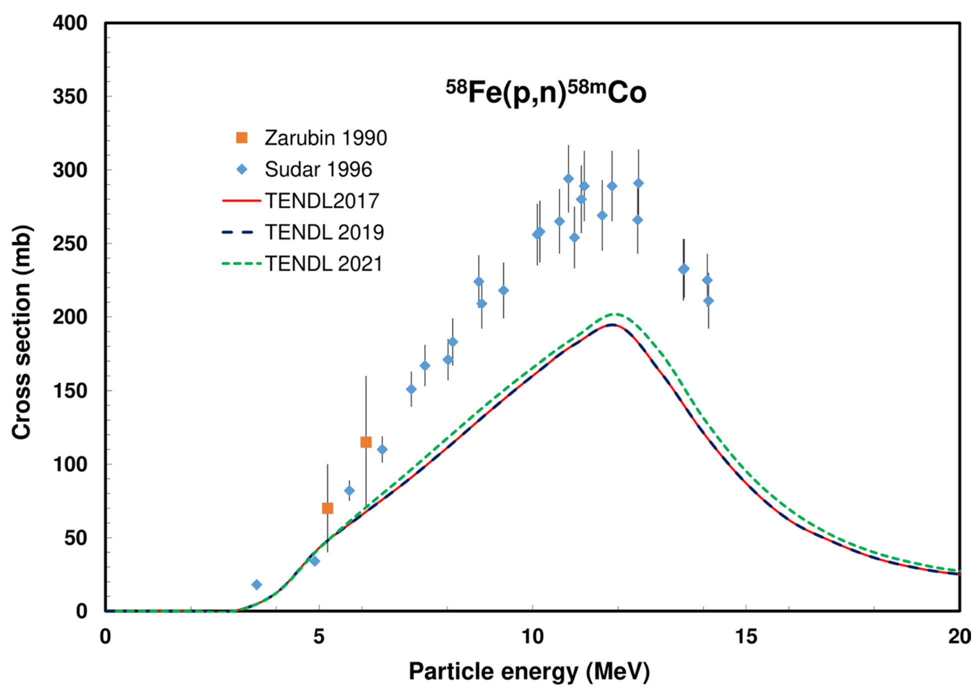

Fig. 21 ^{58}Fe(p,n)^{58m}Co reaction**:** all experimental data and the TENDL theoretical excitation functions

Calculated yields based on recommended fit results are presented in Fig. 51. Experimental yields are reported by Madhusudhan [87] and Janssen [84].

^{79}Br(p,3n)^{77}Kr Ten experimental data sets were found: Lundqvist [88], Diksic [89], Nozaki [78], De Jong [90], Weinreich [91], Sakamoto [92], Deptula [93], Levkovskij [54], Zaitseva [94] and De Villiers [95]. Based on corrections already applied on cross sections for other reactions the Diksic [89] were normalized by a factor of 0.8. and the point at 30 MeV was deselected. The results of Nozaki [78] were normalized by a factor of 0.6. The De Jong [90] high energy data were deselected (above 52 MeV). An outlying point of Lundqvist [88] was not represented and

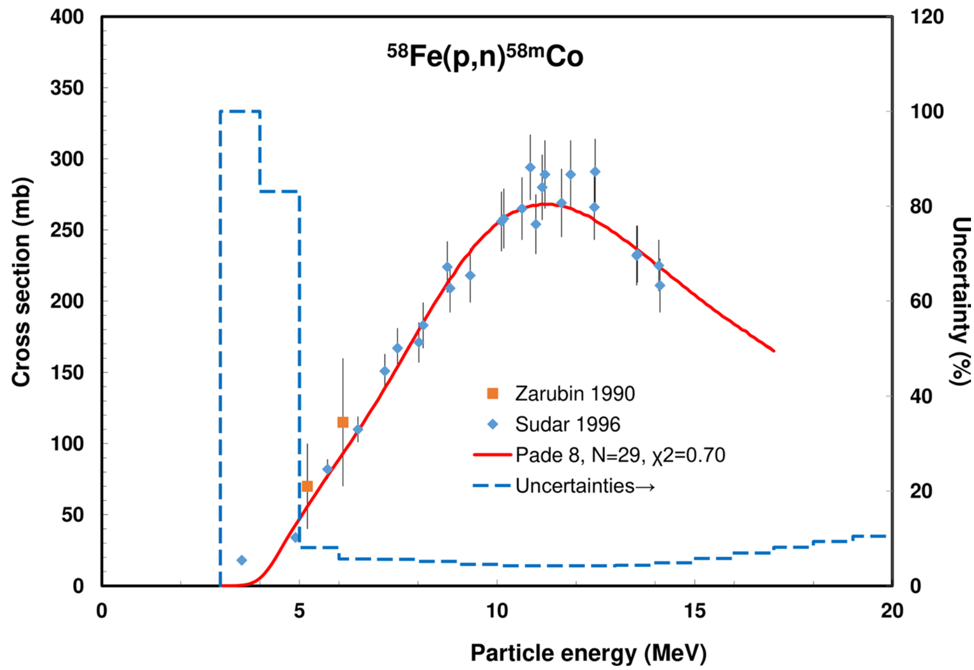

Fig. 22 ^{58}Fe(p,n)^{58m}Co reaction: selected experimental works and Padé fit (solid line) with total derived uncertainties, including 4% systematic uncertainty (dashed line, right-hand scale)

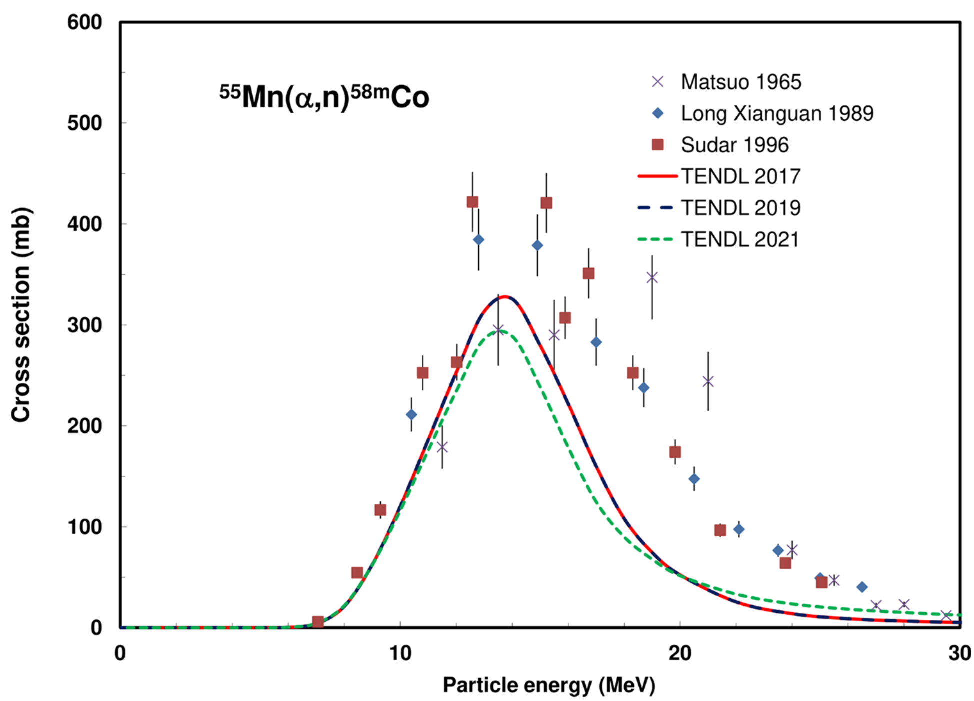

Fig. 23 ^{55}Mn(α,n)^{58m}Co reaction: all experimental data and the TENDL theoretical excitation functions

deselected (> 800mb). Results obtained by experiments on ^{nat}Br targets from 25 MeV on to below the threshold of ^{81}Br(p,5n) were normalized (Lundqvist [85], Nozaki [75], Weinreich [88], Deptula [90], Zaitseva [91], De Villiers [92].

The available data with TENDL predictions are shown in Fig. 44, and the fitted selected data in Fig. 45. The integral yields, calculated from the recommended cross sections obtained through Padé fitting, are shown in Fig. 50. No experimental yield data were found.

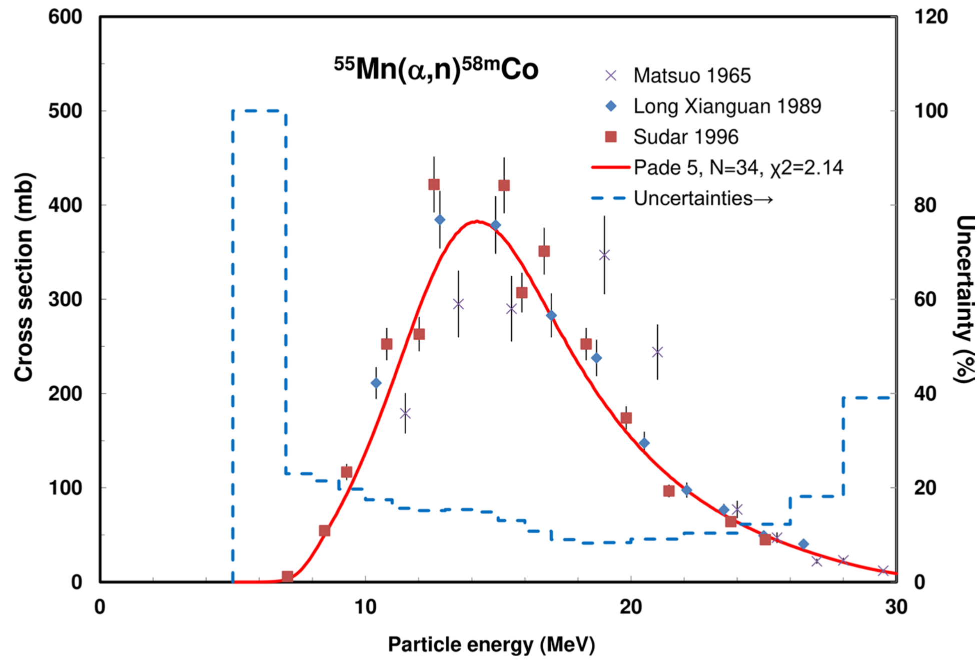

Fig. 24 ^{55}Mn(α,n)^{58m}Co reaction: selected experimental works and Padé fit (solid line) with total derived uncertainties, including 4% systematic uncertainty (dashed line, right-hand scale)

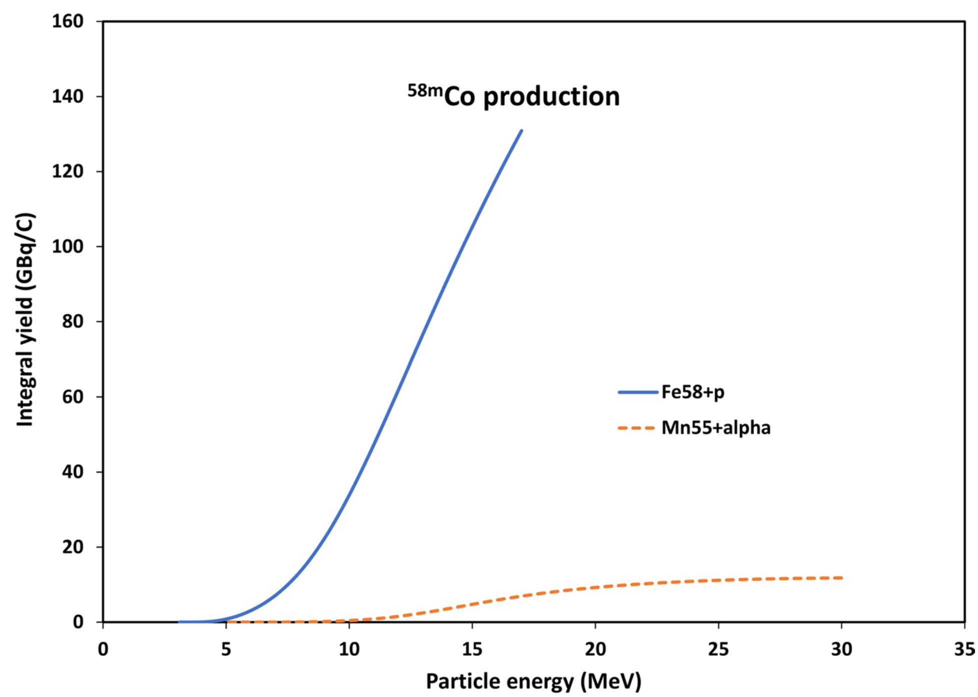

Fig. 25 Yield calculated from the recommended cross sections for ^{58m}Co production

^{75}As(α,2n)^{77}Br Five data sets are available in the literature: Waters [96], Nozaki [78], Alfassi [97], Qaim [98] and Breunig [99] (Fig. 46). All data were selected and fitted as shown in Fig. 47. Calculated yields are presented in Fig. 51. Experimental yield are reported by Dmitriev [85].

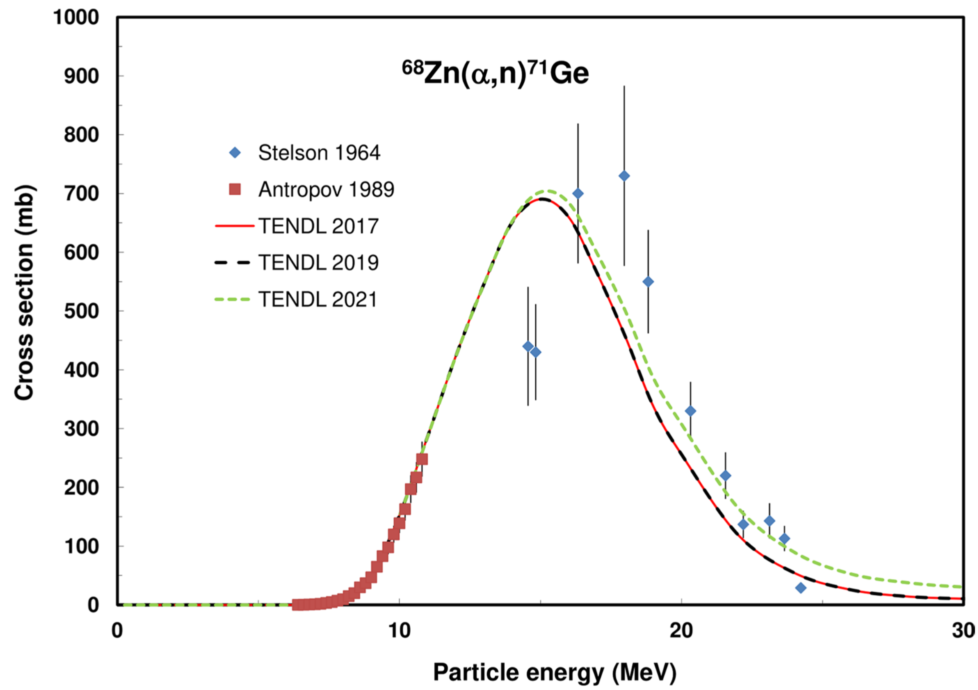

Fig. 26 ^{68}Zn(α,n)^{71}Ge reaction: all experimental data and the TENDL theoretical excitation functions

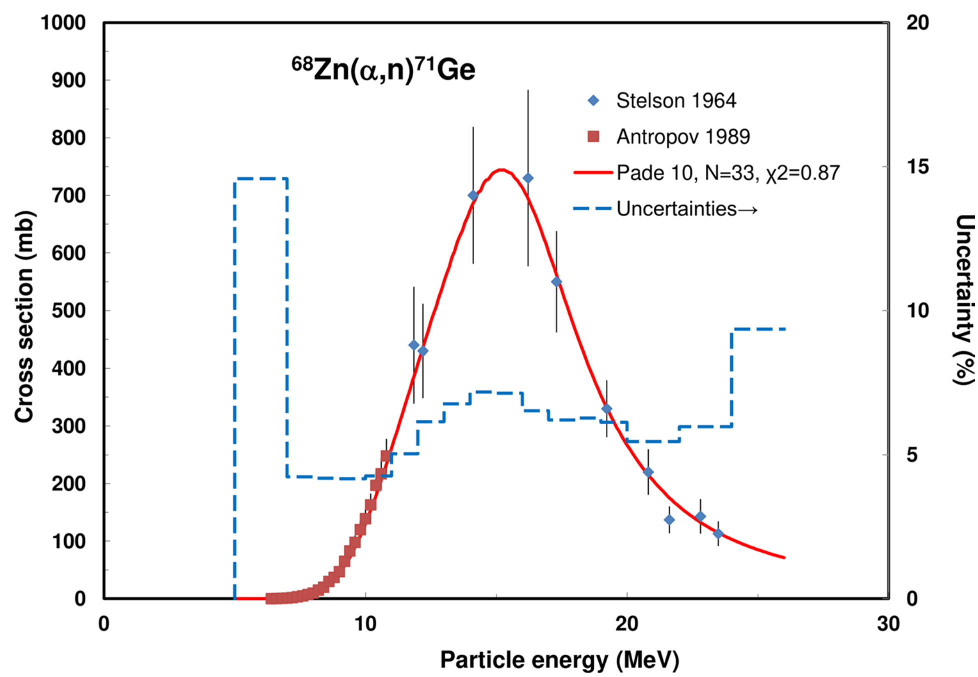

Fig. 27 ^{68}Zn(α,n)^{71}Ge reaction: selected experimental works and Padé fit (solid line) with total derived uncertainties, including 4% systematic uncertainty (dashed line, right-hand scale)

^{nat}Kr(p,x)^{77}Br Two data sets are available: Steyn [100] and Tárkányi [101]. Both data sets were selected. All data, theoretical TENDL predictions and the Padé fits are presented in Figs. 48 and 49, the calculated yield values in Fig. 51. No experimental yield data were found.

Integral yields for ^{77}Kr and ^{77}Br formation Integral yields of reactions related to the production of ^{77}Kr and ^{77}Br are deduced from the recommended values obtained from Padé fittings and are shown in Figs. 50 and 5

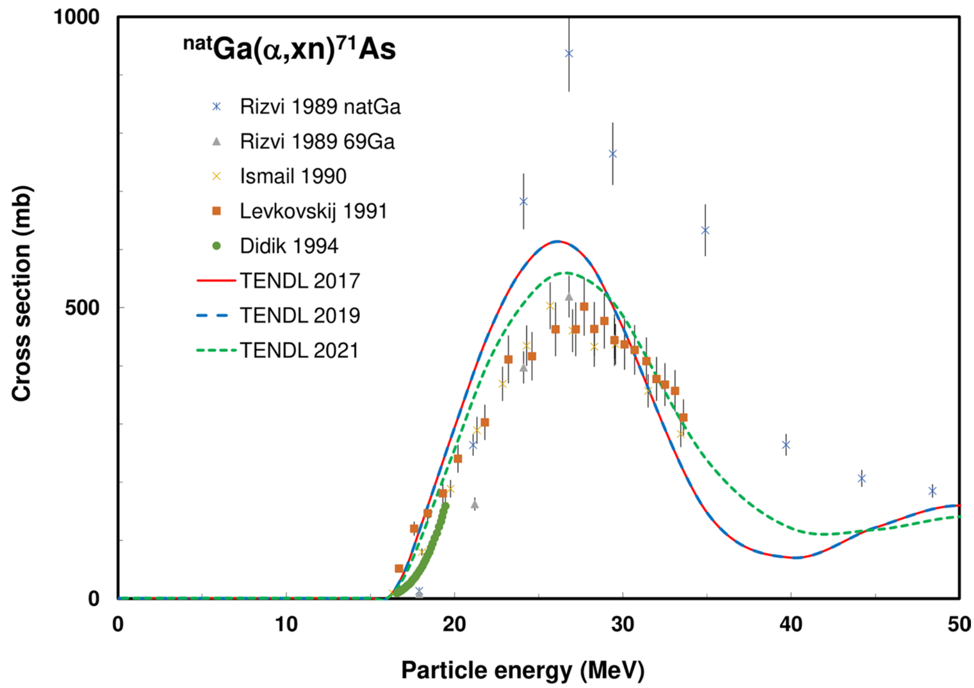

Fig. 28 $^{nat}Ga(\alpha,x)^{71}As$ reaction: all experimental data and the TENDL theoretical excitation functions

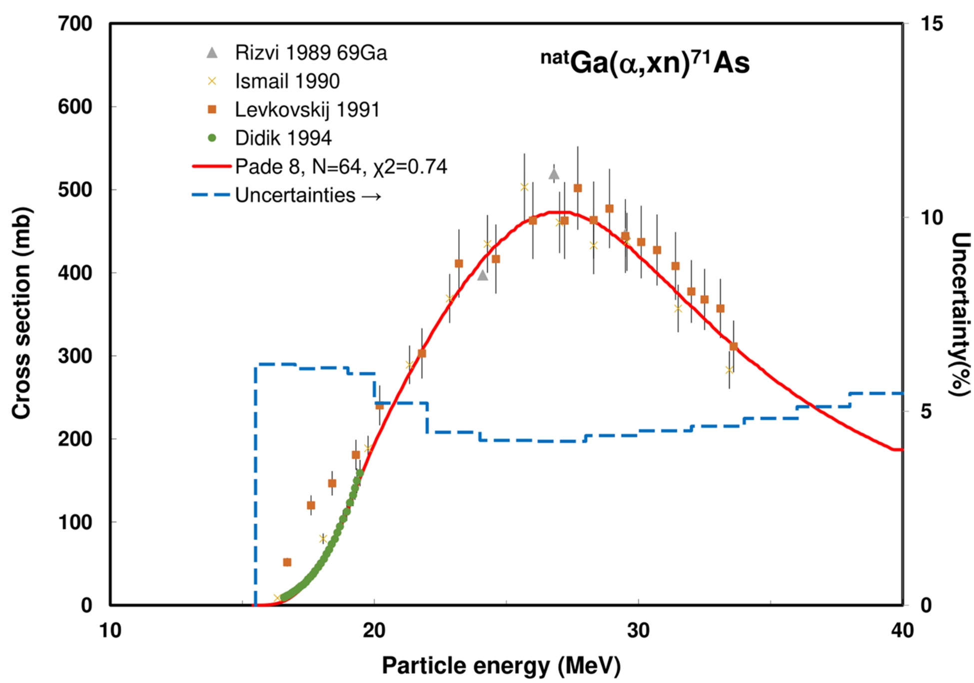

Fig. 29 $^{nat}Ga(\alpha,x)^{71}As$ reaction: selected experimental works and Padé fit (solid line) with total derived uncertainties, including 4% systematic uncertainty (dashed line, right-hand scale)

^{80m}Br production

The Auger electron-emitting nuclide ^{80m}Br ($T_{1/2}=4.43$ h) can be used for therapeutic application. In combination with other radioisotopes of bromine (^{75}Br ($T_{1/2}=96.7$ min PET) and ^{76}Br ($T_{1/2}=16.2$ h, PET), ^{77}Br ($T_{1/2}=57.04$ h, SPECT) it forms a theranostic ensemble. The decay schemes are available in [15] and decay data are displayed in Table 2.

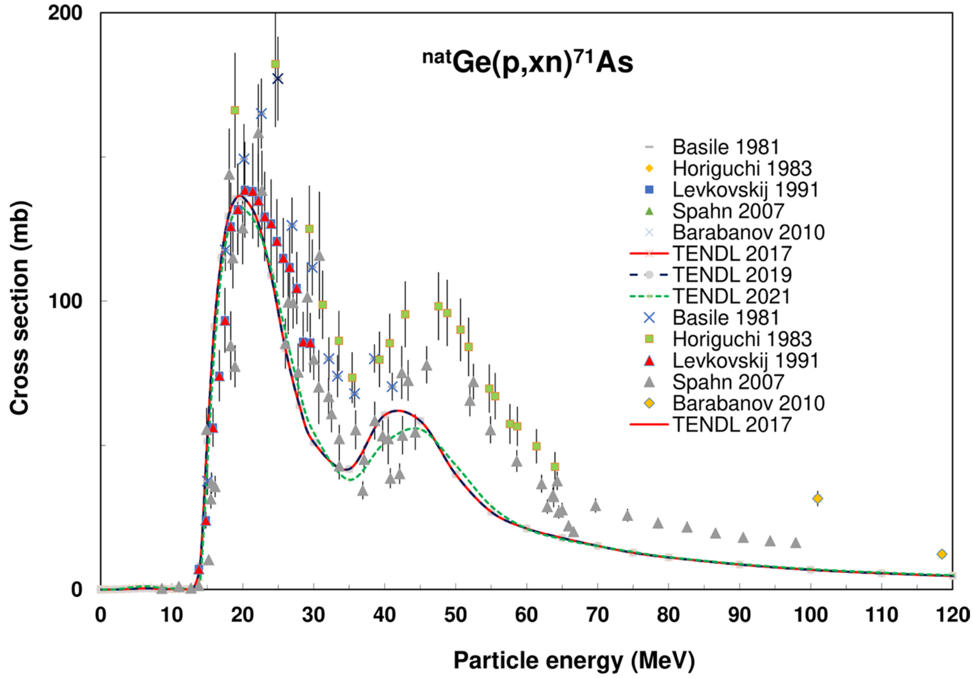

Fig. 30 $^{nat}Ge(p,xn)^{71}As$ reaction: all experimental data and the TENDL theoretical excitation functions

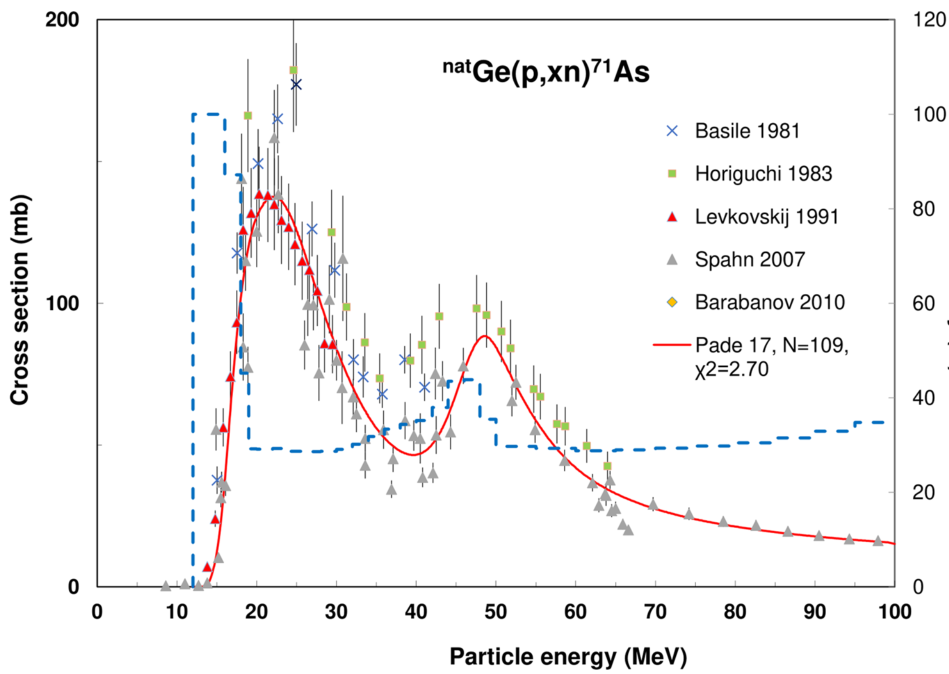

Fig. 31 $^{nat}Ge(p,xn)^{71}As$ reaction: selected experimental works and Padé fit (solid line) with total derived uncertainties, including 4% systematic uncertainty (dashed line, right-hand scale)

Evaluated nuclear reactions for ^{80m}Br formation

The $^{80}Se(p,n)^{80m}Br$, $^{nat}Se(d,xn)^{80m}Br$, $^{nat}Se(p,x)^{80m}Br$, $^{80}Se(d,2n)^{80m}Br$ and $^{nat}Se(\alpha,x)^{80m}Br$ reactions were evaluated.

$^{80}Se(p,n)^{80m}Br$ Five experimental cross section data sets were found: Blaser [102], Debuyst [103], Levkovskij [54], Al-Azony [81] and Spahn [82]. All data were selected and are shown in Figs. 52 and 53 together with the theoretical predictions and the Padé fit. The calculated integral yields for the production of ^{80m}Br are collected in Fig. 62. Nickles [86] reported experimental yield data.

$^{nat}Se(d,xn)^{80m}Br$ For the $^{nat}Se(d,xn)^{80m}Br$ reaction two data sets are available: Debuyst [103] (results on ^{80}Se, normalised) and Tárkányi [104]. The outlying cross section point of Debuyst 1968 [103] at 9.52 MeV was deselected. All data

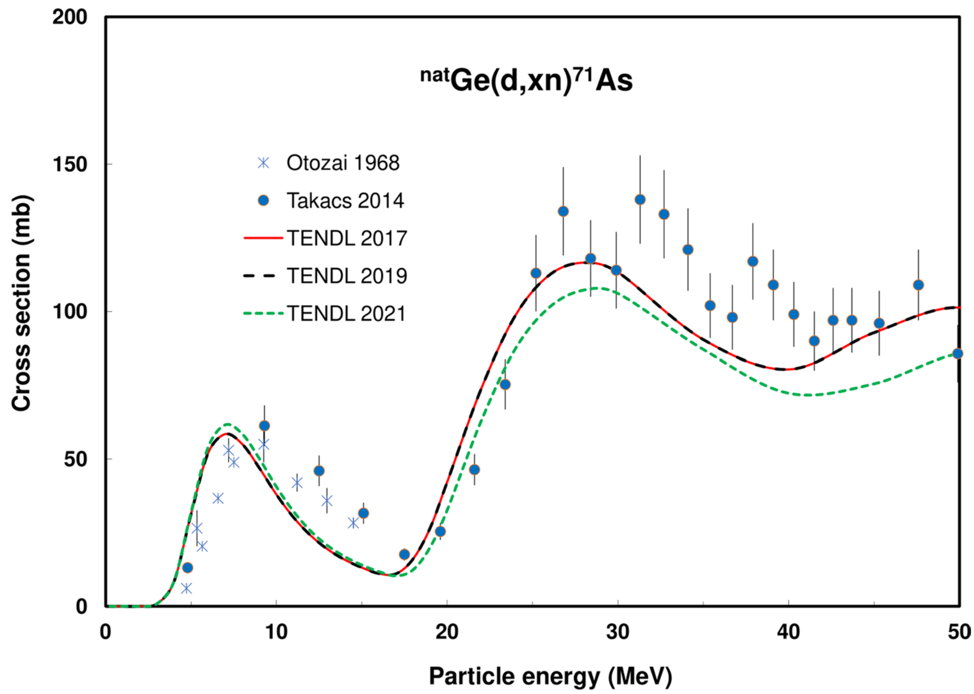

Fig. 32 $^{nat}Ge(d,x)^{71}As$ reaction: all experimental data and the TENDL theoretical excitation functions

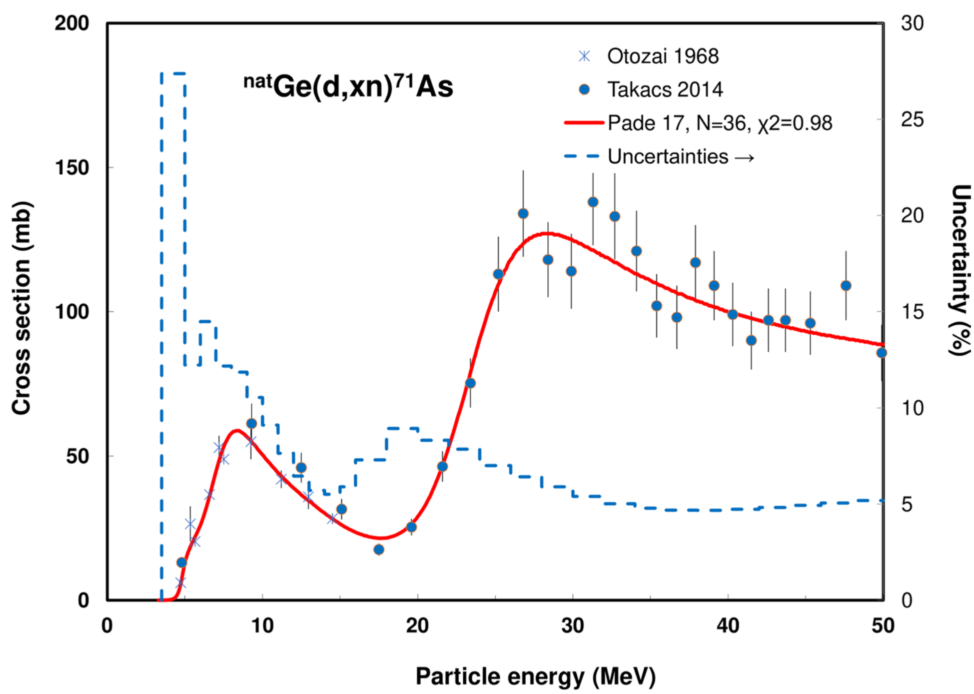

Fig. 33 $^{nat}Ge(d,x).^{71}As$ reaction: selected experimental works and Padé fit (solid line) with total derived uncertainties, including 4% systematic uncertainty (dashed line, right-hand scale)

with TENDL predictions are shown in Fig. 54, the Padé fitted selected data in Fig. 55 and the calculated yield in Fig. 62. No experimental yield data were found.

$^{nat}Se(p,x)^{80m}Br$ Five experimental data sets were published: Blaser [102], Debuyst [103], Levkovskij [54], El-Azony [81] and Spahn [82]. All sets were selected. The too-high value of Spahn [82] at 11.7 MeV was deselected. Experi-

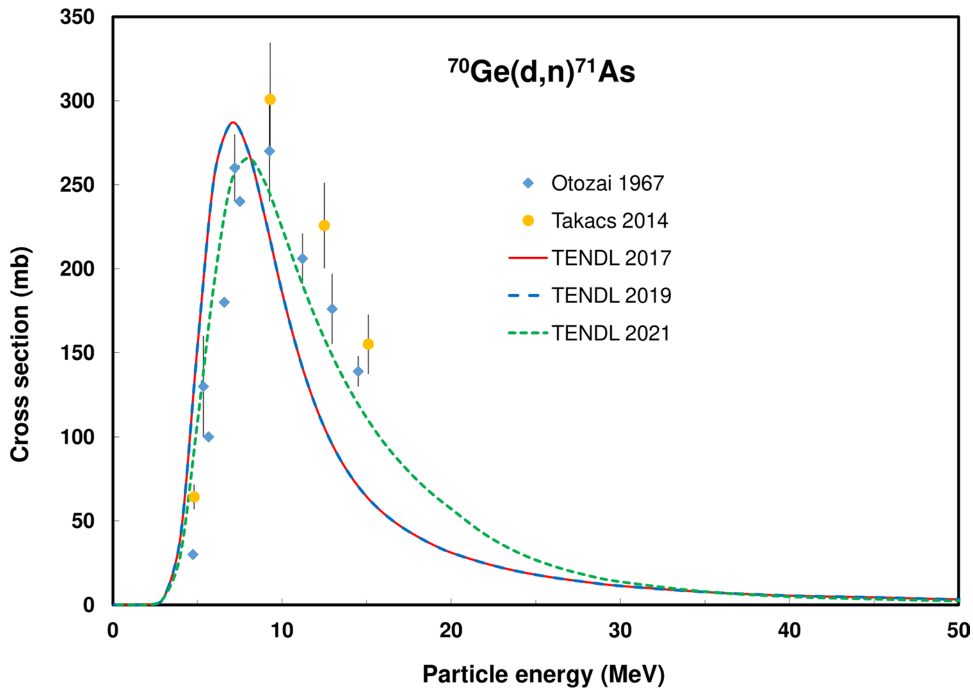

Fig. 34 ^{70}Ge(d,n)^{71}As reaction: all experimental data and the TENDL theoretical excitation functions

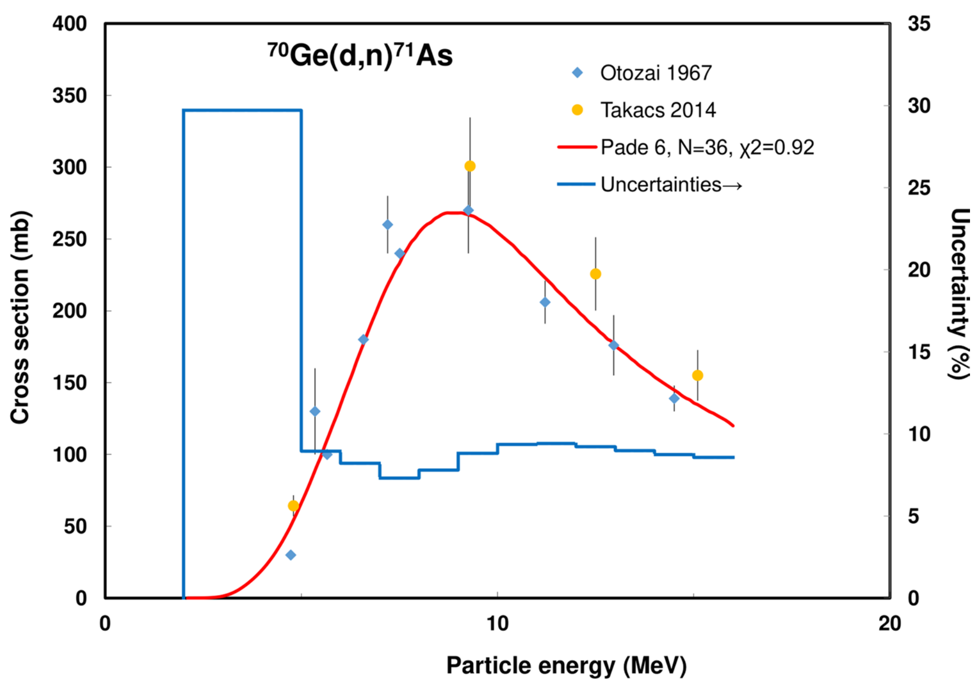

Fig. 35 ^{70}Ge(d,n)^{71}As reaction: selected experimental works and Padé fit (solid line) with total derived uncertainties, including 4% systematic uncertainty (dashed line, right-hand scale)

mental data and the TENDL theoretical excitation functions are shown in Fig. 56, the selected experimental works and Padé fit in Fig. 57. Integral yield based on the recommended values obtained from the fit are displayed in Fig. 62. No experimental yield data were found.

^{80}Se(d,2n)^{80m}Br Two data sets by Debuyst [103] and Tárkányi [104] (obtained on ^{nat}Se, normalized in appropriate energy domain to ^{80}Se abundance for use here) exist. Both were selected, except one outlying point of Debuyst [103] at 9.32 MeV. All data and the TENDL prediction are shown in Fig. 58, selected data with Padé fit in Fig. 59, and the calculated yields in Fig. 62. Vakilova [105] reported experimental yield data.

^{nat}Se(α,x)^{80m}Br Two data sets by Debuyst [103] and Levkovskij [54] exist. Levkovskij [54] has data only for reactions on ^{78}Se (23.78% abundance in ^{nat}Se) and ^{80}Se

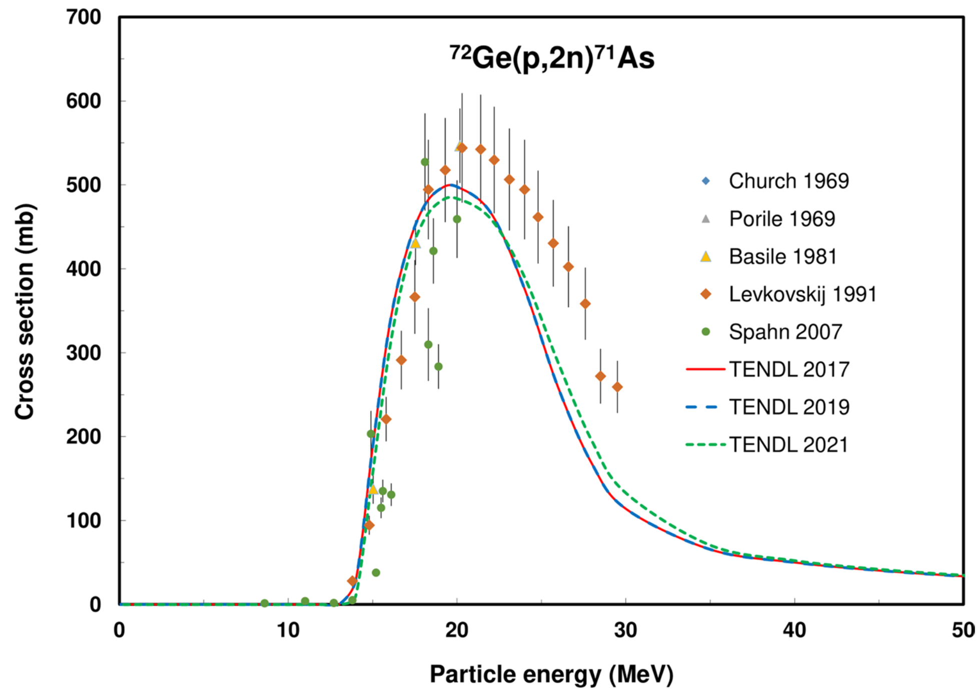

Fig. 36 ^{72}Ge(p,2n)^{71}As reaction: all experimental data and the TENDL theoretical excitation functions

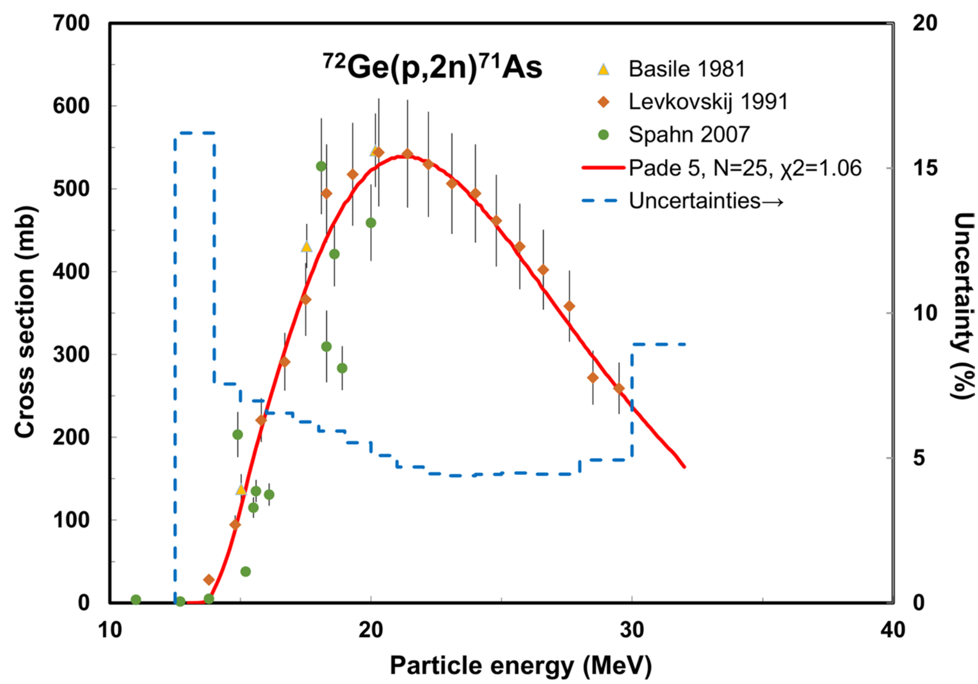

Fig. 37 ^{72}Ge(p,2n)^{71}As reaction: selected experimental works and Padé fit (solid line) with total derived uncertainties, including 4% systematic uncertainty (dashed line, right-hand scale)

(49.61%) targets: the two results were weighted and summed. The contribution of activation on ^{77}Se (7.63% abundance in ^{nat}Se) was considered to be negligible above 20 MeV. The two lowest points of Levkovskij [54] are deselected as they are too low, most probably because no contribution of ^{77}Se is available.

Experimental data, TENDL theoretical predictions, and selected data with Padé fit are shown in Figs. 60 and 61, the calculated yields in Fig. 62. No experimental yield data were found.

Integral yields for ^{80m}Br formation Integral yields of reactions related to the production of ^{80m}Br are deduced from the recommended values obtained from Padé fittings and are shown in Fig. 62.

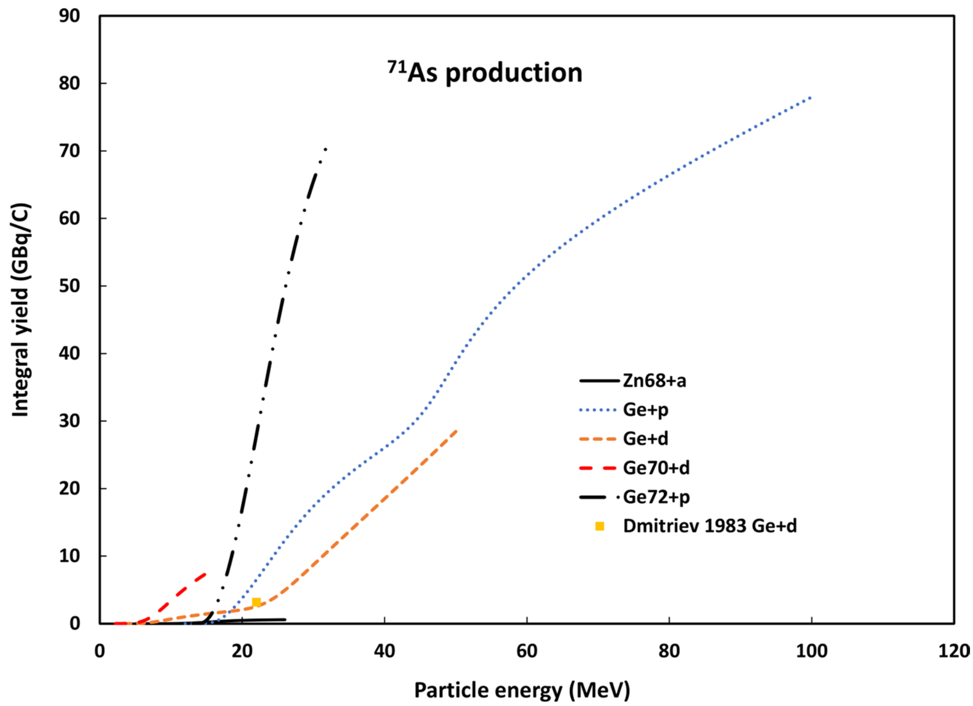

Fig. 38 Yield calculated from the recommended cross sections for ^{71}As production

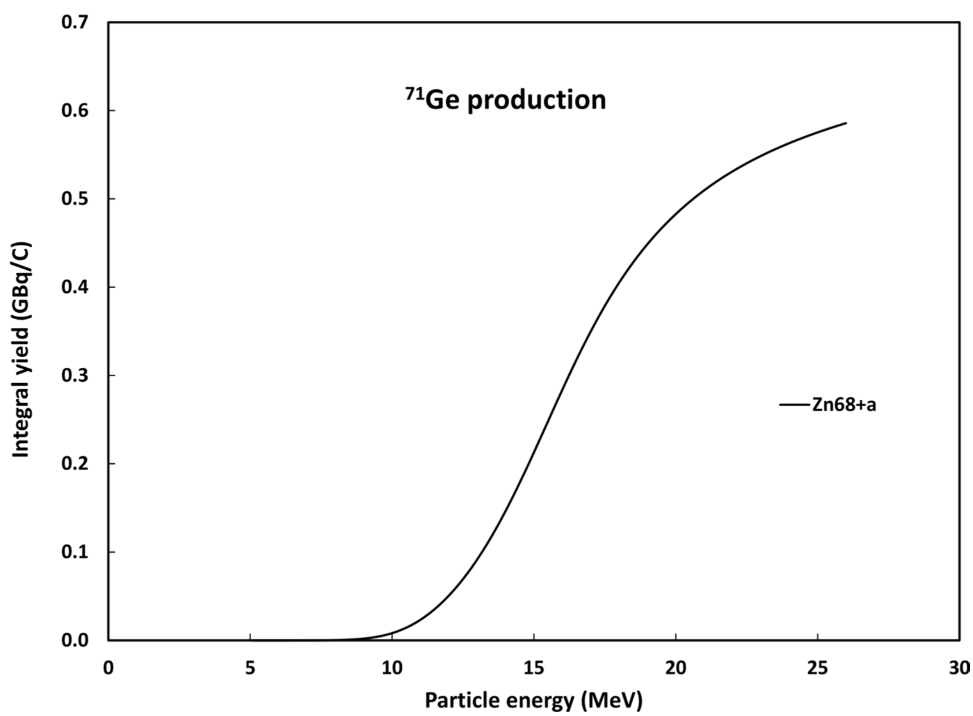

Fig. 39 Yield calculated from the recommended cross sections for ^{71}Ge production

^{103}Pd and ^{103}Ru production

Palladium-103 ($T_{1/2}$ = 16.991 d) and Ruthenium-103 ($T_{1/2}$ = 39.247 d) are the parent isotopes of ^{103m}Rh ($T_{1/2}$ = 56.1 min), which is applied for Auger electron therapy in permanent implants.

The ^{103}Pd and ^{103}Ru decay schemes and decay data are available in [15] and are displayed in Table 2.

Evaluated nuclear reactions for ^{103}Ru and ^{103}Pd formation

The $^{nat}Ag(p,x)^{103}Pd$, $^{nat}Ru(p,x)^{103}Ru$, $^{nat}Ru(d,x)^{103}Ru$ and $^{100}Mo(\alpha,n)^{103}Ru$ reactions were evaluated.

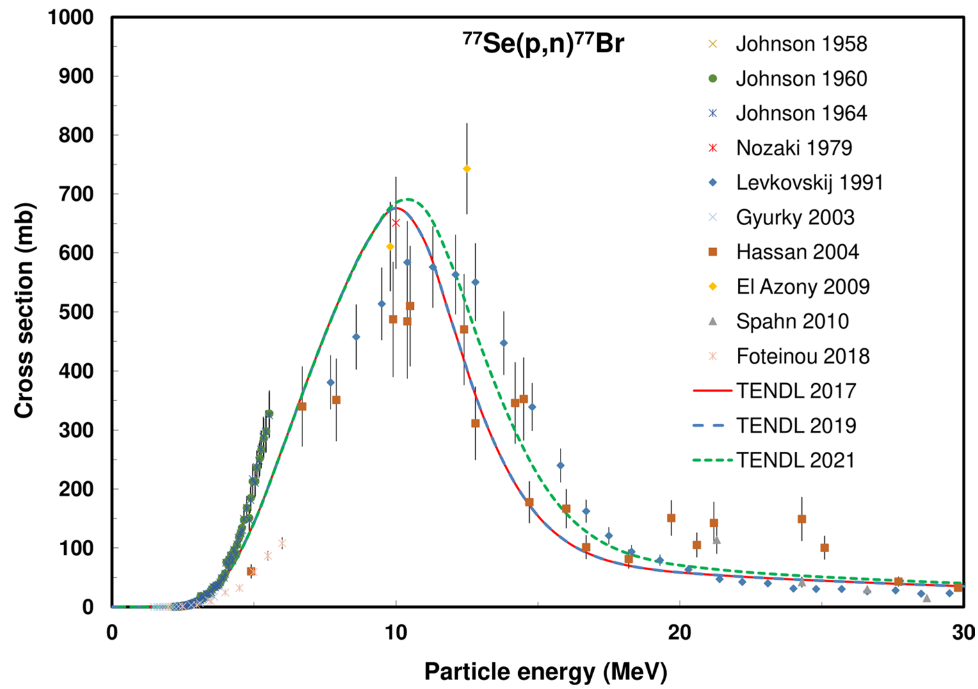

Fig. 40 ^{77}Se(p,n)^{77}Br reaction: all experimental data and the TENDL theoretical excitation functions

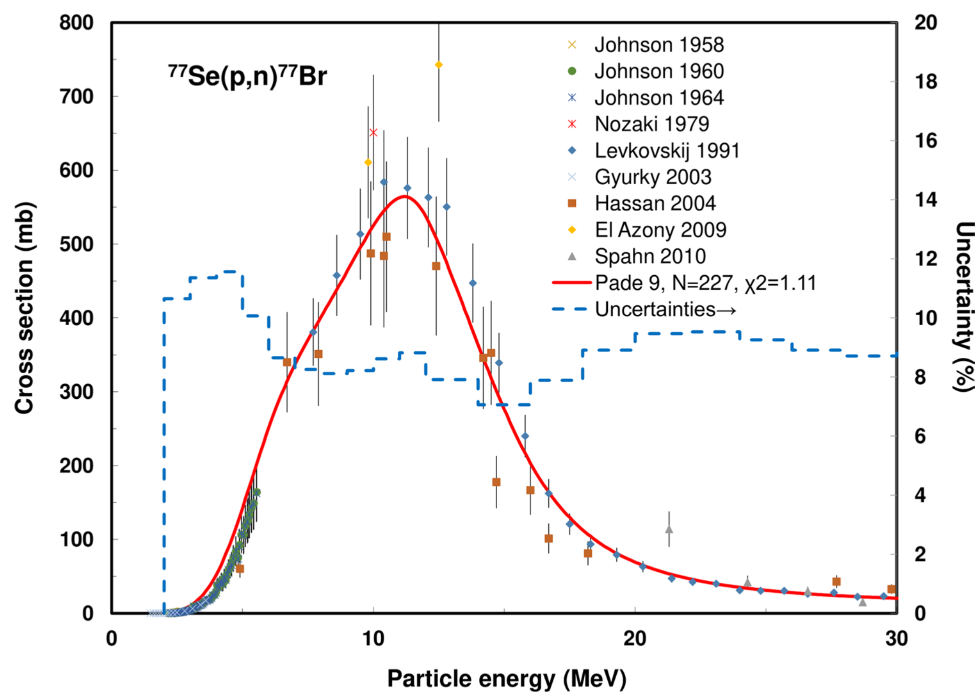

Fig. 41 ^{77}Se(p,n)^{77}Br reaction: selected experimental works and Padé fit (solid line) with total derived uncertainties, including 4% systematic uncertainty (dashed line, right-hand scale)

The ^{103}Rh(p,n)^{103}Pd and ^{103}Rh(d,2n)^{103}Pd reactions were evaluated by us earlier [8] and recommended cross section values are available in the IAEA NDS medical database [106].

^{nat}Ag(p,x)^{103}Pd Two data sets were found: Fassbender [107] and Uddin [108]. The 3 high energy points of Uddin [108] were deselected as they are outlying compared to the TENDL predictions (good summed description of the reactions on the two stable Ag target isotopes) and the Fassbender [107] results. All data, in comparison with the TENDL predictions, are shown in Fig. 63. The selected data with the Padé fit can be seen in Fig. 64. The calculated yields are displayed in Fig. 71. No experimental yield data were found in the literature.

^{nat}Ru(p,x)^{103}Ru Gagnon [109] and Hermanne [110] presented experimental cross section data that are shown in

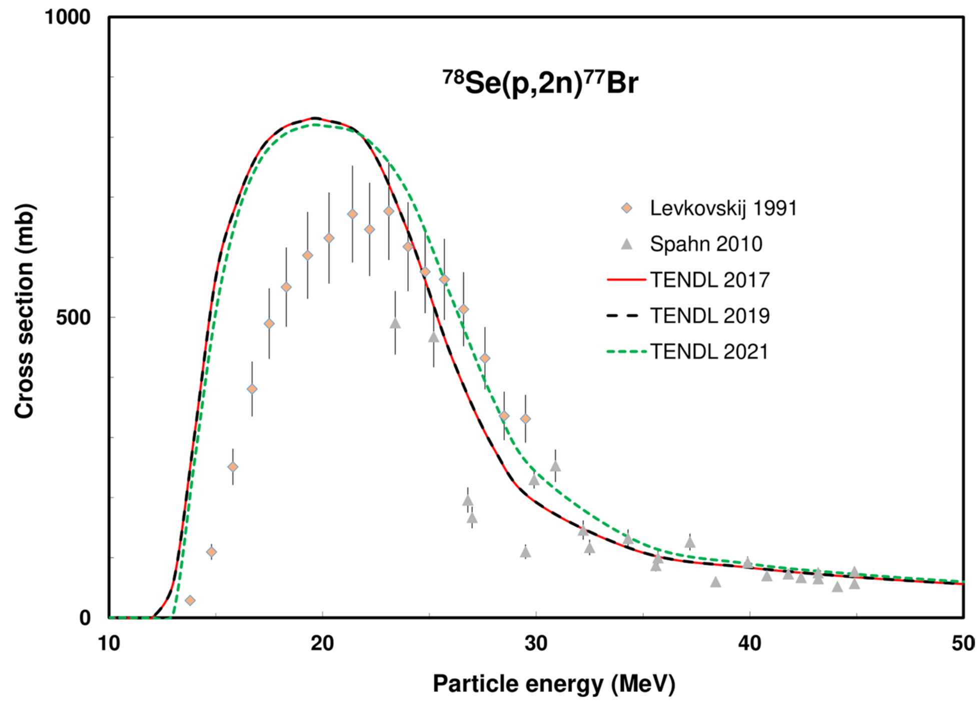

Fig. 42 ^{78}Se(p,2n)^{77}Br reaction: all experimental data and the TENDL theoretical excitation functions

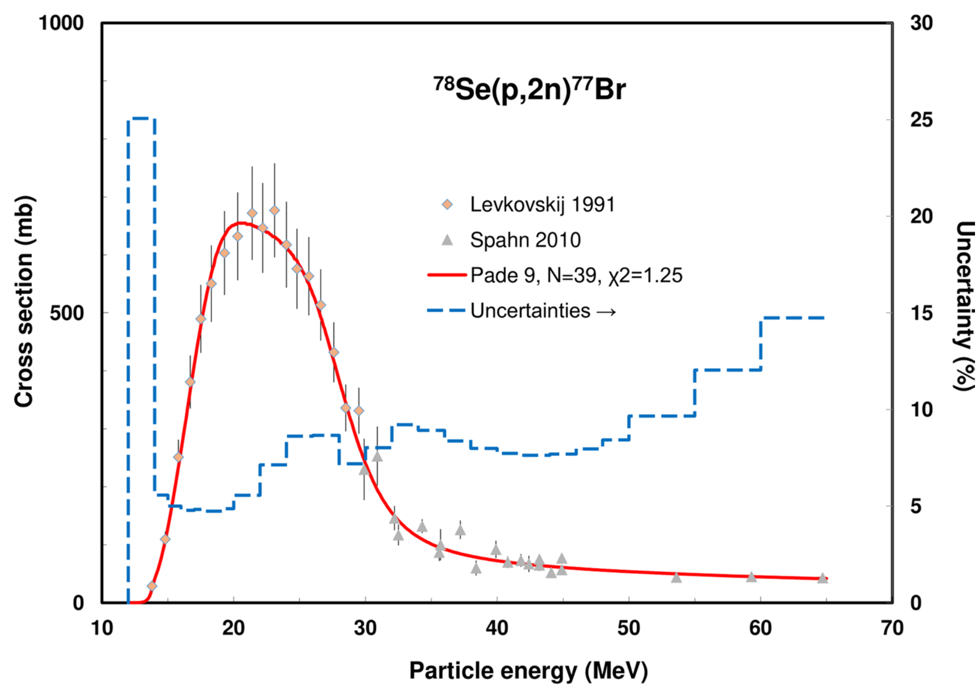

Fig. 43 ^{78}Se(p,2n)^{77}Br reaction: selected experimental works and Padé fit (solid line) with total derived uncertainties, including 4% systematic uncertainty (dashed line, right-hand scale)

Fig. 65 in comparison with the TENDL theoretical predictions. Both sets were selected and fitted (Fig. 66). Calculated physical yields are shown in Fig. 72. No experimental yield data were found.

^{nat}Ru(d,x)^{103}Ru Two data sets are available: Mito [111] (only data on ^{102}Ru target, useful in lower energy range after normalization) and Tárkányi [112] up 50 MeV.

All experimental data, in comparison with the TENDL theoretical prediction, are shown in Fig. 67, the fitted selected data in Fig. 68 and the calculated physical yield in Fig. 72. No experimental yield data were found.

^{100}Mo(α,n)^{103}Ru Four data sets are available in the literature: Esterlund [113], Graf [114], Ditrói [115] and Tárkányi [116]. The Esterlund [113] data were multiplied by a factor

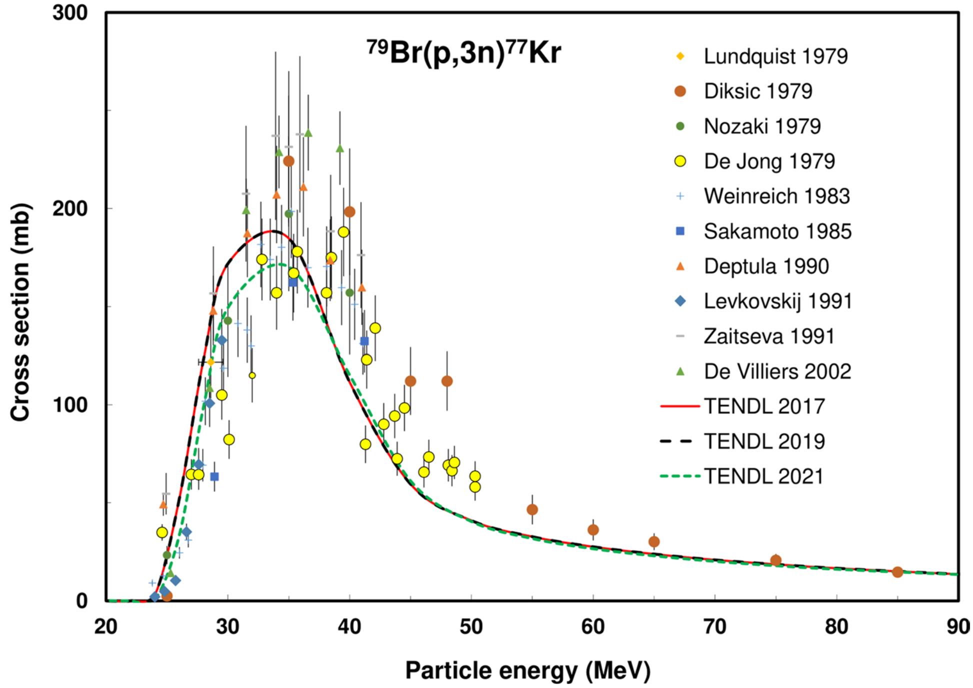

Fig. 44 ^{79}Br(p,3n)^{77}Kr reaction: all experimental data and the TENDL theoretical excitation functions

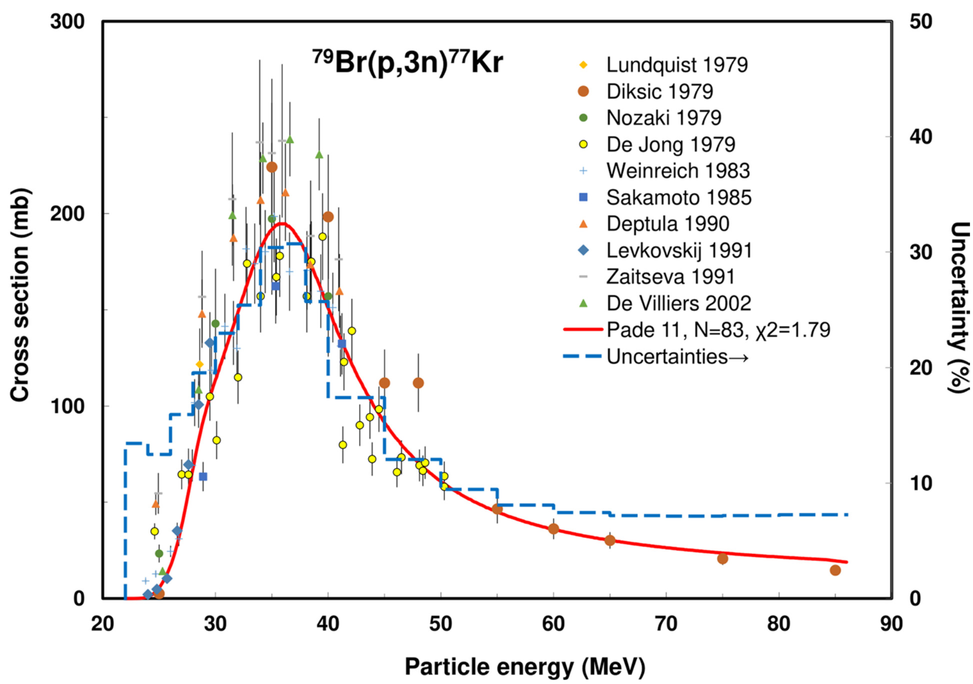

Fig. 45 ^{79}Br(p,3n)^{77}Kr reaction: selected experimental works and Padé fit (solid line) with total derived uncertainties, including 4% systematic uncertainty (dashed line, right-hand scale)

of 2 (correction for incoming particle flux, alpha Z = 2) and the lowest energy point was deselected (below the threshold). All data, in comparison with the TENDL theoretical predictions, are shown in Fig. 69. The selected data and the Padé fit are displayed in Fig. 70, the calculated yield in Fig. 72. No experimental yield data were found.

Integral yields for ^{103}Pd and ^{103}Ru formation Integral yields of reactions related to the production of ^{103}Pd and ^{103}Ru are deduced from the recommended values obtained from Padé fittings and are shown in Figs. 71,72.

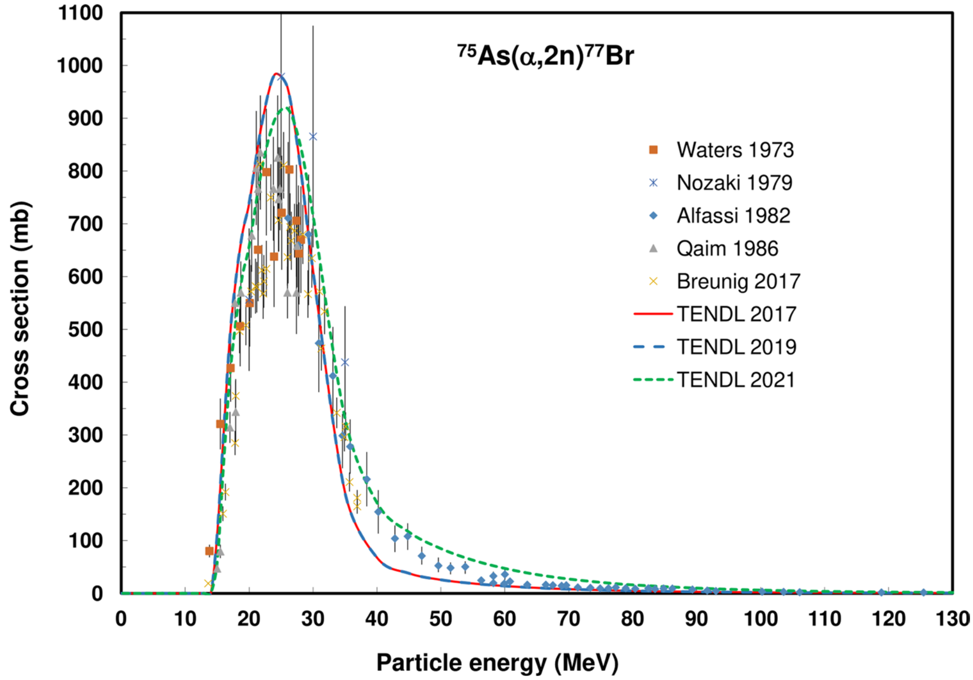

Fig. 46 ^{75}As(α,2n)^{77}Br reaction: all experimental data and the TENDL theoretical excitation functions

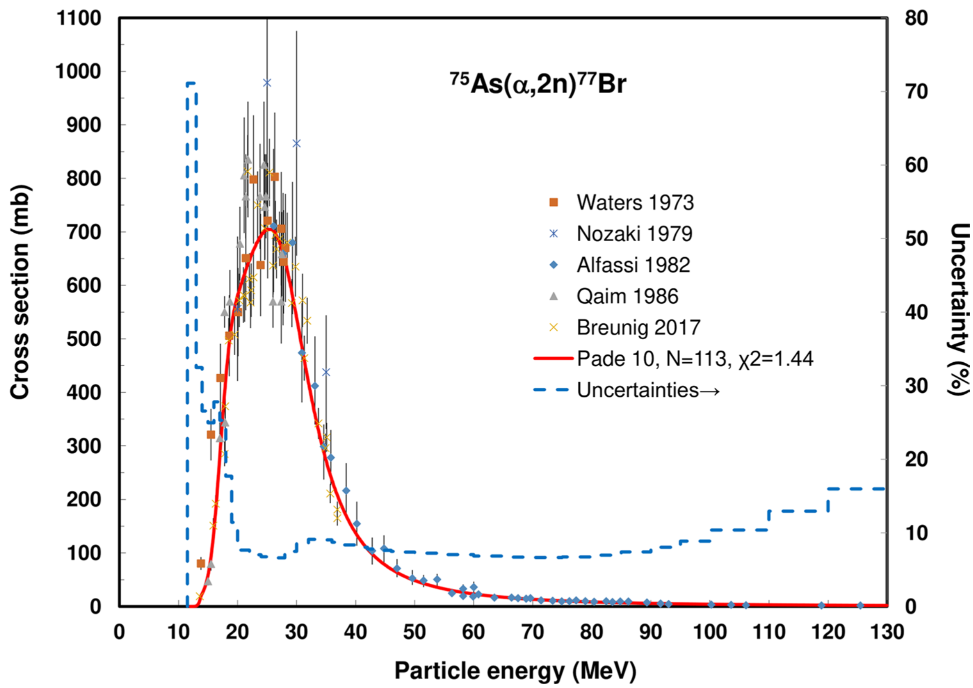

Fig. 47 ^{75}As(α,2n)^{77}Br reaction: selected experimental works and Padé fit (solid line) with total derived uncertainties, including 4% systematic uncertainty (dashed line, right-hand scale)

^{105}Rh production

Rhodium-105 ($T_{1/2}$ = 35.4 h), a mostly reactor-produced radionuclide, decays by β^- emission with moderate energy which makes it suitable for radiotherapy. It also emits γ-rays that are used for SPECT diagnostic experiments. The decay scheme is available in [15] and decay data are displayed in Table 2.

Evaluated nuclear reaction for ^{105}Rh formation

The ^{104}Ru(d,n)^{105}Rh reaction was evaluated.

^{104}Ru(d,n)^{105}Rh Two experimental data sets obtained by Sitarz [57] and Tárkányi [116] were found. The Sitarz [57] data were multiplied by a factor of 1.4 on the basis that all data in this publication show systematically significantly lower values when compared to the results of

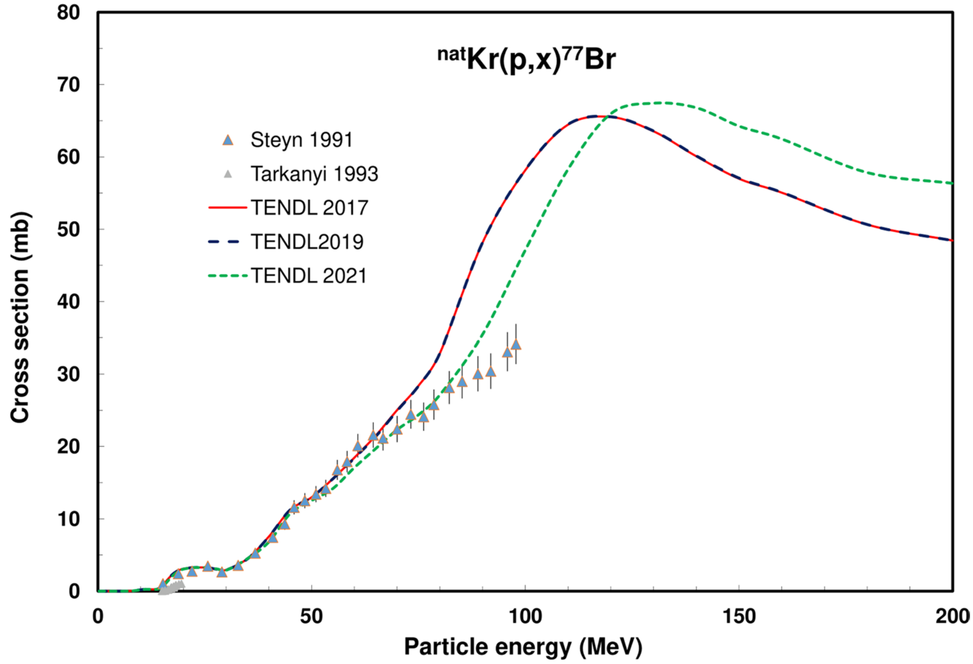

Fig. 48 $^{nat}Kr(p,x)^{77}Br$ reaction: all experimental data and the TENDL theoretical excitation functions

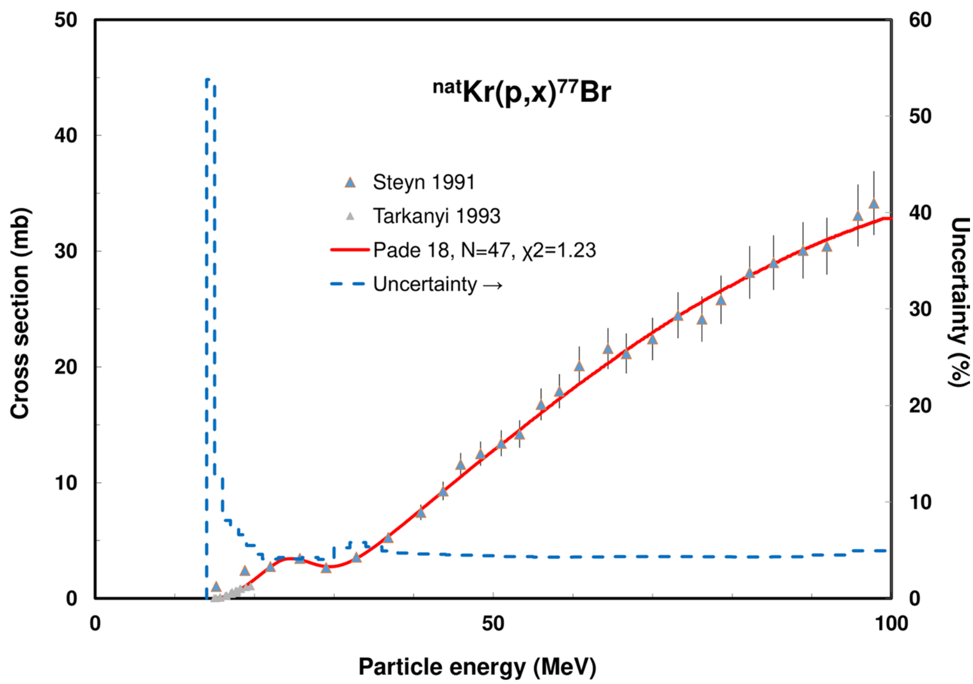

Fig. 49 $^{nat}Kr(p,x)^{77}Br$ reaction: selected experimental works and Padé fit (solid line) with total derived uncertainties, including 4% systematic uncertainty (dashed line, right-hand scale)

other authors (see also Sect. 4.1.9). All data, in comparison with TENDL predictions, and selected data with Padé fit are shown in Figs. 73 and 74. The calculated yield data are displayed in Fig. 75. No experimental yield data were found.

Integral yields for ^{105}Rh formation Integral yield for the $^{104}Ru(d,n)^{105}Rh$ reaction are deduced from the recommended values obtained from Padé fitting and is shown in Fig. 75.

^{117m}Sn production

The radio-isotope ^{117m}Sn ($T_{1/2} = 14$ d) decays for 100% by internal transition to stable ^{117}Sn but emits Auger and conversion electrons, making it a candidate for radiotherapy.

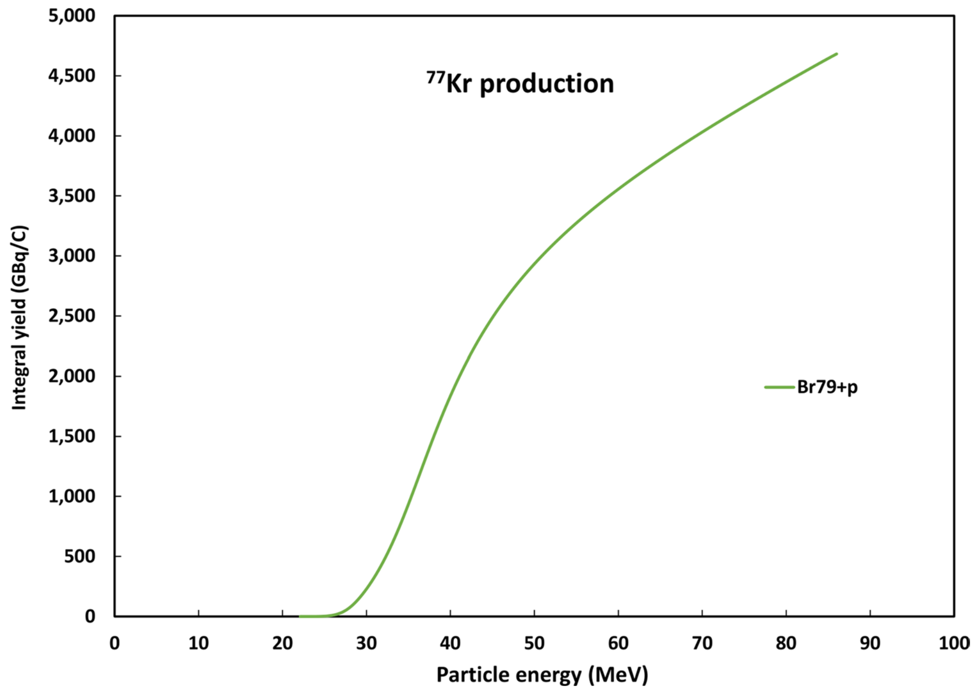

Fig. 50 Yield calculated from the recommended cross sections for ^{77}Kr production

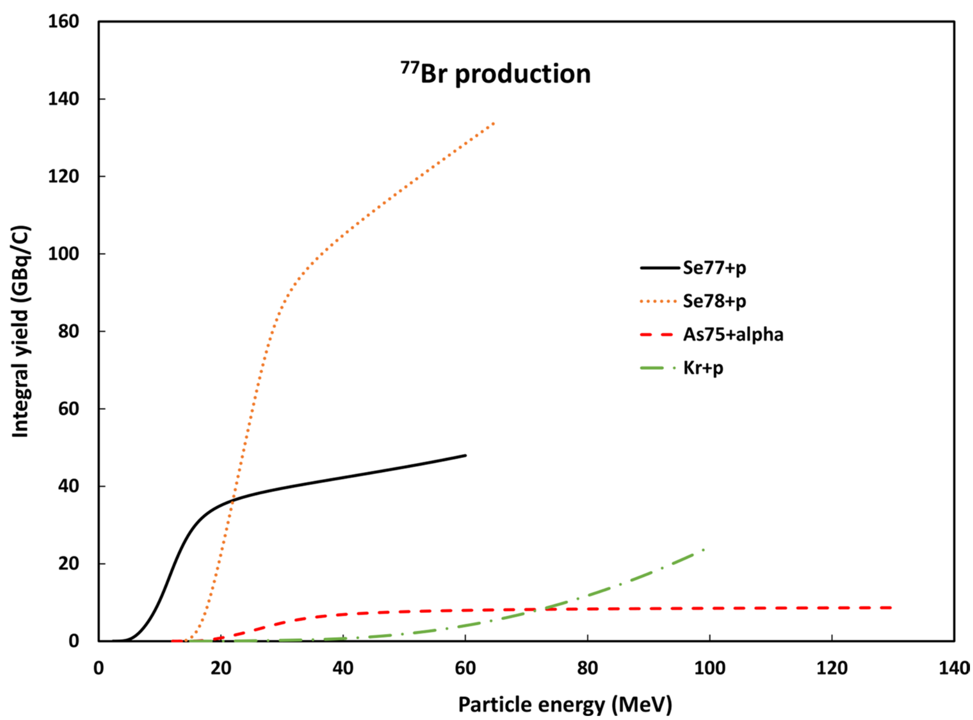

Fig. 51 Yield calculated from the recommended cross sections for ^{77}Br production

The decay scheme is available in [15] and decay data are displayed in Table 2.

Evaluated nuclear reactions for ^{117m}Sn formation

The ^{114}Cd(α,n)^{117m}Sn, ^{116}Cd(α,3n)^{117m}Sn, ^{nat}Cd(α,xn)^{117m}Sn, ^{115}In(α,pn)^{117m}Sn and ^{nat}Sb(p,x)^{117m}Sn reactions were evaluated. For the ^{nat}Sb(d,x)^{117m}Sn reaction only one data set (up to 49.2 MeV) was found.

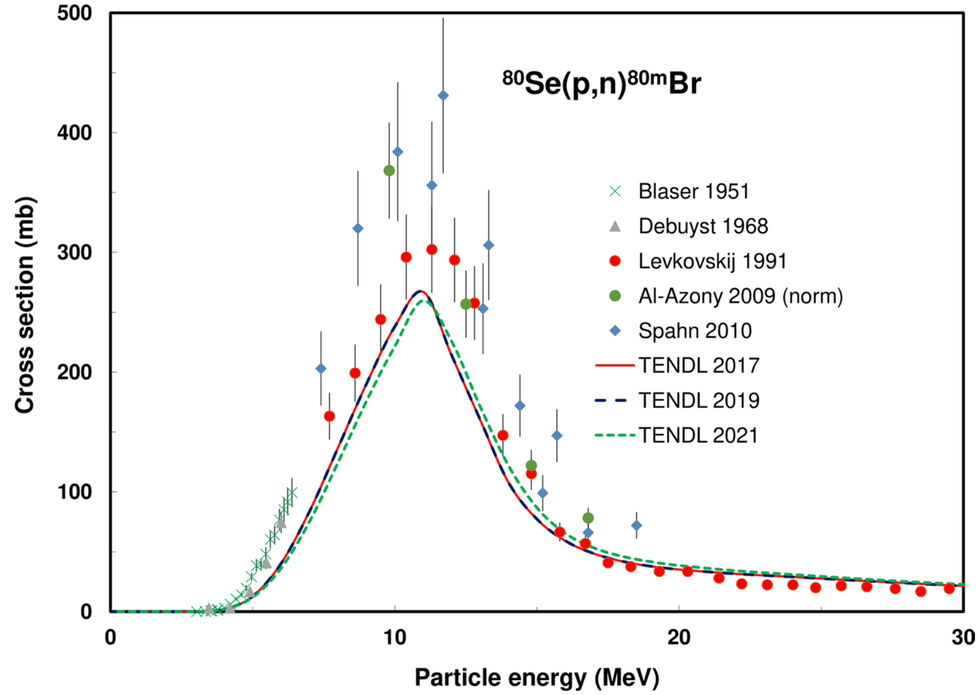

Fig. 52 ^{80}Se(p,n)^{80m}Br reaction: all experimental data and the TENDL theoretical excitation functions

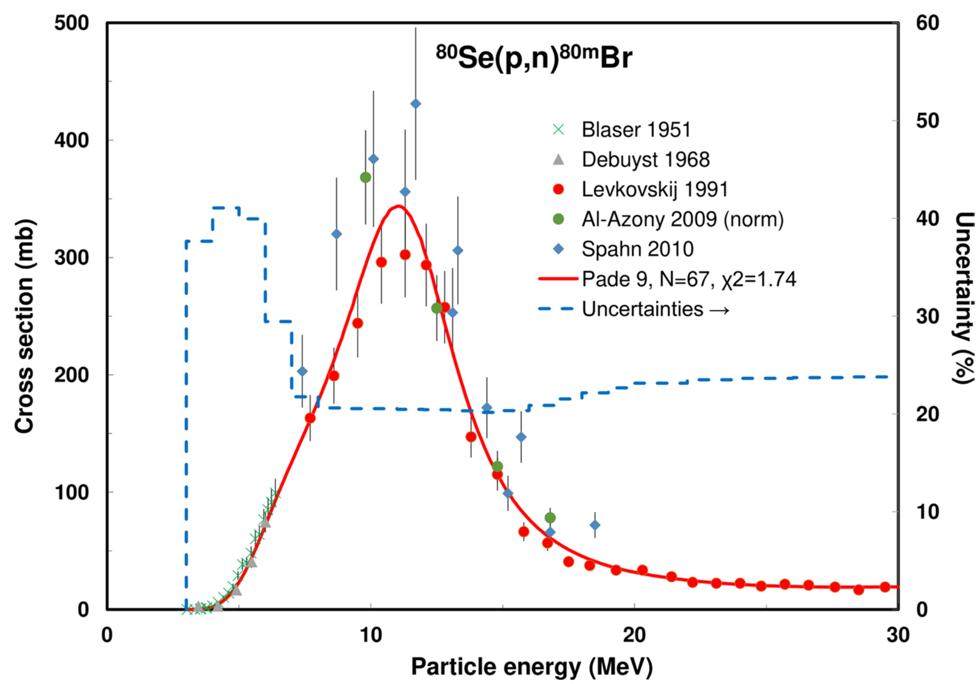

Fig. 53 ^{80}Se(p,n)^{80m}Br reaction: selected experimental works and Padé fit (solid line) with total derived uncertainties, including 4% systematic uncertainty (dashed line, right-hand scale)

^{114}Cd(α,n)^{117m}Sn Five data sets were found in the literature: Qaim [117], Rebeles [118], Hermanne [119], Khandaker [120] and Ditrói [121]. Only the Rebeles [118] data were obtained on a ^{114}Cd target, all other sets were normalized from data obtained on ^{nat}Cd. The Qaim [117] data were deselected due to large scatter (see also Sects. 4.8.2 and 4.8.3). All data, in comparison with the TENDL theoretical prediction, are shown in Fig. 76. anThe selected data and the Padé fit are displayed in Fig. 77. The calculated physical yields for the production of ^{117m}Sn are displayed in Fig. 86. No experimental yield data were found.

^{116}Cd(α,3n)^{117m}Sn Nine data sets were found: Montgomery [122], Qaim [117], Rebeles [118], Hermanne (nat) [119], Khandaker (nat) [120], Ditrói [123], Ditrói (nat) [121], Duchemin (nat) [124]. In Qaim [117] an incident

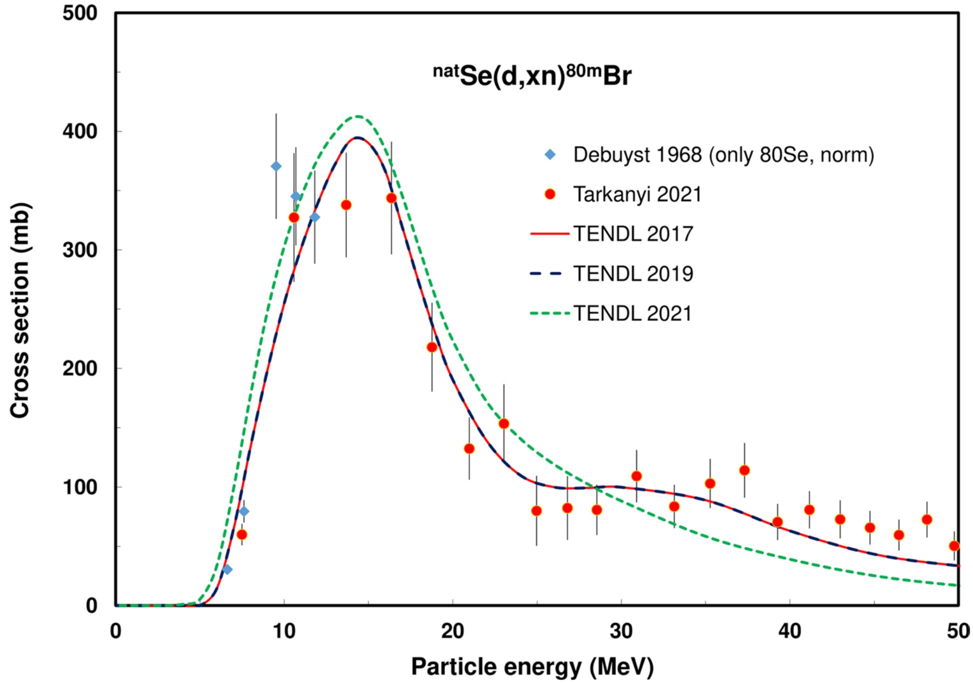

Fig. 54 $^{nat}Se(d,xn)^{80m}Br$ reaction: all experimental data and the TENDL theoretical excitation functions

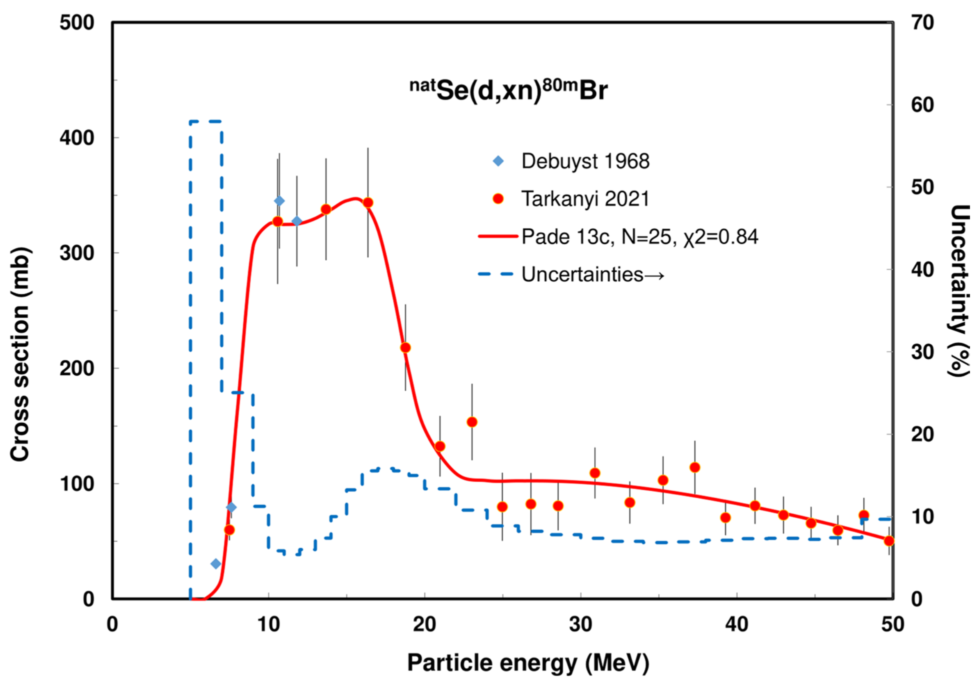

Fig. 55 $^{nat}Se(d,xn)^{80m}Br$ reaction: selected experimental works and Padé fit (solid line) with total derived uncertainties, including 4% systematic uncertainty (dashed line, right-hand scale)

120 MeV energy beam and a stack with many foils was used, unfortunately resulting in a shifted energy scale. A linear downward energy shift was tried out but when agreement for the second peak is attempted, the lowest energy point is shifted nearly 16 MeV to zero MeV.). As part of these corrected data are still scattered, all Qaim [117] data were hence deselected. For the 4 sets obtained on ^{nat}Cd targets, the contribution from the reaction on ^{114}Cd in the natural target was subtracted based on the ^{114}Cd (α,n) results (recommended values after fit) (see Sect. "Evaluated nuclear reactions for 117mSn formation").

The experimental data, the TENDL predictions and the selected data with Padé fit are shown in Figs. 78 and 79. The calculated yield data are displayed in Fig. 86. No experimental yield data were found.

$^{nat}Cd(α,xn)^{117m}Sn$ Five data sets obtained on ^{nat}Cd targets were found: Qaim [117], Hermanne [119], Khandaker [120],

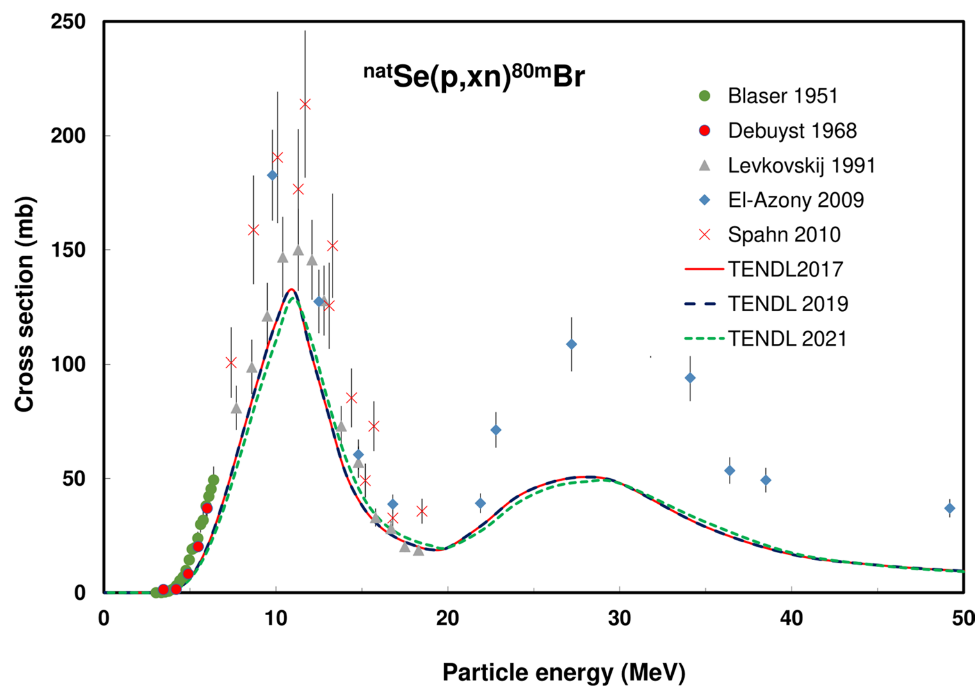

Fig. 56 $^{nat}Se(p,xn)^{80m}Br$ reaction: all experimental data and the TENDL theoretical excitation function

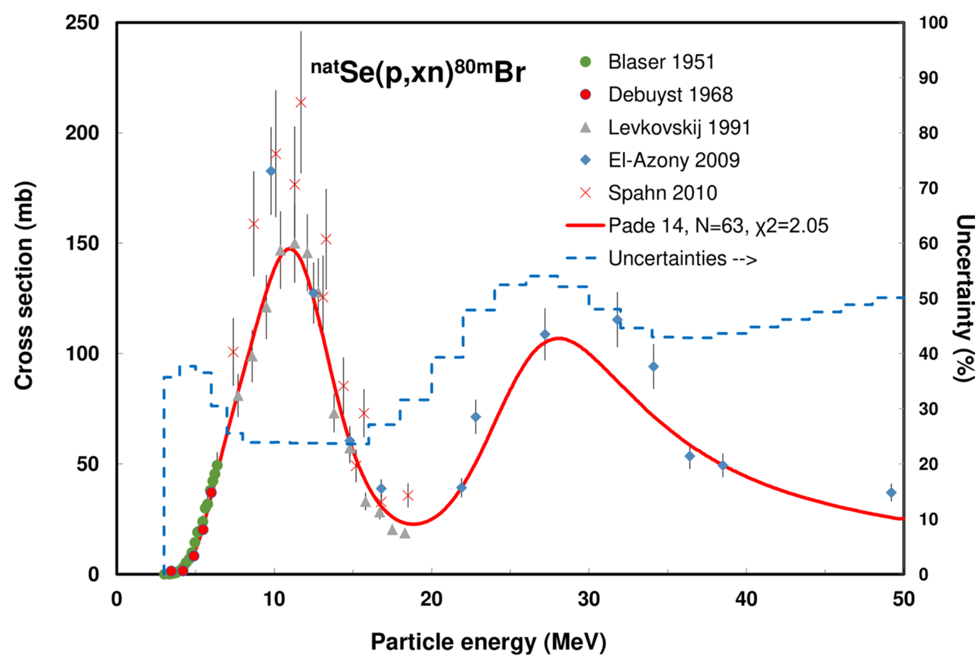

Fig. 57 $^{nat}Se(p,xn)^{80m}Br$ reaction: selected experimental works and Padé fit (solid line) with total derived uncertainties, including 4% systematic uncertainty (dashed line, right-hand scale)

Duchemin [124], Ditrói [123]. By adding the normalized (in relevant limited energy domains) and weighted sums data obtained on enriched ^{114}Cd and ^{116}Cd targets (Montgomery [122] on ^{116}Cd, Rebeles [118] on ^{114}Cd, Rebeles [118] on ^{116}Cd, Ditrói [123] on ^{116}Cd) a total of nine sets became available.

As motivated in the previous section the Qaim [117] set was deselected. The point at 39.5 MeV of Khandaker [120] was also deselected. All data, in comparison with the TENDL prediction, are shown in Fig. 80. The Padé fit of the selected data is displayed in Fig. 81 and the yield calculated from the recommended values based on the Padé fit in Fig. 86. Experimental yields were measured by Dmitriev [125] and Fukushima [126].

$^{115}In(\alpha,pn)^{117m}Sn$ Four data sets were found in literature: Fukushima [127], Qaim [117], Bhardwaj [128], and Aikawa [129]. As the data are very contradicting (Fig. 90), we tried to make reasonable corrections and took the Aikawa [129] values for reference. As mentioned earlier

Fig. 58 ^{80}Se(d,2n)^{80m}Br reaction: all experimental data and the TENDL theoretical excitation functions

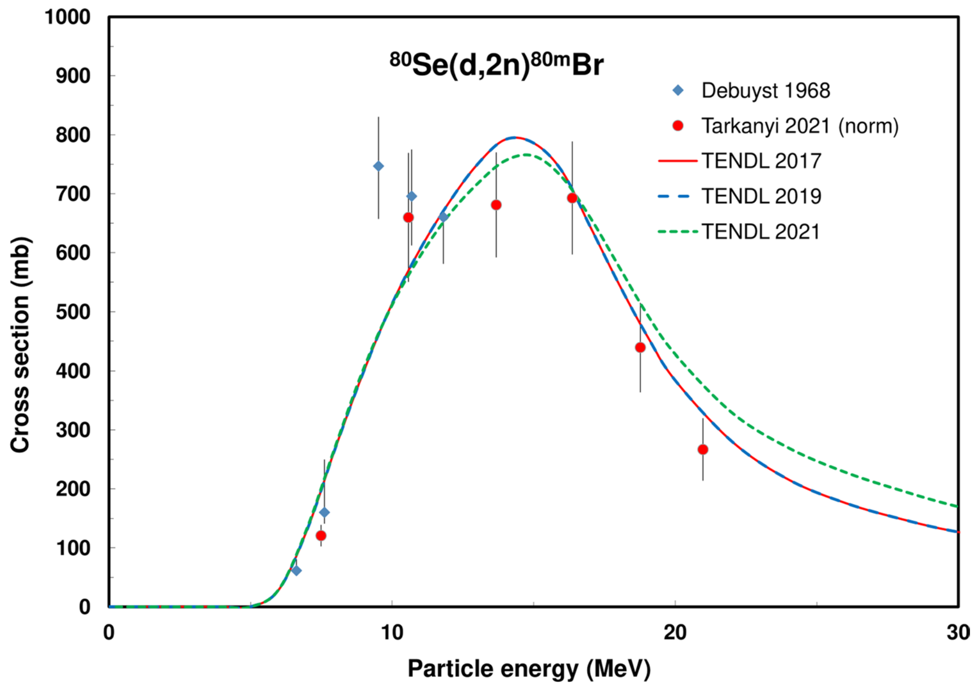

Fig. 59 ^{80}Se(d,2n)^{80m}Br reaction: selected experimental works and Padé fit (solid line) with total derived uncertainties, including 4% systematic uncertainty (dashed line, right-hand scale)

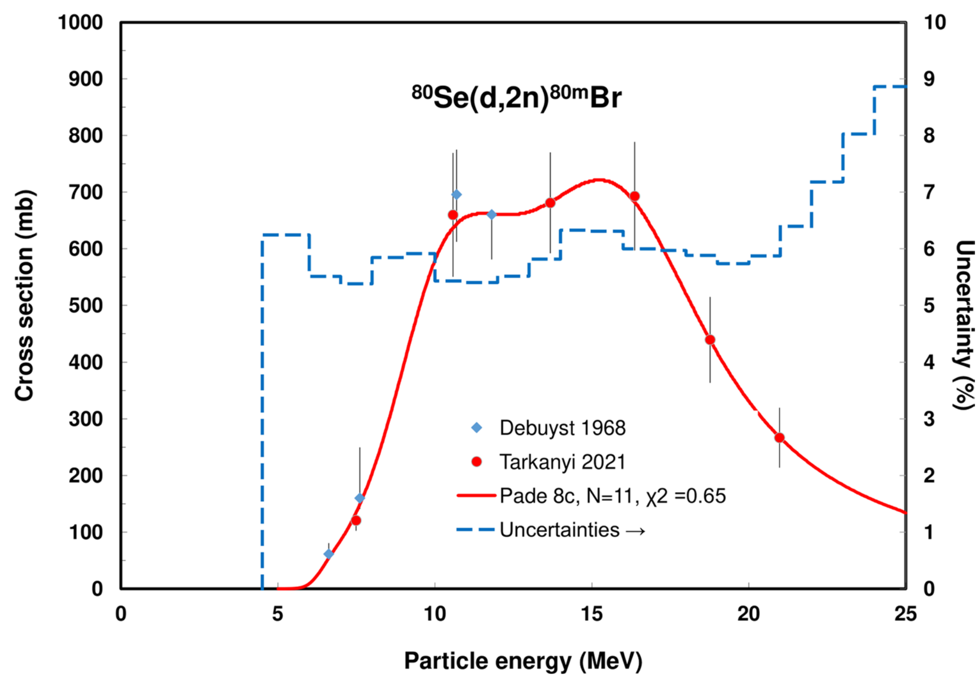

(see Sect. 4.8.2) for all sets in Qaim [117] an important energy shift due to the long stack is noticed and a downward correction of the energy scale was made. Bhardwaj [128] data were divided by a factor of 2 (beam current, Z = 2 for α-particles), while Fukushima [127] data were multiplied by a factor of 4 (beam current). All original data, in comparison with the TENDL theoretical predictions, are shown in Fig. 82. The 4 selected (3 corrected) sets and the Padé fit are displayed in Fig. 83, and the calculated yield in Fig. 86. Dmitriev [125] reported experimental integral data.

^{nat}Sb(p,x)^{117m}Sn Four experimental cross section data sets are available: Ermolaev [130], Takács [131], Mosby [132], and Ermolaev [133]. All data with TENDL predictions and the selected data with Padé fit are shown in Figs. 84 and 85. The deduced integral yields are displayed in Fig. 86. No experimental integral yield data were found.

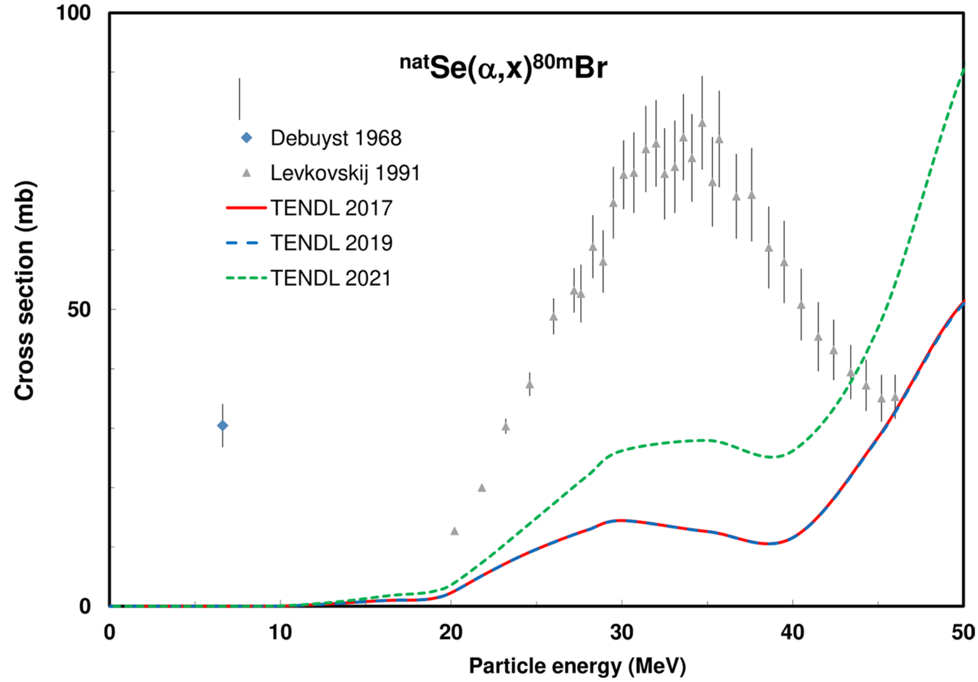

Fig. 60 $^{nat}Se(\alpha,x)^{80m}Br$ reaction: all experimental data and the TENDL theoretical excitation functions

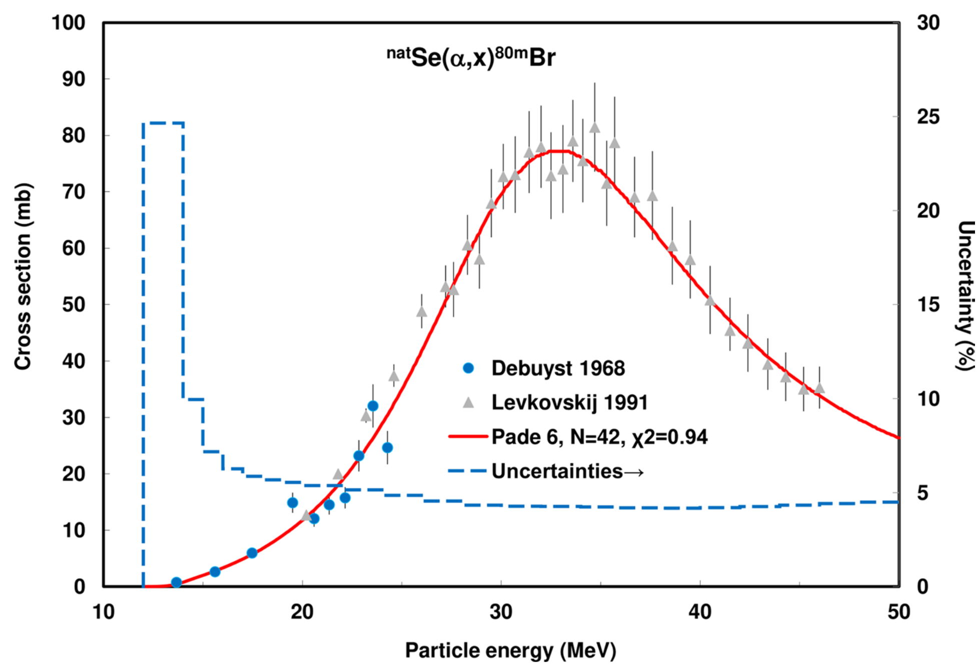

Fig. 61 $^{nat}Se(\alpha,x).^{80m}Br$ reaction: selected experimental works and Padé fit (solid line) with total derived uncertainties, including 4% systematic uncertainty (dashed line, right-hand scale)

Integral yields for ^{117m}Sn formation Integral yields of reactions related to the production of ^{117m}Sn are deduced from the recommended values obtained from Padé fittings and are displayed in Fig. 86.

^{119}Sb production

The ^{119}Sb ($T_{1/2}=38.19$ h) decays by EC followed by emission of low energy Auger electrons (~20 keV, short biological path lengths of~10 µm) and is hence a candidate for targeted radiotherapy. It can be produced directly and through generator decay of its longer-lived ^{119m}Te parent

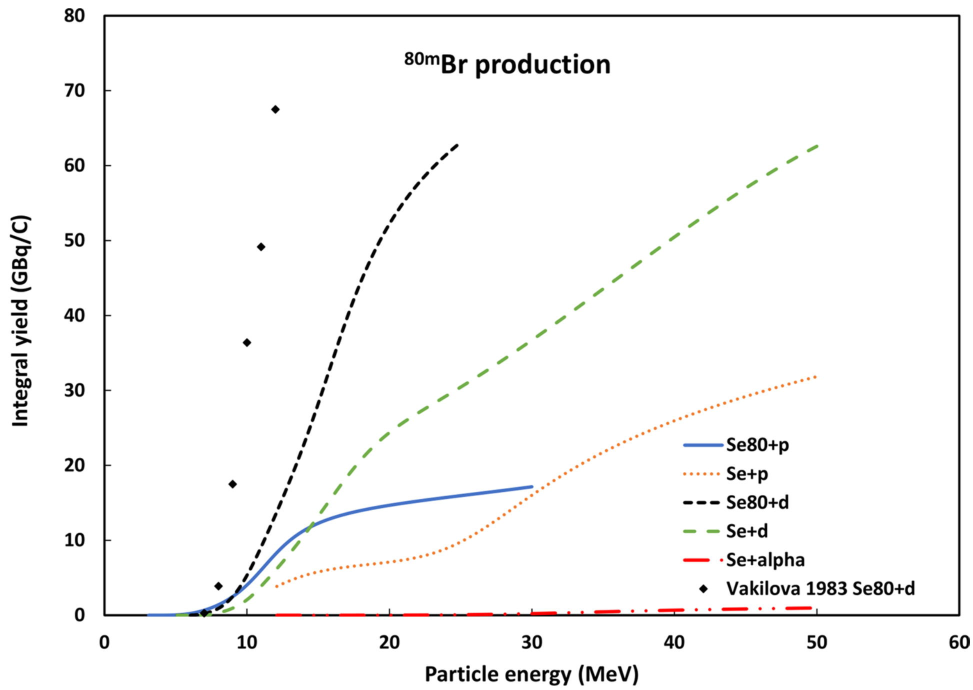

Fig. 62 Yield calculated from the recommended cross sections for ^{80m}Br production

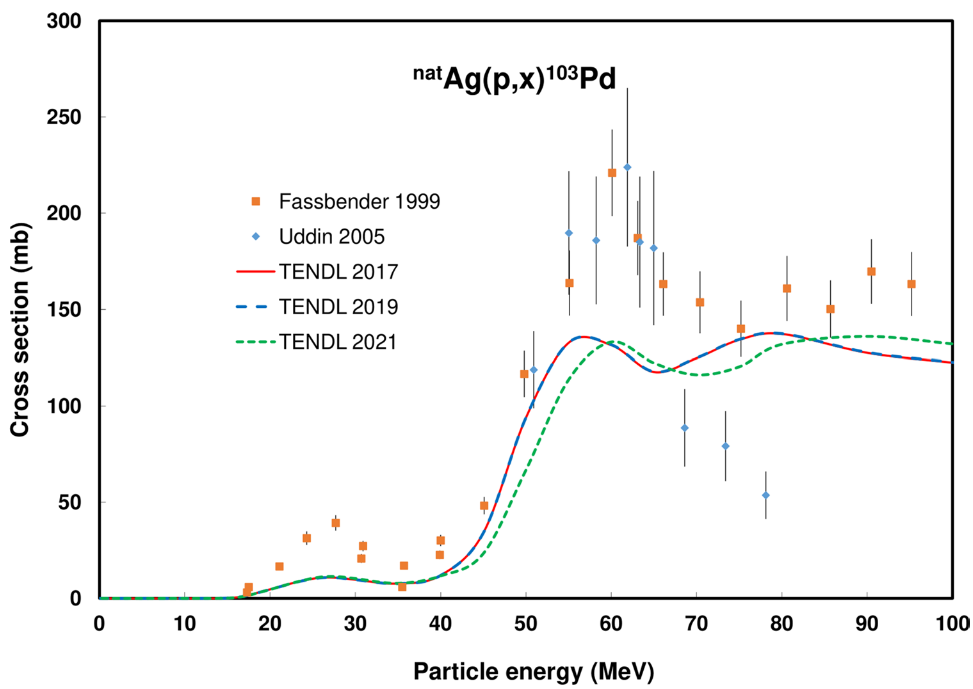

Fig. 63 $^{nat}Ag(p,x)^{103}Pd$ reaction: all experimental data and the TENDL theoretical excitation functions

($T_{1/2}$ = 4.76 d). The decay scheme is available in [15] and decay data are displayed in Table 2.

Evaluated nuclear reactions for ^{119m}Te and ^{119}Sb formation

The $^{119}Sn(p,n)^{119}Sb$ and $^{nat}Sb(p,xn)^{119m}Te$ reactions were evaluated. For each of the $^{nat}Sb(d,xn)^{119}Sb$ (up to 49.2 MeV) and $^{nat}Sb(d,xn)^{119}Te$ (49.2 MeV) reactions four data sets exist.

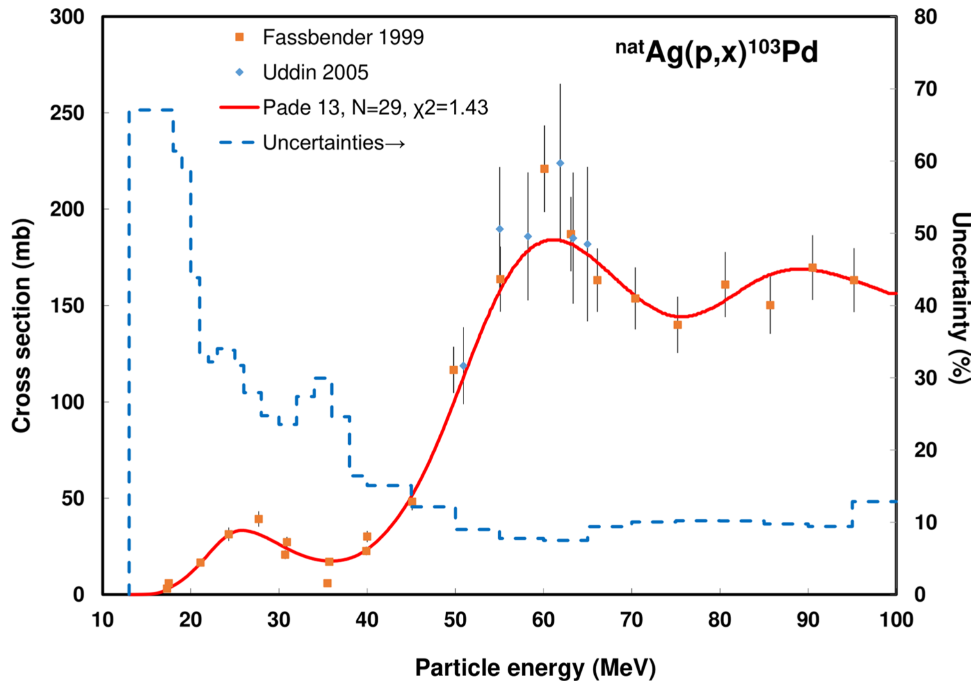

Fig. 64 $^{nat}Ag(p,x)^{103}Pd$ reaction: selected experimental works and Padé fit (solid line) with total derived uncertainties, including 4% systematic uncertainty (dashed line, right-hand scale)

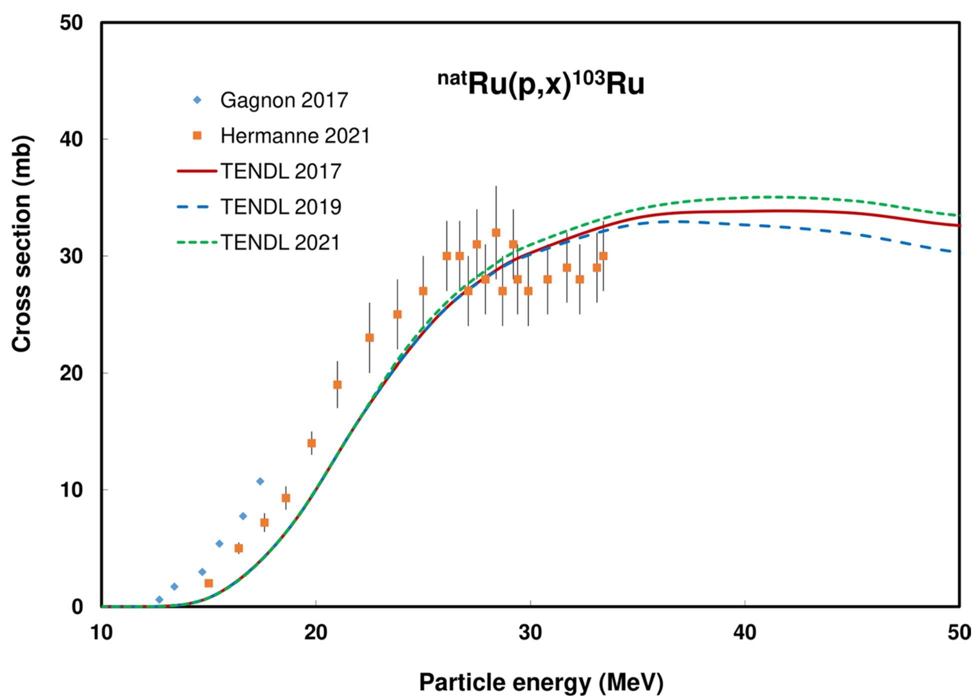

Fig. 65 $^{nat}Ru(p,x)^{103}Ru$ reaction: all experimental data and the TENDL theoretical excitation functions

$^{119}Sn(p,n)^{119}Sb$ Four data sets were found: Klyucharev [134], Johnson [135], Lovchikova [136] and Thisgaard [137]. The Klyucharev [134] data were published as relative and were normalized to the data of Johnson [135]. All available data and the theoretical predictions are shown in Fig. 87, the Padé fit on the selected data in Fig. 88, and the calculated yield in Fig. 100. No experimental yield data were found.

$^{nat}Sb(p,xn)^{119m}Te$ Four experimental data sets are presently available: Lagunas-Solar [138], Yi [139], Takács [131] and Mosby [132] (Fig. 89). All Yi [139] data were deselected because of outlying values in the 35–40 MeV region The Lagunas-Solar [138] data show a strong upward energy shift when compared to the two remaining sets and to the TENDL predictions. is seen for. As this set contains the only data available at high energies they were normalized

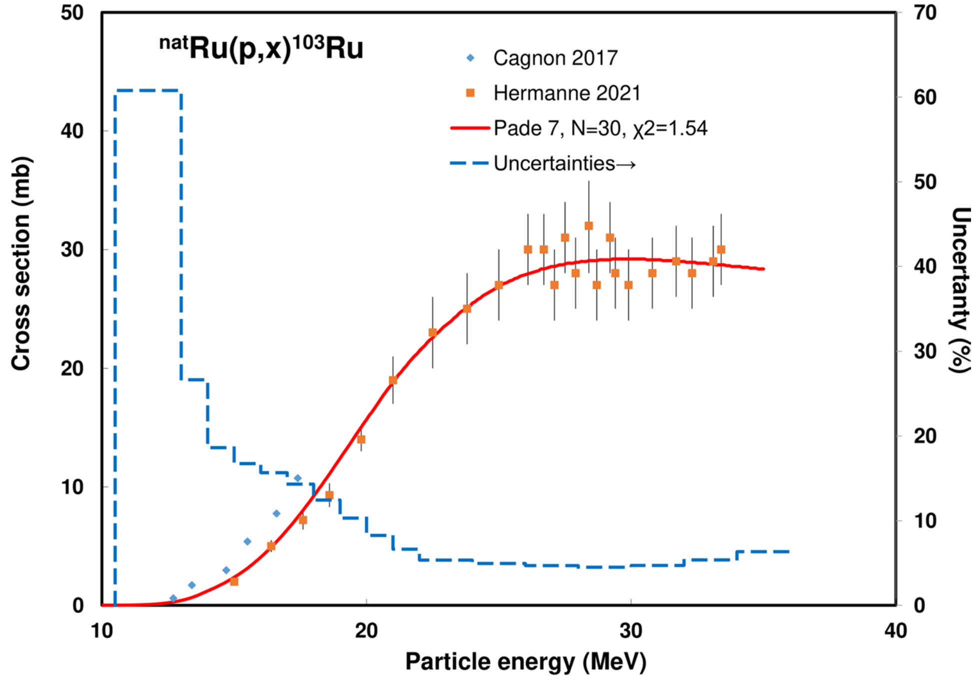

Fig. 66 $^{nat}Ru(p,x)^{103}Ru$ reaction: selected experimental works and Padé fit (solid line) with total derived uncertainties, including 4% systematic uncertainty (dashed line, right-hand scale)

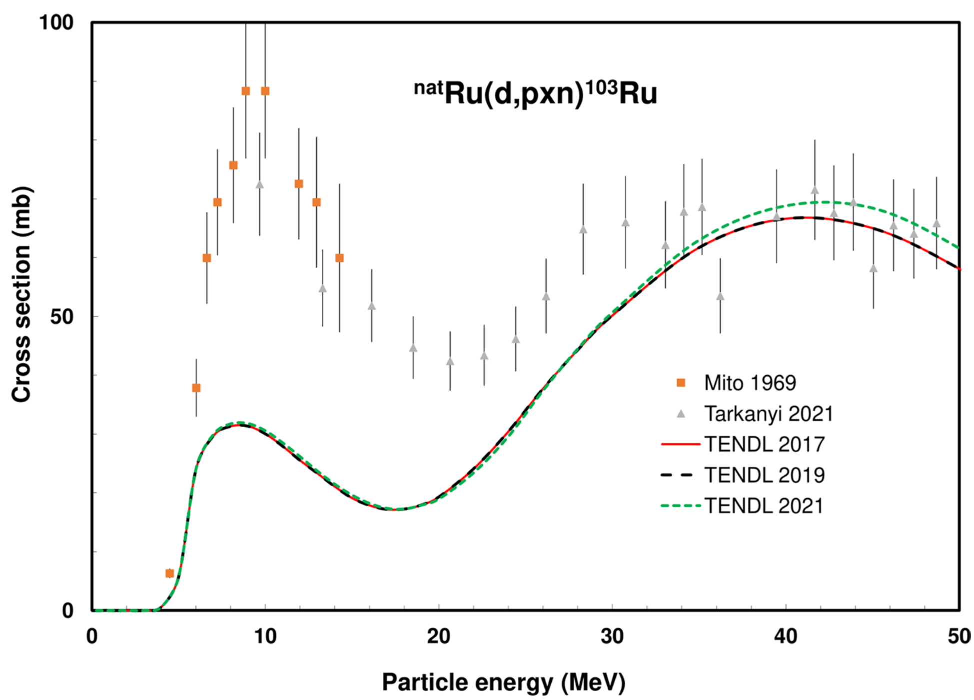

Fig. 67 $^{nat}Ru(d,x)^{103}Ru$ reaction: all experimental data and the TENDL theoretical excitation functions

to recent data (multiplied by a factor of 1.4) and energy corrected via a linear energy shift down to the threshold. The selected data and the Padé fit are shown in Fig. 90, and the calculated integral yield in Fig. 91. Lagunas-Solar [138] reported experimental integral yield data.

Integral yields for ^{119}Sb and ^{139}Te formation Integral yields of reactions related to the production of ^{119}Sb and ^{139}Te are deduced from the recommended values obtained from Padé fittings and are shown in Fig. 91.

$^{134}Ce/^{134}La$ production

The radio-isotope ^{134}Ce ($T_{1/2}$ = 3.16 d) decays for 100% by EC (accompanied by Auger electrons interesting for therapy) to ^{134}La ($T_{1/2}$ = 6.45 min, 100% β^+, 2.7 MeV β^+). It combines

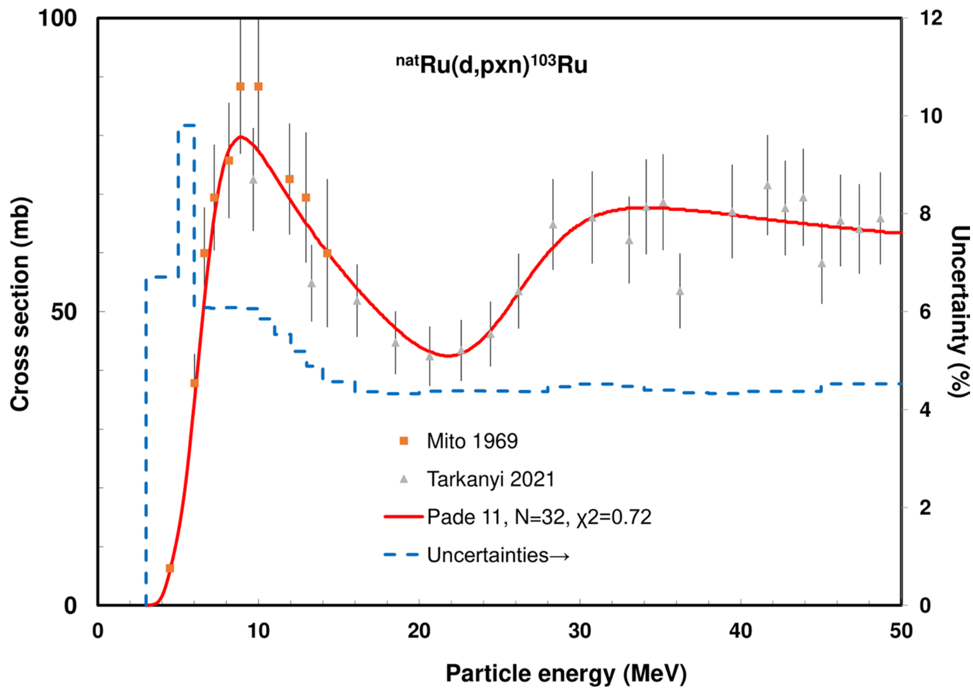

Fig. 68 ${}^{nat}Ru(d,x){}^{103}Ru$ reaction: selected experimental works and Padé fit (solid line) with total derived uncertainties, including 4% systematic uncertainty (dashed line, right-hand scale)

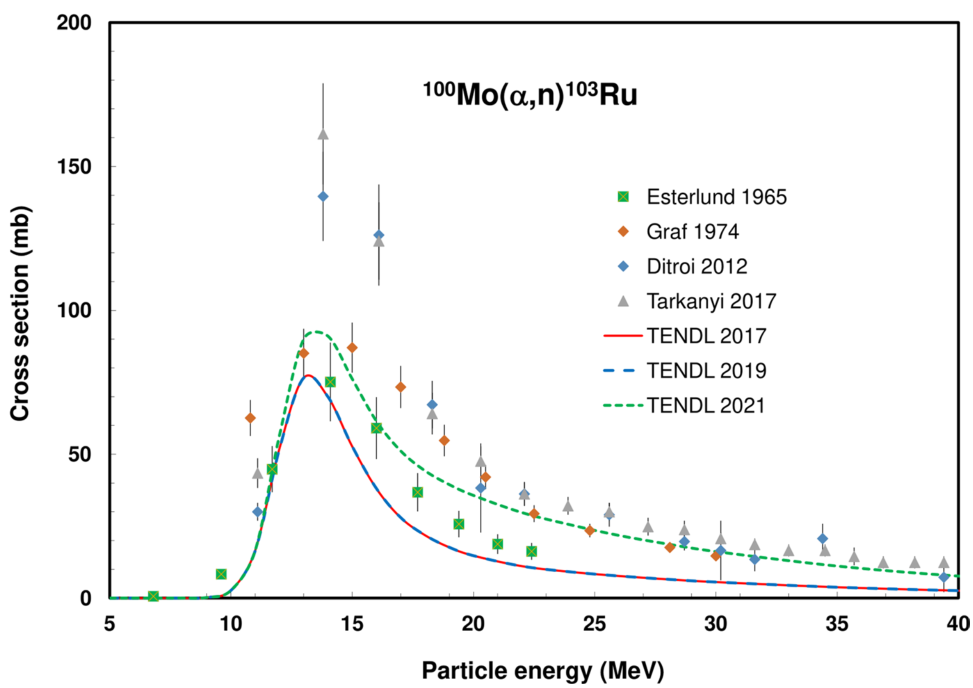

Fig. 69 ${}^{100}Mo(\alpha,n){}^{103}Ru$ reaction: all experimental data and the TENDL theoretical excitation functions

the emission of high-energy beta particles with Auger electrons and can be called a PET “in vivo generator”. The decay schemes are available in [15] and decay data are displayed in Table 2.

Evaluated nuclear reaction for ${}^{134}Ce$ formation

The ${}^{139}La(p,6n){}^{134}C$ e reaction was evaluated.

${}^{139}La(p,6n){}^{134}Ce$ We found 3 experimental sets published by Tárkányi [140], Morell [141] and Becker [142]. All sets were selected and are shown in Fig. 92 with TENDL

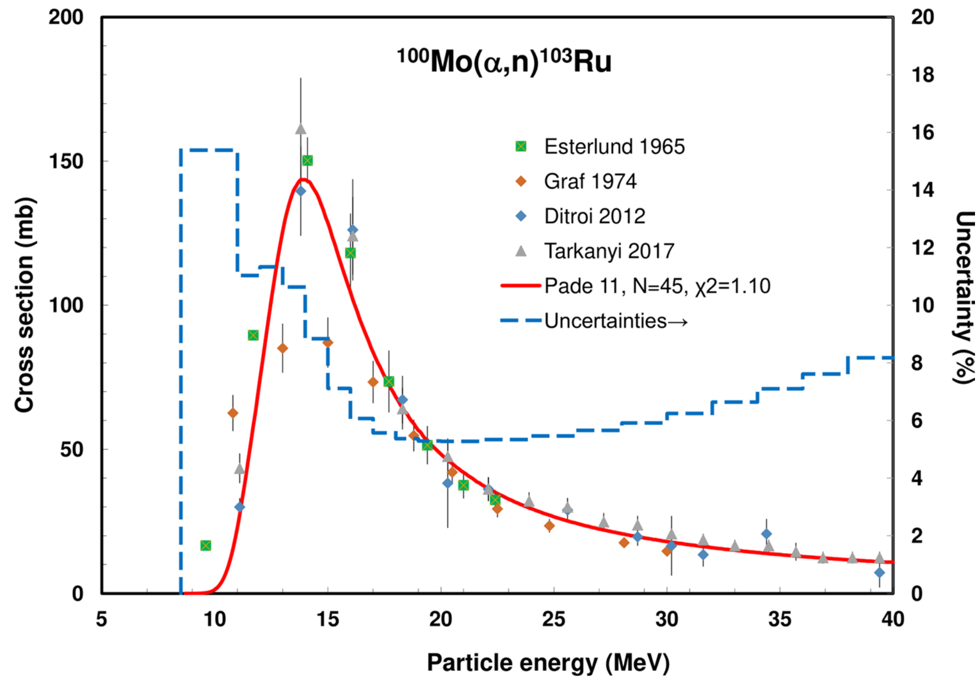

Fig. 70 ^{100}Mo(α,n)^{103}Ru reaction: selected experimental works and Padé fit (solid line) with total derived uncertainties, including 4% systematic uncertainty (dashed line, right-hand scale)

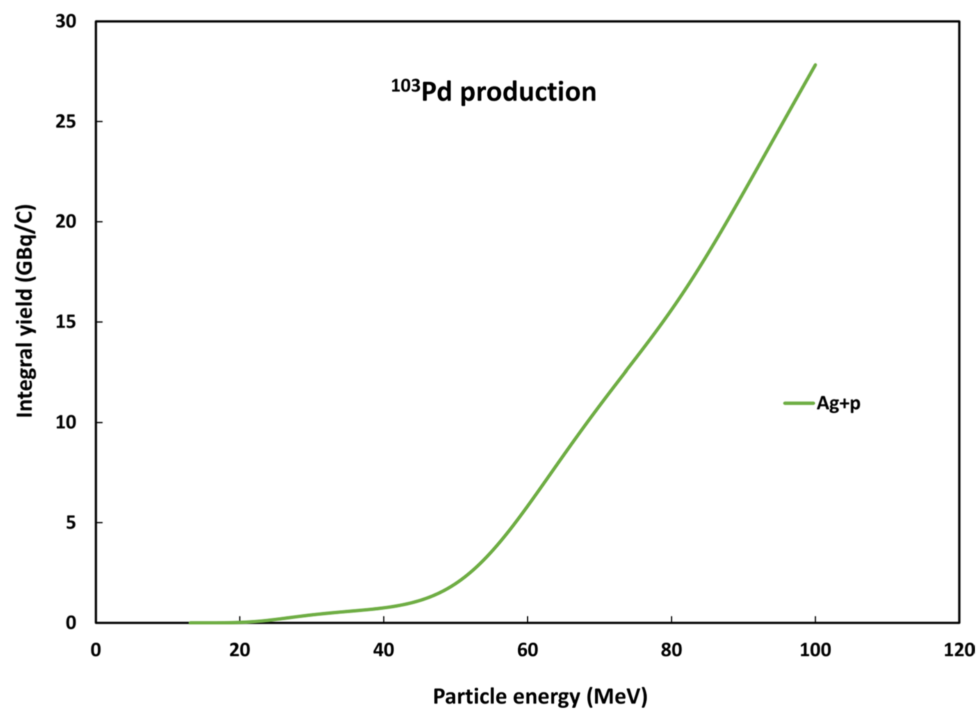

Fig. 71 Yield calculated from the recommended cross sections for ^{103}Pd production

predictions and in Fig. 93 with the Padé fit. The yield data are presented in Fig. 94. No experimental yields were found in the literature.

Integral yields for ^{134}Ce formation Integral yield of the ^{139}La(p,6n)^{134}Ce reaction is deduced from the recommended values obtained from Padé fitting and is shown in Fig. 94.

^{135}La production

^{135}La ($T_{1/2}$ = 19.5 h) decays for 100% to stable ^{135}Ba by electron capture and has favorable nuclear and chemical properties for Auger-based targeted internal radiotherapy. The decay scheme is available in [15] and decay data are displayed in Table 2.

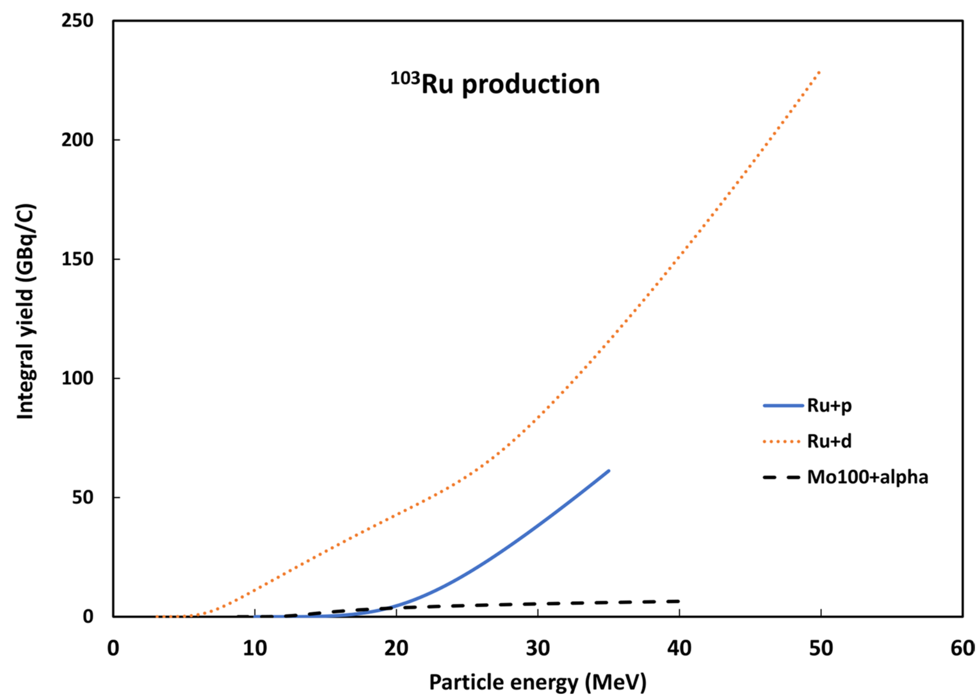

Fig. 72 Yield calculated from the recommended cross sections for ^{103}Ru production

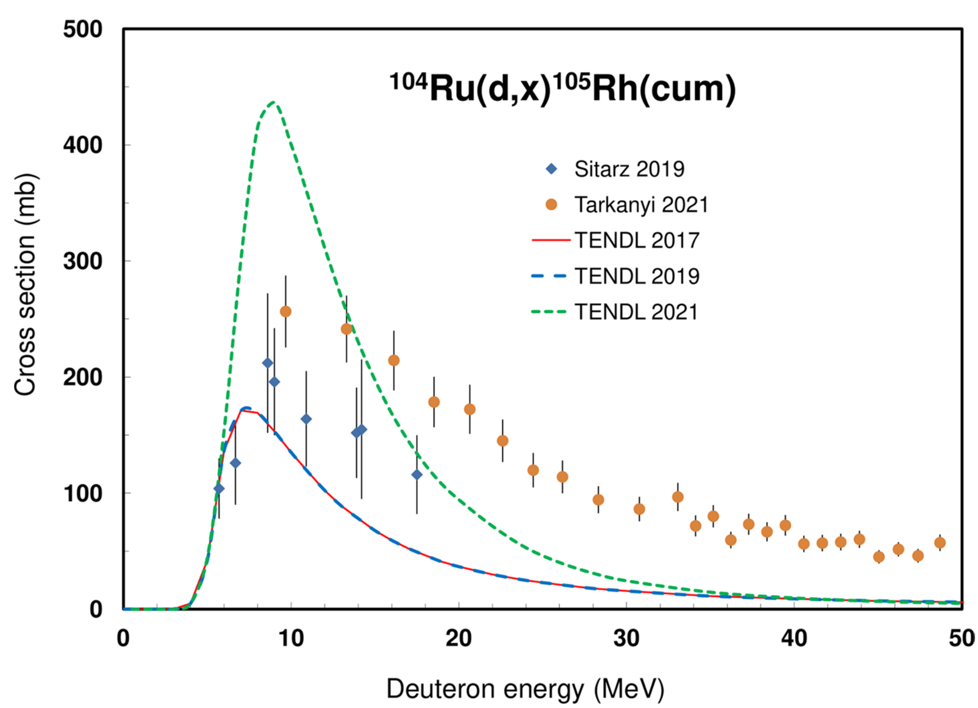

Fig. 73 ^{104}Ru(d,n)^{105}Rh reaction: all experimental data and the TENDL theoretical excitation functions

Evaluated nuclear reaction for ^{135}La formation

The ^{data} (p,xn)^{135}La reaction was evaluated. For the ^{nat}Ba(d,x)^{135}La reaction only a single experimental data set (up to 49.37 MeV) is available.

^{nat}Ba(p,xn)^{135}La Two data sets published by Prescher [143] and Tárkányi [144] were found. Both sets were selected. The experimental and theoretical cross sections are shown in Fig. 95, the Padé fit In Fig. 96 while the calculated yields are seen in Fig. 97. Dmitriev [43] reported experimental integral yield data.

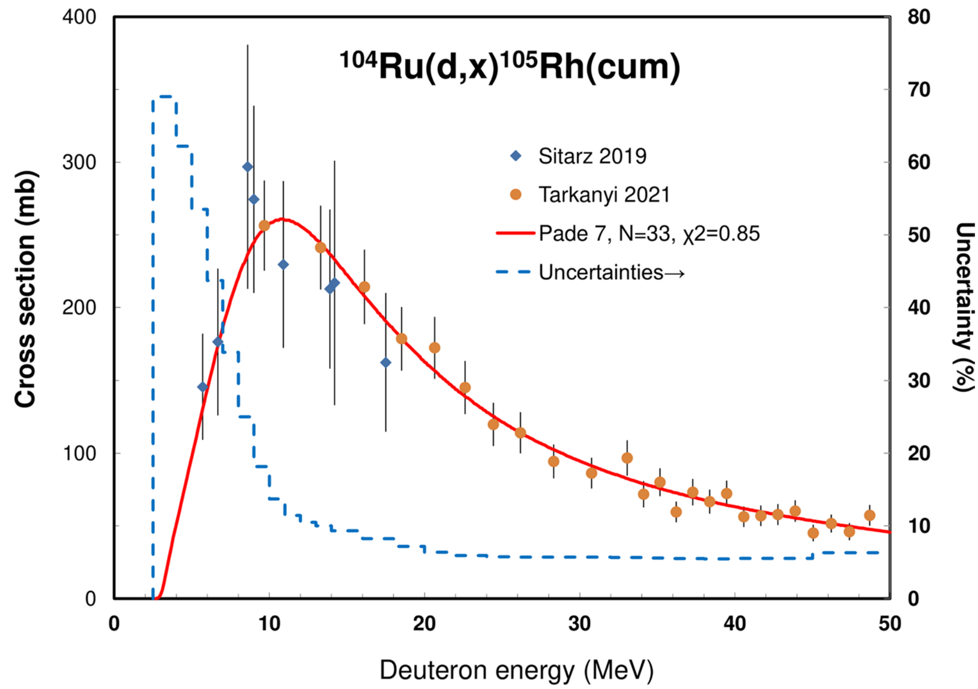

Fig. 74 ^{104}Ru(d,n)^{105}Rh reaction: selected experimental works and Padé fit (solid line) with total derived uncertainties, including 4% systematic uncertainty (dashed line, right-hand scale)

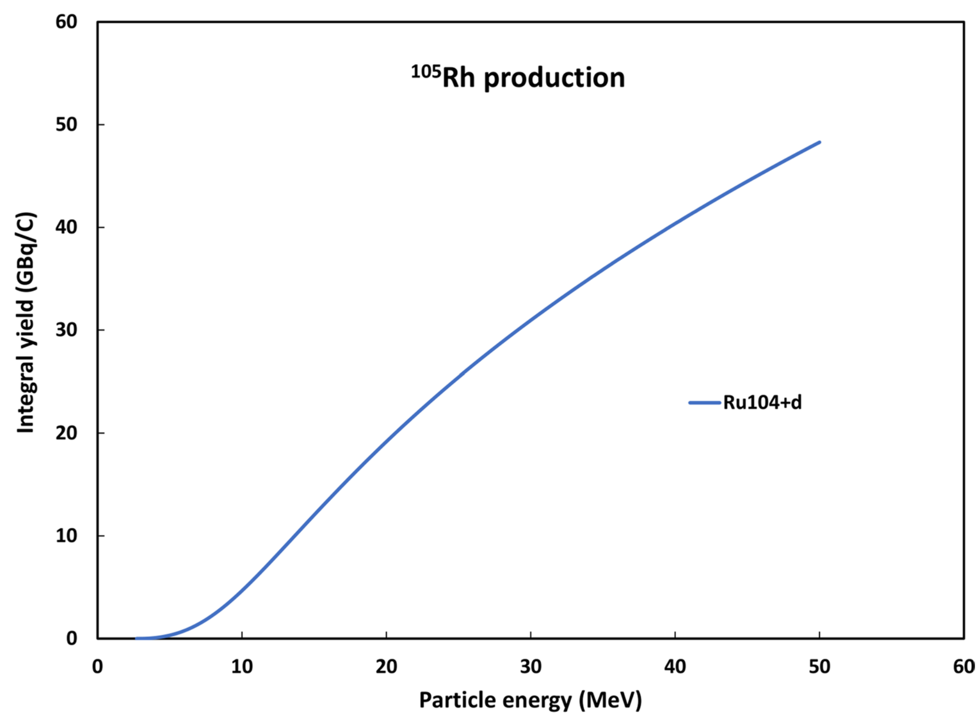

Fig. 75 Yield, calculated from the recommended cross sections for ^{105}Rh production

Integral yields for ^{135}La formation Integral yield of the ^{nat}Ba(p,xn)^{135}La reaction is deduced from the recommended values obtained from Padé fitting and are shown in Fig. 97.

^{149g}Tb production

The ground state of ^{149}Tb (^{149g}Tb, $T_{1/2}$ = 4.118 h) has a complex decay pattern (EC 83.3%; α 16.7%; $E_α$ 3970 keV). As a high-energy alpha-emitter, it has great potential application for radiotherapy.

^{149g}Tb can be obtained in direct nuclear reactions and as an "in production equilibrium" decay product of short-lived

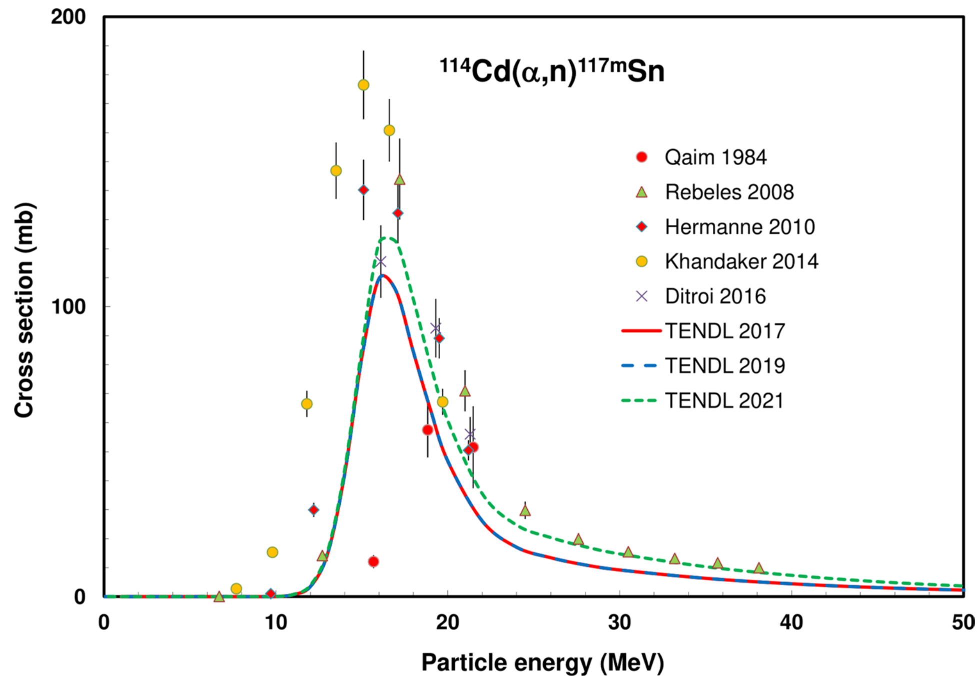

Fig. 76 ^{114}Cd(α,n)^{117m}Sn reaction: all experimental data and the TENDL theoretical excitation functions

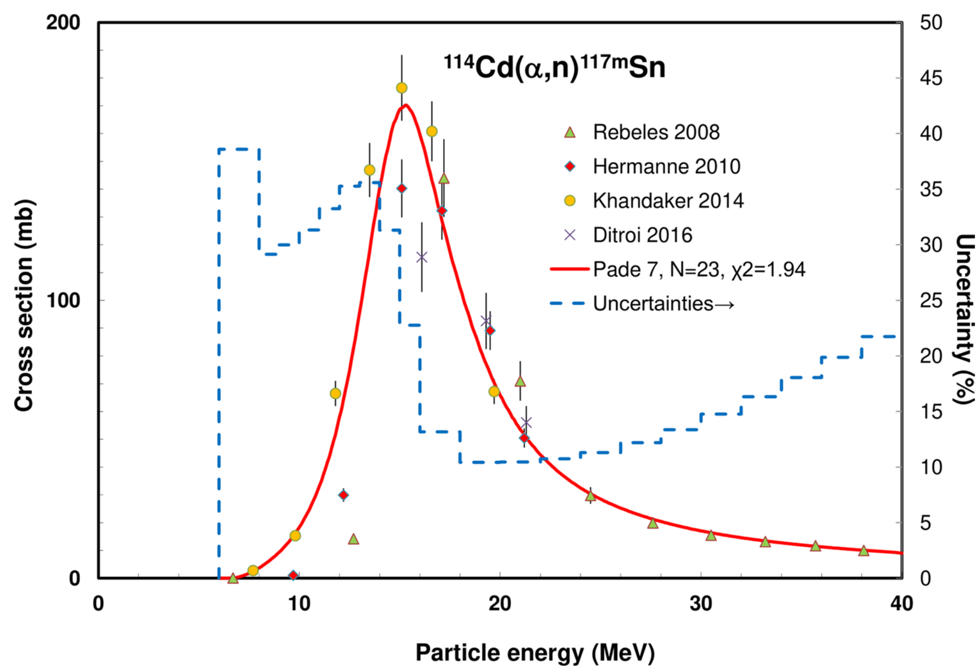

Fig. 77 ^{114}Cd(α,n)^{117m}Sn reaction: selected experimental works and Padé fit (solid line) with total derived uncertainties, including 4% systematic uncertainty (dashed line, right-hand scale)

^{149m,g}Dy (half-lives of 0.5 s and 4.2 min). The decay scheme is available in [15] and decay data are displayed in Table 2.

Evaluated nuclear reaction for ^{149} Tb formation

The ^{nat}Gd(p,xn)^{149g}Tb reaction was evaluated. For the ^{152}Gd(p,xn)^{149} Tb reaction (threshold of 62.5 MeV) only a single experimental data set exists.

^{nat}Gd(p,xn)^{149}Tb Three data sets are reported in literature: Mironov [145], Steyn [146] and Formento-Cavaier [147]. Mironov data [145] were energy shifted. All data and the comparison with disagreeing theoretical TENDL predictions are shown in Fig. 98. The selected data and Padé fit are displayed in Fig. 99, and the Padé fit based integral yield in Fig. 100. No experimental yield values were found.

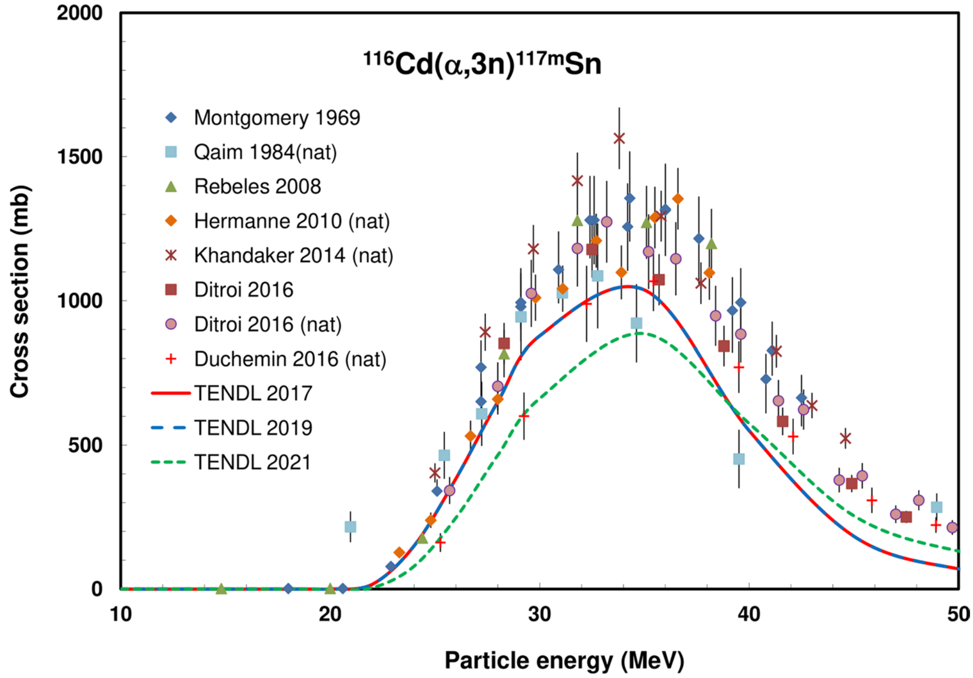

Fig. 78 ^{116}Cd(α,3n)^{117m}Sn reaction: all experimental data and the TENDL theoretical excitation functions

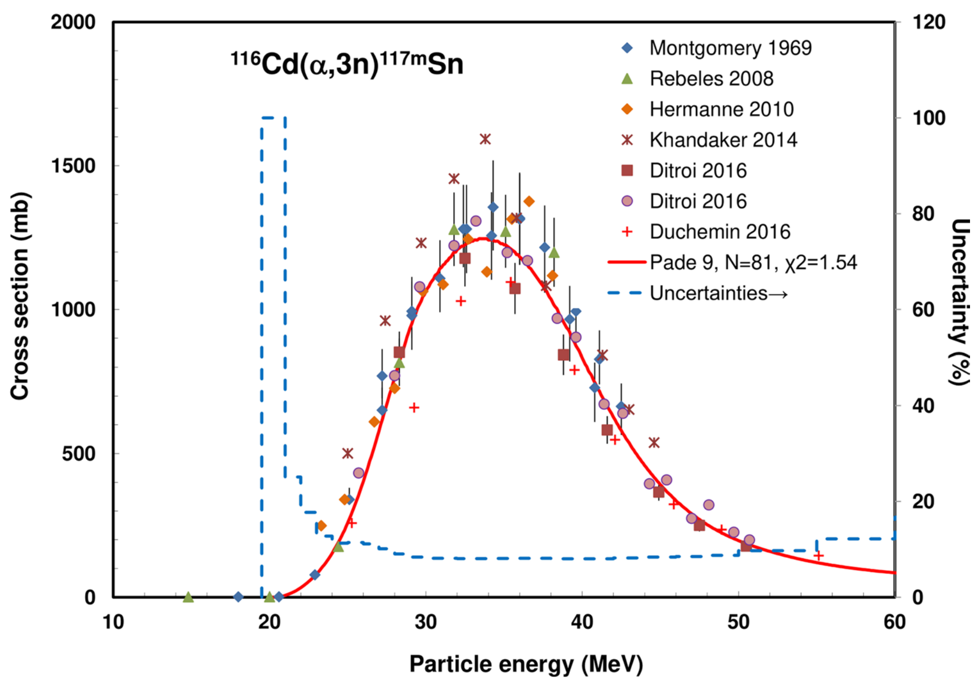

Fig. 79 ^{116}Cd(α,3n)^{117m}Sn reaction: selected experimental works and Padé fit (solid line) with total derived uncertainties, including 4% systematic uncertainty (dashed line, right-hand scale)

Integral yields for ^{149}Tb formation Integral yield of the ^{nat}Gd(p,xn)^{149}Gd reaction was deduced from the recommended values obtained from Padé fitting and is shown in Fig. 100.

^{161}Tb production

During low-energy β^{-} decay ^{161}Tb ($T_{1/2}$ = 6.89 d) emits conversion and Auger electrons making it interesting for radiotherapy. It also emits low-energy photons that could be used for SPECT imaging. The decay schemes are available in [15] and decay data are displayed in Table 2.

Evaluated nuclear reaction for ^{161} Tb formation

The ^{nat}Gd(p,xn)^{161}Tb reaction was evaluated.

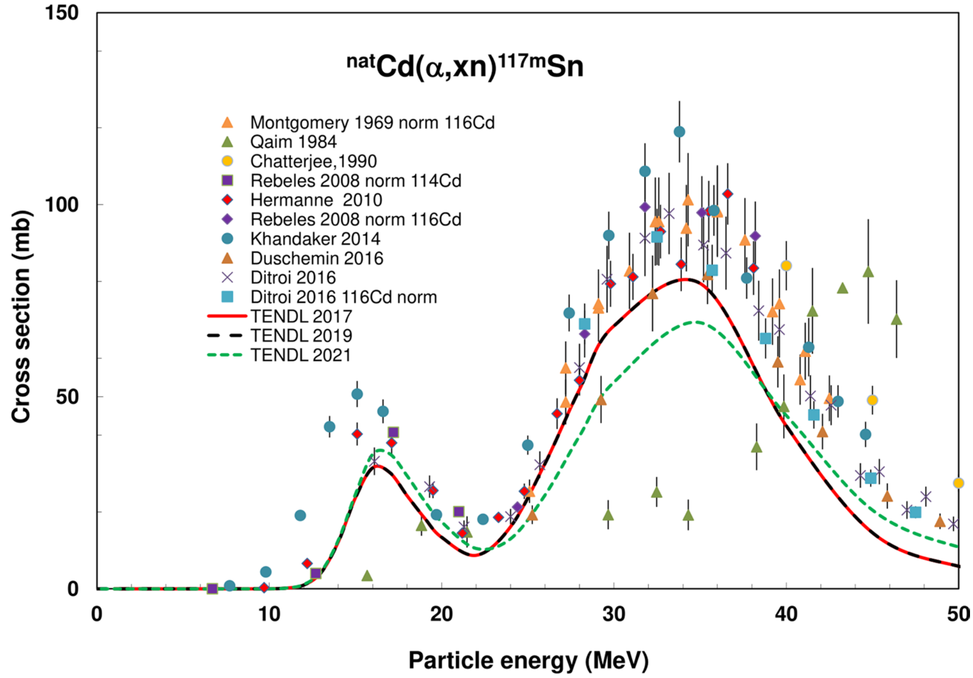

Fig. 80 $^{nat}Cd(\alpha,xn)^{117m}Sn$ reaction: all experimental data and the TENDL theoretical excitation functions

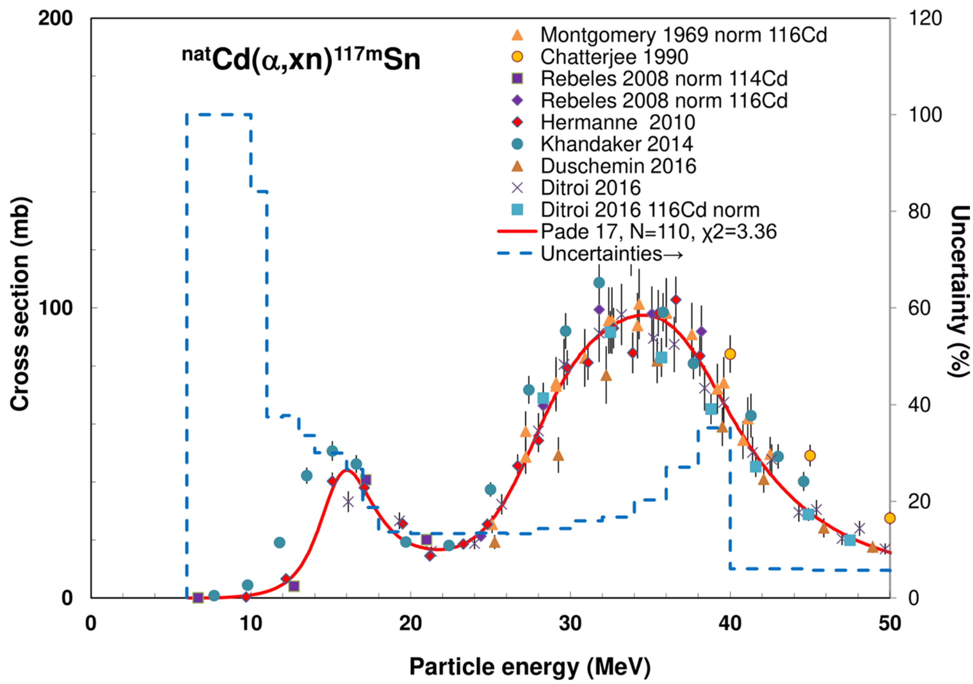

Fig. 81 $^{nat}Cd(\alpha,xn)^{117m}Sn$ reaction: selected experimental works and Padé fit (solid line) with total derived uncertainties, including 4% systematic uncertainty (dashed line, right-hand scale)

$^{160}Gd(d,n)^{161}Tb$ Two data sets are available: Tárkányi [148] and Szelecsenyi [149]. The data show some disagreement. In Tárkányi [148] results obtained in two irradiations at 50 MeV and 20 MeV incident deuterons are discussed and the 20 MeV irradiation shows a better agreement with the data of Szelecsenyi [149] in the 15–20 MeV energy range. All data, in comparison with TENDL predictions, are shown in Fig. 101. The selected data with the Padé fit is in Fig. 102, and the Padé fit based integral yields are in Fig. 103. No experimental yield data were found.

Integral yields for ^{161}Tb formation Integral yield of the $^{160}Gd(d,n)^{161}Tb$ reaction was deduced from the recommended values obtained from Padé fitting and is shown in Fig. 103.

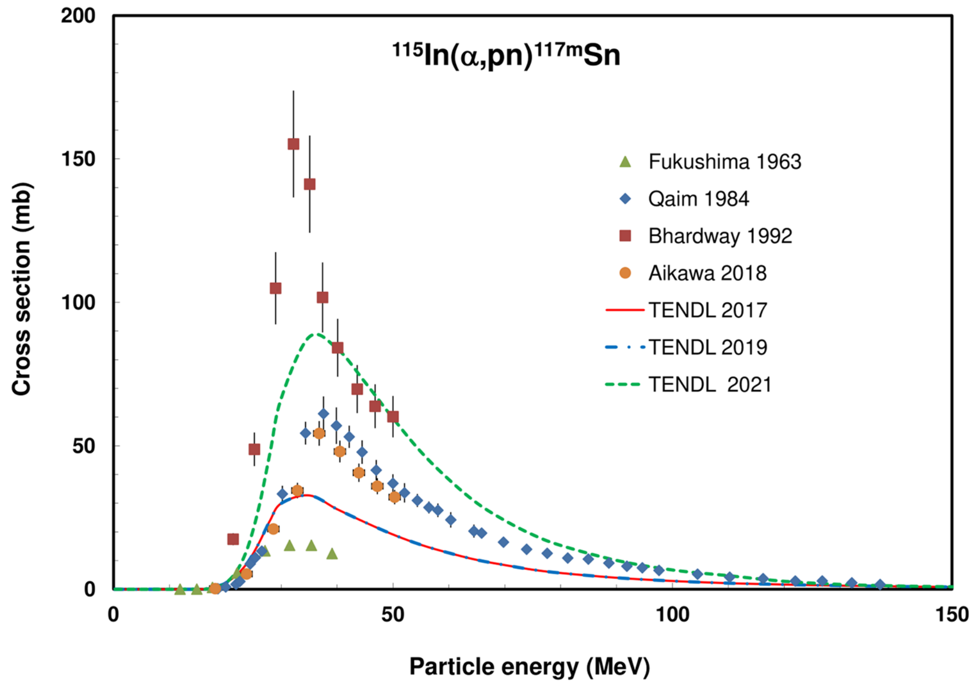

Fig. 82 ^{115}In(α,x)^{117m}Sn reaction: all experimental data and the TENDL theoretical excitation functions

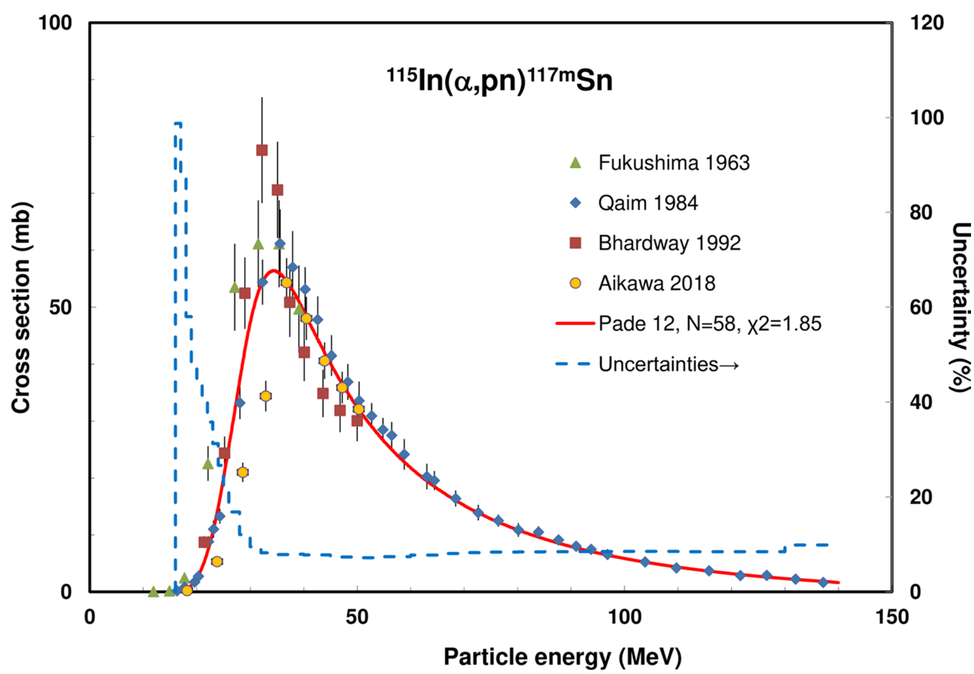

Fig. 83 ^{115}In(α,x)^{117m}Sn reaction: selected experimental works and Padé fit (solid line) with total derived uncertainties, including 4% systematic uncertainty (dashed line, right-hand scale)

^{165}Er production

As ^{165}Er ($T_{1/2}$ = 10.4 h) decays by electron capture (EC), followed by the emission of Auger electrons and low-energy X-rays, it is a candidate for targeted radionuclide therapy.

It can be produced directly and through the EC, β^+ decay of the ^{165}Tm parent ($T_{1/2}$ = 30.06 h).

Evaluated nuclear reactions for ^{165}Tm and ^{165}Er formation

The ^{165}Ho(p,n)^{165}Er, ^{166}Er(p,2n)^{165}Tm, ^{165}Ho(d,2n)^{165}Er, ^{nat}Er(p,xn)^{165}Tm, ^{nat}Er(d,xn)^{165}Tm and ^{166}Er(d,3n)^{165}Tm reactions were evaluated.

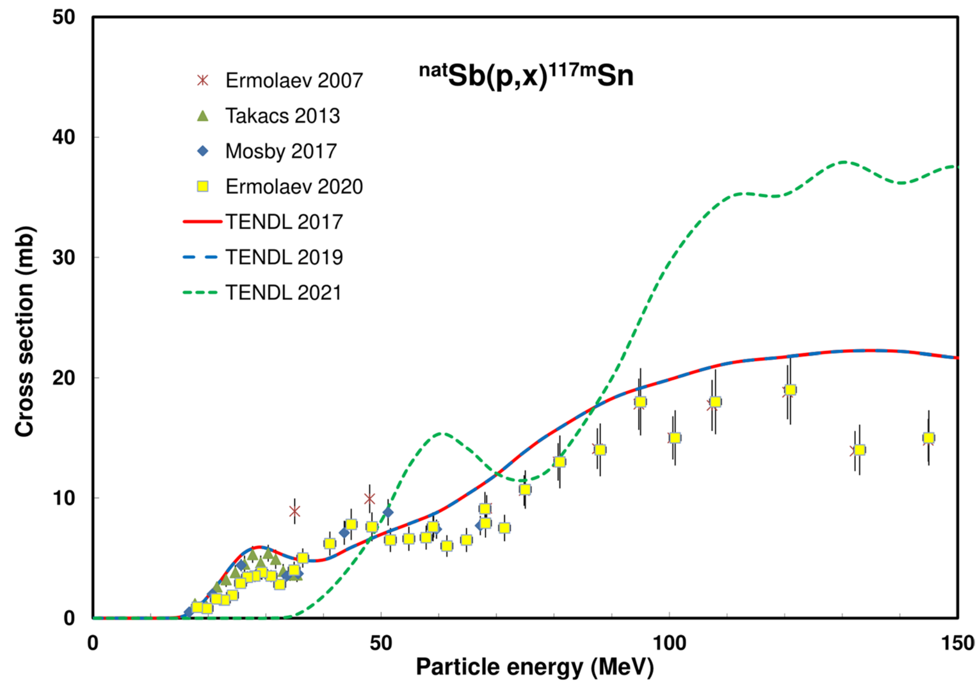

Fig. 84 $^{nat}Sb(p,x)^{117m}Sn$ reaction: all experimental data and the TENDL theoretical excitation functions

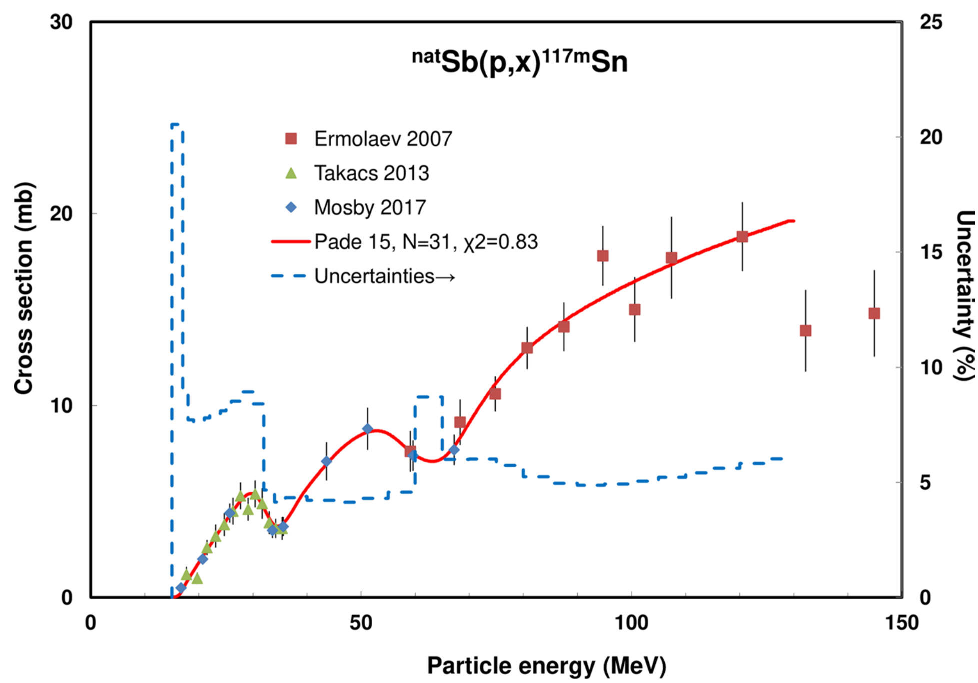

Fig. 85 $^{nat}Sb(p,x)^{117m}Sn$ reaction: selected experimental works and Padé fit (solid line) with total derived uncertainties, including 4% systematic uncertainty (dashed line, right-hand scale)

1 $^{165}Ho(p,n)^{165}Er$

Three data sets were found: Beyer [150], Tárkányi [151] and Gracheva [152]. As Beyer [150] data are energy shifted compared to the two other sets, a linear shift of the energy scale was applied. All data, in comparison with TENDL predictions, are shown in Fig. 104, the Padé fitted selected data in Fig. 105. The calculated integral yields are displayed in Fig. 116. Experimental yield data were reported in Gracheva [152].

$^{166}Er(p,2n)^{165}Tm$ Two experimental data sets obtained on ^{nat}Er targets by Tárkányi [153] and Tárkányi [154] are available in the literature and agree well. The experimental data, the comparison with the TENDL predictions and the Padé fit are shown in Figs. 106 and 107. The calculated yield is

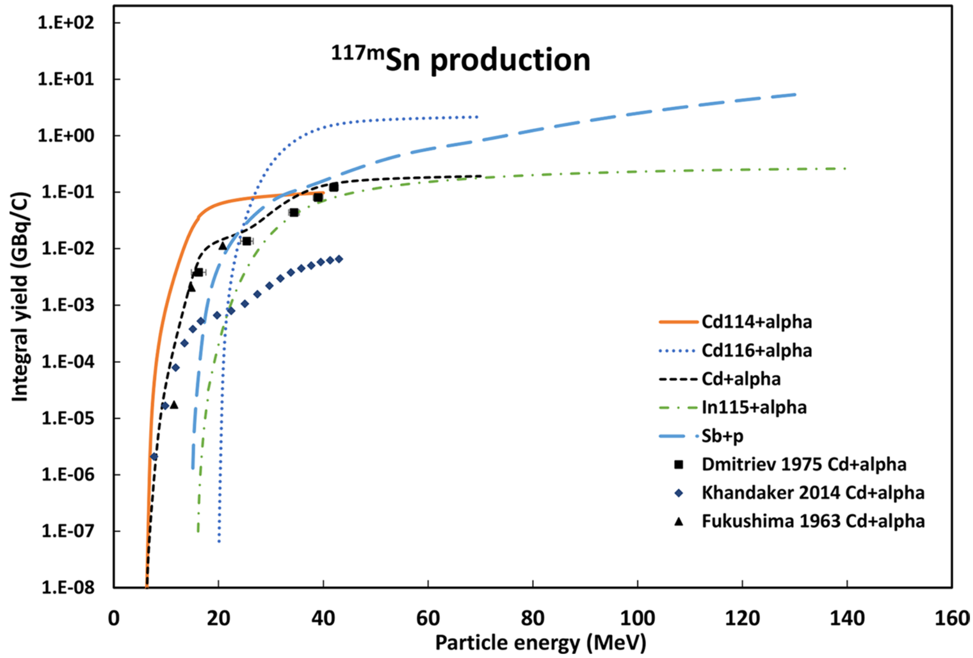

Fig. 86 Yield calculated from the recommended cross sections for ^{117m}Sn production

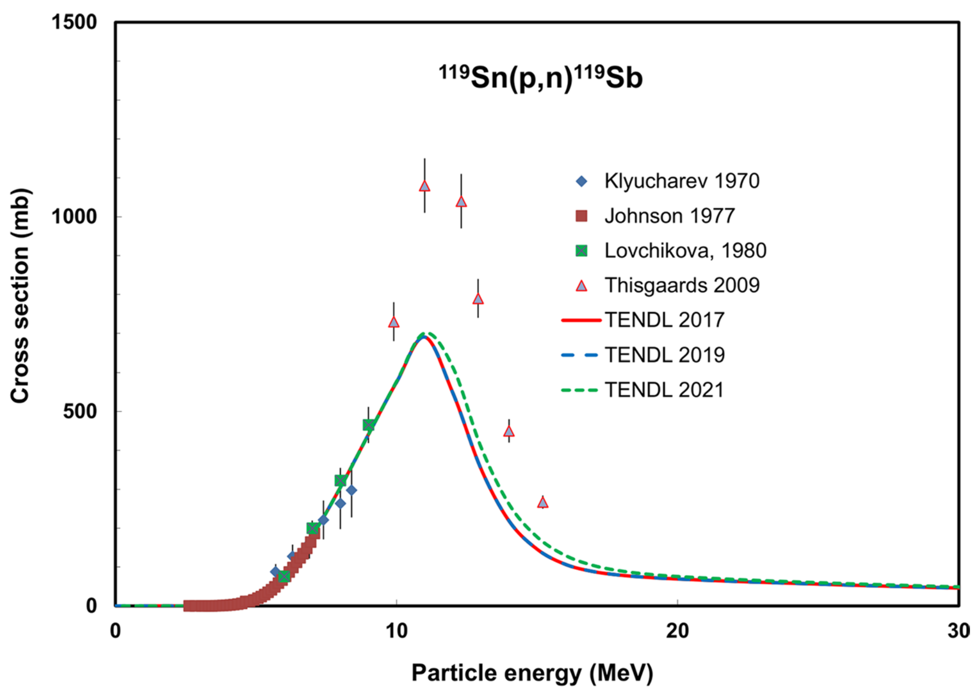

Fig. 87 ^{119}Sn(p,n)^{119}Sb reaction: all experimental data and the TENDL theoretical excitation functions

displayed in Fig. 115. Dmitriev [43] reported experimental thick target yields.

^{165}Ho(d,2n)^{165}Er Two data sets were reported for the ^{165}Ho(d,2n)^{165}Er reaction cross sections by Tárkányi [155] and Hermanne [156]. The outlying data points at 25.2 and 27.3 MeV of Hermanne 2013 [156] were deselected. The original data, with comparison to the TENDL theoretical excitation functions, are in Fig. 108 while the selected data and Padé fit are shown in Fig. 109. The integral yields calculated from the recommended cross sections obtained from the fitted curve are shown in Fig. 116. No experimental yield data were found.

^{nat}Er(p,xn)^{165}Tm Two data sets are available: Tárkányi [153] and Song [157]. Both sets were selected and presented, in comparison with TENDL predictions, in Fig. 110 and with Padé fit in Fig. 111. The calculated integral yields are dis-

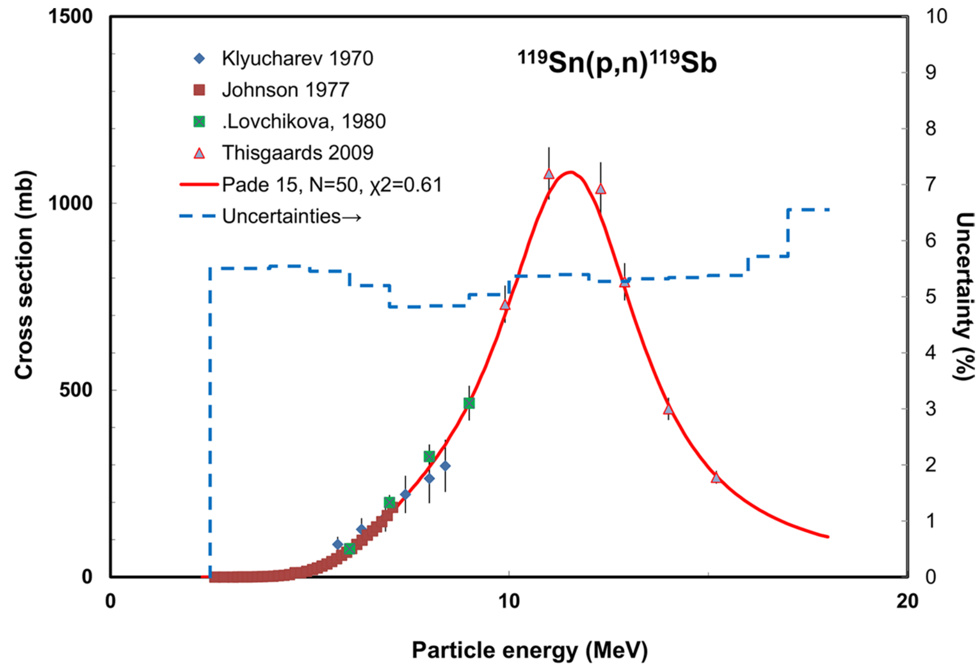

Fig. 88 ^{119}Sn(p,n)^{119}Sb reaction: selected experimental works and Padé fit (solid line) with total derived uncertainties, including 4% systematic uncertainty (dashed line, right-hand scale)

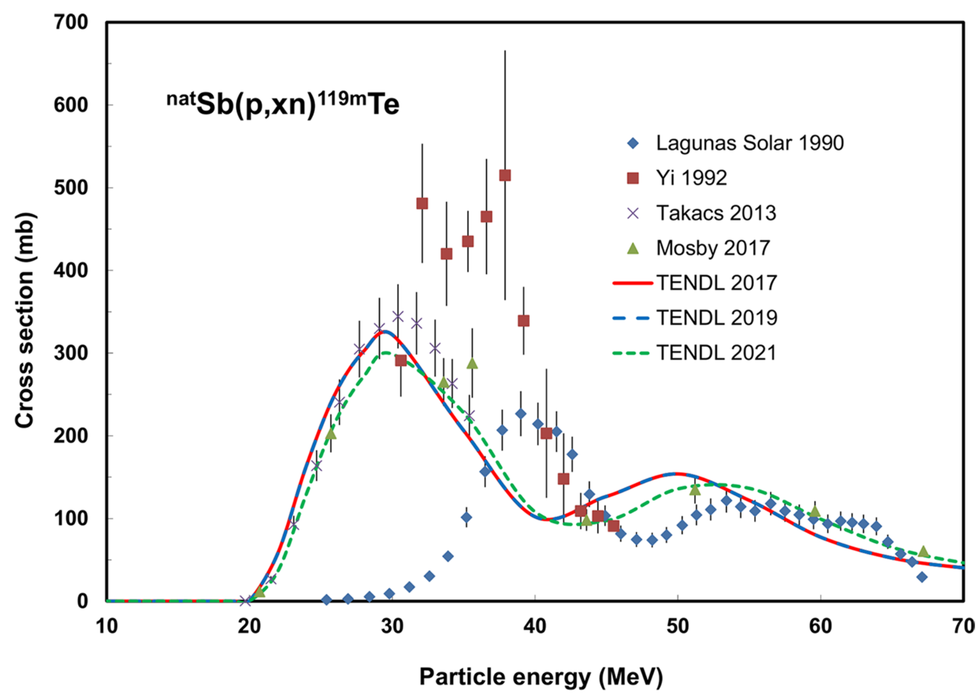

Fig. 89 ^{nat}Sb(p,xn)^{119m}Te reaction: all experimental data and the TENDL theoretical excitation functions

played in Fig. 115. Experimental yields were measured and published by Dmitriev [158] and Dmitriev [43].

^{nat}Er(d,xn)^{165}Tm Three data sets were found: Tárkányi [159], Tárkányi [160] and Khandaker [161]. All data were selected and are shown, in comparison with TENDL predictions, in Fig. 112 and with Padé fit in Fig. 113. The calculated yields are presented in Fig. 115. Dmitriev reported experimental integral yield data in [158] and in [24].

^{166}Er(d,3n)^{165}Tm Only by Hermanne [162] data for the ^{166}Er(d,3n)^{165}Tm reaction were published. Two additional

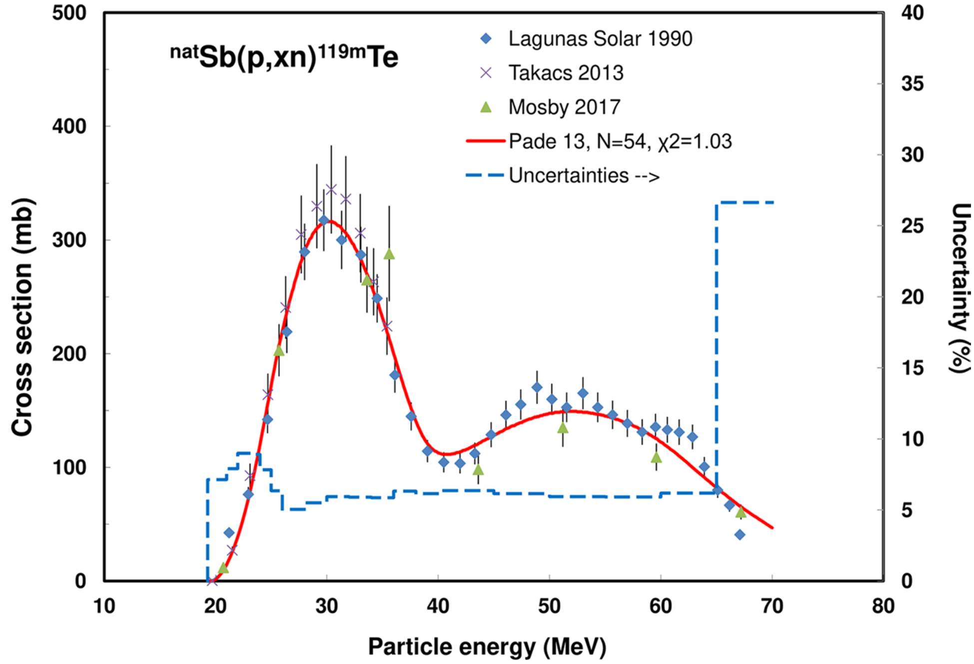

Fig. 90 ^{nat}Sb(p,xn).^{119m}Te reaction: selected experimental works and Padé fit (solid line) with total derived uncertainties, including 4% systematic uncertainty (dashed line, right-hand scale)

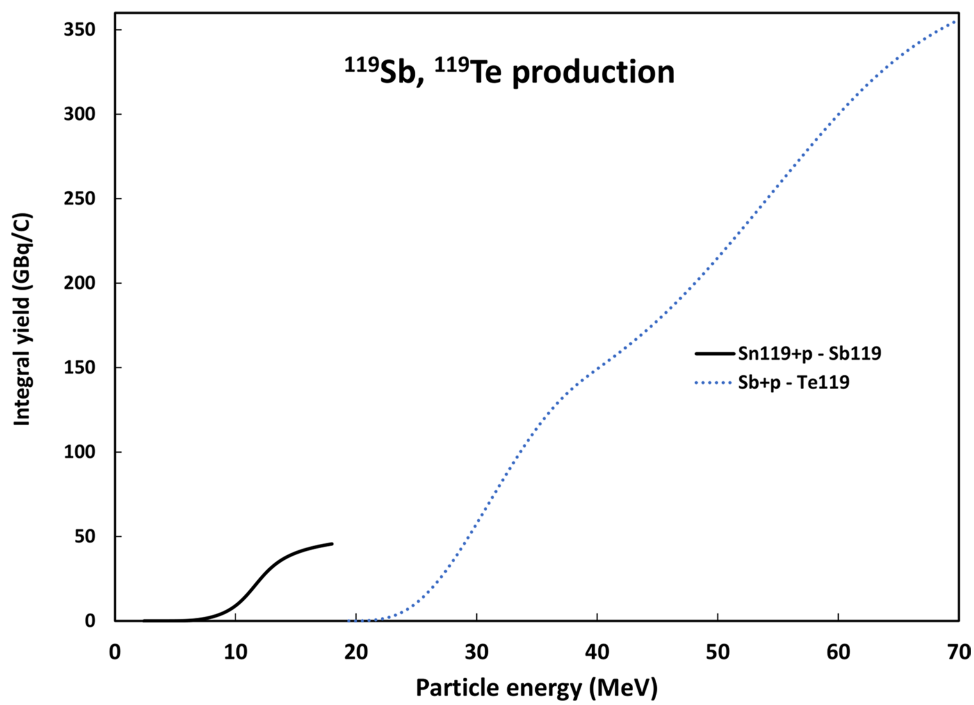

Fig. 91 Yield calculated from the recommended cross sections for ^{119}Sb and ^{119}Te production

sets were deduced from results obtained on ^{nat}Er targets by Tárkányi [159] and Khandaker [161] after subtracting the weak ^{164}Er(d,n) ^{165}Tm contribution, obtained from TENDL prediction and normalization for abundance of the target isotope. Therefore, the additional data are limited up to the ^{167}Er(d,4n)^{165}Tm threshold energy of 19,720.8 keV. All these data were selected and are, in comparison with theoretical TENDL predictions, presented in Fig. 114. The Padé fit is displayed in Fig. 115, and the calculated yield data, based on the recommended values in Fig. 116. Experimental integral yield data were obtained by Dmitriev [158] and Dmitriev [43].

Integral yields for ^{165}Tm and ^{165}Er formation Integral yields of reactions related to the production of ^{165}Tm and ^{165}Er are

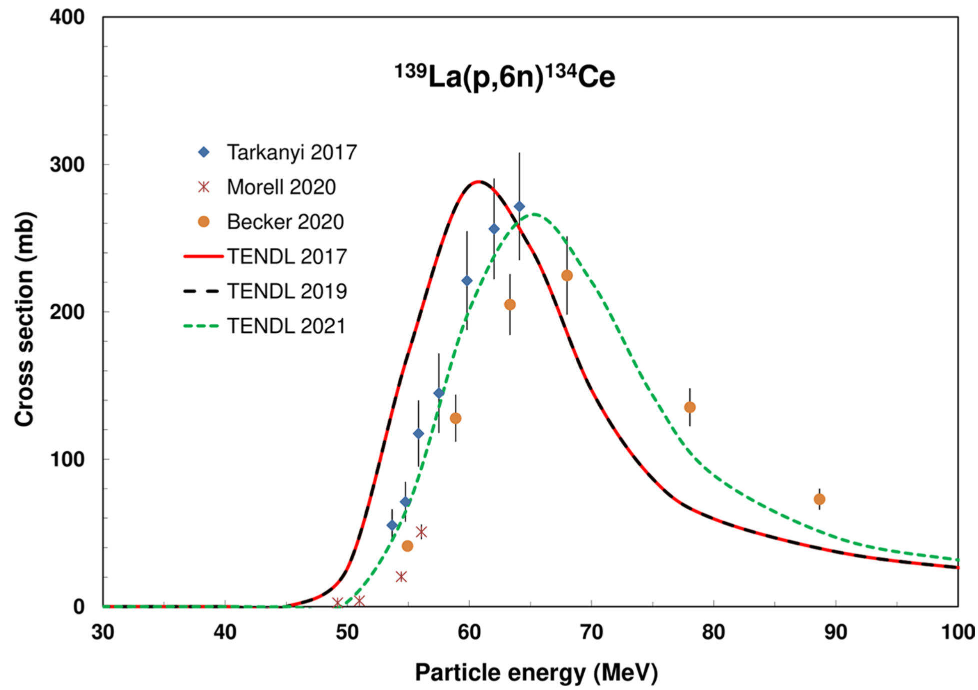

Fig. 92 ^{139}La(p,6n)^{134}Ce reaction: all experimental data and the TENDL theoretical excitation functions

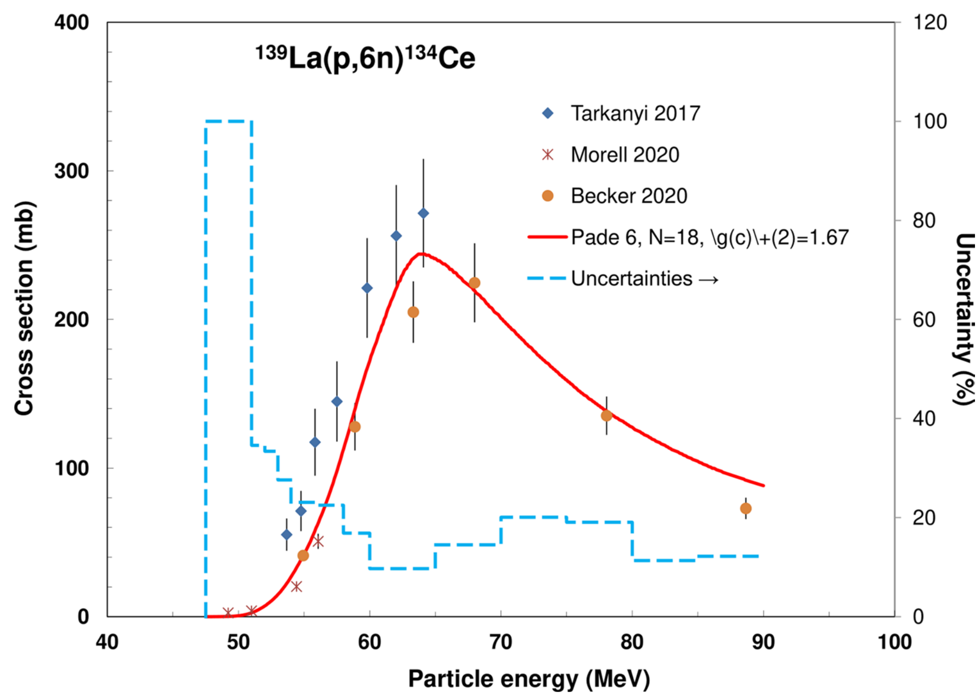

Fig. 93 ^{139}La(p,6n)^{134}Ce reaction: selected experimental works and Padé fit (solid line) with total derived uncertainties, including 4% systematic uncertainty (dashed line, right-hand scale)

deduced from the recommended values obtained from Padé fittings and are shown in Figs. 116,117.

^{167}Tm production

^{167}Tm is useful for therapy by emission of Auger-electrons ($T_{1/2}$ = 9.25 d, E_e(average) = 124.2 keV) and also for SPECT diagnostics by emitting low energy gamma lines. The decay scheme is available in [15] and decay data are displayed in Table 2.

Evaluated nuclear reactions for ^{167}Tm formation

The ^{169}Tm(p,x)^{167}Tm, ^{169}Tm(d,x)^{167}Tm, ^{nat}Er(d,xn)^{167}Tm, ^{nat}Er(p,xn)^{167}Tm, ^{167}Er(p,n)^{167}Tm and ^{165}Ho(α,2n)^{167}Tm reactions were evaluated. For the ^{nat}Yb(d,x)^{167}Tm (up to

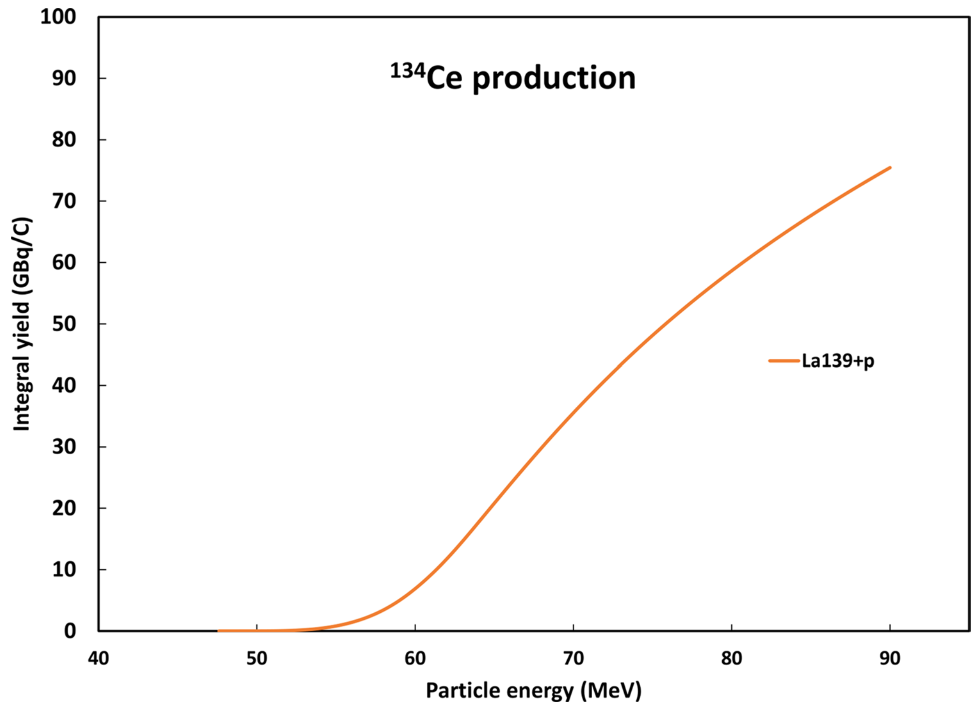

Fig. 94 Yield calculated from the recommended cross sections for ^{134}Ce production

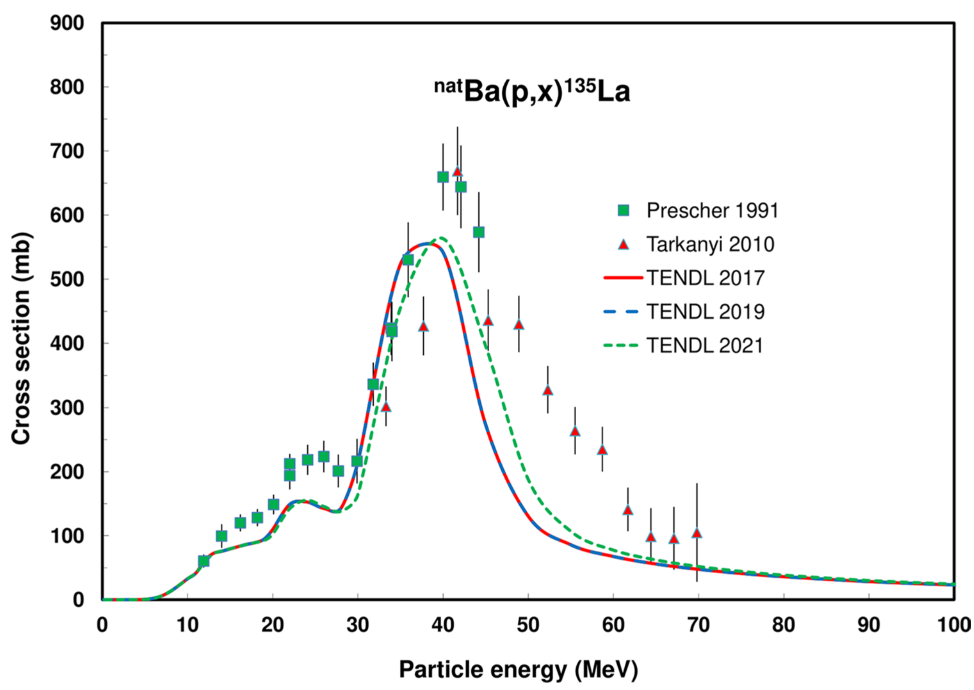

Fig. 95 ^{nat}Ba(p,xn)^{135}La reaction: all experimental data and the TENDL theoretical excitation functions

48.2 MeV) and ^{167}Er(d,2n)^{167}Tm (up to 20.4 MeV) reactions only a single data set is available.

^{169}Tm(p,x)^{167}Tm Two data sets were available and were selected: Tárkányi [163] and Saito [164]. In Saito [164] cross sections at only 3 energies, all below 20 MeV, are given.

All data and comparison with TENDL predictions are shown in Fig. 118, the Padé fit in Fig. 119, and the calculated

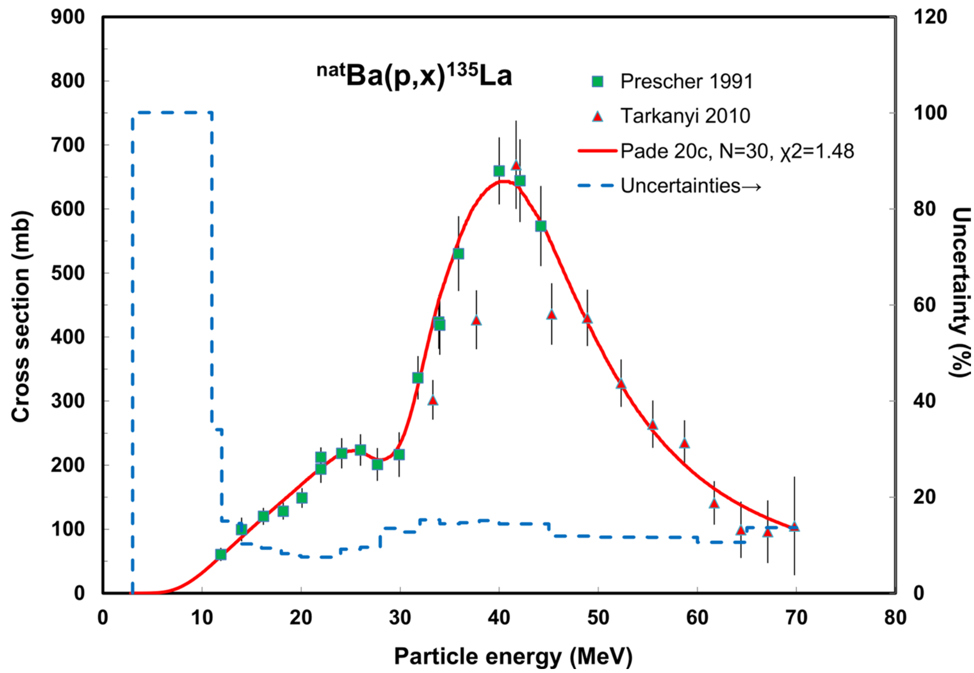

Fig. 96 $^{nat}Ba(p,xn)^{135}La$ reaction: selected experimental works and Padé fit (solid line) with total derived uncertainties, including 4% systematic uncertainty (dashed line, right-hand scale)

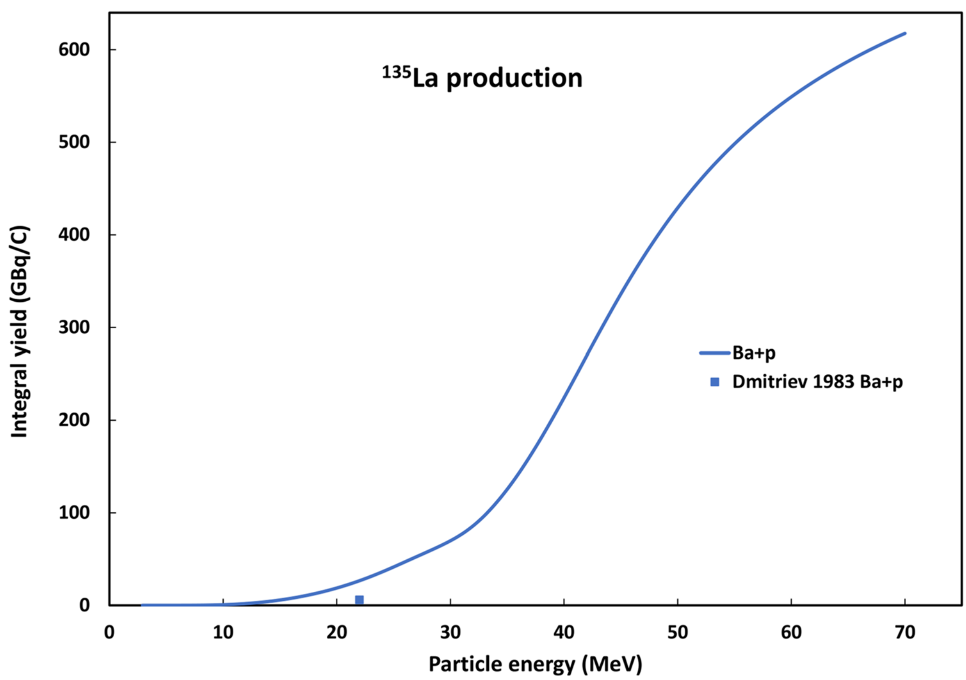

Fig. 97 Yield calculated from the recommended cross sections for ^{135}La production

integral yields in Fig. 130. No experimental yield data were found.

$^{169}Tm(d,x)^{167}Tm$ Four experimental data sets are available: Tárkányi [165], Hermanne [166], Hermanne [167] and Saito [168]. All cross sections and the predictions obtained from TENDL are shown in Fig. 120. All data were selected and Padé fitted (Fig. 121). The calculated yields are shown in Fig. 130. No experimental yield data were found.

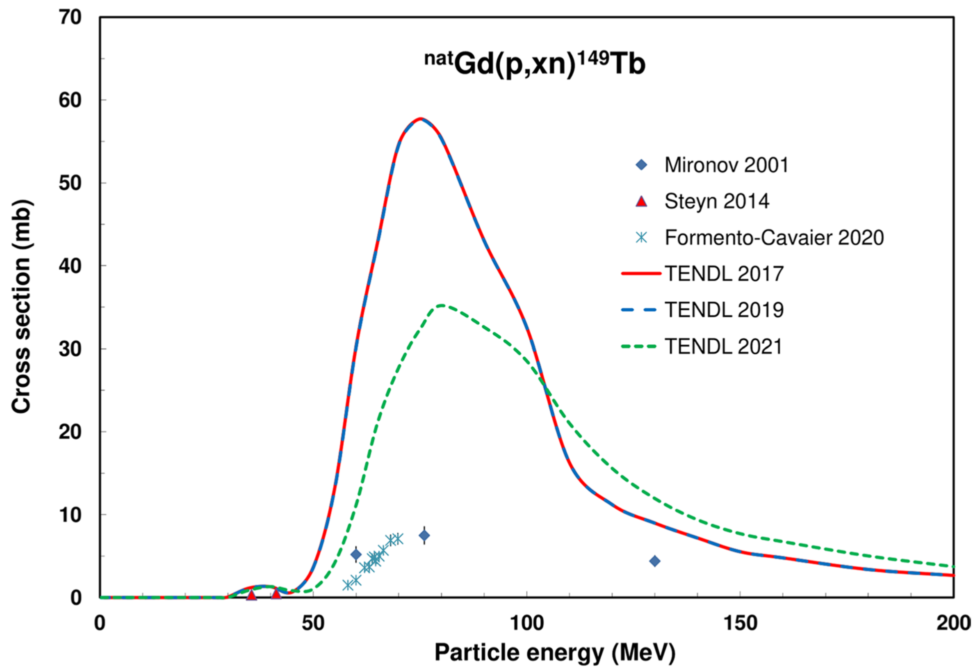

Fig. 98 ^{nat}Gd(p,xn)^{149}Tb reaction: all experimental data and the TENDL theoretical excitation functions

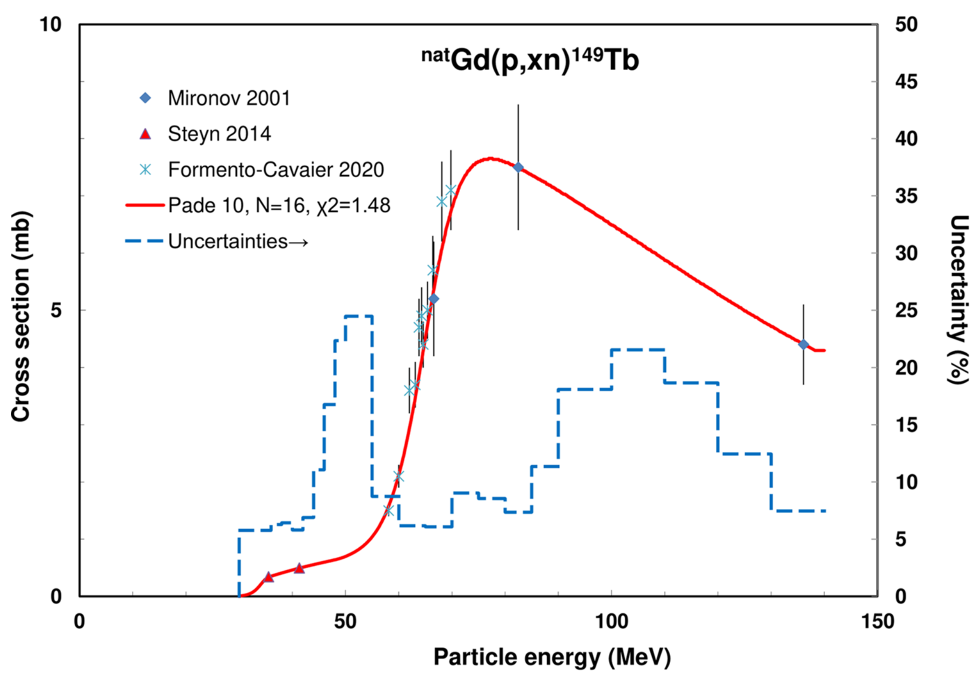

Fig. 99 ^{nat}Gd(p,xn)^{149}Tb reaction: selected experimental works and Padé fit (solid line) with total derived uncertainties, including 4% systematic uncertainty (dashed line, right-hand scale)

^{nat}Er(d,xn)^{167}Tm Three data sets published in Tárkányi [159], Tárkányi [160] and Khandaker [161] were found. All data were selected. The experimental data, in comparison with TENDL theoretical excitation functions, are presented in Fig. 122. The Padé fit is displayed in Fig. 123 and the calculated integral yield in Fig. 130. Experimental yield data were presented by Dmitriev [158] and Dmitriev [24, 43].

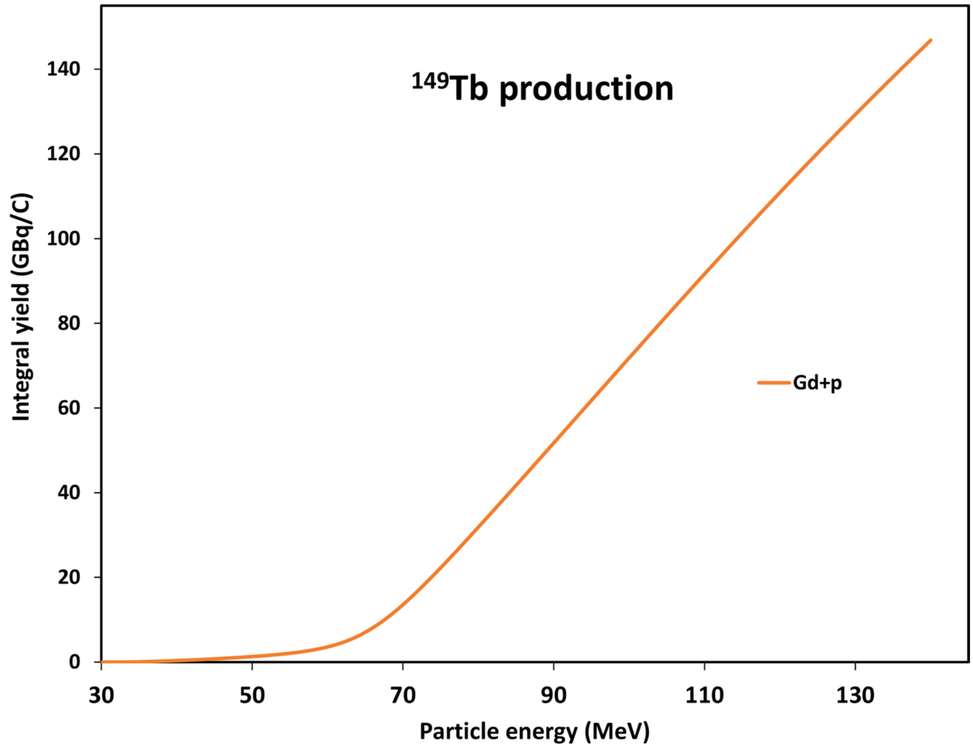

Fig. 100 Yield calculated from the recommended cross sections for ^{149}Tb production

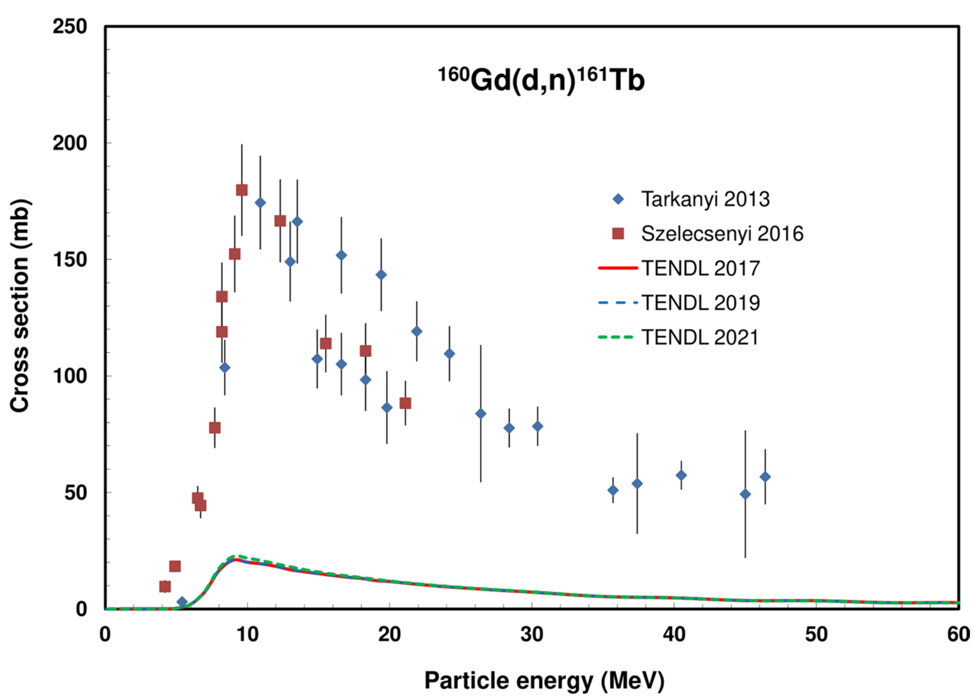

Fig. 101 ^{160}Gd(d,n)^{161}Tb reaction: all experimental data and the TENDL theoretical excitation functions

^{nat}Er(p,xn)^{167}Tm Four experimental cross section data sets are available: Rayudu [169], Tárkányi [170], Tárkányi [154] and Hermanne [171] (Fig. 124). Outlying points of Rayudu 1963 [169] at 14 MeV and Tárkányi [170] at 3.1 MeV were deselected. The Padé fit on the selected data is seen in Fig. 125. The calculated integral yield, based on the recommended values from the Padé fit, is shown in Fig. 130. Experimental yields were reported in Dmitriev [158] and Dmitriev [43].

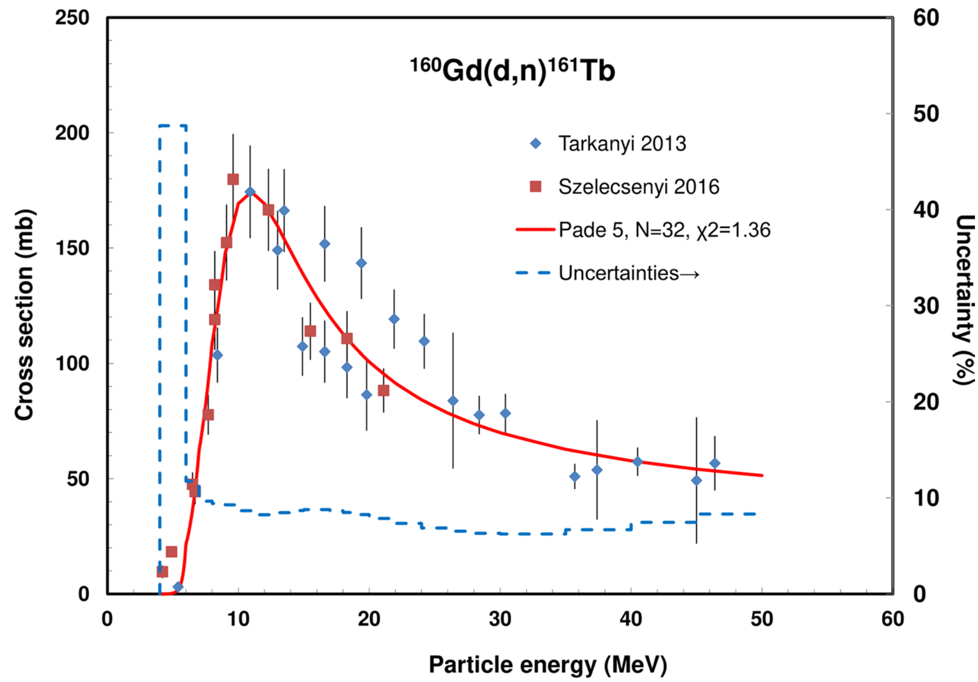

Fig. 102 ^{160}Gd(d,n)^{161}Tb reaction: selected experimental works and Padé fit (solid line) with total derived uncertainties, including 4% systematic uncertainty (dashed line, right-hand scale)

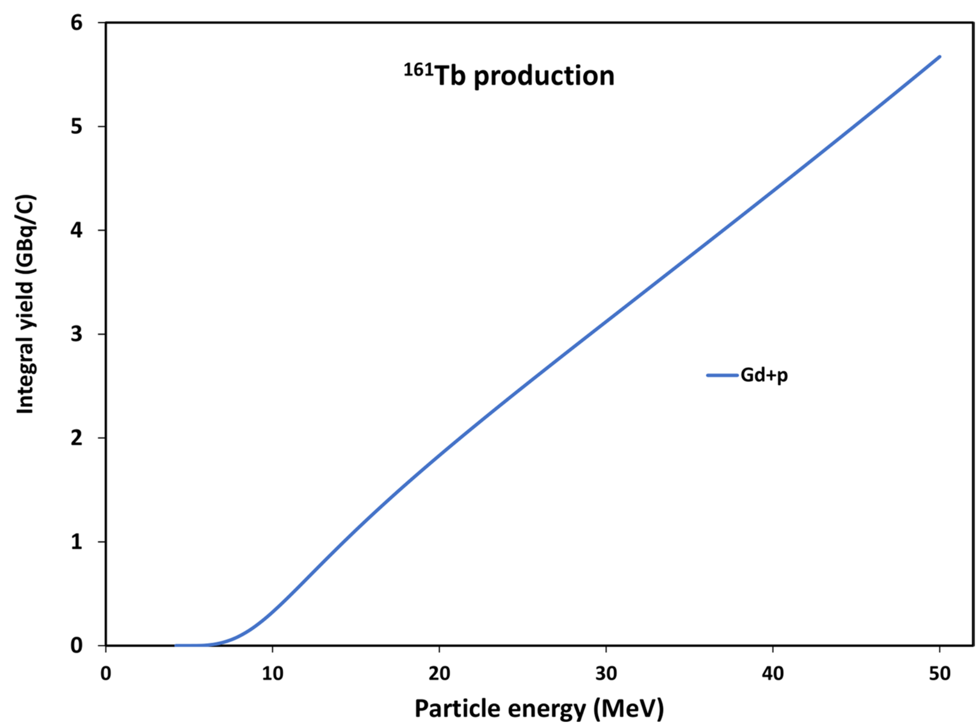

Fig. 103 Yield calculated from the recommended cross sections for ^{161}Tb production

^{167}Er(p,n)^{167}Tm Three data sets were published: Tárkányi [170], Tárkányi [154] and Hermanne [171] (Fig. 126). The two lowest energy points of Tárkányi [170] were deleted. The selected data and the Padé fit are presented in Fig. 127. The calculated integral yield is displayed in Fig. 130. No experimental yield data were found.

^{165}Ho(α,2n)^{167}Tm A large number of sets with cross section data are available in literature: Wilkinson [172], Martin [173], Sau [174], Homma [175], Rama Rao [176], Mukherjee [177], Singh [178], Singh [179], Gadkari [180], Tárkányi [181], Usman [182] (Fig. 128). The sets of Sau

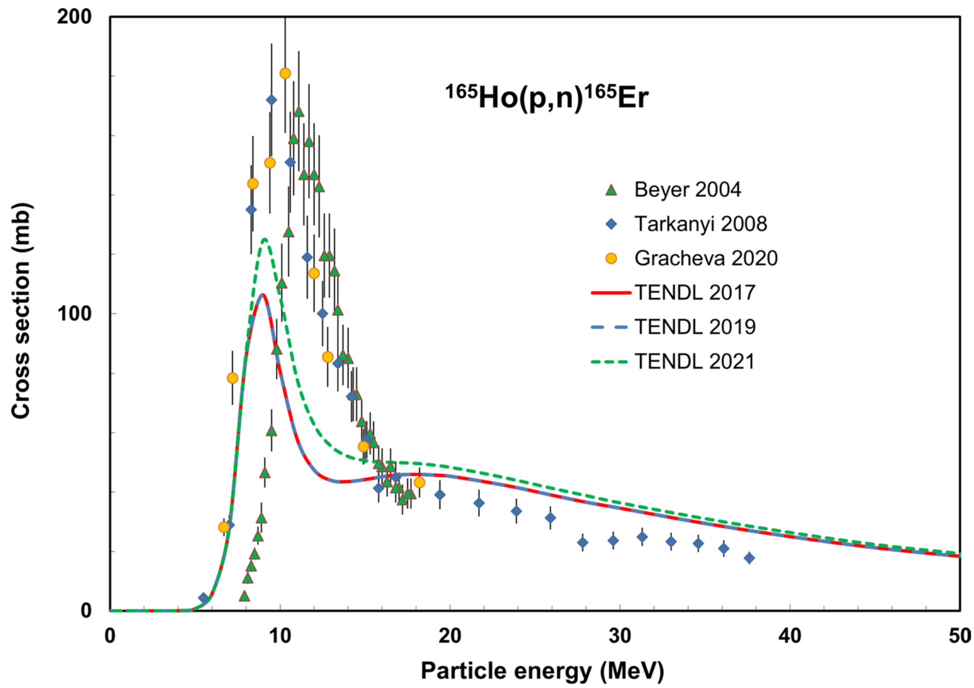

Fig. 104 ^{165}Ho(p,n)^{165}Er reaction: all experimental data and the TENDL theoretical excitation functions

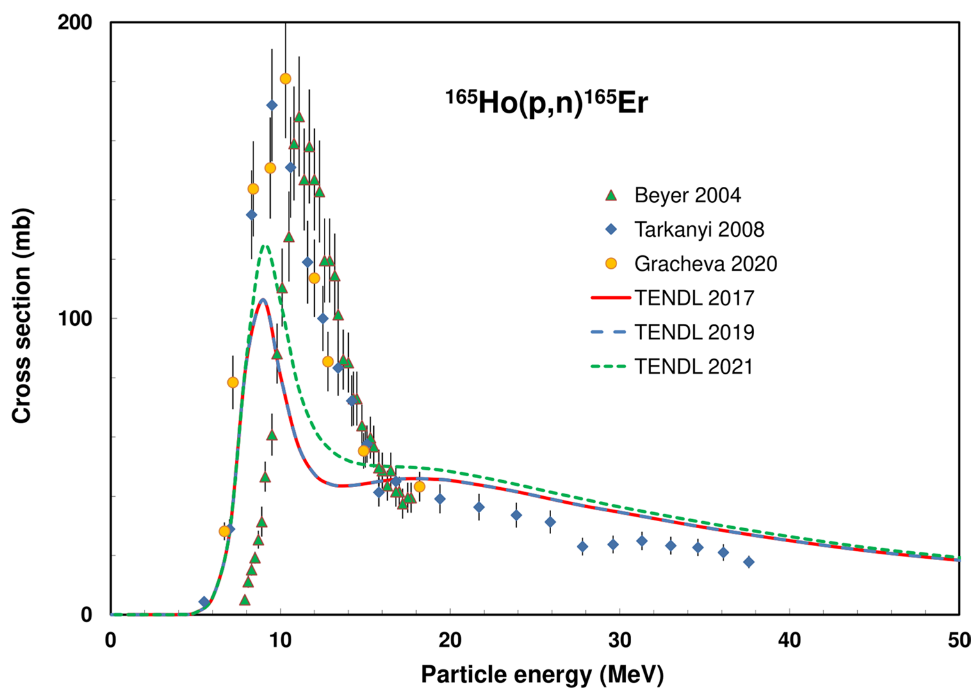

Fig. 105 ^{165}Ho(p,n)^{165}Er reaction: selected experimental works and Padé fit (solid line) with total derived uncertainties, including 4% systematic uncertainty (dashed line, right-hand scale)

[174], Wilkinson [172] and Martin [173] were deselected as all their cross section values are outlying. The too-low values of Gadkari [180], Singh [178] and Rama Rao [176] were multiplied by a factor of 1.8. The values of Singh [179] and Homma [175] were multiplied by a factor of 2. Probably all these authors have a problem with the incoming particle flux by a factor of 2, due to not considering the double charge of the α-particle. The approximation by the factor of 1.8 is due to an additional needed correction for beam intensity. The selected data and the Padé fit

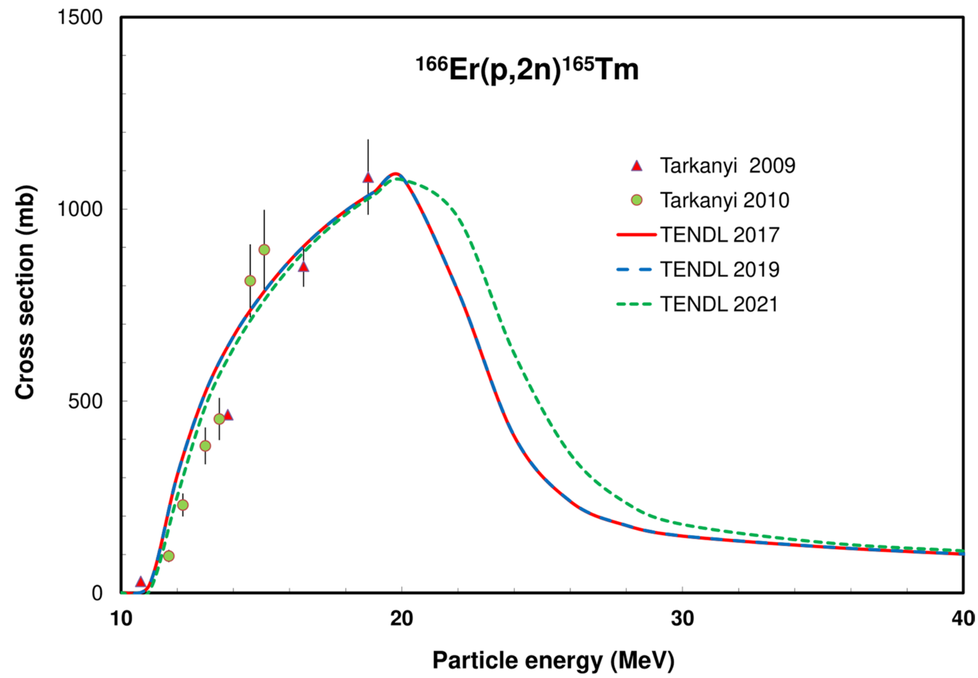

Fig. 106 $^{166}Er(p,2n)^{165}Tm$ reaction: all experimental data and the TENDL theoretical excitation functions

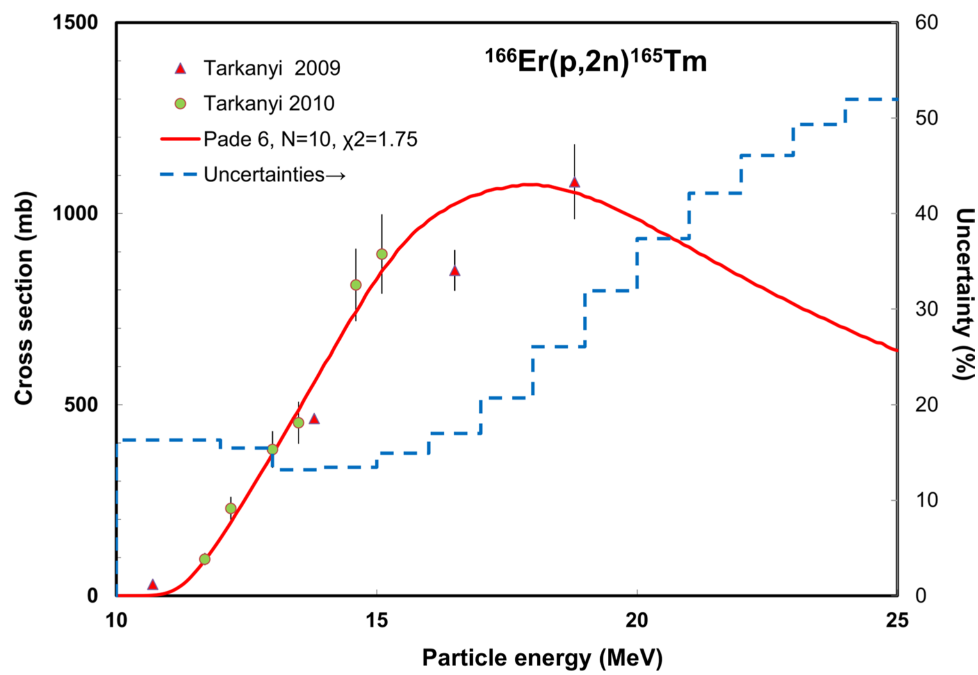

Fig. 107 $^{166}Er(p,2n)^{165}Tm$ reaction: selected experimental works and Padé fit (solid line) with total derived uncertainties, including 4% systematic uncertainty (dashed line, right-hand scale)

are shown in Fig. 129, and the calculated integral yield in Fig. 130. Experimental yield was reported by Dmitriev [158].

Integral yields for ^{167}Tm formation Integral yields of reactions related to the production of ^{167}Tm are deduced from the recommended values obtained from Padé fittings and are shown in Fig. 130.

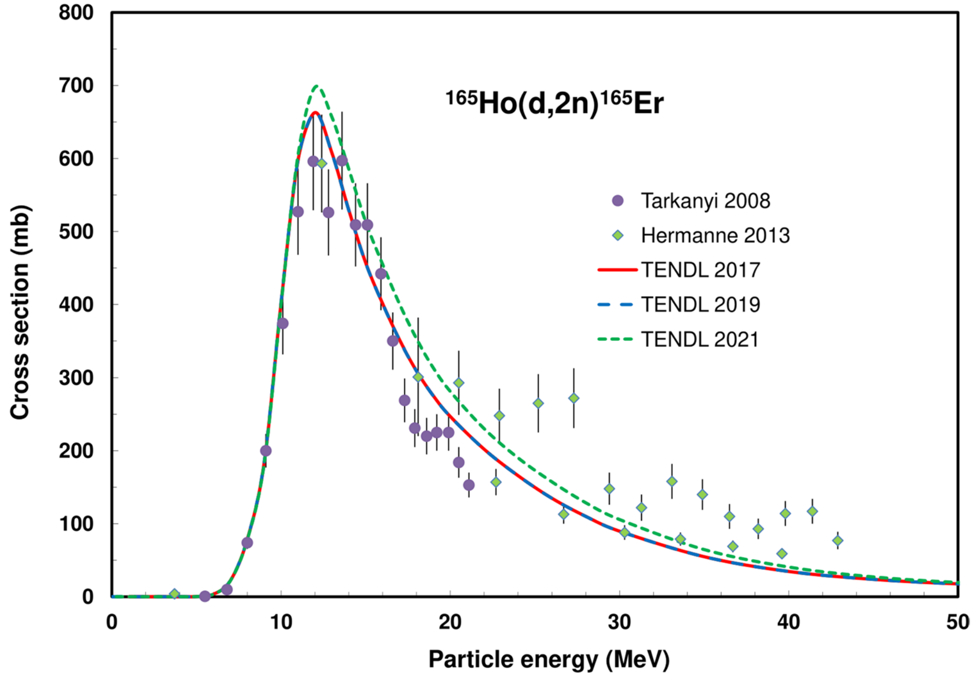

Fig. 108 ^{165}Ho(d,2n)^{165}Er reaction: all experimental data and the TENDL theoretical excitation functions

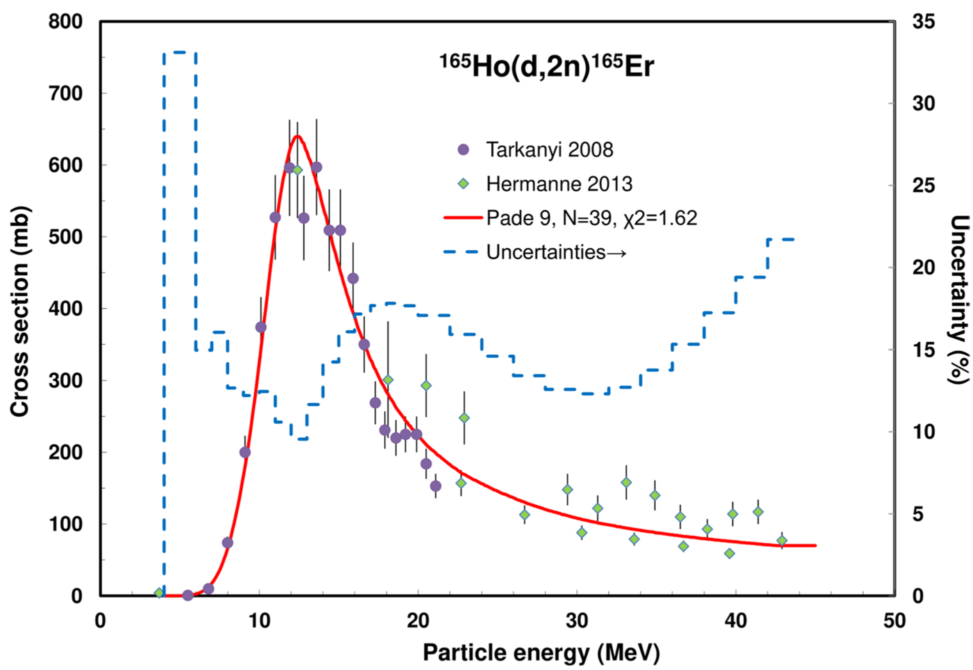

Fig. 109 ^{165}Ho(d,2n)^{165}Er reaction: selected experimental works and Padé fit (solid line) with total derived uncertainties, including 4% systematic uncertainty (dashed line, right-hand scale)

^{197m}Hg/^{197g}Hg production

The γ-emitting isomers ^{197m}Hg ($T_{1/2}$ = 23.8 h, E_γ 134 keV, 34%) and ^{197g}Hg ($T_{1/2}$ = 64.14 h, E_γ 77 keV, 19%, 279 keV, 6%) are suitable for SPECT imaging. Moreover, as their IT and EC decay is accompanied by Auger and conversion electron emission, they have an additional potential interest for therapeutic application. The decay schemes are available in [15] and decay data are displayed in Table 2.

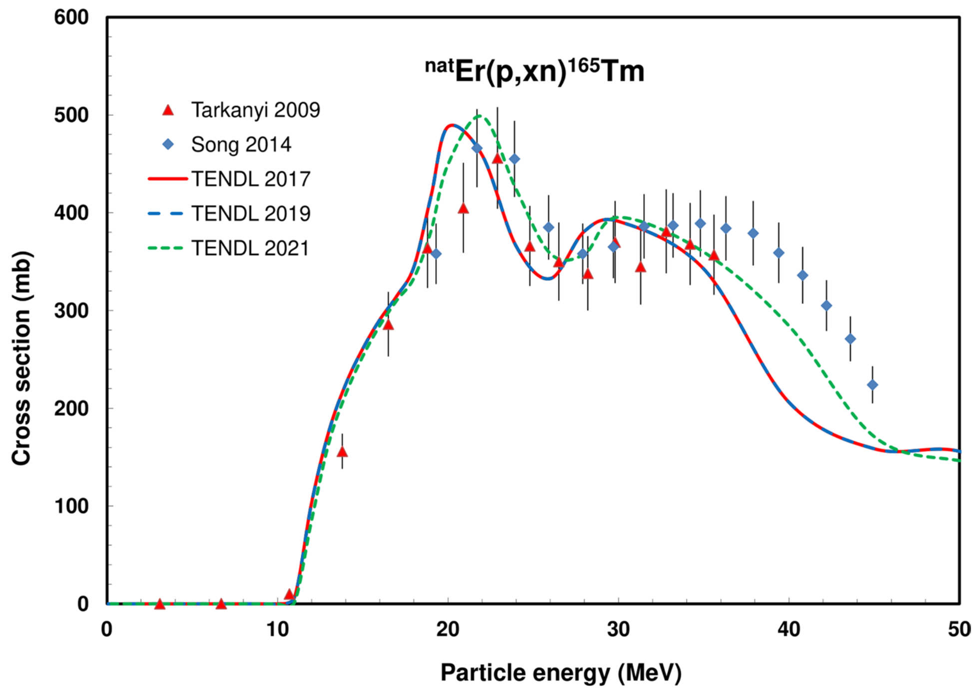

Fig. 110 $^{nat}Er(p,xn)^{165}Tm$ reaction: all experimental data and the TENDL theoretical excitation functions

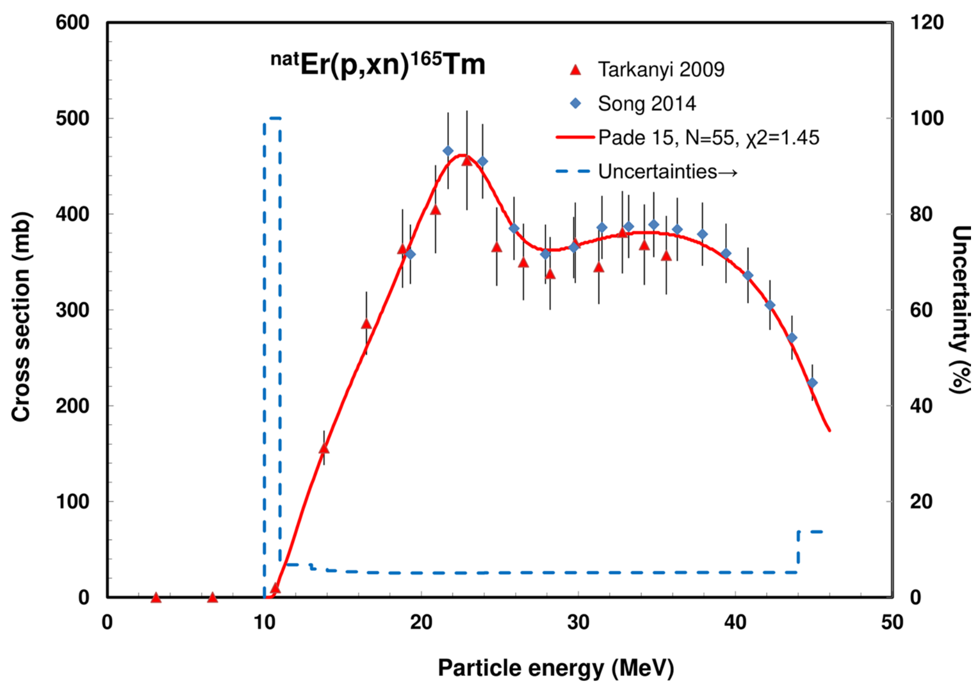

Fig. 111 $^{nat}Er(p,xn)^{165}Tm$ reaction: selected experimental works and Padé fit (solid line) with total derived uncertainties, including 4% systematic uncertainty (dashed line, right-hand scale)

Evaluated nuclear reactions for ^{197m}Hg and ^{197g}Hg formation

The $^{197}Au(p,n)^{197m}Hg$, $^{197}Au(d,2n)^{197m}Hg$, $^{197}Au(p,n)^{197g}Hg$ and $^{197}Au(d,2n)^{197g}Hg$ reactions were evaluated.

$^{197}Au(p,n)^{197m}Hg$ In ten publications (Vandenbosch [183], Hansen [184], Gritsyna [185], Szelecsenyi [186], Michel [28], Szelecsenyi [187], Elmaghraby [188], Satheesh [189], Ditrói [190] and Lebeda [191]) experimental cross section data for the $^{197}Au(p,n)^{197m}Hg$ reaction are reported. The sets of Vandenbosch [183] and Satheesh [189] were deselected, as their values are significantly outlying near the maximum of the excitation curve. All data, in comparison with predictions in the TENDL databases, are shown in Fig. 131. The selected data and the Padé fit are in Fig. 132 while the calculated integral yields for production of ^{197m}Hg and ^{197g}Hg are

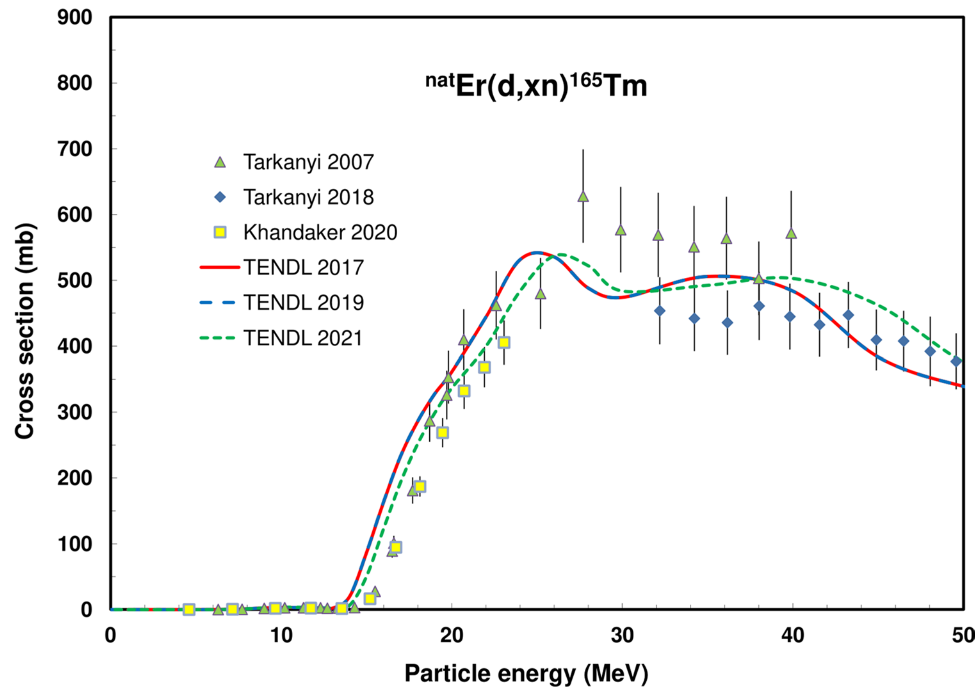

Fig. 112 ^{nat}Er(d,xn)^{165}Tm reaction: all experimental data and the TENDL theoretical excitation functions

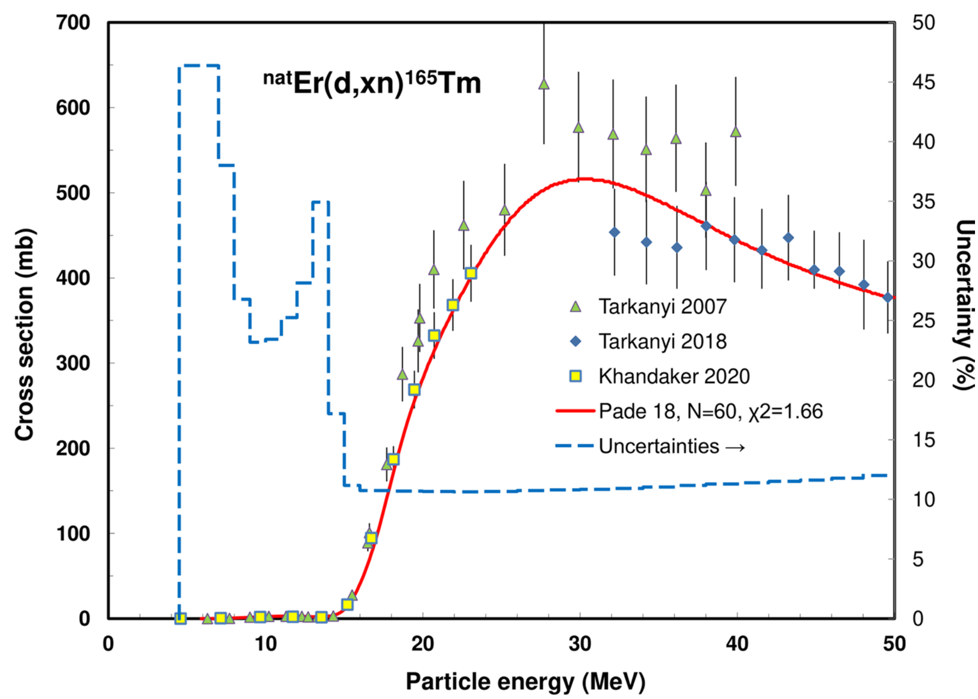

Fig. 113 ^{nat}Er(d,xn)^{165}Tm reaction: selected experimental works and Padé fit (solid line) with total derived uncertainties, including 4% systematic uncertainty (dashed line, right-hand scale)

presented in Fig. 139. Experimental yields were reported by Abe [192] and Birattari [193].

^{197}Au(d,2n)^{197m}Hg Eight experimental data sets were found: Vandenbosch [183], Chevarier [194], Khrisanfov [195], Long [196], Zhao Wenrong [197], Tárkányi [198], Tárkányi [199], Lebeda [191]. The available data, in comparison with the TENDL predictions; are presented in Fig. 133. All data were selected and used for Padé fitting (Fig. 134), the calculated integral yields are shown in Fig. 139. No experimental yield data were found.

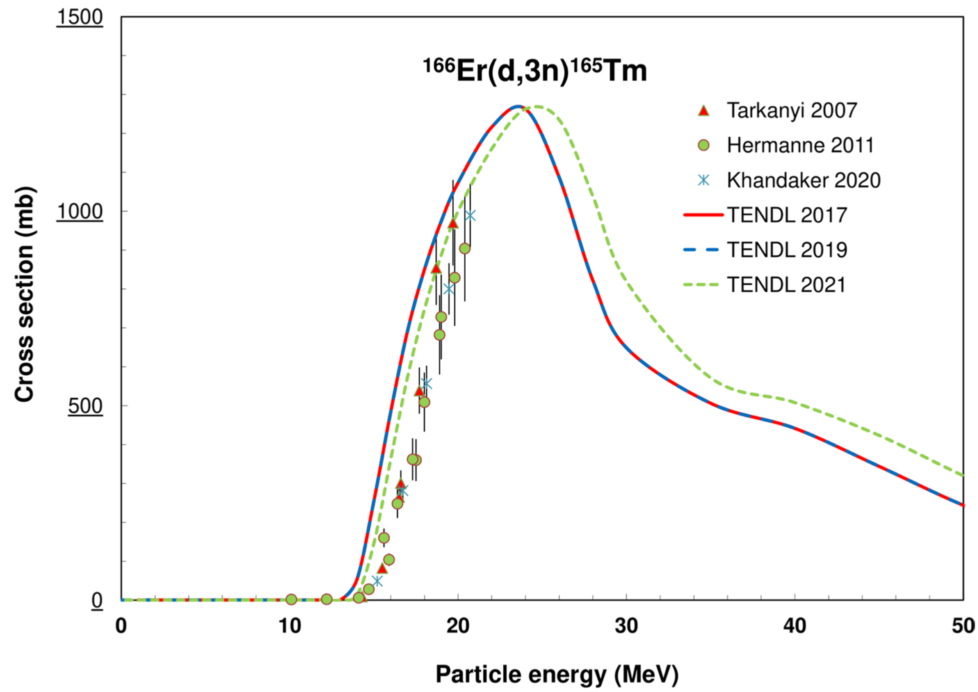

Fig. 114 ^{166}Er(d,3n)^{165}Tm reaction: all experimental data and the TENDL theoretical excitation functions

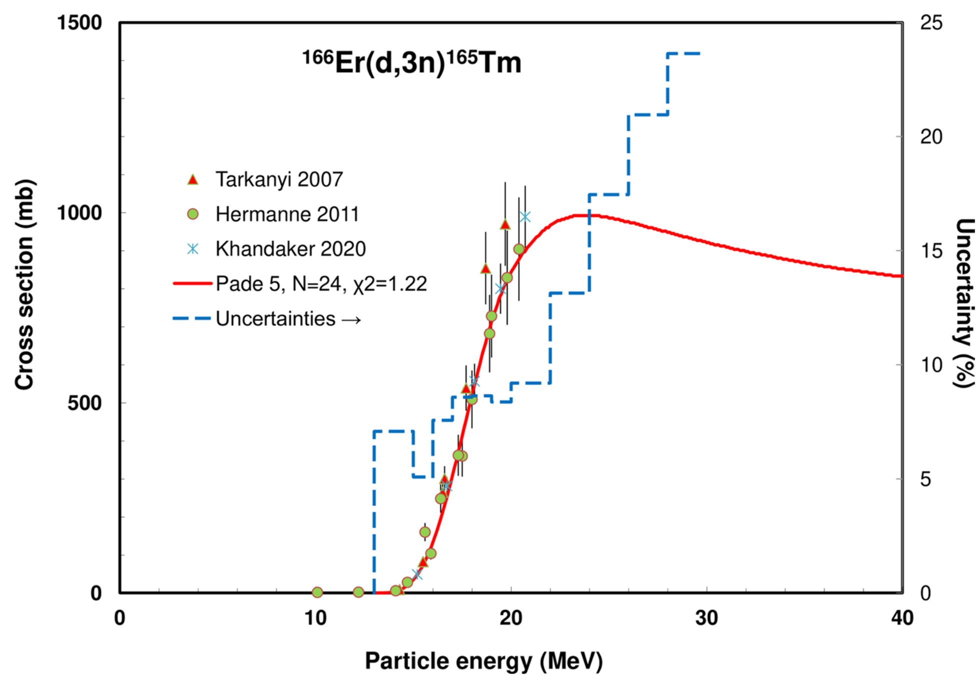

Fig. 115 ^{166}Er(d,3n)^{165}Tm reaction: selected experimental works and Padé fit (solid line) with total derived uncertainties, including 4% systematic uncertainty (dashed line, right-hand scale)

^{197}Au(p,n)^{197g}Hg Eight authors reported experimental cross section data for the ^{197}Au(p,n)^{197g}Hg reaction: Vandenbosch [183], Hansen [200], Gritsyna [185], Chodil [201], Elmaghraby [188], Satheesh [189], Ditrói [190] and Lebeda [191]. Three whole sets were deselected (Vandenbosch [183], Satheesh [189] and Chodil [201]) as they are outlying, especially near the maximum of the excitation curve. The available data, in comparison with the TENDL predictions, are shown in Fig. 135, the selected data with the Padé fit in Fig. 136. The calculated integral yields based

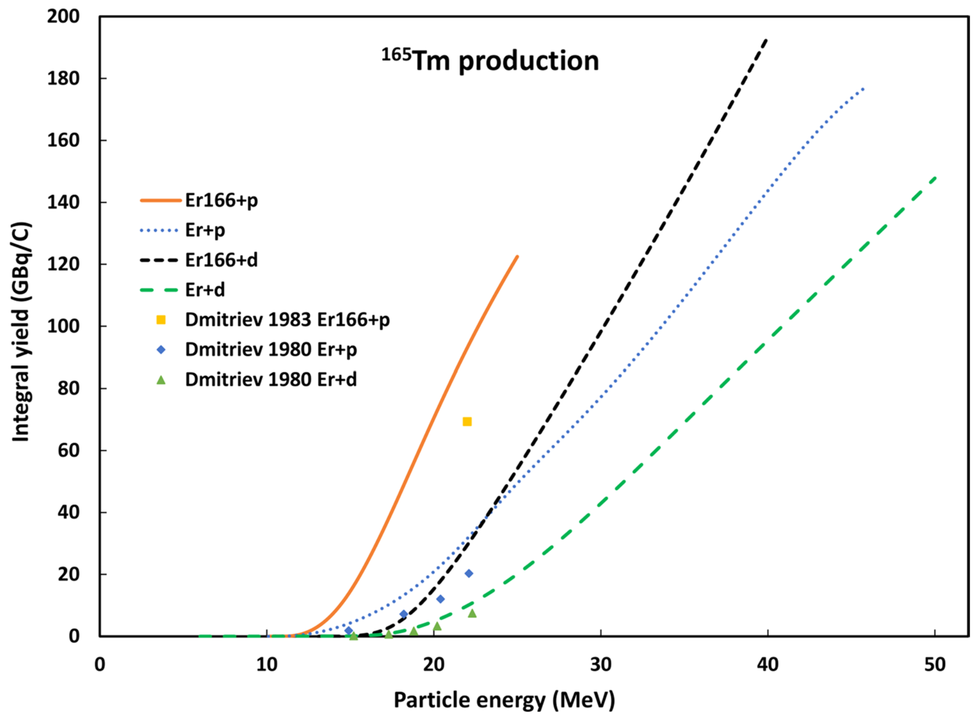

Fig. 116 Yield calculated from the recommended cross sections for ^{165}Tm production

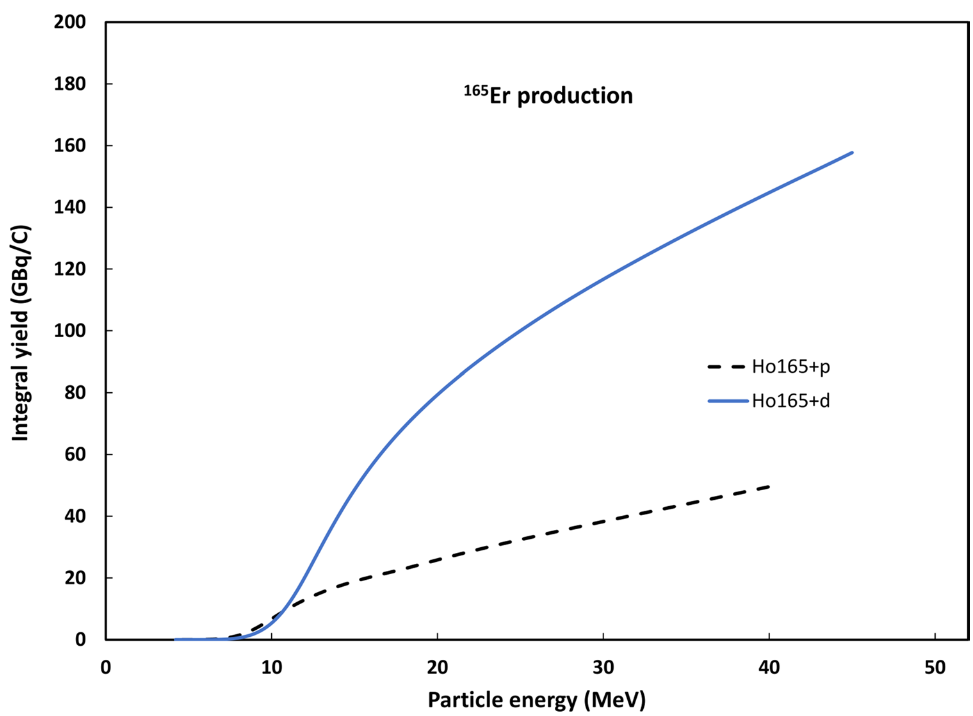

Fig. 117 Yield calculated from the recommended cross sections for ^{165}Er production

on the recommended values from the Padé fit can be seen in Fig. 139. Experimental integral yields were measured by Abe [192] and Birattari [202].

^{197}Au(d,2n)^{197g}Hg Eight data sets were found: Vandenbosch [183], Chevalier [194], Khrisanfov [195], Long [196], Zhao Wenrong [197], Tárkányi [198], Tárkányi

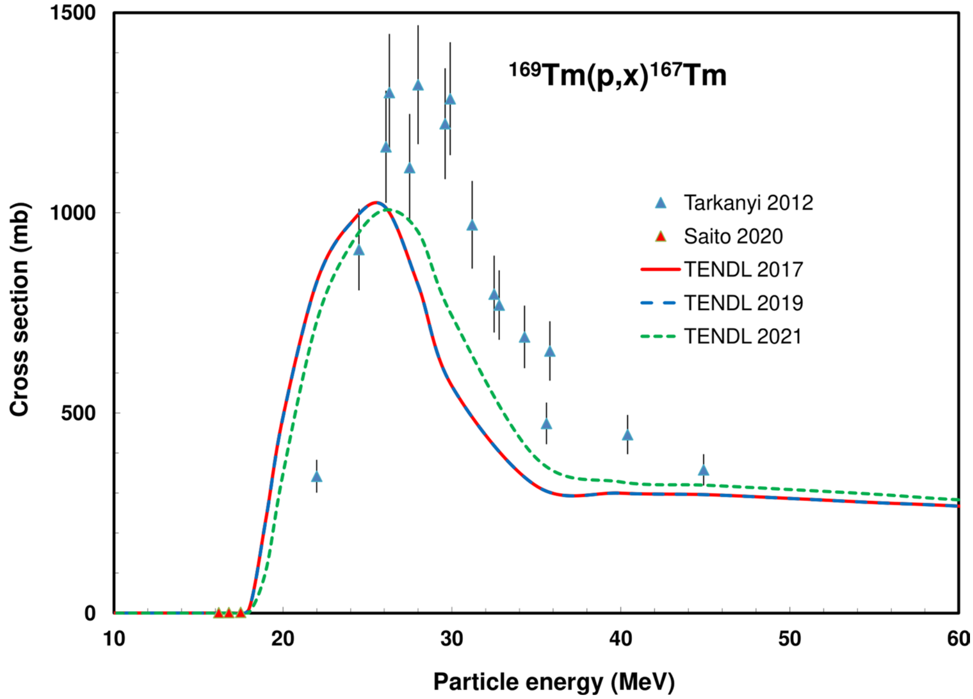

Fig. 118 ^{169}Tm(p,x)^{167}Tm reaction: all experimental data and the TENDL theoretical excitation functions

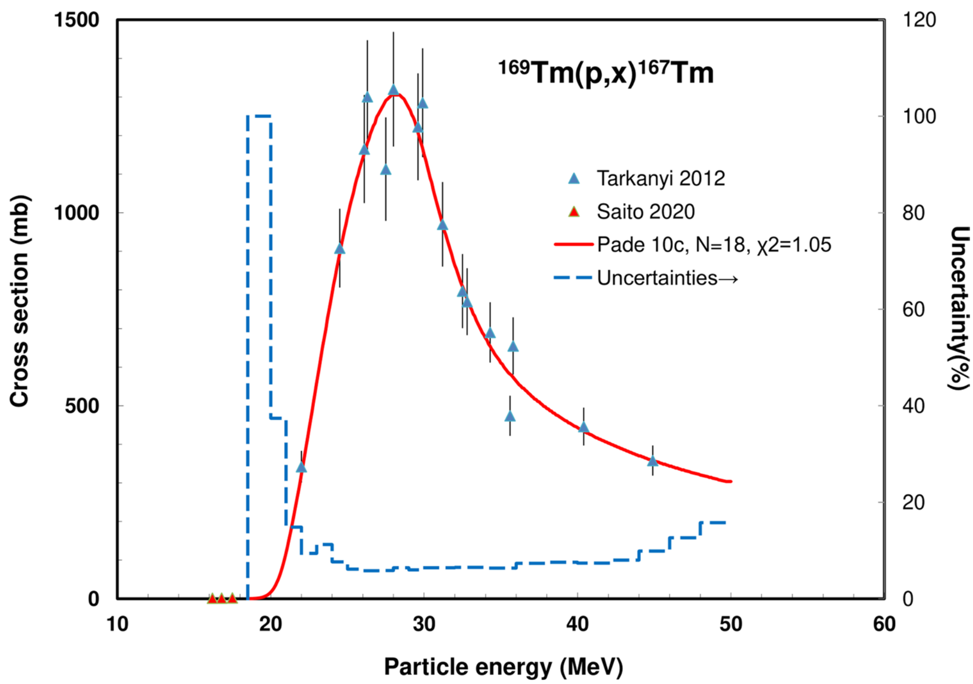

Fig. 119 ^{169}Tm(p,x)^{167}Tm reaction: selected experimental works and Padé fit (solid line) with total derived uncertainties, including 4% systematic uncertainty (dashed line, right-hand scale)

[199] and Lebeda [191] (Fig. 137). The Long [196] and Vandenbosch [183] data sets were deselected. The remaining selected data and the Padé fit are presented in Fig. 138, and the calculated integral yield in Fig. 139. No experimental yield values were found.

Integral yields for ^{197m}Hg and ^{197g}Hg formation Integral yields of reactions related to the production of ^{197m}Hg and ^{197g}Hg are deduced from the recommended values obtained from Padé fittings and are shown in Fig. 139.

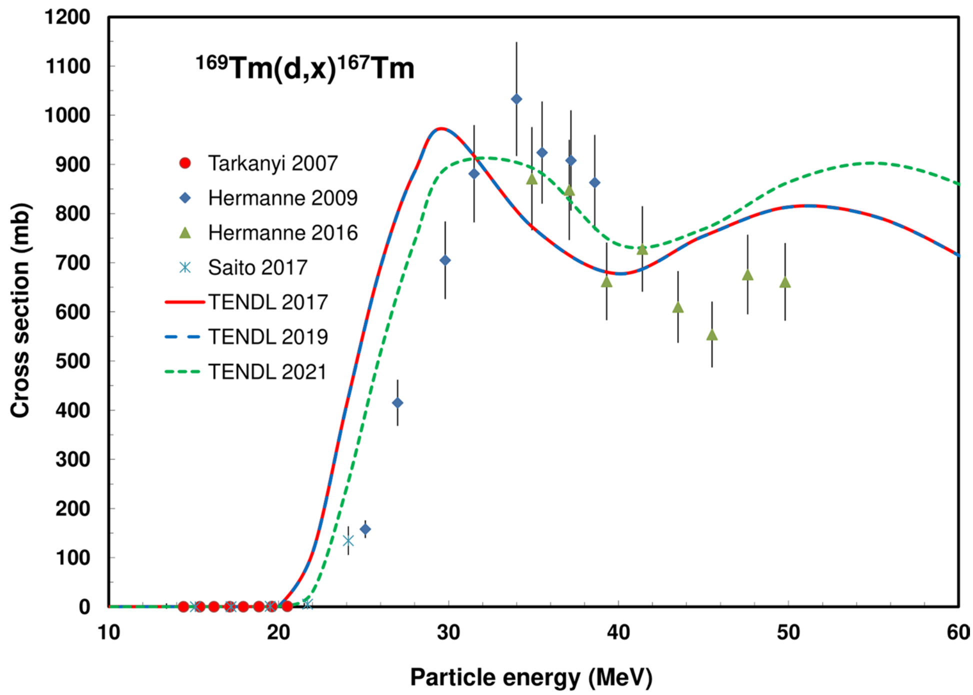

Fig. 120 ^{169}Tm(d,x)^{167}Tm reaction: all experimental data and the TENDL theoretical excitation functions

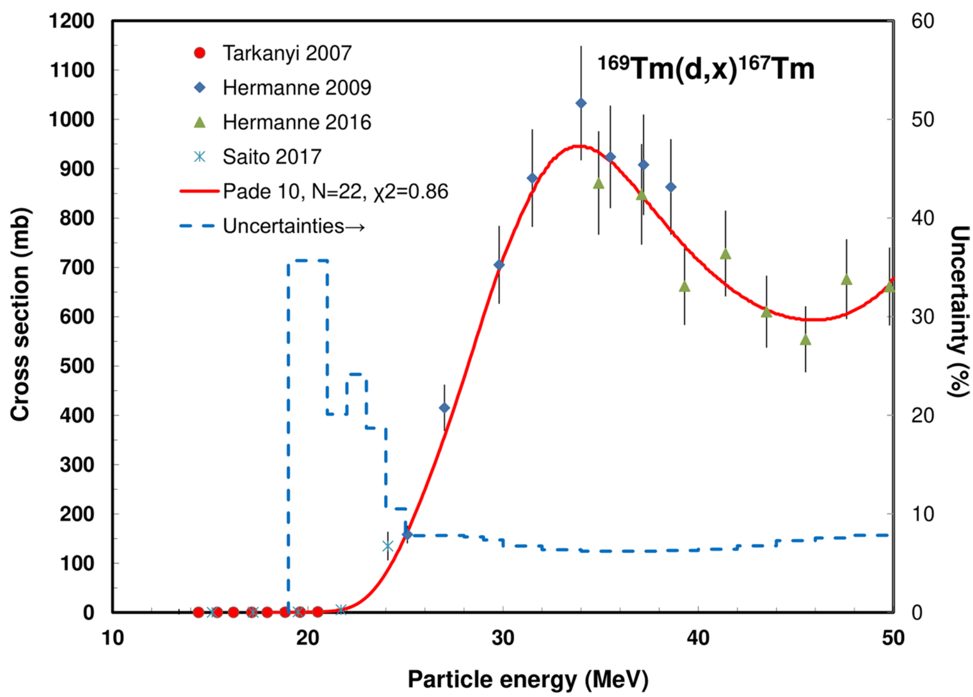

Fig. 121 ^{169}Tm(d,x).^{167}Tm reaction: selected experimental works and Padé fit (solid line) with total derived uncertainties, including 4% systematic uncertainty (dashed line, right-hand scale)

^{198g}Au production

The radionuclide ^{198g}Au ($T_{1/2}$ = 2.6947 d) is a mixed β$^-$ (0.96 MeV, abundance 98.6%) and gamma emitter (0.412 MeV, abundance 95.5%). The emission of β$^-$ particles makes it useful in targeted radiotherapy essentially as permanent seed implant therapy for the prostate gland. The emission of low-energy photons allows for the evaluation of dose distributions by SPECT imaging. The decay

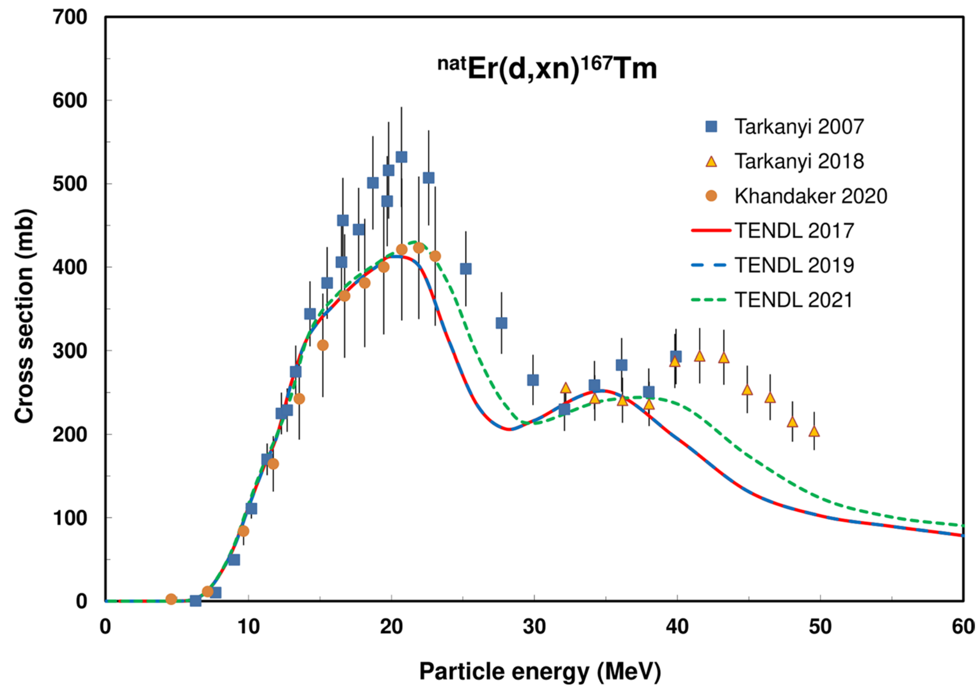

Fig. 122 $^{nat}Er(d,xn)^{167}Tm$ reaction: all experimental data and the TENDL theoretical excitation function

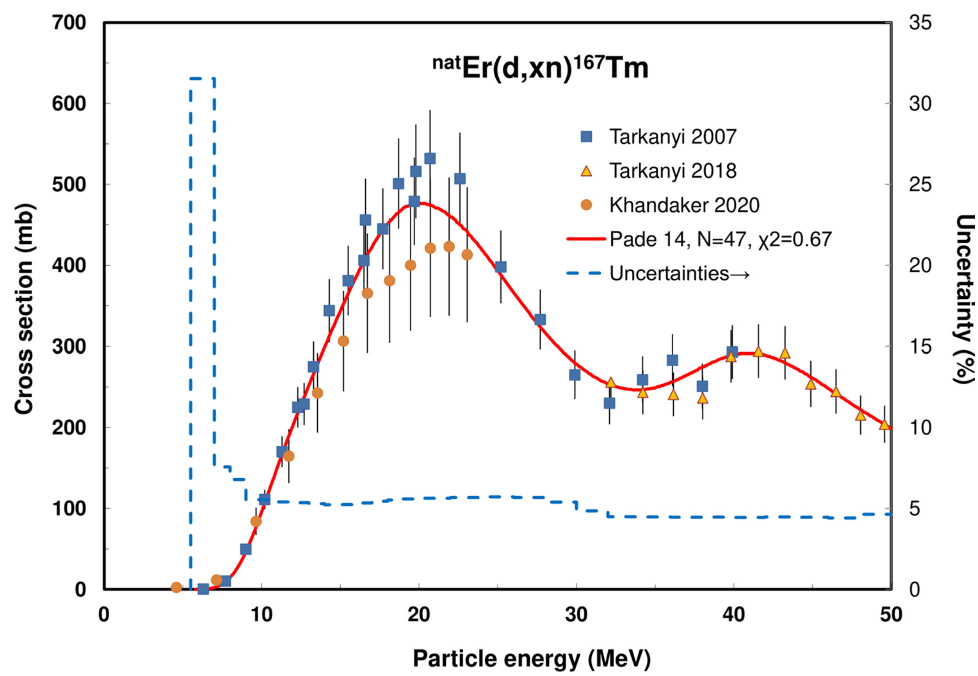

Fig. 123 $^{nat}Er(d,xn)^{167}Tm$ reaction**:** selected experimental works and Padé fit (solid line) with total derived uncertainties, including 4% systematic uncertainty (dashed line, right-hand scale)

schemes are available in [15] and decay data are displayed in Table 2.

Evaluated nuclear reactions for ^{198g}Au formation

The $^{198}Pt(p,x)^{198g}Au$ and $^{198}Pt(d,x)^{198g}Au$ reactions were evaluated.

$^{198}Pt(p,x)^{198g}Au$ Three data sets are reported by Tárkányi [203], Showaimy [204] and Gantumur [205] (Fig. 140). Seven outlying data points in the 16–22 MeV energy range (at 16.3, 17.4,18.4, 19.4, 20.4, 21.3 and 22.2 MeV) of Tárkányi [203] were deleted and a Padé fit was performed on the remaining selected data (Fig. 141).

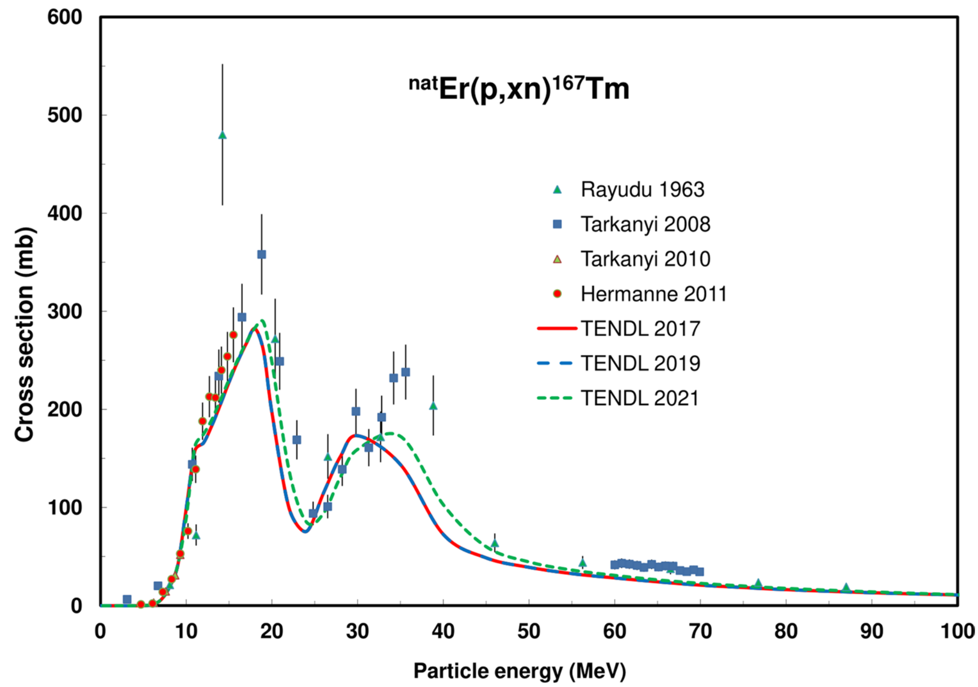

Fig. 124 $^{nat}Er(p,xn)^{167}Tm$ reaction: all experimental data and the TENDL theoretical excitation functions

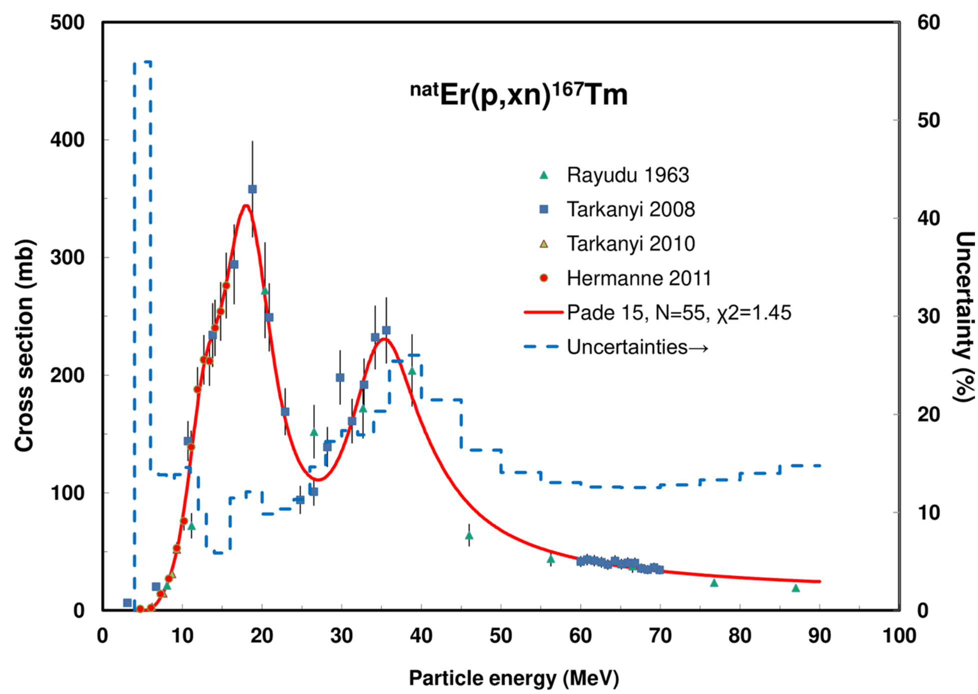

Fig. 125 $^{nat}Er(p,xn)^{167}Tm$ reaction: selected experimental works and Padé fit (solid line) with total derived uncertainties, including 4% systematic uncertainty (dashed line, right-hand scale)

The calculated integral yields are shown in Fig. 144. No experimental yield data were found.

$^{198}Pt(d,2n)^{198g}Au$ Five data sets are available, published by Tárkányi [203], Ditrói [206], Khandaker [207], Ditrói [208] and Tárkányi [209] (Fig. 142). All data were selected and fitted (Fig. 143). Calculated yields are seen in Fig. 144. No experimental yield values were found.

Integral yields for ^{198}Au formation Integral yields of reactions related to the production of ^{198}Au are deduced from the recommended values obtained from Padé fittings and are shown in Fig. 144.

^{230}Pa (^{230}U) production

The α-emitter ^{230}U ($T_{1/2} = 20.8$ d) and its short-lived daughter ^{226}Th ($T_{1/2} = 30.6$ min) are the parents in a

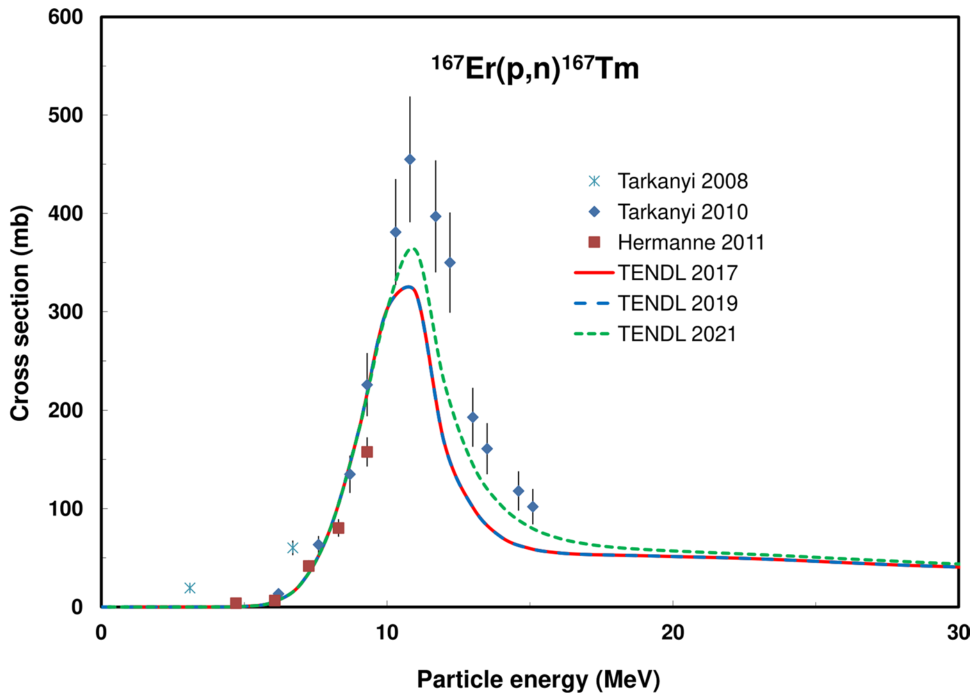

Fig. 126 ^{167}Er(p,n)^{167}Tm reaction: all experimental data and the TENDL theoretical excitation functions

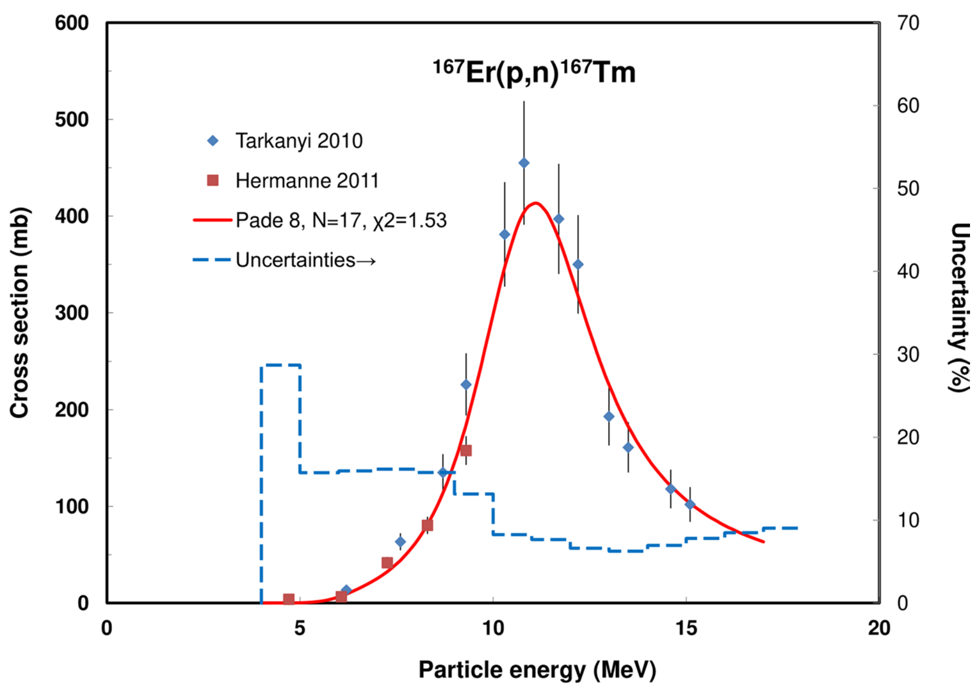

Fig. 127 ^{167}Er(p,n)^{167}Tm reaction: selected experimental works and Padé fit (solid line) with total derived uncertainties, including 4% systematic uncertainty (dashed line, right-hand scale)

generator system of novel therapeutic nuclides for application in targeted radiotherapy. The decay of ^{230}U/^{226}Th is followed by a chain of short-lived radionuclides generating numerous additional α-particles.

By using accelerators, ^{230}U can be obtained through the decay of its ^{230}Pa ($T_{1/2}$ = 17.4 d) parent (β^- decay with a probability of 7.8%) with proton or deuteron activation of thorium nuclei (only ^{232}Th with a half-life of 1.405×10^{10} y occurs naturally). The decay schemes are available in [15] and decay data are displayed in Table 2.

Evaluated nuclear reactions for ^{230}Pa formation

The ^{232}Th(p,3n)^{230}Pa and ^{232}Th(d,4n)^{230}Pa reactions were evaluated.

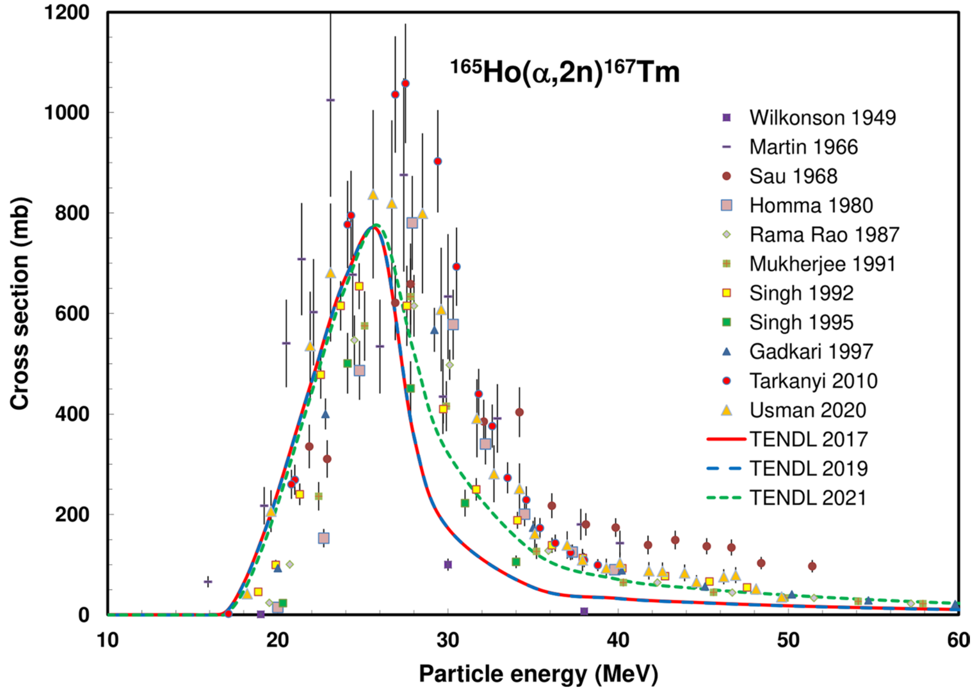

Fig. 128 ^{165}Ho(α, 2n)^{167}Tm reaction: all experimental data and the TENDL theoretical excitation functions

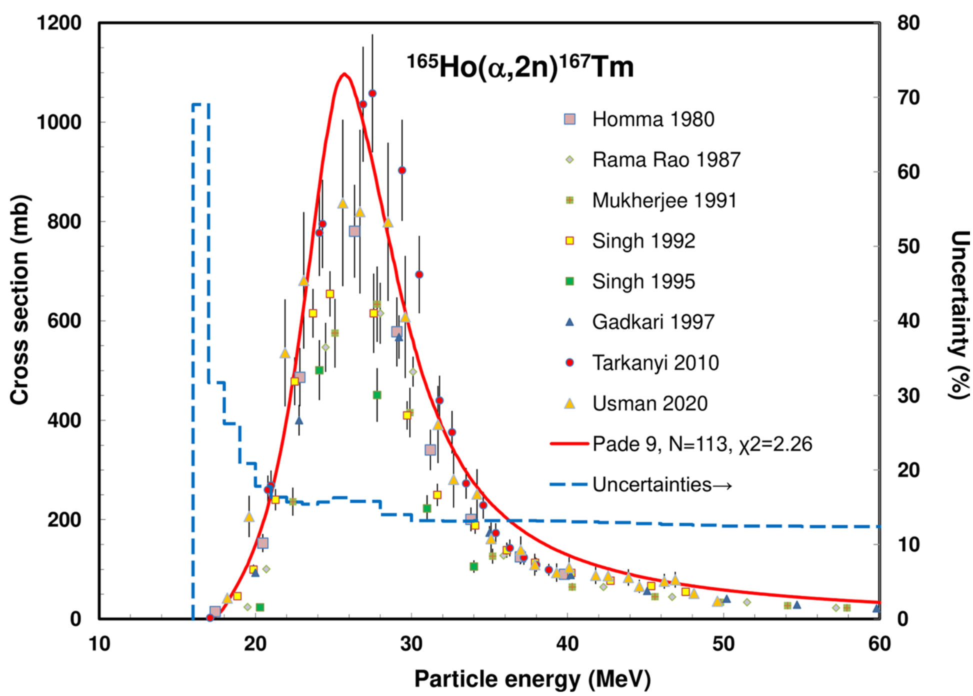

Fig. 129 ^{165}Ho(α,2n)^{167}Tm reaction: selected experimental works and Padé fit (solid line) with total derived uncertainties, including 4% systematic uncertainty (dashed line, right-hand scale)

^{232}Th(p,3n)^{230}Pa Twelve sets with experimental cross section data for this reaction were found: Tewes [210], Tewes [211], Meinke [212] (series1 and series2), Lefort [213], Brun [214], Celler [215], Kudo [216], Chu [217], Roshchin [218], Morgenstern [219], Jost [220] and Radchenko [221] (Fig. 145). Out of them Tewes [211] and

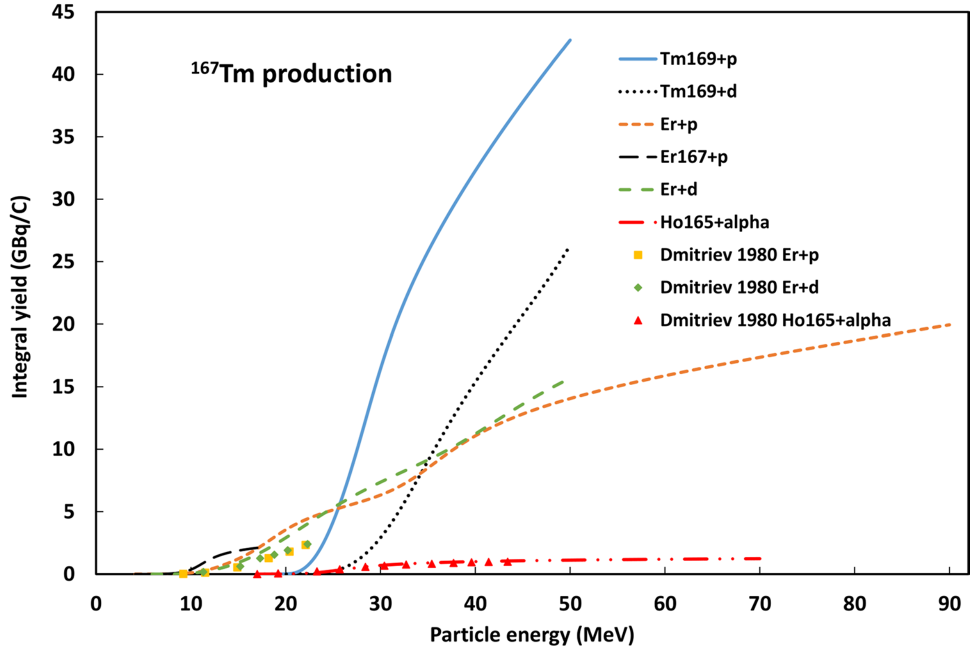

Fig. 130 Yield calculated from the recommended cross sections for ^{167}Tm production

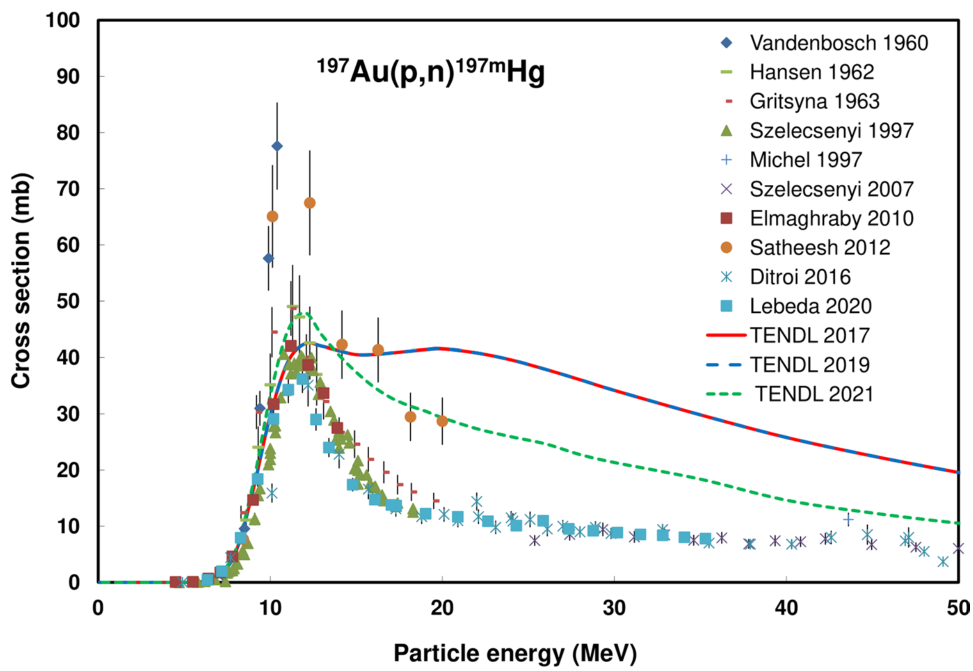

Fig. 131 ^{197}Au(p,n)^{197m}Hg reaction: all experimental data and the TENDL theoretical excitation functions

the two series of Meinke [212] were deselected, for Brun [214] the energy was rescaled and for Lefort [213] the two lowest energy points were deleted. The selected data and the Padé fit with uncertainties can be seen in Fig. 146. The Padé fit based integral yield data is shown in Fig. 149. Experimental yields were reported by Friend [222].

^{232}Th(d,4n)^{230}Pa Two data sets, measured by Rama Rao [223] and Duchemin [224], are available and both were selected. The experimental data, in comparison to the prediction by TENDL, are shown in Fig. 147, the Padé fit with uncertainties in Fig. 148 while the calculated integral yields are shown in Fig. 149. No experimental yield data were found.

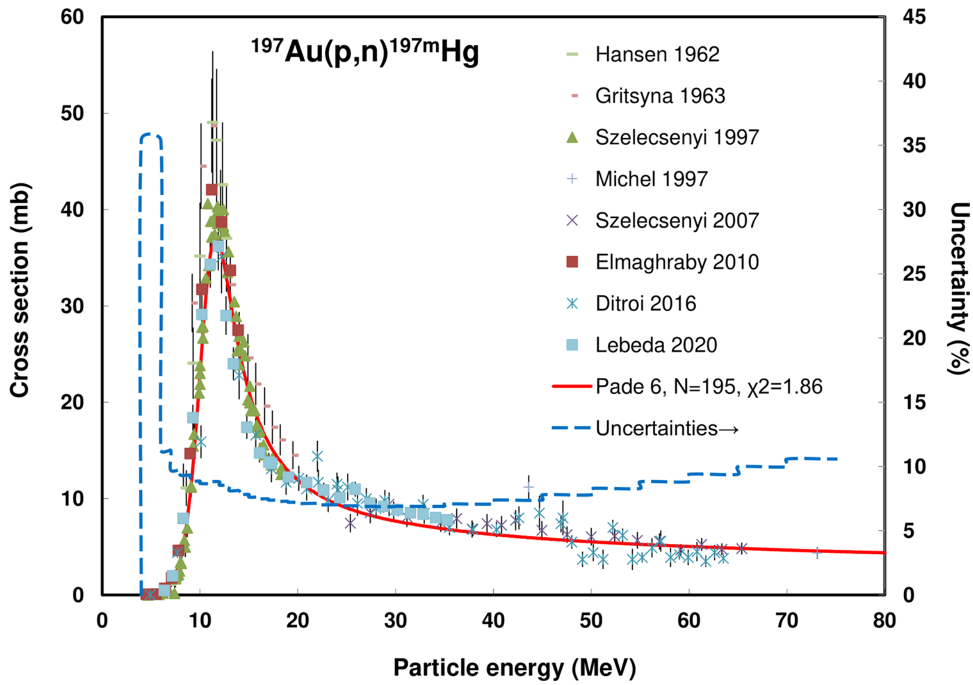

Fig. 132 ^{197}Au(p,n)^{197m}Hg reaction: selected experimental works and Padé fit (solid line) with total derived uncertainties, including 4% systematic uncertainty (dashed line, right-hand scale)

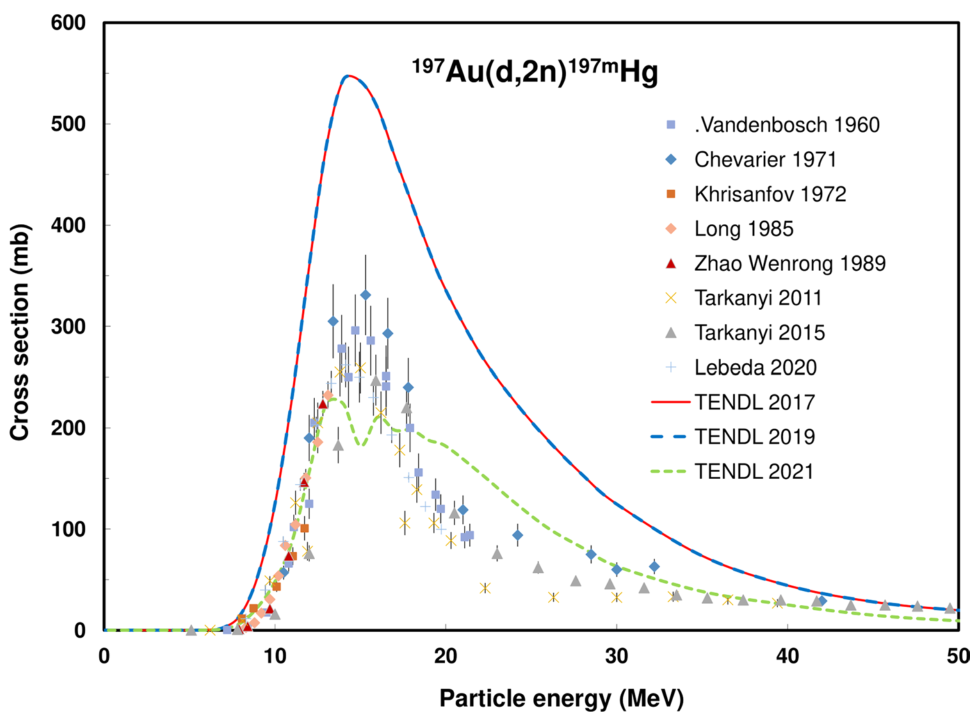

Fig. 133 ^{197}Au(d,2n)^{197m}Hg reaction: all experimental data and the TENDL theoretical excitation functions

Integral yields for ^{230}Pa formation Integral yields of reactions related to the production of ^{230}Pa are deduced from the recommended values obtained from Padé fittings and are shown in Fig. 149.

Summary and conclusions

Evaluations of production cross sections and their uncertainties were performed on sixty reactions for direct, indirect and generator production of the ^{47}Sc,^{47}Ca(^{47}Sc), ^{58m}Co, ^{71}As(^{71}Ge), ^{71}Ge, ^{77}Br, ^{80m}Br, ^{103}Pd (^{103m}Rh), ^{103}Ru(^{103m}Rh), ^{105}Rh, ^{117m}Sn, ^{119}Sb, ^{134}Ce, ^{135}La, ^{161}Tb,

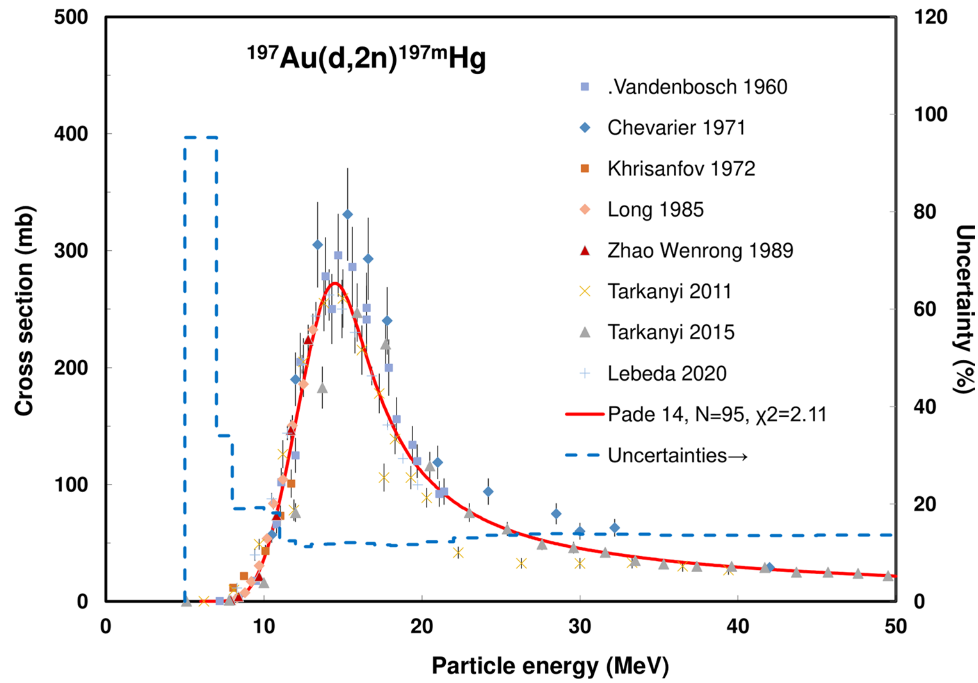

Fig. 134 ^{197}Au(d,2n)^{197m}Hg reaction: selected experimental works and Padé fit (solid line) with total derived uncertainties, including 4% systematic uncertainty (dashed line, right-hand scale)

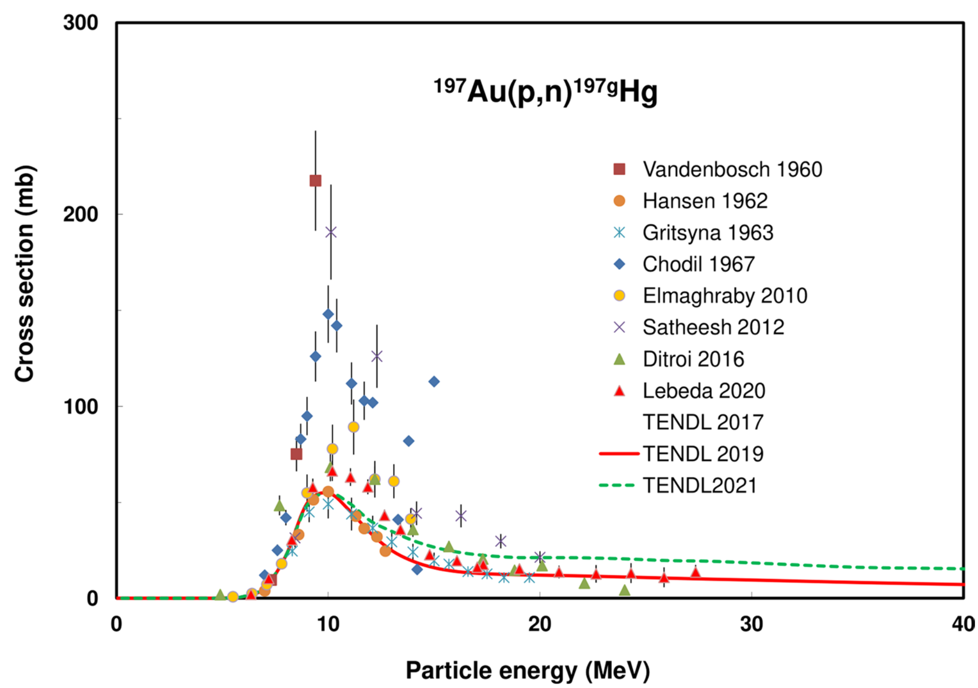

Fig. 135 ^{197}Au(p,n)^{197g}Hg reaction: all experimental data and the TENDL theoretical excitation functions

^{165}Er, ^{165}Tm(^{165}Er), ^{167}Tm, ^{197m}Hg, ^{197g}Hg, ^{198g}Au and ^{230}Pa(^{230}U) radioisotopes. The collected experimental data were compared with the theoretical predictions to be found in the TENDL-2017, 2019 and 2021 libraries. While the predictions in TENDL-2017 and 2019 are nearly the same, the description obtained in TENDL-2021 is better but still in some cases significant disagreements in the magnitude and shape of the resulting excitation functions exist (especially when considering isomeric states or deuteron-induced reactions).

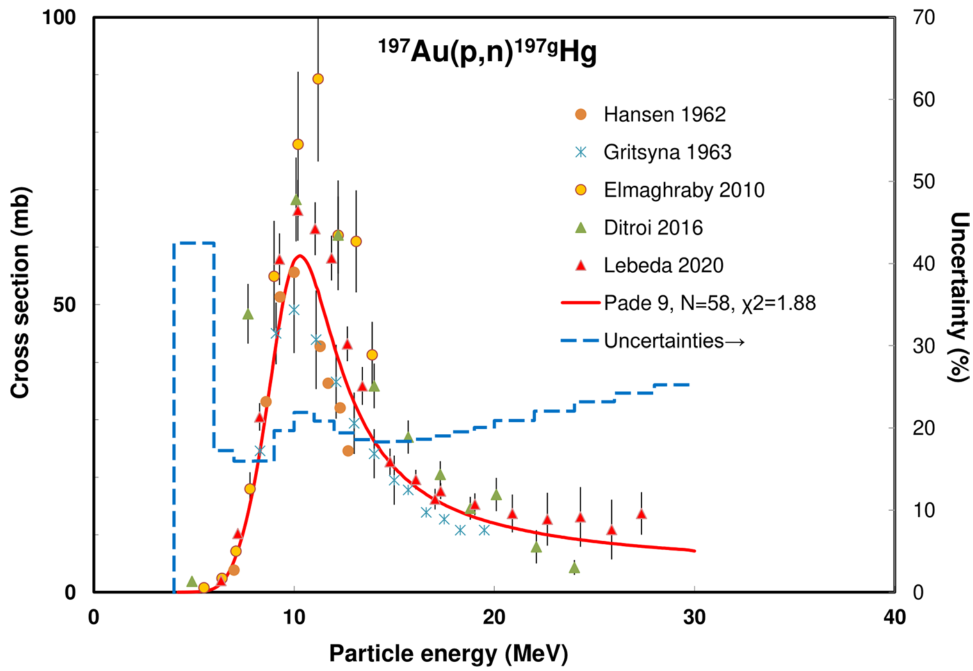

Fig. 136 $^{197}Au(p,n)^{197g}Hg$ reaction: selected experimental works and Padé fit (solid line) with total derived uncertainties, including 4% systematic uncertainty (dashed line, right-hand scale)

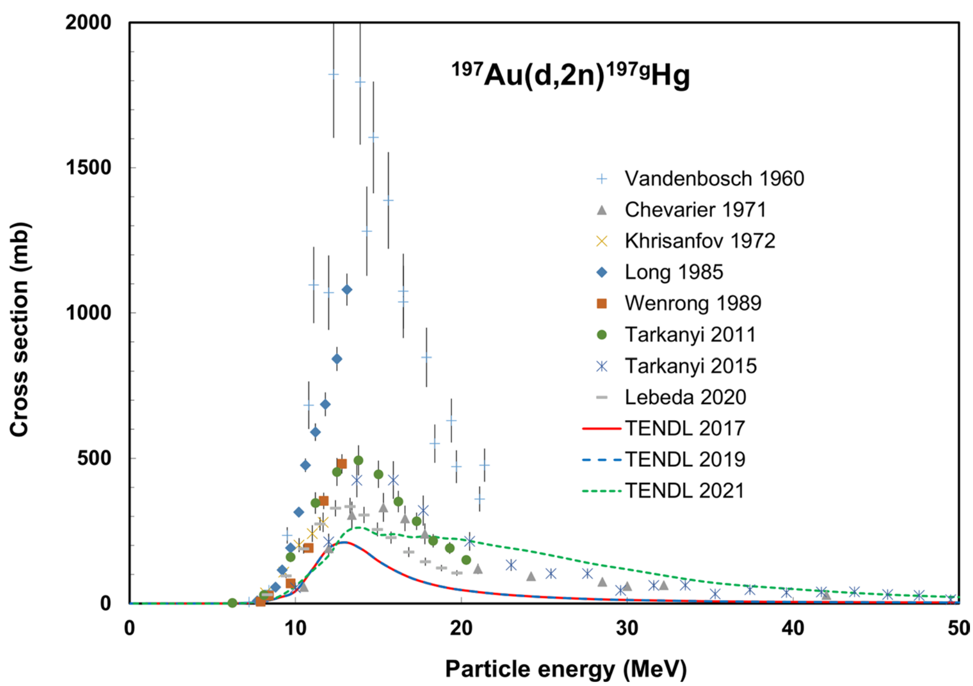

Fig. 137 $^{197}Au(d,2n)^{197g}Hg$ reaction: all experimental data and the TENDL theoretical excitation functions

A Padé fitting method was applied to the selected datasets, and uncertainties for all recommended cross-section data were deduced. The recommended cross-section data have been used to determine integral yields for practical radionuclide production.

The recommended data may also have a useful role in other fields of non-energy related nuclear studies (e.g., accelerator technology, activation analysis and thin layer activation) and further development of the theory and modelling of nuclear reactions.

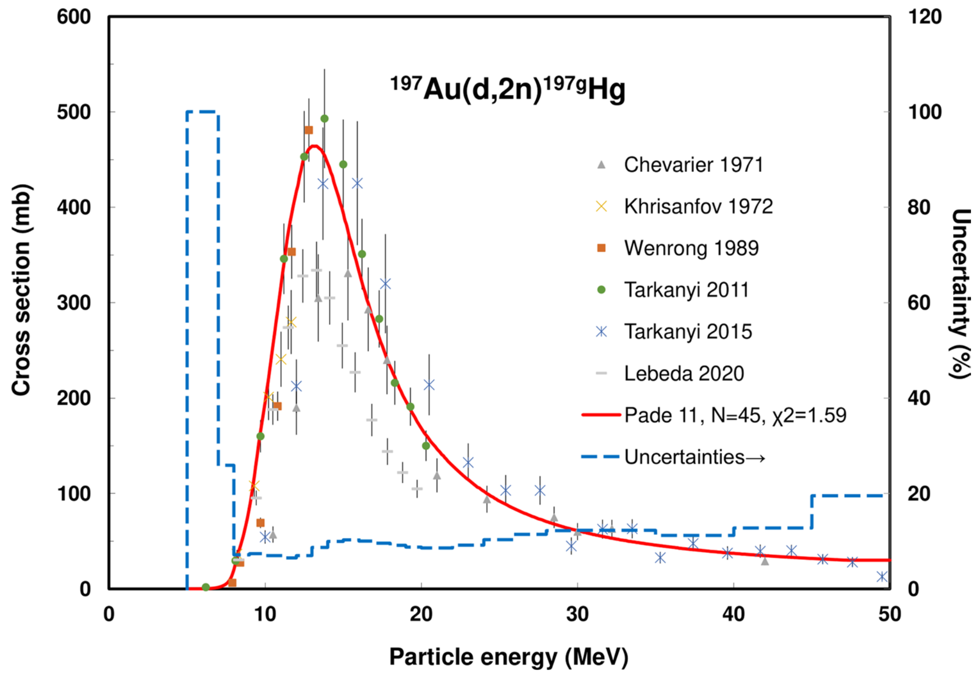

Fig. 138 ^{197}Au(d,2n)^{197g}Hg reaction: selected experimental works and Padé fit (solid line) with total derived uncertainties, including 4% systematic uncertainty (dashed line, right-hand scale)

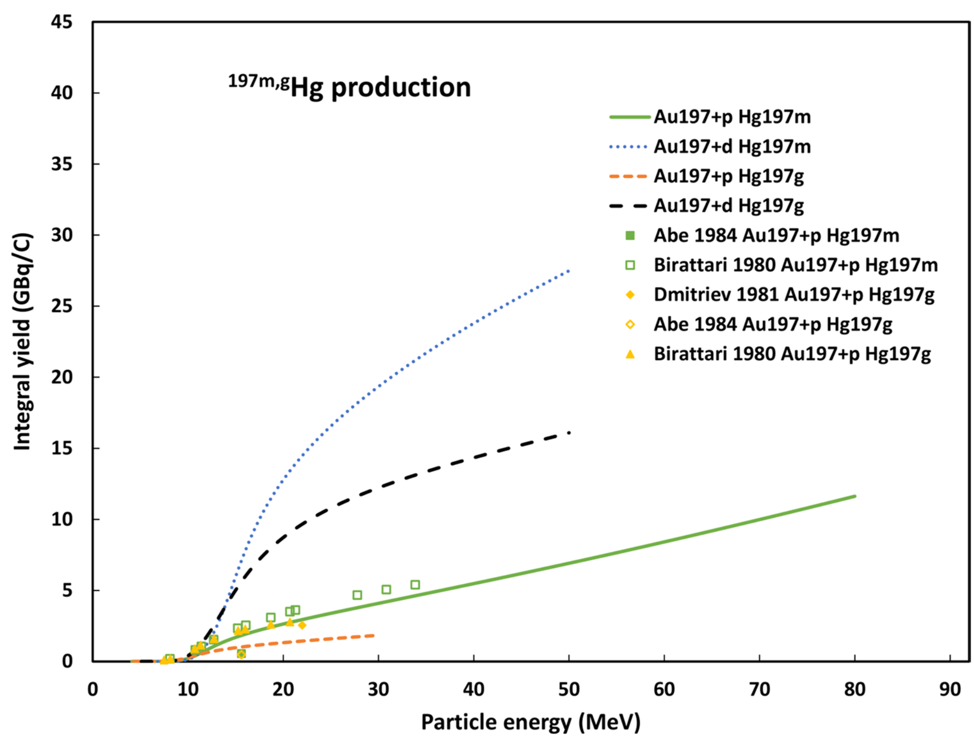

Fig. 139 Yield calculated from the recommended cross sections for ^{197m}Hg and ^{197g}Hg production

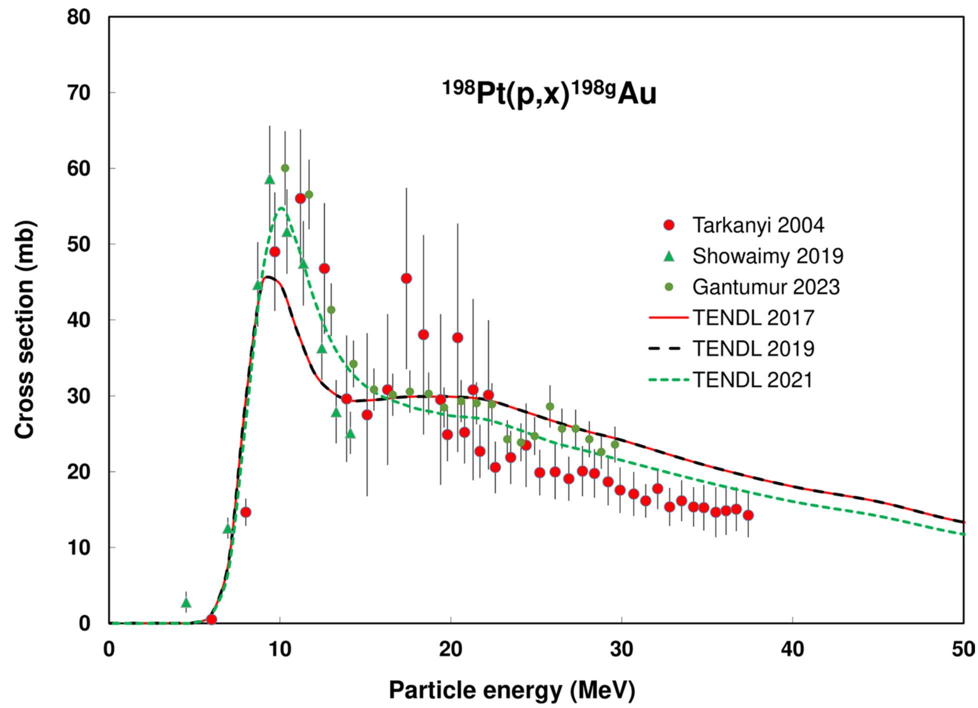

Fig. 140 ^{198}Pt(p,n)^{198g}Au reaction: all experimental data and the TENDL theoretical excitation functions

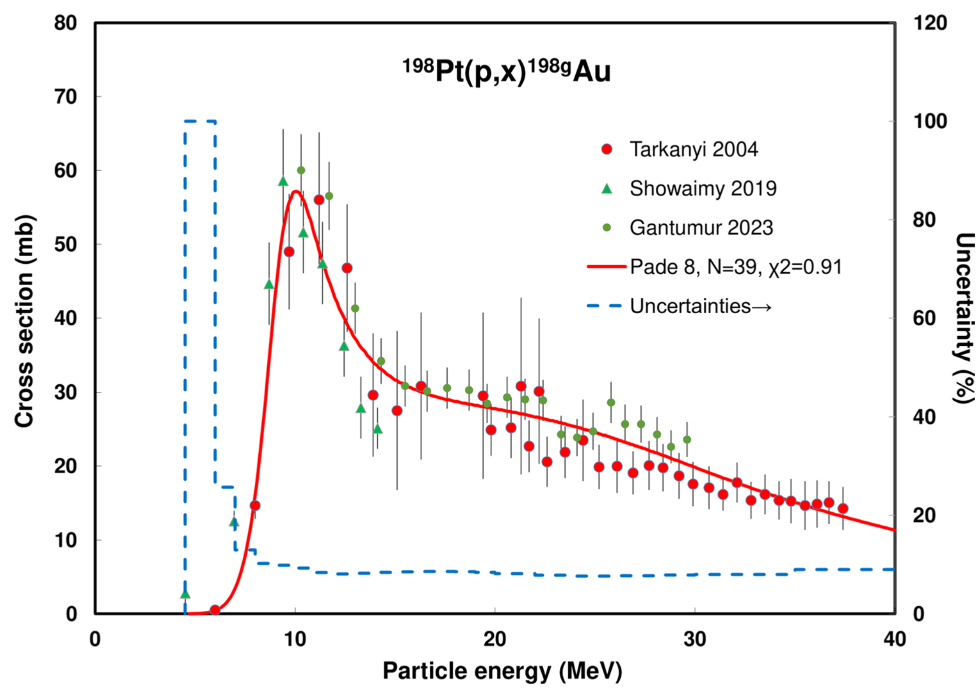

Fig. 141 ^{198}Pt(p,n)^{198g}Au reaction: selected experimental works and Padé fit (solid line) with total derived uncertainties, including 4% systematic uncertainty (dashed line, right-hand scale)

Fig. 142 ^{198}Pt(d,2n)^{198g}Au reaction: all experimental data and the TENDL theoretical excitation functions

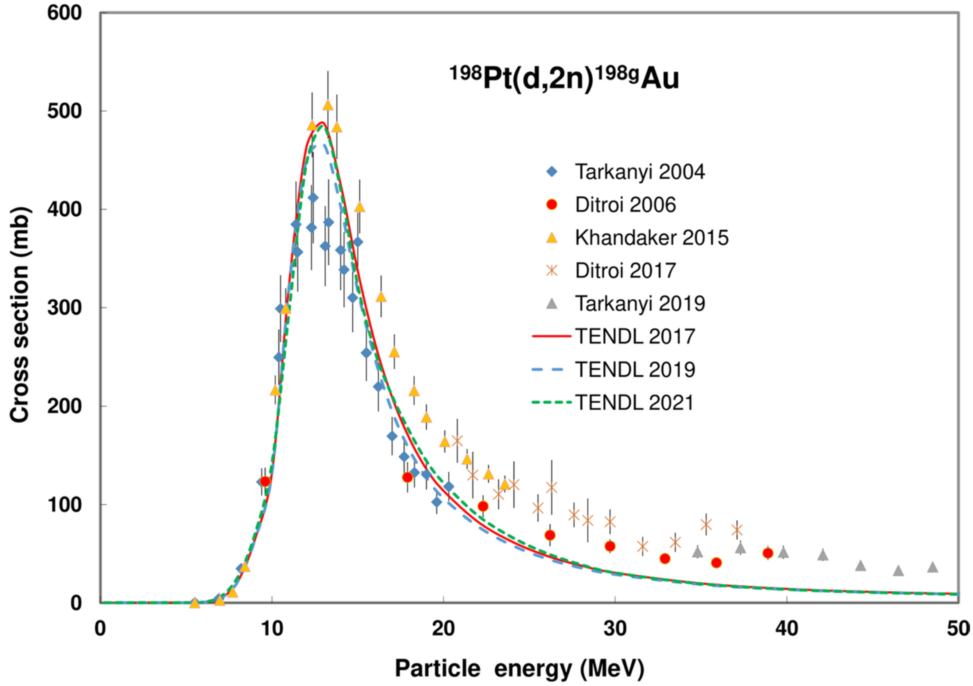

Fig. 143 ^{198}Pt(d,2n)^{198g}Au reaction: selected experimental works and Padé fit (solid line) with total derived uncertainties, including 4% systematic uncertainty (dashed line, right-hand scale)

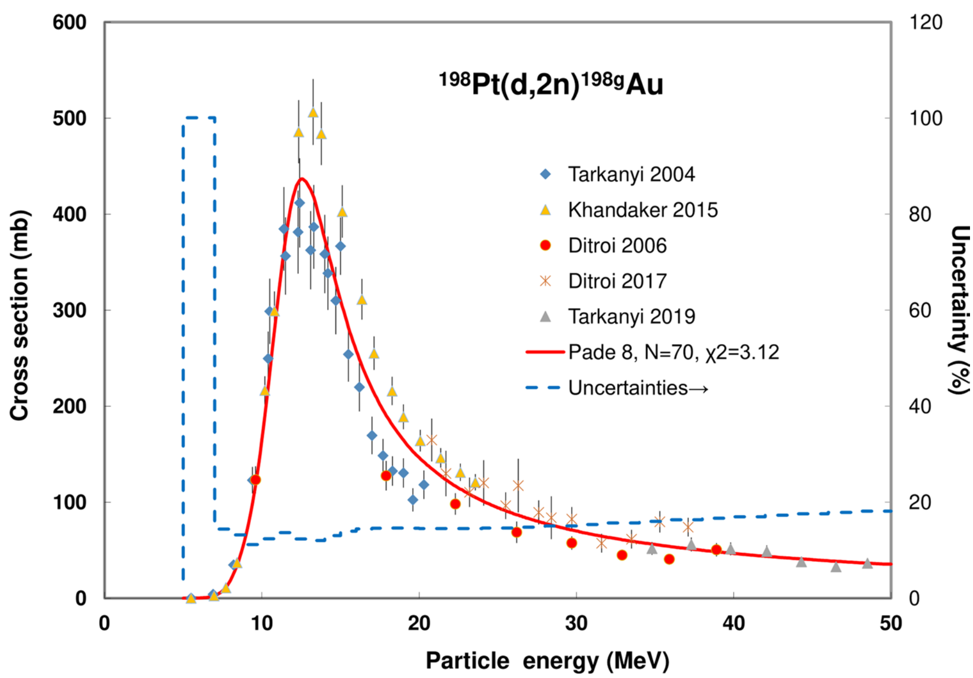

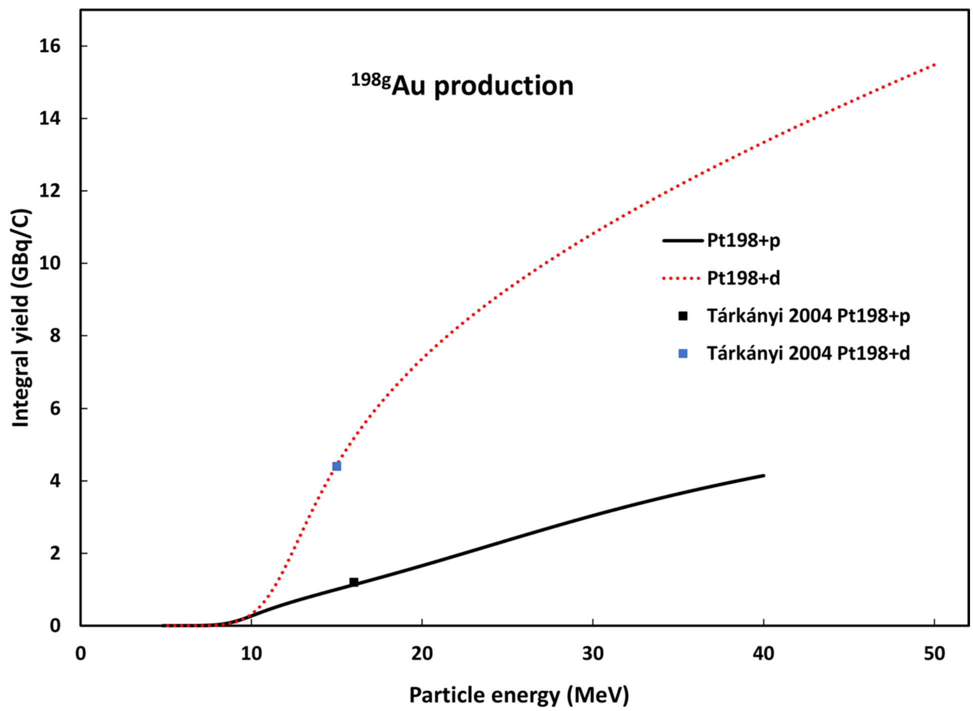

Fig. 144 Yield calculated from the recommended cross sections for ^{198g}Au production

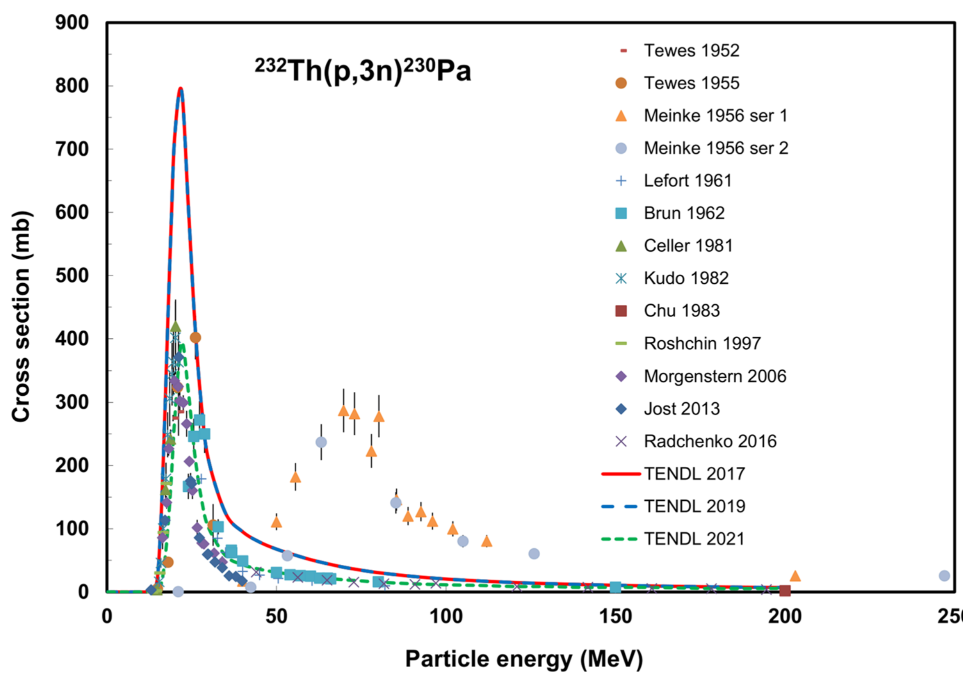

Fig. 145 ^{232}Th(p,3n)^{230}Pa reaction: all experimental data and the TENDL theoretical excitation functions

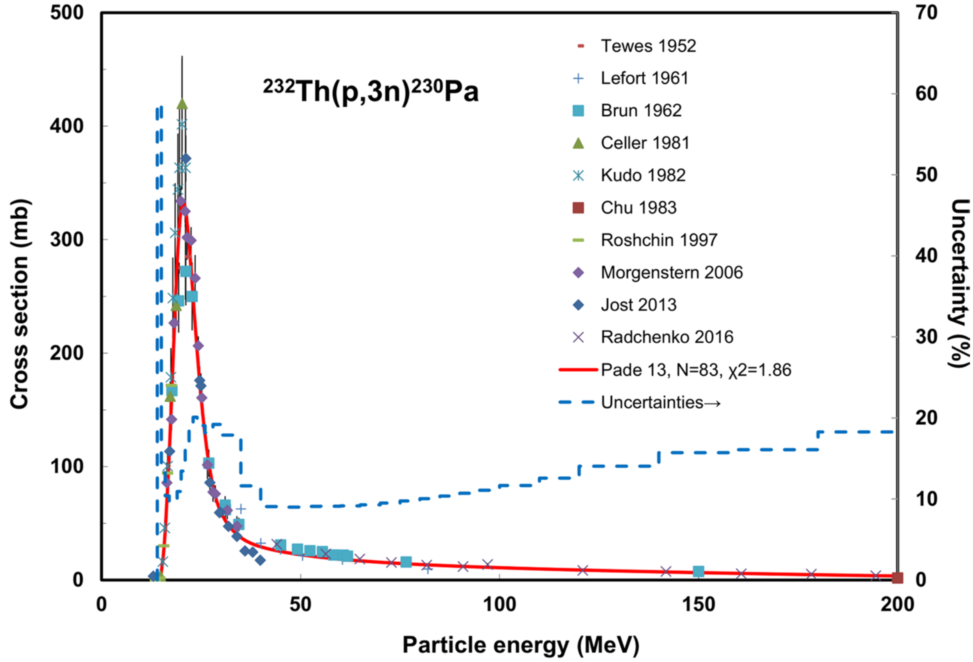

Fig. 146 $^{232}Th(p,3n).^{230}Pa$ reaction: selected experimental works and Padé fit (solid line) with total derived uncertainties, including 4% systematic uncertainty (dashed line, right-hand scale)

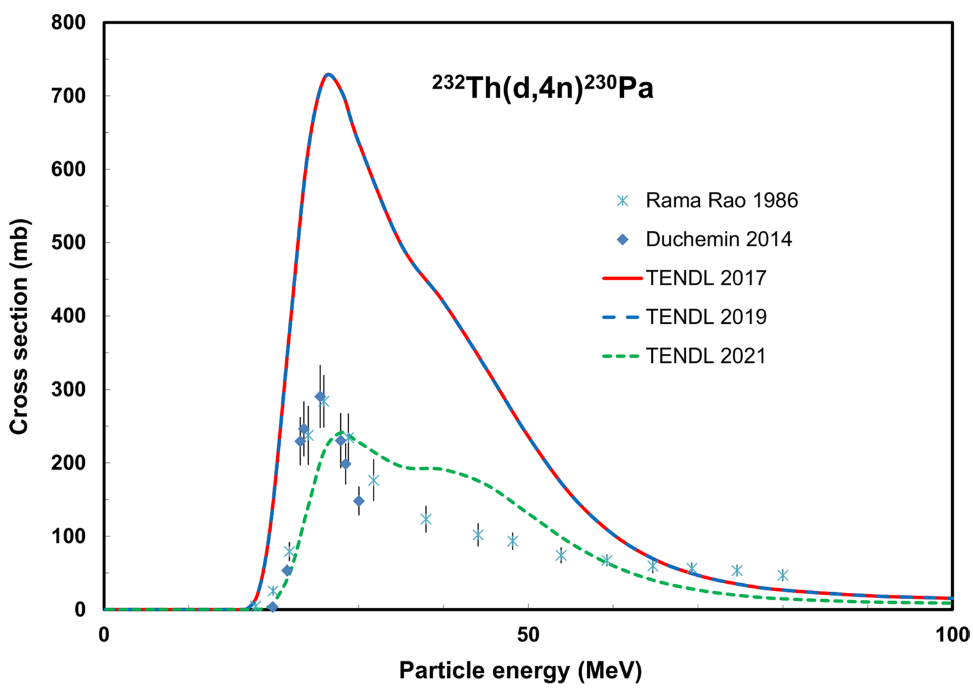

Fig. 147 $^{232}Th(d,4n)^{230}Pa$ reaction: all experimental data and the TENDL theoretical excitation functions

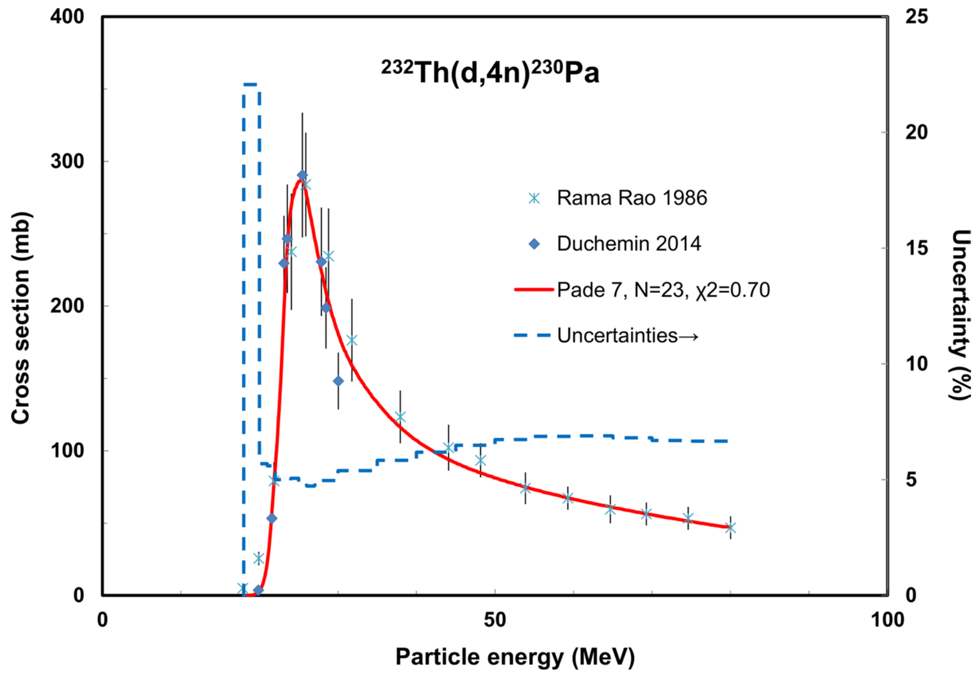

Fig. 148 ^{232}Th(d,4n)^{230}Pa reaction: selected experimental works and Padé fit (solid line) with total derived uncertainties, including 4% systematic uncertainty (dashed line, right-hand scale)

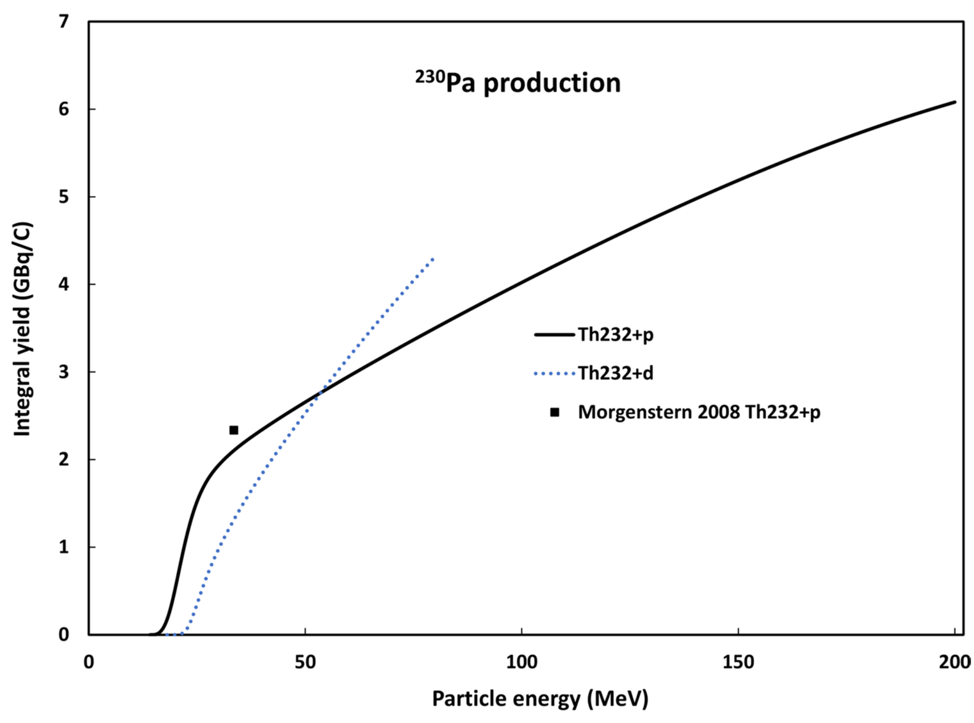

Fig. 149 Yield calculated from the recommended cross sections for ^{230}Pa production

Acknowledgements This work was partly supported by Project No. NKTA-42, which has been implemented with the support provided by the Ministry of Innovation and Technology of Hungary from the National Research, Development and Innovation Fund, financed under the TKP2021 funding scheme.

Funding Open access funding provided by ELKH Institute for Nuclear Research.

References

1. Tárkányi F, Takács S, Gul K, Hermanne A, Mustafa MG, Nortier M, Oblozinsky P, Qaim SM, Scholten B, Shubin YN, Youxiang Z (2001) Charged particles cross-sections database for medical radioisotope production, Beam monitors reactions, in: IAEA (Ed.) TECDOC-1211 http://www-nds.iaea.org/medical, IAEA
2. Betak E, Caldeira AD, Capote R, Carlson BV, Choi HD, Guimaraes FB, Ignatyuk AV, Kim SM, Király B, Kovalev SF, Menapace E, Nortier FM, Pompeia P, Qaim SM, Scholten B, Shubin YN, Sublet J-C, Tárkányi F, Nichols AL (2011) Nuclear data for the production of therapeutic radionuclides. In: Qaim SM, Tárkányi F, Capote R (eds) Technical Reprots Series. IAEA, Vienna, pp 1–377
3. Hermanne A, Ignatyuk AV, Capote R, Carlson BV, Engle JW, Kellett MA, Kibedi T, Kim G, Kondev FG, Hussain M, Lebeda O, Luca A, Nagai Y, Naik H, Nichols AL, Nortier FM, Suryanarayana SV, Takacs S, Tarkanyi FT, Verpelli M (2018) Reference cross sections for charged-particle monitor reactions. Nucl Data Sheets 148:338–382
4. Tarkanyi FT, Ignatyuk AV, Hermanne A, Capote R, Carlson BV, Engle JW, Kellett MA, Kibedi T, Kim GN, Kondev FG, Hussain M, Lebeda O, Luca A, Nagai Y, Naik H, Nichols AL, Nortier FM, Suryanarayana SV, Takacs S, Verpelli M (2019) Recommended nuclear data for medical radioisotope production: diagnostic positron emitters. J Radioanal Nucl Chem 319:533–666
5. Engle JW, Ignatyuk AV, Capote R, Carlson BV, Hermanne A, Kellett MA, Kibedi T, Kim G, Kondev FG, Hussain M, Lebeda O, Luca A, Nagai Y, Naik H, Nichols AL, Nortier FM, Suryanarayana SV, Takacs S, Tarkanyi FT, Verpelli M (2019) Recommended Nuclear Data for the Production of Selected Therapeutic Radionuclides. Nucl Data Sheets 155:56–74
6. Hermanne A, Tárkányi FT, Ignatyuk AV, Takács S, Capote R (2023) Evaluated and recommended cross-section data for production of radionuclides with emerging interest in nuclear medicine imaging. Part 1: Positron emission tomography (PET). Nucl Instrum Methods Phys Res Sect B Beam Interact Mater Atoms 535:149–192
7. Hermanne A, Tárkányi F, Ignatyuk A, Takács S, Capote R (2021) Upgrade of IAEA recommended data of selected nuclear reactions for production of PET and SPECT isotopes. Nucl Data Sheets 173:285–308
8. Tárkányi F, Hermanne A, Ignatyuk A, Takács S, Capote R (2022) Upgrade of recommended nuclear cross section data base for production of therapeutic radionuclides. J Radioanal Nucl Chem 331:1163–1206
9. Qaim SM, Tárkányi F, Capote R (2011) Nuclear data for the production of therapeutic radionuclides, technical reports series 473. IAEA, Vienna, p 1
10. Engle JW, Nichols AI, Capote Noy R (2018) Summary report: technical meeting on nuclear data for medical applications. IAEA, Vienna
11. Pade HE (1892) Sur la représentation d'une fonction par des fractions rationnelles. Ann L'Ecole Norm 9:3–93
12. Baker JGA, Gammel JL (1970) The padé approximants in theoretical physics. Academic Press, New York
13. Graves-Morris PR (1973) Padé approximants and their applications. Academic Press, New York
14. Otuka N, Takács S (2015) Definitions of radioisotope thick target yields. Radiochim Acta 103:1–6
15. NNDC (2022) NUDAT 3.0, Brookhaven National Laboratory, https://www.nndc.bnl.gov/nudat3/
16. Heininger CG, Wiig EO (1956) Spallation of vanadium with 60-, 100-, 175-, and 240-Mev Protons. Phys Rev 101:1074–1076
17. Hontzeas S, Yaffe L (1963) Interaction of vanadium with protons of energies up to 84 MeV. Can J Chem 41:2194
18. Michel R, Peiffer F, Stuck R (1985) Measurement and hybrid model analysis of integral excitation-functions for proton-induced reactions on vanadium, manganese and cobalt up to 200 Mev. Nucl Phys A 441:617–639
19. Michel R, Brinkmann G, Weigel H, Herr W (1979) Measurement and hybrid-model analysis of proton-induced reactions with V, Fe and Co. Nucl Phys A 322:40–60
20. Levkovskii VN (1991) The cross-sections of activation of nuclides of middle-range mass (A=40-100) by protons and alpha particles of middle range energies (E=10-50 MeV). Inter-Vesy, Moscow
21. Pupillo G, Mou L, Boschi A, Calzaferri S, Canton L, Cisternino S, De Dominicis L, Duatti A, Fontana A, Haddad F, Martini P, Pasquali M, Skliarova H, Esposito J (2019) Production of Sc-47 with natural vanadium targets: results of the PASTA project. J Radioanal Nucl Chem 322:1711–1718
22. Barbaro F, Canton L, Carante M, Colombi A, De Dominicis L, Fontana A, Haddad F, Mou L, Pupillo G (2021) New results on proton-induced reactions on vanadium for 47Sc production and the impact of level densities on theoretical cross sections. Phys Rev C 104:044619
23. Acerbi E, Birattari C, Castiglioni M, Resmini F (1976) Nuclear applied physics at milan cyclotron. J Radioanal Chem 34:191–217
24. Dmitriev PP, Krasnov NN, Molin GA (1983) Yields of radioactive nuclides formed by bombardment of a thick target with 22-MeV Deuterons, INDC(CCP)-210/L
25. Qaim S, Probst H (1984) Excitation-functions of deuteron induced nuclear reactions on vanadium with special reference to the production of K-43 - systematics of (d, xn) reaction cross-sections relevant to the formation of highly neutron deficient radioisotopes. Radiochim Acta 35:11–14
26. Tarkanyi F, Ditroi F, Takacs S, Hermanne A, Baba M, Ignatyuk AV (2011) Investigation of activation cross-sections of deuteron induced reactions on vanadium up to 40 MeV. Nucl Instrum Methods Phys Res Sect B Beam Interact Mater Atoms 269:1792–1800
27. Sonzogni A, Romo A, Mosca H, Nasiff S (1993) Alpha and deuteron induced reactions on vanadium. J Radioanal Nucl Chem 170:143–156
28. Michel R, Bodemann R, Busemann H, Daunke R, Gloris M, Lange HJ, Klug B, Krins A, Leya I, Lüpke M, Neumann S,

Reinhardt H, Schnatz-Büttgen M, Herpers U, Schiekel T, Sudbrock F, Holmqvist B, Condé H, Malmborg P, Suter M, Dittrich-Hannen B, Kubik PW, Synal HA, Filges D (1997) Cross sections for the production of residual nuclides by low- and medium-energy protons from the target elements C, N, O, Mg, Al, Si, Ca, Ti, V, Mn, Fe Co, Ni, Cu, Sr, Y, Zr, Nb, Ba and Au. Nucl Instrum Methods Phys Res Sect B 129:153–193
29. Neumann S (1999) Activation experiments with medium-energy neutrons and the production of cosmogenic nuclides in extraterrestrial matter (dissertation)
30. Michel R, Brinkmann G, Weigel H, Herr W (1978) Proton-induced reactions on titanium with energies between 13 and 45 MeV. J Inorg Nucl Chem 40:1845–1851
31. Michel R, Brinkmann G (1980) On the depth-dependent production of radionuclides (44-Less-Than-or-Equal-to-a-Less-Than-or-Equal-to-59) by solar protons in extraterrestrial matter. J Radioanal Chem 59:467–510
32. Fink D, Sisterson J, Vogt S, Herzog G, Klein J, Middleton R, Koehler A, Magliss A (1990) Production of Ca-41 and K, Sc and V short-lived isotopes by the irradiation of Ti with 35 to 150 Me\V protons - applications to solar cosmic-ray studies. Nucl Instrum Methods Phys Res Sect B Beam Interact Mater Atoms 52:601–607
33. Brodzinski RL, Rancitelli LA, Cooper JA, Wogman NA (1971) High-energy proton spallation of titanium. Phys Rev C 4:1250–1257
34. Kopecky P, Szelecsényi F, Molnar T, Mikecz P, Tárkányi F (1993) Excitation-functions of (P, Xn) reactions on (Nat)Ti - monitoring of bombarding proton-beams. Appl Radiat Isot 44:687–692
35. Zarie K, Al-Hammad N, Azzam A (2006) Experimental study of excitation functions of some proton induced reactions on Ti-nat for beam monitoring purposes. Radiochim Acta 94:795–799
36. Khandaker MU, Kim K, Lee MW, Kim KS, Kim GN, Cho YS, Lee YO (2009) Investigations of the natTi(p, x)43,44m,44g,46,47,48Sc,48V nuclear processes up to 40MeV. Appl Radiat Isot 67:1348–1354
37. Garrido E, Duchemin C, Guertin A, Haddad F, Michel N, Metivier V (2016) New excitation functions for proton induced reactions on natural titanium, nickel and copper up to 70 MeV. Nucl Instrum Methods Phys Res Sect B Beam Interact Mater Atoms 383:191–212
38. Parashari S, Mukherjee S, Nayak B, Naik H, Suryanarayana S, Makwana R, Singh N (2019) Excitation function of the natTi(p, x)V-48, Sc-47, Sc-46, Sc-44m reactions within the energy range of 10–22 MeV. Nucl Phys A 987:128–143
39. Cervenak J, Lebeda O (2020) New cross-section data for proton-induced reactions on Ti-nat and Cu-nat with special regard to the beam monitoring. Nucl Instrum Methods Phys Res Sect B Beam Interact Mater Atoms 480:78–97
40. Azzam A, Hamada M, Said S, Mohamed G, Al-abyad M (2020) Excitation functions for proton-induced reactions on Te and Ti-nat targets: Measurements and model calculations special relevant to the Te-128(p, n)I-128 reaction. Nucl Phys a 999:121790
41. Voyles A, Lewis A, Morrell J, Basunia M, Bernstein L, Engle J, Graves S, Matthews E (2021) Proton-induced reactions on Fe, Cu, and Ti from threshold to 55 MeV. Eur Phys J a 57:1–23
42. Liu B, Han R, Yuan C, Sun H, Chen Z, Tian G, Shi F, Zhang X, Luo P, Jia H (2021) Excitation functions of proton induced reactions on titanium and copper. Appl Radiat Isot 173:109713
43. Dmitriev PP (1983) Systematics of nuclear reaction yields for thick target at 22 MeV proton energy. Vop. At. Nauki i Tekhn. Ser.Yadernye Konstanty 57:2
44. Sabbioni E, Marafante E, Goetz L, Birattari C (1977) Cyclotron production of carrier free V-48 and preparation of different V-48 compounds for metabolic studies in rats. Radiochem Radioanal Lett 31:39–46
45. Takács S, Sonck M, Scholten B, Hermanne A, Tárkányi F (1997) Excitation functions of deuteron induced nuclear reactions on Ti-nat up to 20 MeV for monitoring deuteron beams. Appl Radiat Isot 48:657–665
46. Hermanne A, Sonck M, Takács S, Tárkányi F (2000) Experimental study of excitation functions for some reactions induced by deuterons (10–50 Mev) on natural Fe and Ti. Nucl Inst Methods Phys Res Sect B Beam Interact Mater Atoms 161:178–185
47. Takács S, Király B, Tárkányi F, Hermanne A (2007) Evaluated activation cross sections of longer-lived radionuclides produced by deuteron induced reactions on natural titanium. Nucl Inst Methods Phys Res Sect B Beam Interact Mater Atoms 262:7–12
48. Gagnon K, Avila-Rodriguez M, Wilson J, McQuarrie S (2010) Experimental deuteron cross section measurements using single natural titanium foils from 3 to 9 MeV with special reference to the production of V-47 and Ti-51. Nucl Inst Methods Phys Res Sect B Beam Interact Mater Atoms 268:1392–1398
49. Khandaker M, Haba H, Kanaya J, Otuka N (2013) Excitation functions of (d, x) nuclear reactions on natural titanium up to 24 MeV. Nucl Inst Methods Phys Res Sect B Beam Interact Mater Atoms 296:14–21
50. Khandaker MU, Haba H, Kanaya J, Otuka N, Kassim HA (2014) Activation cross-sections of deuteron-induced nuclear reactions on natural titanium. Nucl Data Sheets 119:252–254
51. Lebeda O, Stursa J, Ralis J (2015) Experimental cross-sections of deuteron-induced reaction on Y-89 up to 20 MeV; comparison of Ti-nat(d, x)V-48 and Al-27(d, x)Na-24 monitor reactions. Nucl Inst Methods Phys Res Sect B Beam Interact Mater Atoms 360:118–128
52. Duchemin C, Guertin A, Haddad F, Michel N, Metivier V (2015) Cross section measurements of deuteron induced nuclear reactions on natural titanium up to 34 MeV. Appl Radiat Isot 103:160–165
53. Gadioli E, Gadioli Erba E, Hogan JJ, Burns KI (1981) Emission of alpha particles in the interaction of 10–85 MeV protons with48,50Ti. Zeitschrift für Physik A Atoms Nuclei 301:289–300
54. Levkovskii VN (1991) Activation cross sections for the nuclides of medium mass region (A=40-100) with medium energy (E=10-50 MeV) protons and alppha-particles (Experiment and Systematics). Inter-Vesti, Moscow
55. Levenberg I, Pokrovsky V, Yutlandov I (1963) Simple nuclear reactions on Ca48 induced by high energy protons. Nucl Phys 41:504–510
56. Carzaniga T, Braccini S (2019) Cross-section measurement of Sc-44m, Sc-47, Sc-48 and Ca-47 for an optimized Sc-47 production with an 18 MeV medical PET cyclotron. Appl Radiat Isot 143:18–23
57. M. Sitarz (2019) Research on production of new medical radioisotopes with cyclotron, PhD thesis, niversité de Nantes, Nantes, France
58. Misiak R, Walczak R, Was B, Bartyzel M, Mietelski J, Bilewicz A (2017) Sc-47 production development by cyclotron irradiation of Ca-48. J Radioanal Nucl Chem 313:429–434
59. Zarubin P, Abuissa N, Smirnov A, Antropov A (1990) The total cross section of the reaction Fe-58(p, n) at Ep=5.2 and 6.1 MeV. Izv Akad Nauk, Ser Fiz 54:104–108
60. Sudar S, Qaim S (1996) Isomeric cross-section ratio for the formation of Co-58(m, g) in neutron, proton, deuteron, and alpha-particle induced reactions in the energy region up to 25 MeV. Phys Rev C 53:2885–2892
61. Matsuo T, Matuszek JM, Dudey ND, Sugihara TT (1965) Cross-section ratios of isomeric nuclides produced in medium-energy

($\ensuremath{\alpha}, \mathrm{xn}$) reactions. Phys Rev 139:B886–B895
62. Long X-G, He F-Q, Peng X-F, Liu M-T (1990) Excitation functions for the Mn-55(a, n)Co-58-m, g, Mn-55(a,2n)Co-57 and Mn-55(a, a+n)Mn-54 reactions. Chin Phys C 14:444–450
63. Stelson PH, McGowan FK (1964) Cross sections for (alpha, n) reactions for medium-weight nuclei. Phys Rev 133:B911–B919
64. Antropov AE, Valid K, Smirnov AV, Gusev VP, Abu Issa NN, Z PP, Kolozhvari AA (1989) The investigation of reaction ^{68}Zn(a ,n)^{71}Ge at alpha particles energy 14–244 MeV, 39. In: Conf. Nucl. Spectrosc. and Nucl. Struct., Tashkent, pp 352
65. Rizvi I, Bhardawaj M, Ansari M, Chaubey A (1989) Non-equilibrium effects in alpha particle induced reactions on gallium isotopes. Can J Phys 67:870–875
66. Ismail M (1990) Measurement and analysis of the excitation function for alpha-induced reactions on Ga and Sb isotopes. Phys Rev C 41:87–108
67. Didik V, Malkovich R, Skoryatina E, Kozlovskii V (1994) Experimental determination of the cross-sections of nuclear reactions by the method of analysis of the concentration profiles of transmutation nuclides. At Energ 77:570–572
68. Basile D, Birattari C, Bonardi M, Goetz L, Sabbioni E, Salomone A (1981) Excitation-functions and production of arsenic radioisotopes for environmental toxicology and biomedical purposes. Int J Appl Radiat Isot 32:403–410
69. Horiguchi T, Kumahora H, Inoue H, Yoshizawa Y (1983) Excitation functions of Ge(p, xnyp) reactions and production of Ge-68. Appl Radiat Isot 34:1531–1535
70. Spahn I, S GF, Kandil SA, Coenen HH, Qaim SM (2007) New nuclear data for production of ^{73}As, ^{88}Y and ^{153}Sm: important radionuclides for environmental and medical applications<h1 data-test-id="paper-detail-title">. In: international conference on nuclear data for science and technology 2007, EDPS, Nice, pp 1363–1366
71. Barabanov I, Bezrukov L, Gurentsov V, Zhuykov B, Kianovsky S, Kornoukhov V, Kohanuk V, Yanovich E (2010) Measurement of the cross sections for the production of the isotopes As-74, Ge-68, Zn-65, and Co-60 from natural and enriched germanium irradiated with 100-MeV protons. Phys At Nucl 73:1106–1110
72. Otozai K, Kuze S, Okamura H, Mito A, Nishi T, Fujiwara I (1968) Excitation functions for deuterium-induced reactions. Nucl Phys Sect A 107:427–435
73. Takacs S, Takacs MP, Hermanne A, Tarkanyi F, Adam-Rebeles R (2014) Excitation functions of longer lived radionuclides formed by deuteron irradiation of germanium. Nucl Instrum Methods Phys Res Sect B Beam Interact Mater Atoms 336:81–95
74. Spahn I, Steyn G, Nortier F, Coenen H, Qaim S (2007) Excitation functions of Ge-nat(p, xn)(71,72,73,74) As reactions up to 100 MeV with a focus on the production of As-72 for medical and As-73 for environmental studies. Appl Radiat Isot 65:1057–1064
75. Johnson CH, Galonsky A, Ulrich JP (1958) Proton strength functions from (p, n) cross sections. Phys Rev 109:1243
76. Johnson CH, Galonsky A, Inskeep CN (1960) Cross sections for (p, n) reactions in intermediate-weight nuclei. Phys Rev A 136:B1719–B1729
77. Johnson CH, Trail CC, Galonsky A (1964) Thresholds for (p, n) reactions on 26 intermediate- weight nuclei. Phys Rev B 136:1719
78. Nozaki T, Iwamoto M, Itoh Y (1979) Production of Br-77 by various nuclear reactions. Appl Radiat Isot 30:79–83
79. Gyurky G, Fulop Z, Somorjai E, Kokkoris M, Galanopoulos S, Demetriou P, Harissopulos S, Rauscher T, Goriely S (2003) Proton induced reaction cross section measurements on Se isotopes for the astrophysical p process. Phys Rev C 68:055803
80. Hassan H, Qaim S, Shubin Y, Azzam A, Morsy M, Coenen H (2004) Experimental studies and nuclear model calculations on proton-induced reactions on Se-nat, Se-76 and Se-77 with particular reference to the production of the medically interesting radionuclides Br-76 and Br-77. Appl Radiat Isot 60:899–909
81. El-Azony K, Suzuki K, Fukumura T, Szelecsenyi F, Kovacs Z (2009) Excitation functions of proton induced reactions on natural selenium up to 62 MeV. Radiochim Acta 97:71–77
82. Spahn I, Steyn G, Vermeulen C, Kovacs Z, Szelecsenyi F, Shehata M, Spellerberg S, Scholten B, Coenen H, Qaim S (2010) New cross section measurements for the production of the Auger electron emitters Br-77 and Br-80m. Radiochim Acta 98:749–755
83. Foteinou V, Harissopulos S, Axiotis M, Lagoyannis A, Provatas G, Spyrou A, Perdikakis G, Zarkadas C, Demetriou P (2018) Cross section measurements of proton capture reactions on Se isotopes relevant to the astrophysical p process. Phys Rev C 97:035806
84. Janssen AGM, Van Den Bosch RLP, De Goeij JJM, Theelen HMJ (1980) The reactions 77Se(p, n) and 78Se(p, 2n) as production routes for 77Br. Int J Appl Radiat Isot 31:405–409
85. Dmitriev PP, Panarin MV, Dmitrieva ZP (1982) ^{76}Br, ^{77}Br, and ^{82}Br yield in nuclear reactions with protons, deuterons, and alpha particles. Sov At Energy 52:99
86. Nickles RJ (1991) A shotgun approach to the chart of the nuclides. Radiotracer production with an 11 MeV proton cyclotron. Acta Radiol Suppl 376:69–71
87. Madhusudhan C, Treves S, Wolf A, Lambrecht R (1979) Cyclotron isotopes and radiopharmaceuticals.31. improvements in Br-77 production and radichemical separation from enriched Se-78+. J Radioanal Chem 53:299–305
88. Lundqvist H, Malmborg P, Langstrom B, Chiengmai S (1979) Simple production of Br-77(-) and I-123(-) and their use in the labelling of [BRUDR-Br-77 and [IUDR-I-123. Int J Appl Radiat Isot 30:39–43
89. Diksic M, Galinier J, Marshall H, Yaffe L (1979) Br-79 and Br-81 (p, xn) and (p, pxn) excitation functions in the energy range 10 MeV 85 MeV. Phys Rev C 19:1753–1761
90. Dejong D, Kooiman H, Veenboer J (1979) Br-76 and Br-77 from decay of cyclotron produced Kr-76 and Kr-77. Appl Radiat Isot 30:786–788
91. Weinreich R, Knieper J (1983) Production of Kr-77 and Kr-79 for medical applications via proton irradiation of bromine - Excitation functions, yields, and separation procedure. Appl Radiat Isot 34:1335–1338
92. Sakamoto K, Dohniwa M, Okada K (1985) Excitation functions for (p, xn) and (p, pxn) reactions on natural 79 + 81Br, 85 + 87Rb, 127I and 133Cs upto Ep=52 MeV. Int J Appl Radiat Isot 36:481–488
93. Deptula C, Khalkin VA, Kim SH, Knotek O, Konov VA, Mikecz P, Poponenkova LM, Rurarz E, Zaitseva NG (1990) Excitation functions and yields for medically generator Sr82-Rb82, Xe123-I123 and Bi201-Pb201-Tl201 obtained with 100 MeV protons. Nukleonika 35:3–47
94. Zaitseva N, Deptula C, Knotek O, Khan K, Mikolaewski S, Mikecz P, Rurarz E, Khalkin V, Konov V, Popinenkova L (1991) Gross-sections for the 100 MeV proton induced nuclear reactions and yields of some radionuclides used in nuclear medicine. Radiochim Acta 54:57–71
95. de Villiers D, Nortier M, Richter W (2002) Experimental and theoretical excitation functions for Br-nat(p, x) reactions. Appl Radiat Isot 57:907–913
96. Waters SL, Nunn AD, Thakur ML (1973) Cross-section measurements for the 75As(α,2n)77Br reaction. J Inorg Nucl Chem 35:3413–3416
97. Alfassi Z, Weinreich R (1982) The production of positron emitters Br-75 and Br-76 - excitation functions and yields for He-3

and alpha-particle induced nuclear reactions on arsenic. Radiochim Acta 30:67–71
98. Qaim SM, Blessing G, Ollig H (1986) Excitation functions of 75As (α, n)78Br and 75As (α, 2n)77m, gBr reactions from threshold to 28 MeV. Radiochim Acta 39:57–60
99. Breunig K, Spahn I, Hermanne A, Spellerberg S, Scholten B, Coenen H (2017) Cross section measurements of As-75(alpha, xn)Br-76, Br-77, Br-78 and As-75(alpha, x)As-74 nuclear reactions using the monitor radionuclides Ga-67 and Ga-66 for beam evaluation. Radiochim Acta 105:431–439
100. Steyn G, Mills S, Nortier F, Haasbroek F (1991) Integral excitation functions for Kr-nat + p up to 116 MeV and optimization of the production of Rb-81 for Kr-81m generators. Appl Radiat Isot 42:361–370
101. Tárkányi F, Kovács Z, Qaim SM (1993) Excitation-functions of proton-induced nuclear-reactions on highly enriched ^{78}Kr - relevance to the production of ^{75}Br and ^{77}Br at a small cyclotron. Appl Radiat Isot 44:1105–1111
102. Blaser JP, Boehm F, Marmier P, Scherrer P (1951) Anregungsfunctionen und Wirkungsquerschnitte der (p, n)-Reaktion (II). Helv Phys Acta 24:441
103. Debuyst R, Vander Stricht A (1968) Excitation functions and yield ratios for the isomeric pair 80Br 80mBr formed in (d, 2n), (α, np), (α, p) and (p, n) reactions on selenium. J Inorg Nucl Chem 30:691–698
104. Tarkanyi F, Takacs S, Ditroi F, Szucs Z, Brezovcsik K, Hermanne A, Ignatyuk A (2021) Investigation of cross sections of deuteron induced nuclear reactions on selenium up to 50 MeV. Eur Phys J a 57:117
105. Vakilova G, Vasidov A, Mukhammedov S, Pardaev E, Rakhmanov A, Saidmuradov Z (1983) Sensitivity of the determination of some elements with Z less-than-or-equal-to 42 by a deuteron activational method in a cyclotron, soviet. At Energ 55:598–602
106. Tárkányi F, Takács S, Gul K, Hermanne A, Mustafa MG, Nortier M, Oblozinsky P, Qaim SM, Scholten B, Shubin YN, Youxiang Z (2001) Beam monitor reactions (Chapter 4). Charged particle cross-section database for medical radioisotope production: diagnostic radioisotopes and monitor reactions., TECDOC 1211, IAEA, pp 49
107. Fassbender M, Nortier F, Schroeder I, van der Walt T (1999) The production of Pd-103 via the Ag-nat(p, x)Pd-103 nuclear process. Radiochim Acta 87:87–91
108. Uddin MS, Hagiwara M, Baba M, Tárkányi F, Ditrói F (2005) Experimental studies on excitation functions of the proton-induced activation reactions on silver. Appl Radiat Isot 62:533–540
109. Gagnon K, Wilson JS, Holt CMB, Lapi SE, Ferguson S, Mitlin D, McQuarrier SA (2017) Excitation functions for proton-induced reactions on natRu from 7 to 18 MeV. J Label Compd Radiopharm 60:S324
110. Hermanne A, Tarkanyi F, Takacs S (2021) Excitation functions for Rh, Ru and Tc radionuclides obtained by proton irradiation of natRu up to 33.6 MeV. Nucl Instrum Methods Phys Res Sect B Beam Interact Mater Atoms 502:205–218
111. Mito A, Komura K, Mitsugashira T, Otozai K (1969) Excitation functions for the (d, p) reactions on 96Ru, 102Ru and 104Ru. Nucl Phys A 129:165–171
112. Tárkányi F, Ditrói F, Takács S, Hermanne A, Ignatyuk AV, Spahn I, Spellerberg S (2021) Investigation of activation cross-sections of deuteron induced reactions on ruthenium up to 50 MeV. Appl Radiat Isot 168:109401
113. Esterlund EA, Pate BD (1965) Analysis of excitation functions via the compound statistical model. Nucl Phys 69:401
114. Graf HP, Munzel H (1974) Excitation Functions for α-Particle Reactions with Molybdenum Isotopes. J Inorg Nucl Chem 36:3647
115. Ditroi F, Hermanne A, Tarkanyi F, Takacs S, Ignatyuk AV (2012) Investigation of the alpha-particle induced nuclear reactions on natural molybdenum. Nucl Instrum Methods Phys Res Sect B Beam Interact Mater Atoms 285:125–141
116. Tarkanyi F, Hermanne A, Ditroi F, Takacs S, Ignatyuk A (2017) Investigation of activation cross section data of alpha particle induced nuclear reaction on molybdenum up to 40 MeV: review of production routes of medically relevant Ru-97, Ru-103. Nucl Instrum Methods Phys Res Sect B Beam Interact Mater Atoms 399:83–100
117. Qaim SM, Dohler H (1984) Production of carrier-free Sn-117m. Int J Appl Radiat Isot 35:645–650
118. Rebeles RA, Hermanne A, Van den Winkel P, Tárkányi F, Takács S, Daraban L (2008) Alpha induced reactions on Cd-114 and Cd-116: an experimental study of excitation functions. Nucl Instrum Methods Phys Res Sect B Beam Interact Mater Atoms 266:4731–4737
119. Hermanne A, Daraban L, Rebeles RA, Ignatyuk A, Tárkányi F, Takács S (2010) Alpha induced reactions on natCd up to 38.5 MeV: Experimental and theoretical studies of the excitation functions. Nucl Instrum Methods Phys Res Sect B 268:1376–1391
120. Khandaker MU, Kim K, Lee M, Kim G (2014) Investigation of activation cross-sections of alpha-induced nuclear reactions on natural cadmium. Nucl Instrum Methods Phys Res Sect B Beam Interact Mater Atoms 333:80–91
121. Ditroi F, Takacs S, Haba H, Komori Y, Aikawa M (2016) Cross section measurement of alpha particle induced nuclear reactions on natural cadmium up to 52 MeV. Appl Radiat Isot 118:266–276
122. Montgomery DM, Porile NT (1969) Reactions of ^{116}Cd with intermediate energy ^{3}He and ^{4}He ions. Nucl Phys A 130:65–76
123. Ditrói F, Takács S, Haba H, Komori Y, Aikawa M, Szűcs Z, Saito M (2016) Excitation function of the alpha particle induced nuclear reactions on enriched ^{116}Cd, production of the ^{117m}Sn theranostic isotope. Nucl Inst Methods Phys Res B 385:1–8
124. Duchemin C, Essayan M, Guertin A, Haddad F, Michel N, Métivier V (2016) How to produce high specific activity tin-117 m using alpha particle beam. Appl Radiat Isot 115:113–124
125. Dmitriev PP, Panarin MV, Molin GA, Dmitrieva ZP (1975) Yields of Sn-113 and Sn-117m in nuclear-reactions with protons, deuterons, and alpha-particles, soviet. At Energ 39:734–735
126. Fukushima S, Hayashi S, Kume S, Okamura H, Otozai K, Sakamoto K, Tsujini R (1963) The production of high specific activities of tin. Bull Chem Soc Jp 36:1225
127. Fukushima S, Hayashi S, Kume S, Okamura H, Otozai K, Sakamoto K, Tsujino R, Yoshizawa Y (1963) The production of high specific activities of tin. Bull Chem Soc Jpn 36:1225
128. Bhardwaj MK, Rizvi IA, Chaubey AK (1992) Excitation function studies for the alpha induced reactions in indium. Int J Modern Phys E 1:389–396
129. Aikawa M, Saito M, Ukon N, Komori Y, Haba H (2018) Activation cross sections of alpha-induced reactions on natIn for 117mSn production. Nucl Instrum Methods Phys Res Sect B 426:18–21
130. Ermolaev S, Zhuikov B, Kokhanyuk V, Srivastava S (2007) Production yields of (117m)sn from natural antimony target in proton energy range 145–35 MeV. J Label Compd Radiopharm 50:611–612
131. Takács S, Takács MP, Hermanne A, Tárkányi F, Adam Rebeles R (2013) Cross sections of proton induced reactions on natSb. Nucl Instrum Methods Phys Res Sect B Beam Interact Mater Atoms 297:44–57

132. Mosby M, Birnbaum E, Nortier F, Engle J (2017) Cross sections for proton-induced reactions on Sb-nat up to 68 MeV. Nucl Instrum Methods Phys Res Sect B Beam Interact Mater Atoms 412:34–40
133. Ermolaev S, Zhuikov B, Kokhanyuk V, Matushko V, Srivastava S (2020) Cross sections and production yields of Sn-117m and other radionuclides generated in natural and enriched antimony with protons up to 145 MeV. Radiochim Acta 108:327–351
134. Klyucharev AP, Skakun EA, Rakivnenko YN, Romanii IA (1970) Excitation functions on reactions (p, n) on some Sn isotopes and isomeric ratios. Yadern Fiz 11:953
135. Johnson CH, Bair JK, Jones CM, Penny SK, Smith DW (1977) p-wave size resonances observed by the (p, n) reaction for 26- to 7-MeV protons incident on isotopes of Sn. Phys Rev C 15:196–216
136. Lovchikova G, Salnikov O, Simakov S, Trufanov A, Kotelnikova G, Pilz V, Streil T (1980) Study of the mechanism of the reactions Zr-94(p, n)Nb-94, Sn-119(p, n)Sb-119, and Sn-122(p, n) Sb-122 in the proton energy range 6–9 MeV. Soviet J Nucl Phys Ussr 31:1–5
137. Thisgaard H, Jensen M (2009) Production of the Auger emitter Sb-119 for targeted radionuclide therapy using a small PET-cyclotron. Appl Radiat Isot 67:34–38
138. Lagunassolar M, Carvacho O, Yang S, Yano Y (1990) Cyclotron production of PET radionuclides Sb-118 (3.5 min - beta+ 75-% - EC 25-%) from high energy protons on natural Sb targets. Appl Radiat Isot 41:521–529
139. Yi J, Miller D (1992) Cross-sections of SB-NAT(P, X) reactions for 30 46 mev protons. Appl Radiat Isot 43:1103–1106
140. Tarkanyi F, Hermanne A, Ditroi F, Takacs S (2017) Activation cross section data of proton induced nuclear reactions on lanthanum in the 34–65 MeV energy range and application for production of medical radionuclides. J Radioanal Nucl Chem 312:691–704
141. Hermanne A, Tárkányi F, Takács S, Ditroi F, Ignatyuk A (2020) Deuteron induced reactions on tellurium: an alternative for production of 123I? Nucl Instrum Methods Phys Res Sect B 466:20–30
142. Becker K, Vermeulen E, Kutyreff C, O'Brien E, Morrell J, Birnbaum E, Bernstein L, Nortier F, Engle J (2020) Cross section measurements for proton induced reactions on natural La. Nucl Instrum Methods Phys Res Sect B Beam Interact Mater Atoms 468:81–88
143. Prescher K, Peiffer F, Stueck R, Michel R, Bodemann R, Rao MN, Mathew KJ (1991) Thin-target cross sections of proton-induced reactions on barium and solar cosmic ray production rates of xenon-isotopes in lunar surface materials. Nucl Instrum Methods Phys Res Sect B 53:105–121
144. Tarkanyi F, Ditroi F, Kiraly B, Takacs S, Hermanne A, Yamazaki H, Baba M, Mohammadi A, Ignatyuk AV (2010) Study of activation cross sections of proton induced reactions on barium: production of 131Ba–>131Cs. Appl Radiat Isot 68:1869–1877
145. Mironov YT (2001) Features of excitation function study of the nuclear reactions at internal beam in the PNPI synchrocyclotron. In: Conf. Nucl. Spectrosc. Nucl. Struct., Sarov, Russia, pp 276
146. Steyn GF, Vermeulen C, Szelecsényi F, Kovács Z, Hohn A, van der Meulen NP, Schibli R, van der Walt TN (2014) Cross sections of proton-induced reactions on 152Gd, 155Gd and 159Tb with emphasis on the production of selected Tb radionuclides. Nucl Instrum Methods Phys Res Sect B 319:128–140
147. Formento-Cavaier R, Haddad F, Alliot C, Sounalet T, Zahi I (2020) New excitation functions for proton induced reactions on natural gadolinium up to 70 MeV with focus on 149Tb production. Nucl Instrum Methods Phys Res Sect B 478:174–181
148. Tárkányi F, Hermanne A, Takács S, Ditrói F, Csikai J, Ignatyuk AV (2013) Cross-section measurement of some deuteron induced reactions on ^{160}Gd for possible production of the therapeutic radionuclide ^{161}Tb. J Radioanal Nucl Chem. https://doi.org/10.1007/s10967-013-2507-x
149. Szelecsényi F, Kovács Z, Nagatsu K, Zhang M-R, Suzuki K (2016) Investigation of deuteron-induced reactions on natGd up to 30 MeV: possibility of production of medically relevant 155Tb and 161Tb radioisotopes. J Radioanal Nucl Chem 307:1877–1881
150. Beyer GJ, Zeisler SK, Becker DW (2004) The Auger-electron emitter Er-165: excitation function of the Ho-165(p, n)Er-165 process. Radiochim Acta 92:219–222
151. Tarkanyi F, Hermanne A, Takacs S, Ditroi F, Kiraly B, Kovalev SF, Ignatyuk AV (2008) Experimental study of the (165)Ho(p, n) nuclear reaction for production of the therapeutic radioisotope (165)Er. Nucl Instrum Methods Phys Res Sect B Beam Interact Mater Atoms 266:3346–3352
152. Gracheva N, Carzaniga T, Schibli R, Braccini S, van der Meulen N (2020) Er-165: a new candidate for Auger electron therapy and its possible cyclotron production from natural holmium targets. Appl Radiat Isot 159:109079
153. Tarkanyi F, Takacs S, Hermanne A, Ditroi F, Kiraly B, Baba M, Ohtsuki T, Kovalev SF, Ignatyuk AV (2009) Investigation of production of the therapeutic radioisotope 165 Er by proton induced reactions on erbium in comparison with other production routes. Appl Radiat Isot 67:243–247
154. Tarkanyi F, Hermanne A, Takacs S, Kiraly B, Spahn I, Ignatyuk AV (2010) Experimental study of the excitation functions of proton induced nuclear reactions on (167)Er for production of medically relevant (167)Tm. Appl Radiat Isot 68:250–255
155. Tarkanyi F, Hermanne A, Takacs S, Ditroi F, Kiraly B, Kovalev SF, Ignatyuk AV (2008) Experimental study of the Ho-165(d, 2n) and Ho-165(d, p) nuclear reactions up to 20 MeV for production of the therapeutic radioisotopes Er-165 and Ho-166g. Nucl Instrum Methods Phys Res Sect B Beam Interact Mater Atoms 266:3529–3534
156. Hermanne A, Adam-Rebeles R, Tárkányi F, Takács S, Csikai J, Takács MP, Ignatyuk AV (2013) Deuteron induced reactions on Ho and La: experimental excitation functions and comparison with code results. Nucl Instrum Methods Phys Res Sect B Beam Interact Mater Atoms 311:102–111
157. Song TY, Kim JW, Kim HI, Lee CW, Lee YO, Yang SC, Kim KS, Kim GN (2014) Measurement of activation cross sections of erbium irradiated by proton beam. Nucl Data Sheets 119:249–251
158. Dmitriev PP, Molin GA, Panarin MV (1980) Yields of Tu-165, Tu-166, Tu-167, Tu-168, and Tu-170 in reactions with protons, deuterons, and alpha-particles, soviet. At Energ 48:419–421
159. Tarkanyi F, Hermanne A, Kiraly B, Takacs S, Ditroi F, Baba M, Ohtsuki T, Kovalev SF, Ignatyuk AV (2007) Study of activation cross-sections of deuteron induced reactions on erbium: production of radioisotopes for practical applications. Nucl Instrum Methods Phys Res Sect B Beam Interact Mater Atoms 259:829–835
160. Tarkanyi F, Hermanne A, Ditroi F, Takacs S (2018) Study of activation cross sections of deuteron induced reactions on erbium in the 32–50 MeV energy range. Appl Radiat Isot 135:67–71
161. Khandaker M, Haba H, Komori Y, Otuka N (2020) Excitation functions of deuteron-induced nuclear reactions on erbium in the energy range of 4–24 MeV. Nucl Instrum Methods Phys Res Sect B Beam Interact Mater Atoms 470:1–9
162. Hermanne A, Rebeles RA, Tarkanyi F, Takacs S, Spahn I, Ignatyuk AV (2011) High yield production of the medical

radioisotope 167Tm by the 167Er(d,2n) reaction. Appl Radiat Isot 69:475–481
163. Tarkanyi F, Hermanne A, Takacs S, Ditroi F, Spahn I, Ignatyuk AV (2012) Activation cross-sections of proton induced nuclear reactions on thulium in the 20–45 MeV energy range. Appl Radiat Isot 70:309–314
164. Saito M, Aikawa M, Murata T, Komori Y, Haba H, Takács S, Ditrói F, Szűcs Z (2020) Production cross sections of 169Yb by the proton-induced reaction on 169Tm. Nucl Instrum Methods Phys Res Sect B 471:13–16
165. Tarkanyi F, Hermanne A, Takacs S, Ditroi F, Spahn I, Kovalev SF, Ignatyuk AV, Qaim SM (2007) Activation cross sections of the 169Tm(d,2n) reaction for production of the therapeutic radionuclide 169Yb. Appl Radiat Isot 65:663–668
166. Hermanne A, Tárkányi F, Takács S, Ditrói F, Baba M, Ohtshuki T, Spahn I, Ignatyuk AV (2009) Excitation functions for production of medically relevant radioisotopes in deuteron irradiations of Pr and Tm targets. Nucl Instrum Methods Phys Res Sect B Beam Interact Mater Atoms 267:727–736
167. Hermanne A, Tarkanyi F, Takacs S, Ditroi F (2016) Extension of excitation functions up to 50 MeV for activation products in deuteron irradiations of Pr and Tm targets. Nucl Instrum Methods Phys Res Sect B Beam Interact Mater Atoms 383:81–88
168. Saito M, Aikawa M, Komori Y, Haba H, Takács S (2017) Production cross sections of 169Yb and Tm isotopes in deuteron-induced reactions on 169Tm. Appl Radiat Isot 125:23–26
169. Rayudu GVS, Yaffe L (1963) Reaction produced on erbium by protons of energies between 6 and 87 MeV. Can J Chem 41:2544–2556
170. Tarkanyi F, Takacs S, Hermanne A, Ditroi F, Kiraly B, Baba M, Ohtsuki T, Kovalev SF, Ignatyuk AV (2008) Study of activation cross sections of proton induced reactions on erbium for practical applications. Nucl Instrum Methods Phys Res Sect B Beam Interact Mater Atoms 266:4872–4876
171. Hermanne A, Rebeles RA, Tarkanyi F, Takacs S, Kiraly B, Ignatyuk AV (2011) Cross sections for production of longer lived Tm-170, Tm-168, Tm-167 in 16 MeV proton irradiation of Er-nat. Nucl Instrum Methods Phys Res Sect B Beam Interact Mater Atoms 269:695–699
172. Wilkinson G, Hicks HG (1949) Radioactive isotopes of the rare earths. I. Experimental techniques and thulium isotopes. Phys Rev 75:1370–1378
173. Martin GC, Pilger RC (1966) Absolute cross sections and excitation functions for α-particle-induced reactions of 165Ho, 164Er, 166Er and 167Er. Nucl Phys 89:481–496
174. Sau J, Demeyer A, Chéry R (1968) Etude expérimentale et analyse des fonctions d'excitation 165Ho(α, χn) et 169Tm (α, χn). Nucl Phys A 121:131–144
175. Homma Y, Sugitani Y, Matsui Y, Matsuura K, Kurata K (1980) Cyclotron production of Tm-167 from natural erbium and natural holmium. Int J Appl Radiat Isot 31:505–508
176. Rao JR, Rao AVM, Mukherjee S, Upadhyay R, Singh NL, Agarwal S, Chaturvedi L, Singh PP (1987) Non-equilibrium effects in alpha-particle-induced reactions in light, medium and heavy nuclei up to 120 MeV. J Phys G Nucl Phys 13:535
177. Mukherjee S, Rao AVM, Rao JR (1991) Preequilibrium analysis of the excitation-functions of (Alpha, Xn) reactions on silver and holmium. Nuovo Cimento Della Societa Italiana Di Fisica a-Nuclei Particles Fields 104:863–874
178. Singh NL (1992) Pre-equilibrium neutron emission in alpha particle induced reactions. J Phys G: Nucl Part Phys 18:927
179. Singh BP, Prasad R (1995) Measurement and analysis of excitation functions for the reactions 165Ho(α, xn) (x = 1–3) in the energy range ≈ 10–40 MeV. Phys Scr 51:440
180. Gadkari MS, Patel HB, Shah DJ, Singh NL (1997) Study of preequilibrium decay in (α, xn) reactions in holmium up to 70 MeV. Phys Scr 55:147
181. Tarkanyi F, Hermanne A, Kiraly B, Takacs S, Ignatyuk AV (2010) Study of excitation functions of alpha-particle induced nuclear reactions on holmium for 167Tm production. Appl Radiat Isot 68:404–411
182. Usman AR, Khandaker MU, Haba H, Otuka N, Murakami M (2020) Production cross sections of thulium radioisotopes for alpha-particle induced reactions on holmium. Nucl Instrum Methods Phys Res Sect B 469:42–48
183. Vandenbosch R, Huzienga JR (1960) Isomeric cross-section ratios for reactions producing the isomeric pair Hg197,197m. Phys Rev 120:1313
184. Hansen LF, Albert RD (1962) Statistical theory predictions for 5- to 11-MeV (p, n) and (p, p´) nuclear reactions i^{n} 51V˒ 59Co˒ 63Cu˒ 65Cu, an^{d} ^{1}03Rh. Phys Rev 128:291
185. Gritsyna VT, Klyucharev AP, Remaev VV, Reshetova LN (1963) Ratio of the cross sections for the production of the isomer and ground states of nuclei in the (p, n) reaction at the energies from the threshold to 20 MeV. Sov Phys JETP 17:1186
186. Szelecsényi F, Takács S, Fenyvesi A, Szûcs Z, Tárkányi F, Heselius S-J, Bergman J, Boothe TE (1997) Study of the 197Au(p, pn)196ml, m2, gAu and 197Au(p, n)197mHg reactions and their application for proton beam monitoring in radioisotope production. In: Reffo G, Ventura A, Grandi C (eds) International Conference on Nuclear Data for Science and Technology. Italian Physical Society, Trieste, Italy, p 1483
187. Szelecsényi F, Steyn GF, Kovács Z, van der Walt TN (2007) Application of Au + p nuclear reactions for proton beam monitoring up to 70 MeV. In: international conference on nuclear data for science and technology 2007, EDP Sciences, Nice, France, pp 1259
188. Elmaghraby EK, Hassan KF, Omara H, Saleh ZA (2010) Production of the mercury-197 through proton induced reaction on gold. Appl Radiat Isot 68:1694–1698
189. Satheesh B, Musthafa MM, Singh BP, Prasad R (2012) Study of Isomeric Cross-Section Ratio and Pre-Equilibrium Fraction in Proton and Alpha Particle Induced Nuclear Reactions on Au-197. Int J Modern Phys E Nucl Phys 21:Artn1250059
190. Ditroi F, Tarkanyi F, Takacs S, Hermanne A (2016) Activation cross sections of proton induced nuclear reactions on gold up to 65 MeV. Appl Radiat Isot 113:96–109
191. Lebeda O, Červenák J (2020) Revised cross-sections for formation of theranostic 197m, gHg in proton- and deuteron-induced reactions on 197Au. Nucl Instrum Methods Phys Res Sect B 478:85–91
192. Abe K, Iizuka A, Hasegawa A, Morozumi S (1984) Induced Radioactivity of Component Materials by 16-Mev Protons and 30-Mev Alpha-Particles. J Nucl Mater 123:972–976
193. Bonardi M, Birattari C (1984) Excitation functions for the Au(p, 3n)195m, 195Hg nuclear reactions and 95m, 195Hg/195mAu generator yields. Int J Appl Radiat Isot 35:564
194. Chevarier N, Chevarier A, Demeyer A, Duc TM (1971) Reactions induitessurl'or par des deutons de 10 a 70 MeV. J Phys (Paris) 32:483
195. Khrisanfov YV, Padalko VY, Zarubin PP (1972) Excitation functions for ^{197}Au+ d Reactions, J. Izv. Rossiiskoi Akademii Nauk. Ser Fiz 36:641–643
196. Long X, Peng X, He F (1985) Activation cross-sections of Au-197 with deuterons, Inst.of Nucl.Sci.and Technol.,Sichuan U. Reports
197. Zhao W, Lu H (1989) Measurements of cross sections for ^{197}Au(d, x) reaction. Chin J Nucl Phys 11:83
198. Tarkanyi F, Ditroi F, Hermanne A, Takacs S, Kiraly B, Yamazaki H, Baba M, Mohammadi A, Ignatyuk AV (2011)

Activation cross-sections of deuteron induced nuclear reactions on gold up to 40 MeV. Nucl Instrum Methods Phys Res Sect B Beam Interact Mater Atoms 269:1389–1400
199. Tarkanyi F, Hermanne A, Ditroi F, Takacs S, Rebeles RA, Ignatyuk AV (2015) New data on cross-sections of deuteron induced nuclear reactions on gold up to 50 MeV and comparison of production routes of medically relevant Au and Hg radioisotopes. Nucl Instrum Methods Phys Res Sect B Beam Interact Mater Atoms 362:116–132
200. Hansen LF, Jopson RC, Mark H, Swift CD (1962) Ta181(p, n) W181 and Au197(p, n)Hg197 excitation functions between 4 and 13 MeV. Nucl Phys 30:389
201. Chodil G, Jopson RC, Mark H, Swift CD, Thomas RG, Yates MK (1967) (p, n) and (p,2n) cross sections on nine elements between 7.0 and 15.0 MeV. Nucl Phys A 93:648
202. Birattari C, Bonardi M (1980) Excitation functions for nuclear reactions (p, xn) and (p, pxn) on targets of gold and study of the production of the ultra-short-lived radioisotope Au-195-m. INFN Reports/ Various Techniques Series, IFNF, Italy
203. Tárkányi F, Hermanne A, Takács S, Shubin YN, Dityuk AI (2004) Cross sections for production of the therapeutic radioisotopes Au-198 and Au-199 in proton and deuteron induced reactions on Pt-198. Radiochim Acta 92:223–228
204. Showaimy H, Solieman AHM, Hamid ASA, Khalaf AM, Saleh ZA (2019) Measurements of activation cross sections for proton induced reactions on natural platinum targets leading to the formation of gold radioisotopes. Radiat Phys Chem 157:97–101
205. Gantumur D, Aikawa M, Khishigjargal T, Norov E, Ukon N, Haba H (2023) Activation cross sections of proton-induced reactions on natural platinum up to 30 MeV. Appl Radiat Isot 192:110621
206. Ditroi F, Tarkanyi F, Csikai J, Uddin M, Hagiwara M, Baba M, Shubin Y, Kovalev S (2006) Excitation functions of long lived products in deuteron induced nuclear reactions on platinum up to 40 MeV. Nucl Instrum Methods Phys Res Sect B Beam Interact Mater Atoms 243:20–27
207. Khandaker MU, Haba H, Murakami M, Otuka N, Abu Kassim H (2015) Excitation functions of deuteron-induced nuclear reactions on natural platinum up to 24 MeV. Nucl Instrum Methods Phys Res Sect B Beam Interact Mater Atoms 362:151–162
208. Ditroi F, Tarkanyi F, Takacs S, Hermanne A (2017) Extension of activation cross section data of long lived products in deuteron induced nuclear reactions on platinum up to 50 MeV. Nucl Instrum Methods Phys Res Sect B Beam Interact Mater Atoms 401:56–70
209. Tárkányi F, Ditrói F, Takács S, Hermanne A, Ignatyuk AV (2019) Experimental and theoretical cross section data of deuteron induced nuclear reactions on platinum. J Radioanal Nucl Chem 321:747–764
210. Tewes HA, James RA (1952) Proton induced reactions of thorium–-fission yield curves. Phys Rev 88:860–867
211. Tewes HA (1955) Excitation functions for some proton-induced reactions of thorium. Phys Rev 98:25–27
212. Meinke WW, Wick GC, Seaborg GT (1956) High-energy excitation functions in the heavy region. J Inorg Nucl Chem 3:69–92
213. Lefort M, Simonoff GN, Tarrago X (1961) Re´actions nucle´aires de spallation induites sur le thorium par des protons de 150 et 82 MeV. Nucl Phys 25:216–247
214. Brun C, Simonoff GN (1962) Compétition fission-évaporation. Etude des fonctions d'excitation dans différents noyaux de protactinium. J Phys Radium 23:12–16
215. Celler A, Luontama M, Kantele J, Zylicz J (1981) Cross sections of 232Th (p, xn+yp) reactions at Ep = 68 to 202 MeV. Phys Scripta 24:930
216. Kudo H, Muramatsu H, Nakahara H, Miyano K, Kohno I (1982) Fission fragment yields in the fission of ^{232}Th by protons of energies 8 to 22 MeV. Phys Rev C 25:3011–3023
217. Chu YY, Zhou ML (1983) Comparison of the (p, xn) cross sections from 238U, 235U and 232Th targets irradiated with 200 MeV protons. IEEE Trans Nucl Sci 30:1153–1155
218. Roshchin A, Yavshits S, Jakovlev V, Karttunen E, Aaltonen J, Heselius S (1997) Cross sections for nonfission reactions induced in Th-232 by low-energy protons. Phys At Nucl 60:1941–1945
219. Morgenstern A, Apostolidis C, Bruchertseifer F, Capote R, Gouder T, Simonelli F, Sin M, Abbas K (2008) Cross-sections of the reaction 232Th(p,3n)230Pa for production of 230U for targeted alpha therapy. Appl Radiat Isot 66:1275–1280
220. Jost CU, Griswold JR, Bruffey SH, Mirzadeh S, Stracener DW, Williams CL (2013) Measurement of cross sections for the 232Th(P,4n) 229Pa reaction at low proton energies. In: AIP conference proceedings, pp 520–524
221. Radchenko V, Engle JW, Wilson JJ, Maassen JR, Nortier MF, Birnbaum ER, John KD, Fassbender ME (2016) Formation cross-sections and chromatographic separation of protactinium isotopes formed in proton-irradiated thorium metal. Radiochim Acta 104:291–304
222. Friend MT, Mastren T, Parker TG, Vermeulen CE, Brugh M, Birnbaum ER, Nortier FM, Fassbender ME (2020) Production of 230Pa by proton irradiation of 232Th at the LANL isotope production facility: precursor of 230U for targeted alpha therapy. Appl Radiat Isot 156:108973
223. Rao JR, Ernst J, Machner H (1986) Comparative study of d- and 6Li-induced reactions on 232Th in terms of breakup and preequilibrium processes. Nucl Phys A 448:365–380
224. Duchemin C, Guertin A, Haddad F, Michel N, Metivier V (2014) 232Th(d, xn)230,232,233Pa cross section measurements. Nucl Data Sheets 119:267–269